Qualitative and quantitative analysis of spindle assembly checkpoint signaling in *Schizosaccharomyces pombe*

Dissertation

der Mathematisch-Naturwissenschaftlichen Fakultät

der EBERHARD KARLS UNIVERSITÄT TÜBINGEN

zur Erlangung des Grades eines

Doktors der Naturwissenschaften

(Dr. rer. nat.)

vorgelegt von

Stephanie Heinrich

aus Gera

Tübingen

2013

Tag der mündlichen Qualifikation:	20.12. 2013
Dekan:	Prof. Dr. Wolfgang Rosenstiel
1. Berichterstatter:	Dr. Silke Hauf
2. Berichterstatter:	Prof. Dr. Gerd Jürgens

For my parents

Rita and Gunter Heinrich

ACKNOWLEDGEMENTS

I would like to thank everyone who has been part of this journey and who helped me through the completion of this dissertation, including many people not mentioned below.

First and foremost, I would like to express my sincere gratitude to Dr. Silke Hauf for the opportunity to perform my doctoral work in her lab. I am grateful for the immeasurable support and guidance she has provided throughout this study. Her continuous encouragement, advice and enthusiasm had a great influence on the success of this work.

I would like to thank Prof. Dr. Gerd Jürgens for agreeing to be my Ph.D. supervisor and, together with Dr. Wolfram Antonin, for participating in my annual progress report and providing helpful advice when discussing my results. Furthermore, I am thankful to Prof. Dr. Gerd Jürgens, Prof. Dr. Boris Maček, Prof. Dr. Doron Rapaport and Dr. Silke Hauf for agreeing to be my Ph.D. examiners.

I am thankful to Eva-Maria Geissen, Prof. Dr. Nicole Radde and Dr. Jan Hasenauer for great teamwork and making our collaboration this successful.

I am truly grateful to all members of the Hauf lab, present and past, for a great working atmosphere full of support, fruitful discussions, laughter and fun. Thanks to Julia, Hanna, André, Asha, Yu-Hua, Maria, Eva I., Eva S., Nicole, Sabine, Armin, Nadine and Katharina for being great lab mates. I also want to thank the internship and undergraduate students Julia B., Julia S., Fatih, Christoph, Janet, Melanie, Katrin and Vera for assisting me in my projects. I am very grateful to Eva I. for excellent technical help and great lab organization. Special thanks to Julia for making everyday madness enjoyable.

Furthermore I would like to thank all my other friends on an off campus for making me feel at home in Tübingen.

Finally, I will forever be indebted to my parents for their continuous support and for always believing in me.

TABLE OF CONTENTS

LIST OF FIGURES

ABBREVIATIONS

A	Adenine
Ala	Alanine (A)
APC/C	Anaphase promoting complex/Cyclosome
Arg	Arginine (R)
Ark1	Aurora related kinase 1
Blinkin	Bub1-linking protein
Bub	Budding uninhibited by benzimidazole
BubR1	Bub1-related protein 1
Cdc	Cell division cycle
Cdk	Cyclin-dependent kinase
C. elegans	*Caenorhabditis elegans*
CENP	Centromere associated protein
CPC	Chromosomal passenger complex
d	Day
Da	Dalton
D. melanogaster	*Drosophila melanogaster*
DMSO	Dimethyl sulfoxide
DAPI	4',6-diamidino-2-phenylindole
DNA	Deoxyribonucleic acid
DTT	Dithiothreitol
EDTA	Ethylenediaminetetraacetic acid
EMM	Edinburgh minimal medium
GFP	Green fluorescent protein
GLEBS	Gle2-binding sequence
Glu	Glutamate (E)
h	Hour
HEPES	2-[4-(2-hydroxyethyl)piperazin-1-yl]ethanesulfonic acid
HORMA	protein domain named after the Hop1p, Rev7p and MAD2 proteins
IP	Immunoprecipitation
K	Lysine (Lys)
KMN	KNL1 /Mis12 complex/Ndc80 complex
KNL1	Kinetochore-null protein 1
L	Liter

Leu	Leucine (L)
Mad	Mitotic arrest deficient
MBC	Carbendazim, methyl-2-benizimidazole carbamate
Met	Methionine (M)
Mis	Missegregation
μg	Microgram
min	Minute
mL	Milliliter
μL	Microliter
Mps1	Monopolar spindle 1
Mph1	Monopolar spindle homolog 1
N	Asparagine (Asp)
Ndc	Nuclear division cycle
NPC	Nuclear pore complex
Nup	Nucleoporin
PEM	A buffer consisting of PIPES, EGTA and magnesium sulphate
PFA	Paraformaldehyde
PP1	Protein phosphatase 1
PP2A	Protein phosphatase 2A
Q	Glutamine (Gln)
RNAi	RNA interference
rpm	Rotations per minute
SAC	Spindle assembly checkpoint
S. cerevisiae	*Saccharomyces cerevisiae* (budding yeast)
SDS	Sodium dodecyl sulphate
Ser	Serine (S)
Sgo	Shugoshin
siRNA	small interfering RNA
Slp1	Sleepy homolog
SPB	Spindle pole body
S. pombe	*Schizosaccharomyces pombe* (fission yeast)
Thr	Threonine (T)
TPR	Tetratricopeptide repeat (protein motif)
Tpr	Translocated promoter region (Nup211 homolog)
Tris	Tris(hydroxymethyl)aminomethane

WCE	Whole cell extract
X. laevis	*Xenopus laevis*
YEA	Yeast extract supplemented with adenine

SUMMARY

The spindle assembly checkpoint (SAC) is a conserved eukaryotic surveillance mechanism, which maintains genomic integrity by delaying mitotic progression until all chromosomes have become properly attached to the mitotic spindle via their kinetochores. Malfunction of this checkpoint leads to chromosome segregation errors and has been implicated in tumorigenesis. SAC protein localization to unattached kinetochores is considered to be required for checkpoint signaling.

This study shows that *Schizosaccharomyces pombe* checkpoint proteins display a hierarchical kinetochore localization, with Ark1 and Mph1 being the most upstream components in the signaling cascade. The sole function of Ark1 in the checkpoint is to recruit Mph1, with the N-terminal region of Mph1 being required to dock the protein to kinetochores. Both proteins are the only checkpoint components still enriching at kinetochores in cells lacking *bub3*, and their localization is crucial for checkpoint activity in this situation.

To shed light on the connection between upstream and downstream segments of the checkpoint signaling cascade, we examined the link between Bub1 and Mad1. A conserved motif in Bub1 and the Mad1 C-terminus are required for Mad1 localization and checkpoint function. Moreover, we provide evidence for a role of Mad1 in checkpoint signaling that goes beyond its function in localizing and presenting Mad2.

Reliable checkpoint signaling needs robustness towards slight SAC protein level fluctuations, as they inevitably occur due to gene expression noise. We observed that slight changes in checkpoint protein abundance can strongly affect SAC signaling. To avoid this critical zone, cells keep the noise of relevant checkpoint proteins low. Some abundance changes caused non-genetic variability in checkpoint signaling, with one population of cells failing to arrest in mitosis and the other population maintaining a mitotic arrest. We describe stoichiometric inhibition of Slp1 as the basis for this population split. In addition, changes in nutrient conditions influence Slp1 abundance, which suggests that cells respond to changes in the environment by altering checkpoint signaling.

Taken together, the SAC protein interaction network structure and SAC protein abundance are equally important for reliable checkpoint signaling.

ZUSAMMENFASSUNG

Der ‘Spindle assembly checkpoint’ (SAC) ist ein konservierter, eukaryontischer, zellulärer Überwachungsmechanismus, der die genomische Integrität aufrechterhält, indem er das Fortschreiten der Mitose verzögert bis alle Chromosomen über ihre Kinetochore korrekt mit der mitotischen Spindel verknüpft sind. Fehlfunktionen dieses Kontrollmechanismus führen zu Fehlern in der Chromosomensegregation und können zur Tumorentstehung beitragen. SAC-Proteine binden an unangeheftete Kinetochoren, was als Voraussetzung für das Entstehen des SAC-Signals angesehen wird.

Diese Studie zeigt, dass *Schizosaccharomyces pombe* SAC-Proteine hierarchisch an unangeheftete Kinetochore binden, und die Signalkaskade mit den Proteinen Ark1 und Mph1 beginnt. Die Lokalisation von Mph1 ist die einzige Funktion von Ark1 im Checkpoint. Die N-terminale Region in Mph1 ist dabei notwendig, um das Protein ans Kinetochor zu bringen. Beide Proteine sind die einzigen SAC-Proteine, die in Zellen mit fehlendem Bub3 noch an unangeheftete Kinetochore binden und ihre Lokalisation ist essentiell um einen aktiven Checkpoint aufrechtzuerhalten.

Um zu verstehen wie obere und untere Segmente der SAC-Signalkaskade miteinander verknüpft sind, haben wir die Verbindung zwischen dem Bub1 und Mad1 untersucht. Ein konserviertes Motiv in Bub1 und der C-terminus von Mad1 sind notwendig, damit Mad1 an Kinetochore binden kann. Mad1 hat zudem eine Rolle im Checkpoint, die über die bekannte Funktion hinausgeht Mad2 an unangehefteten Kinetochoren zu präsentieren.

Entscheidend für ein zuverlässiges SAC-Signal ist dessen Robustheit gegenüber kleinen Veränderungen in der Menge an SAC-Proteinen, wie sich durch Genexpressions-Rauschen entstehen. Überraschenderweise fanden wir, dass geringe Änderungen der SAC-Proteinmengen das SAC-Signal stark beeinflussen können. Um diese kritische Zone zu vermeiden, halten die Zellen das Protein-Rauschen in engen Grenzen. Einige Proteinmengen-Veränderungen verursachten eine nicht-genetische Signal-Variabilität, bei der nur ein Teil der Population einen stabilen mitotischen Arrest aufrechterhält. Die stöchiometrische Inhibierung von Slp1 kann das Aufspalten in zwei Population erklären. Zusätzlich zeigen wir, dass Änderungen der Nährstoffbedingungen die Slp1-Proteinmenge beeinflussen, was darauf hinweist, dass Zellen auf Unterschiede des Milieus mit einer Veränderung des SAC-Signals reagieren.

Zusammenfassend sind sowohl das SAC-Protein-Interaktionsnetzwerk als auch die SAC-Proteinmenge gleichermaßen wichtig für ein zuverlässiges SAC-Signal.

1 Introduction

1.1 Cells

Organisms, be it a bacterium, a yeast, a plant or a mammal, share a similar building concept as they are composed of cells. Cells were first discovered in 1665, when Robert Hooke described microscopic units found in slices of cork as 'little chambers' and named them after the latin word cellula ('small room'). Over a century later, the more general 'cell theory' was formulated by the German botanist Matthias Jakob Schleiden (1838) and by the zoologist Theodor Schwann (1839), when they reported that plants and animals are composed of or formed by cells. Schleiden hypothesized that new cells emerge by a spontaneous crystallization process inside another cell, which he called 'free cell formation'. In 1852 Robert Remak and in 1858 Rudolf Virchow, among other scientists, disproved this concept and postulated that new cells are formed through scission of pre-existing cells, which Virchow summarized in the term 'omnis cellula e cellula' (every cell from pre-existing cell), which is now the basis of classical cell theory.

1.2 The cell cycle

Eukaryotic cells reproduce in an elegant, highly coordinated fashion. The progression through the different phases is called the cell cycle. It can be divided into four major steps. Replication of the DNA as carrier of the genetic information is accomplished in the synthetic or S phase, and its equal distribution to the two emerging daughter cells is executed in the mitotic or M phase. These two events of duplication and division are spaced by two gap phases (G1 and G2), which provide time for the take up of nutrients and cellular growth. The period between two M phases is called interphase, and comprises G1, S and G2 phase. The length of individual cell cycle phases can vary, and even the order of events is flexible to a certain extent: during early *Drosophila melanogaster* embryonic development, DNA replication and nuclear division can occur without cellular division and gap phases, resulting in a multi-nuclear syncytium (Morgan, 2007). Cells in multicellular organisms can exit the cell cycle and go from an active to a quiescent state, a so-called G0 phase, by stopping to proliferate. 'G0 cells' include damaged or senescent cells, but also cells that are terminally differentiated (Morgan,

2007).

The cell cycle is a highly coordinated, precise and reliable system, in which a complex regulatory network of proteins controls the correct and timely order of events. Key components that mediate cell cycle progression are the cyclin-dependent kinases (CDKs). CDK activities rise and fall during each cell cycle which leads to cyclical changes in the phosphorylation status of each of its substrates, which in turn influences cell cycle events. The driving force behind its oscillating activity is the binding to activator proteins called cyclins. While cyclin synthesis and degradation fluctuate in distinct cell cycle phases, CDK abundance is constant during the cell cycle (Morgan, 1995; Morgan, 1997). Cyclin abundance and thus CDK activity is low when cells enter G1, but increases to allow cells to progress through S phase, G2 phase and M phase. CDK activity drops again at the end of mitosis to allow for exit from M phase (Coudreuse & Nurse, 2010; Morgan, 2007). Reduction of CDK activity is achieved by degradation of mitotic cyclin B, which is mediated by the multi-subunit E3 ubiquitin ligase called the anaphase promoting complex/cyclosome (APC/C) (Morgan, 2007; Pines, 2011).

1.3 Mitosis

M phase is the phenotypically most distinct stage of the cell cycle and comprises nuclear division (mitosis or karyokinesis) and cellular division (cytokinesis). During a complex series of events, the genetic material is split in two and each daughter cell obtains one set of identical DNA masses. The term ‘mitosis’ was first mentioned by Walther Flemming in 1882, when he named the process after the appearance of condensed chromosomes (Greek ‘mito’ or ‘thread’). Mitosis can be divided into distinct phases, which have been defined based on the morphological changes of the nucleus or the cell: prophase, prometaphase, metaphase, anaphase and telophase. In prophase, chromosomes start to undergo condensation, while centrosomes (or ‘microtubule-organizing centers’) initiate spindle establishment by microtubule nucleation (Pereira & Schiebel, 1997). In prometaphase, the nuclear envelope breaks down in some organisms (which is called an ‘open’ mitosis) and chromosomes condense further to visibly distinguishable pairs of sister chromatids. Spindle microtubules emanating from both centromeres contact and capture kinetochores, large proteinaceous structures that assemble on centromeres of each sister chromatid (DeLuca & Musacchio, 2012; Hori & Fukagawa, 2012; Westhorpe & Straight, 2013). In metaphase, stable ‘end-on’ attachments are formed between microtubules and

kinetochores (Kops et al, 2010) and all chromosomes are aligned at the spindle equator (also referred to as 'metaphase plate'). Correct attachment of sister chromatids to microtubules from opposing spindle poles is essential for proper bipolar attachment and accurate chromosome segregation. If all chromosomes are correctly attached, the connection between the two sister chromatids is abruptly dissolved and the separated sister chromatids are pulled to the opposing poles (anaphase A). Anaphase events are triggered by the activation of the APC/C, which adds poly-ubiquitin chains to its major substrates securin and cyclin B and thereby marks them for destruction by the 26S proteasome (Peters, 2006; Pines, 2011). Both securin and cyclin B contain destruction (D)-box and/or KEN-box degrons, which are important substrate recognition sites for Cdc20, the mitotic co-activator of the APC/C (Primorac & Musacchio, 2013). Degradation of cyclin B leads to a reduction in CDK activity, whereas degradation of securin frees its interaction partner separase, a protease which cleaves the Scc1 subunit of the cohesin ring that holds sister chromatids together (Oliveira & Nasmyth, 2010). In anaphase B, the spindle poles move further apart, the spindle itself elongates and transfers the two sister chromatids away from each other to the ends of the dividing cell. In the final phase of mitosis, telophase, the spindle disassembles, while chromosomes decondense and are packaged together with other nuclear components into a new nucleus (Sullivan & Morgan, 2007). Subsequently, at the cleavage furrow the cytoplasm is pinched in two halves (abscission) and cytokinesis occurs (Burgess & Chang, 2005).

In some eukaryotes, not all the stages above are precisely discernable. In yeast such as *Schizosaccharomyces pombe* (fission yeast) or *Saccharomyces cerevisiae* (budding yeast), prophase and prometaphase are not clearly distinguishable as the nucleus stays intact and a spindle is formed inside the nucleus, resulting in a 'closed' mitosis. The spindle emanates from the functional equivalent of a centrosome, called a 'spindle pole body' (SPB), which in budding yeast is an integral part of the nuclear envelope during the cell cycle (Jaspersen & Winey, 2004), but in fission yeast lies on the cytoplasmic surface of the nucleus during interphase, becomes integrated into the nuclear membrane during mitosis and is excluded again in late anaphase (Ding et al, 1997). In *Caenorhabditis elegans*, the nuclear envelope persists until anaphase (Lee et al, 2000). The only traditional mitotic stages that are relatively well conserved are anaphase and telophase, because the disjunction and segregation of replicated sister chromatids, and the generation of new cells are minimum requirements for cell reproduction (Pines & Rieder, 2001).

1.4 The kinetochore

The kinetochore provides the crucial link between chromosomes and the mitotic spindle to facilitate faithful chromosome segregation. It consists of around 100 proteins that are hierarchically assembled on centromeric DNA and couples forces generated by microtubule dynamics to chromosome movements (Foley & Kapoor, 2013). The kinetochore can be divided into three sub-structures, which assemble on top of each other: the inner kinetochore, the outer kinetochore and the 'corona'. The inner kinetochore is composed of the constitutive centromere-associated network (CCAN) and makes direct contact to a specialized stretch of centromeric nucleosomes that contain the histone variant CENP-A instead of histone H3 (De Rop et al, 2012; Westhorpe & Straight, 2013). The outer kinetochore provides the platform for binding microtubules and is formed by the KMN network, which comprises KNL1 (Spc7 in *S. pombe*), the MIS12 complex (MIS12-C, composed of Mis12, Dsn1, Nnf1, and Nsl1), and the NDC80 complex (NDC80-C, composed of Ndc80, Nuf2, Spc24, and Spc25) (DeLuca & Musacchio, 2012; Foley & Kapoor, 2013). The conserved inner and outer kinetochore proteins are accompanied by a set of dynamic accessory proteins, such as components of the spindle assembly checkpoint (see later) (Musacchio & Salmon, 2007). The outermost 'corona' is a fibrous structure seen by electron microscopy to stretch out 100-150 nm from the outer kinetochore. Proteins shown to localize to the fibrous structure are the microtubule-interacting molecular motor CENP-E or the microtubule interactor CENP-F (Varma et al, 2013; Wan et al, 2009).

In vivo, depletion of any of the KMN protein components decreases the capacity to form functional kinetochore–microtubule connections, with the strongest defects observed in cells depleted of NDC80-C components, suggesting that the NDC80-C is largely responsible for direct attachments (DeLuca & Musacchio, 2012). *In vitro* binding assays (Cheeseman et al, 2006) and force measurements (McIntosh et al, 2008; Powers et al, 2009) with purified NDC80-C and microtubules are consistent with the hypothesis that this complex connects chromosome movement to microtubule dynamics. KNL1 also has microtubule-binding activity *in vitro* (Cheeseman et al, 2006). The MIS12-C interacts with the C-terminus of KNL and the Spc24/Spc25 subunit of the NDC80-C (Petrovic et al, 2010). MIS12-C further serves as bridge between NDC80-C, KNL1 and the CCAN by directly binding to the CCAN component CENP-C (Przewloka et al, 2011; Screpanti et al, 2011).

Spindle assembly checkpoint proteins

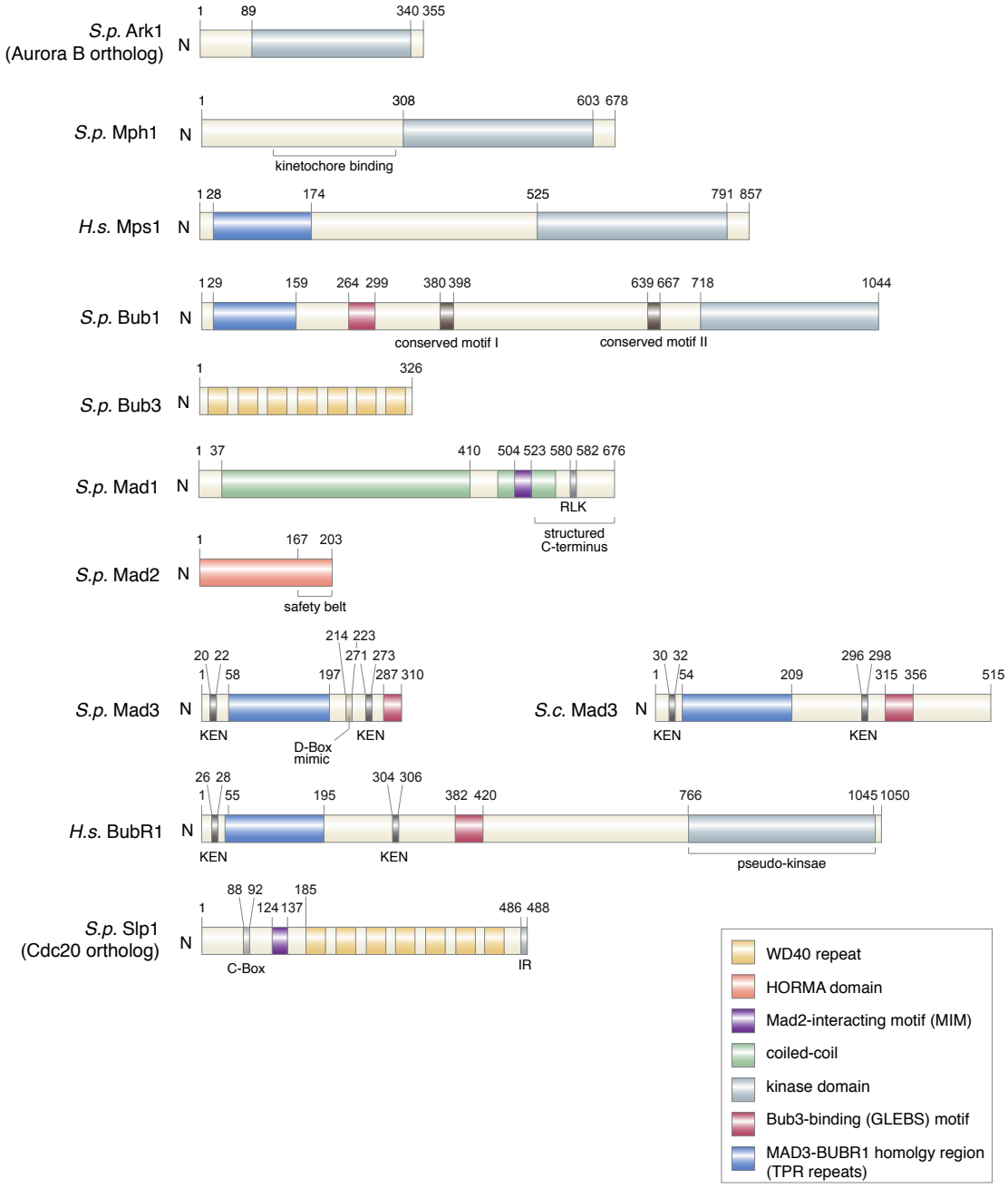

Figure 1 Structural organization of spindle assembly checkpoint proteins in *Schizosaccharomyces pombe* (adapted from Musacchio and Salmon, 2007; see text for details)
S.p. = Schizosaccharomyces pombe; S.c. = Saccharomyces cerevisiae; H.s.= Homo sapiens. All proteins are drawn to scale.
The Mad3 proteins in *S. pombe* and *S. cerevisiae* differ from the Mad3 ortholog BubR1, in that the latter contains an additional C-terminal kinase domain. Similar to BubR1, also Ark1 (Aurora B ortholog), Mph1 (Mps1 ortholog) and Bub1 contain kinase domains. The tetratricopeptide repeats (TPR) in Bub1 and BubR1 have been shown to interact with the kinetochore component KNL1. Both Slp1 (Cdc20 ortholog) and Bub3 contain WD40 repeats that fold into 7-bladed propellers. The Slp1 C-box and IR tail are both required for interaction with APC/C. Mad2 is composed of the globular HORMA domain (for Hop1, Rev7, Mad2), a two-layered structure of beta-sheets and alpha-helices. The 'safety belt' in Mad2 consists of 2 beta-sheets that undergo a strong conformational change upon switch from open (O-) Mad2 to closed (C-) Mad2, which is required for entrapping either Mad1 or Slp1.

During the formation of microtubule-kinetochore attachments, errors can occur and are resolved by an error correction mechanism, which involves the kinase Aurora B, a subunit of the chromosomal passenger complex (CPC) (Carmena et al, 2012; Ditchfield et al, 2003; Hauf et al, 2003; Lampson et al, 2004). Phosphorylation of multiple kinetochore components, including members of the KMN network (Cheeseman et al, 2006; DeLuca et al, 2006), destabilize the interaction of these proteins with microtubules, resolve erroneous attachments and create free kinetochores that can re-interact with microtubules for proper bi-oriented attachment.

1.5 The spindle assembly checkpoint

If cells encounter problems in the completion of a cell cycle event, dedicated control systems will delay the initiation of later events until those problems have been solved. For example, erroneous kinetochore-microtubule attachments must be resolved prior to anaphase to ensure correct chromosome segregation. To this end, the cell cycle is equipped with several checkpoints, which monitor the status of a cell at transition points and halt cell cycle progression if conditions are unfavorable. During mitosis, the spindle assembly checkpoint (SAC) senses improperly attached kinetochores and inhibits cell cycle progression beyond metaphase until all chromosomes have achieved proper bi-orientation (Jia et al, 2013; Lara-Gonzalez et al, 2012; Musacchio & Salmon, 2007). Conserved core components of the SAC are Mad1, Mad2, Mad3 (or BubR1, depending on the organism), Bub1, Bub3 as well as Mps1 (Mph1 in *S. pombe*) and Aurora B (Ark1 in *S. pombe*) (Figure 1). The discovery of the MAD (mitotic arrest-deficient) and BUB (budding uninhibited by benzimidazole) proteins dates back to 1991, when two independent budding yeast screens identified mutants that failed to induce a cell cycle delay in the presence of microtubule-depolymerizing drugs (Hoyt et al, 1991; Li & Murray, 1991). The checkpoint function of the serine/threonine kinases Mps1 and Aurora B was revealed in subsequent studies (see later and (Biggins & Murray, 2001; Weiss & Winey, 1996).

Elegant experiments using micromanipulation and laser ablation have linked spindle checkpoint signaling with defective kinetochore-microtubule attachments (Li & Nicklas, 1995; Rieder et al, 1995). Applying tension to a mis-attached chromosome using a micromanipulation needle, which simulates proper attachment and biorientation to the mitotic spindle, drastically reduced a checkpoint-induced mitotic delay (Li & Nicklas, 1995). Similarly, complete destruction of the last unattached kinetochore by laser ablation

caused a rapid exit from mitosis (Rieder et al, 1995). Moreover, specific mutants of kinetochore components impair proper kinetochore formation and SAC activation, which result in a

precocious split of sister chromatids and subsequent chromosome mis-segregation (He et al, 2001). Checkpoint components have been described to enrich at unattached kinetochores during early mitosis, which has been interpreted as initial stage of checkpoint signaling (Musacchio & Salmon, 2007). To allow for a robust block in prometaphase to correct chromosome attachment errors, the signal at the kinetochore has to be translated into an inhibitory signal for cell cycle progression. This is achieved by negative regulation of APC/C activity. The ultimate molecular target of the SAC is Cdc20 (Slp1 in *S. pombe*), the mitotic activator of the E3 ubiquitin ligase APC/C (Peters, 2006; Primorac & Musacchio, 2013), which is temporarily sequestered by the checkpoint proteins Mad2 and Mad3. Inhibition of the APC/C blocks ubiquitination and subsequent degradation of securin and cyclin B and prevents progression to anaphase.

1.6 SAC signaling at the kinetochore and beyond

1.6.1 Generating the checkpoint signal – Aurora B and Mps1 at the kinetochore

On a molecular level, the trigger for initiating SAC component recruitment to unattached kinetochores is unknown. However, recent studies have illuminated certain aspects of how kinetochore and checkpoint components contact each other and modulate kinetochore-microtubule connections and checkpoint signaling. The outer kinetochore KMN network has been shown to operate as connecting platform, as it serves both as receptor for microtubules and interacts directly or indirectly with checkpoint components (Jia et al, 2013) (Figure 2). Similar to the hierarchical structure of the kinetochore, checkpoint components also enrich at the centromere-kinetochore interface in an ordered fashion, with Aurora B and Mps1 being the most upstream components of the SAC signaling pathway (Foley & Kapoor, 2013; Musacchio & Salmon, 2007). Aurora B, as part of the chromosomal passenger complex (CPC), localizes to the centromeric region of chromosomes, where it dynamically modulates kinetochore-microtubule attachment (Carmena et al, 2012). If kinetochores are improperly attached, Aurora B phosphorylates kinetochore components such as Ndc80 (Cheeseman et al, 2002; Ciferri et al, 2008), which reduces their affinity to microtubules and thus allows the establishment of new

contacts between the kinetochore and the mitotic spindle (Cheeseman et al, 2006; Ciferri et al, 2008). In addition, Aurora B influences Mps1 enrichment at kinetochores in many organisms except *S. cerevisiae* (no inter-dependence found) and *C. elegans* (no Mps1 ortholog found) (Essex et al, 2009; Maure et al, 2007). In human cells, reports on the relationship between Aurora B and Mps1 have been contradictory. Upon reduction of Aurora B activity, Mps1 recruitment to kinetochores is perturbed (Hewitt et al, 2010; Santaguida et al, 2010; Saurin et al, 2011), which is in accordance to results from *Xenopus laevis*, which places Aurora B upstream of Mps1 (Vigneron et al, 2004). Conversely, Mps1 reduction by shRNA reduces Aurora B activity, although centromeric Aurora B localization is preserved (Jelluma et al, 2008). Modification of Aurora B activity has been reported to depend on the direct phosphorylation of the CPC protein Borealin/Dasra by Mps1 (Jelluma et al, 2008). However, other studies employing Mps1 knock-down approaches, Mps1 inhibitors or analog-sensitive alleles of Mps1 to specifically perturb Mps1 kinase activity could not observe an involvement of Mps1 in promoting Aurora B localization or activity in human cells (Hewitt et al, 2010; Maciejowski et al, 2010; Santaguida et al, 2010; Saurin et al, 2011), so that the role of Mps1 in Aurora B regulation remains uncertain.

Mps1 has been shown to phosphorylate the kinetochore component KNL1 at multiple MELT motifs (MELT standing for the amino acids Met, Glu, Leu, Thr), which allows direct binding of Bub1 and Bub3 (Krenn et al, 2012; London et al, 2012; Primorac et al, 2013; Shepperd et al, 2012; Yamagishi et al, 2012) (Figure 2–1). The recruitment of Bub1 and Bub3 to phosphorylated KNL1 is required to enrich the checkpoint components Mad1, Mad2 and Mad3/BubR1 at the kinetochore (Essex et al, 2009; Gillett et al, 2004; Kadura et al, 2005; Meraldi et al, 2004; Sharp-Baker & Chen, 2001; Vanoosthuyse et al, 2009; Windecker et al, 2009). In metazoans, Mps1 additionally recruits the three-subunit RZZ complex (Rod, Zwilch and Zw10), which in turn is required for recruitment of Mad1 and Mad2 (Buffin et al, 2005; Essex et al, 2009; Karess, 2005; Maciejowski et al, 2010; Santaguida et al, 2010). Interestingly, the RZZ complex also targets a dynein/dynactin complex to kinetochores. This complex has been implicated in stripping off Mad1 and Mad2 from kinetochores in metaphase, and moving them along microtubules to spindle poles, thereby contributing to checkpoint silencing (Howell et al, 2000; Howell et al, 2001; Sivaram et al, 2009). In yeast, no functional homologs of the RZZ components have been identified and dynein seems not to be involved in Mad2 removal from kinetochores in *S. pombe* (Courtheoux et al, 2007).

1.6.2 Bub1 and Bub3 at the kinetochore

Bub1 interaction with KNL1 is mediated by its N-terminus. Two N-terminal regions that occur both in Bub1 and in Mad3/BubR1 have been suggested to mediate kinetochore recruitment, either by binding to the outer kinetochore or by interacting with Bub3. The first region consists of an array of three motifs that each adopt a tetratricopeptide repeat(TPR)-like fold (Bolanos-Garcia et al, 2009). Deletion of these motifs in *S. pombe* Bub1 weakens kinetochore localization, fails to recruit Bub3 and Mad3 to kinetochores and abolishes checkpoint function (Vanoosthuyse et al, 2004). Contradictory reports exist for human cells (Klebig et al, 2009; Krenn et al, 2012; Taylor et al, 1998). Whereas Klebig *et al.* (2009) were unable to detect kinetochore recruitment of Bub1 upon deletion of the N-terminal 150 amino acids, analysis of the N-terminal 146 or 150 amino acids by Krenn *et al.* (2012) or Taylor *et al.* (1998), respectively, indicates that the TPR repeats are neither required nor sufficient to localize Bub1 to kinetochores. A direct interaction between the TPR motif and one of two kinetochore interaction (KI) motifs of KNL1 has been shown *in vitro* and subsequently been visualized by X-ray crystallography (Krenn et al, 2012). Point mutants perturbing the interaction of Bub1 and KNL1 *in vitro* did not alter Bub1 kinetochore localization *in vivo* (Krenn et al, 2012), suggesting only a minor contribution of the TPR motif to Bub1-kinetochore interaction. Indeed, the second Mad3/BUB1 homology region, often referred to as the GLEBS motif (short for Gle2-binding sequence) or – more recently – as the Bub3-binding motif, has been shown to be the major contributor to kinetochore recruitment of Bub1 (Klebig et al, 2009; Logarinho et al, 2008; Taylor et al, 1998; Vanoosthuyse et al, 2009; Windecker et al, 2009). The GLEBS motif, which was first described as an interaction motif between the nuclear pore component Nup98 and the mRNA export factor and Bub3 homolog Gle2/Rae1(Bailer et al, 1998), mediates interaction between Bub1 and Bub3 (Klebig et al, 2009; Larsen et al, 2007; Taylor et al, 1998; Vanoosthuyse et al, 2009). In fission yeast cells expressing Bub1 that lacks the GLEBS motif, neither Bub1 nor Bub3 are able to localize to kinetochores (Windecker et al, 2009), indicating that complex formation mediates kinetochore binding. Consistently, cells with reduced or absent Bub1 fail to recruit Bub3 to kinetochores and vice versa (Gillett et al, 2004; Kerscher et al, 2003; Logarinho et al, 2008; Shepperd et al, 2012; Vanoosthuyse et al, 2004; Windecker et al, 2009). Both biochemical (Yamagishi et al, 2012) and structural analysis (Primorac et al, 2013) showed that the presence of both Bub1 and Bub3 is necessary to allow interaction with the kinetochore protein KNL1 (Figure 2–1).

The contribution of the GLEBS motif to checkpoint signaling is controversial. Whereas human cells lacking the Bub1-Bub3 interaction have a clear checkpoint defect (Klebig et al, 2009), fission yeast cells expressing *bub1-ΔGLEBS* preserve checkpoint activity (Vanoosthuyse et al, 2009; Windecker et al, 2009). The same observation has been made for Bub3: altered Bub3 levels cause checkpoint defects in several organisms (Campbell & Hardwick, 2003; Essex et al, 2009; Kalitsis et al, 2000; Logarinho et al, 2008; Lopes et al, 2005), but fission yeast cells lacking *bub3* are able to maintain checkpoint signaling despite defective kinetochore enrichment of Bub1 and Mad1, Mad2, and Mad3 (Tange & Niwa, 2008; Vanoosthuyse et al, 2009; Windecker et al, 2009). The molecular basis for this discrepancy is unclear, but at least for fission yeast, it has been proposed that Bub3 acts as an inhibitory chaperone that blocks Bub1 both at the kinetochore and in the nucleoplasm (Yamagishi et al, 2012). If Bub1 is released from its inhibition by Bub3 in *bub3Δ* or *bub1-Δ*GLEBS cells, Bub1 might be precociously activated, which could result in a faster and/or stronger checkpoint signal. In turn, abolished interaction between Bub1 and Bub3 might impede checkpoint inactivation if Bub1 remains active. Indeed, fission yeast Bub3 has been implicated in checkpoint silencing after transient mitotic arrest (Vanoosthuyse et al, 2009). Interestingly, the situation in fission yeast also shows that kinetochore enrichment of checkpoint components may not be a pre-requisite for checkpoint signaling.

Bub1 also harbors a kinase domain at its C-terminus. However, Bub1 kinase activity is not required for Bub1 kinetochore recruitment and only seems to play a minor role in checkpoint signaling. A kinase-dead version of Bub1 (Klebig et al, 2009; Sharp-Baker & Chen, 2001; Vanoosthuyse et al, 2004; Warren et al, 2002; Yamaguchi et al, 2003) or a Bub1 lacking the complete kinase domain (Klebig et al, 2009; Warren et al, 2002; Yamaguchi et al, 2003) still facilitates a mitotic arrest in cells with perturbed kinetochore-microtubule attachments. Whereas the kinase domain is dispensable for checkpoint signaling, a conserved region between the GLEBS motif and the kinase domain, termed the conserved motif I, has been shown to be essential for SAC function. In human cells (Klebig et al, 2009), budding yeast (Warren et al, 2002) and fission yeast (Nadine Schmidt, unpublished data), deletion of this motif abolishes checkpoint activity and impedes Mad1 recruitment, although Bub1 interaction with the kinetochore remained intact. It has therefore been suggested that Bub1 can directly interact with Mad1. *In vivo* studies in budding yeast determined a mitosis-specific Mad1-Bub1 complex by co-immunoprecipitation (Brady & Hardwick, 2000; Warren et al, 2002), potentially together with Bub3 (Brady & Hardwick, 2000). On the Mad1 side, a small, 3-amino-acid motif (RLK)

in the C-terminus of the protein has been shown to be required for interaction with Bub1 and Bub3 in budding yeast (Brady & Hardwick, 2000). It remains to be seen if this interaction is direct and conserved across species. However, even if the Bub1-Mad1 interaction was a common feature in SAC protein kinetochore recruitment, it is likely not the only pathway to regulate Mad1 localization to unattached kinetochores. Artificial recruitment of *S. pombe* Mph1 to kinetochores in interphase has been shown to co-recruit Bub1 and Bub3, but fails to co-recruit Mad1, suggesting additional mechanisms for regulating kinetochore association of Mad1 in mitosis (Ito et al, 2012).

Once at the kinetochore, Bub1 remains stably associated with a low turnover rate as shown by fluorescence recovery after photobleaching (FRAP) (Howell et al, 2004; Shah et al, 2004). Similar measurements have been performed for Bub3, but showed a much more rapid turnover (Howell et al, 2004). This is interesting, as it suggests that the Bub1-Bub3 interaction is dynamic and Bub3 potentially releases Bub1 at the kinetochore. How complex disassembly can be achieved without loosing the interaction with KNL1 and which additional checkpoint role(s) Bub3 might have is unknown.

1.6.1 Mad1 at the kinetochore

Mad1 and Mad2 are both recruited to unattached kinetochores and de-localize from kinetochores upon microtubule binding (Foley & Kapoor, 2013; Lara-Gonzalez et al, 2012). In interphase, Mad1 and Mad2 are re-localizing to the nuclear rim and interact with nuclear pores (Lara-Gonzalez et al, 2012). Mad1 is essential for SAC signaling as cells without Mad1 do not localize Mad2 to kinetochores and are deficient in arresting cells in a perturbed mitosis with defective kinetochore-microtubule attachments (Essex et al, 2009; Gillett et al, 2004; Heinrich et al, 2012; Luo et al, 2002; Martin-Lluesma et al, 2002). Conversely, cells with sustained Mad1 kinetochore localization co-recruit Mad2 and artificially arrest in a metaphase-like state despite correctly attached kinetochores (Maldonado & Kapoor, 2011). Mad1 has therefore been suggested to be the kinetochore receptor of Mad2 and kinetochore localization of the Mad1 is considered a crucial determinant of active checkpoint signaling (Figure 2–2). Mad1 is composed of a long N-terminal coiled-coil region, followed by the Mad2-interacting motif (MIM) and a C-terminal region. The N-terminus comprises almost 75% of the protein and has been shown to be required for Mad1 dimerization *in vitro* (Sironi et al, 2002). The Mad1 C-terminus consists of an alpha-helical, coiled-coil forming region followed by a globular ‘head’ domain containing beta-sheets and alpha-helices (Kim et al, 2012).

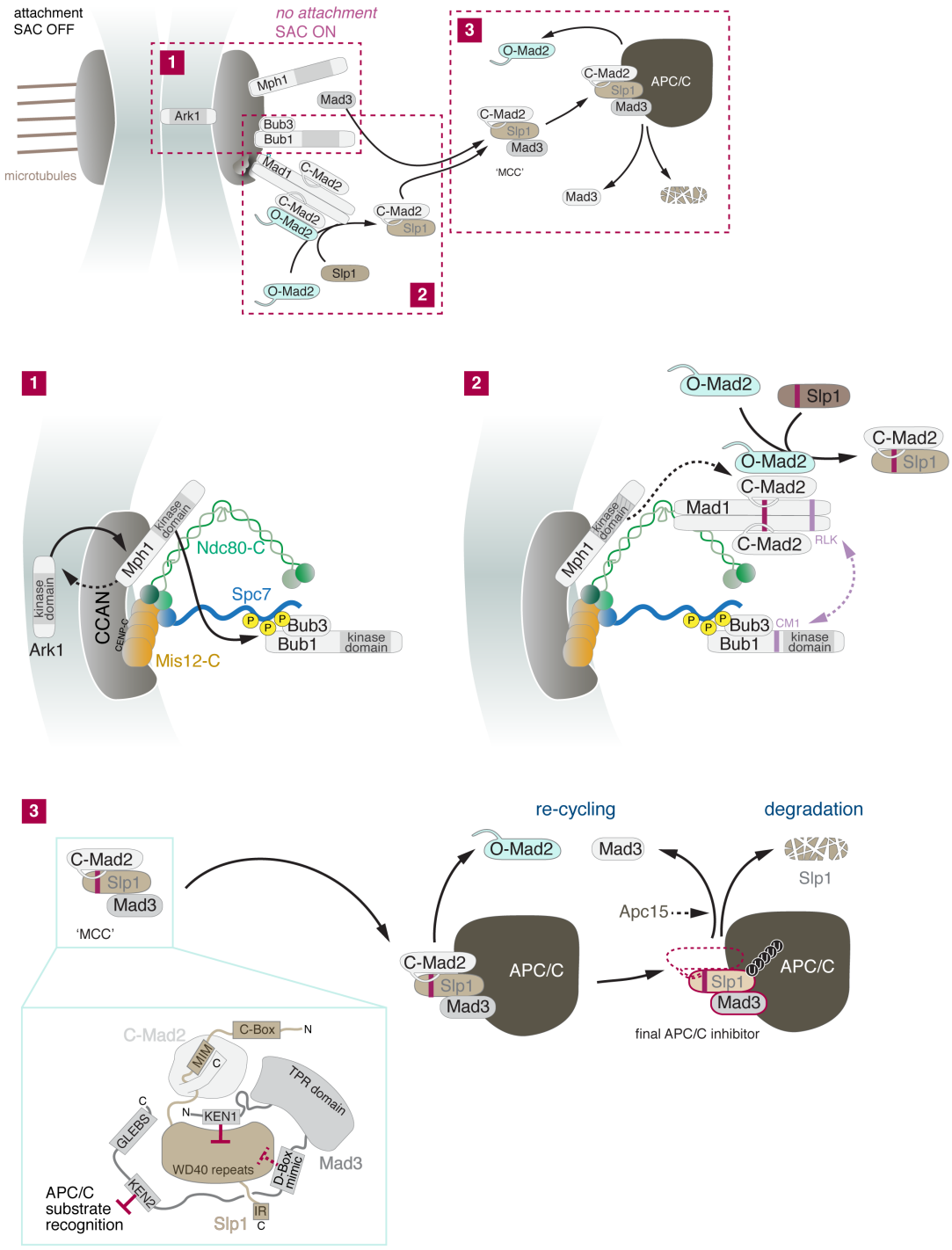

Figure 2 Spindle assembly checkpoint signaling

(adapted from Heinrich et al. 2012 and Foley and Kapoor 2012; see text for details)

The upper panel displays a general scheme of checkpoint signaling at the kinetochore and in the nucleoplasm triggered by kinetochores that are not attached to the mitotic spindle. Numbered insets show critical steps in checkpoint signaling:

(2–1) Kinetochore composition and recruitment of upstream checkpoint proteins

(2–2) Kinetochore recruitment of the Mad1–Mad2 complex and the 'Mad2 template model'

(2–3) MCC formation and APC/C inhibition

Solid lines indicate a direct modification (e.g. protein-protein interaction or phosphorylation); dashed lines show a connection between proteins that is indirect or where the exact type of interaction is unclear. The extension at O-/C-Mad2 displays the C-terminal 'safety belt' required for Mad1- or Slp1 interaction. The Mad2-binding motif (MIM) on both Mad1 and Slp1 is highlighted in pink.

'O-Mad2' = Mad2 in the open conformation; 'C-Mad2' = Mad2 in the closed conformation; 'P' = phosphorylation; 'U' = ubiquitin

Yeast two-hybrid analysis suggested an interaction of the N-terminus of human Mad1 with the kinetochore component Ndc80/Hec1 (Martin-Lluesma et al, 2002), which could be a mediator of Mad1 kinetochore recruitment. Findings in *X. laevis* also supported an involvement of the Mad1 N-terminus in kinetochore localization (Chung & Chen, 2002). However, the C-terminus has also been implicated in kinetochore targeting. The crystal structure by Kim et al. (2012) revealed a striking similarity to the structural arrangement of the Ndc80 complex components Spc24-Spc25, which serve as the contact point for kinetochore binding of the NDC80-C. The Mad1 C-terminus could therefore employ a similar binding mode to kinetochores. However, the authors could not attribute Mad1 kinetochore targeting to a single domain within Mad1 and rather favored the existence of multiple binding sites within Mad1 (Kim et al, 2012). In yeast, the mode of kinetochore recruitment seems to differ as the C-terminus instead of the N-terminus in both budding yeast (Kastenmayer et al, 2005; Scott et al, 2005) and fission yeast (Heinrich, Hauf et al., ms. submitted) is required for localization of Mad1 to kinetochores. The molecular basis for this inter-species difference is not understood.

1.6.2 The ‘Mad2 template model’

The ultimate target of the checkpoint is Cdc20, the co-activator of the APC/C. Mad2 has been found to bind Cdc20 and inhibit APC/C activity *in vitro* and *in vivo* (Fang et al, 1998; Hwang et al, 1998; Kim et al, 1998). Mad2-binding to Cdc20 is essential to facilitate checkpoint signaling, as Mad2 mutants unable to bind Cdc20 (De Antoni et al, 2005; Nezi et al, 2006; Sironi et al, 2001) as well as Cdc20 mutants lacking crucial residues for Mad2 interaction (Hwang et al, 1998; Kim et al, 1998) fail to establish a functional checkpoint. To understand the connection between Cdc20 inhibition and SAC signaling at the unattached kinetochore, a set of biochemical, cell biological and structural methods have been employed to dissect the individual signaling steps. The resulting model of molecular action has been termed the ‘Mad2 template model’ (De Antoni et al, 2005). The structural basis of this model is the drastic conformational change of Mad2 from an ‘open’ form (O-Mad2 or ‘N1’-Mad2) to a ‘closed’ form (C-Mad2 or ‘N2’-Mad2), thereby binding and sequestering Cdc20 (Luo et al, 2002; Luo et al, 2004; Sironi et al, 2002). To enable this conformational change, a kinetochore-bound complex of Mad1 and C-Mad2 provides a ‘template’ C-Mad2 for asymmetric dimerization with a free O-Mad2 molecule, which is then converted into its closed form bound to Cdc20 (De Antoni et al, 2005; DeAntoni et al, 2005; Mapelli et al, 2007) (Figure 2–2).

Mad1 and Cdc20 share a similar, short sequence motif, which enables them to interact with Mad2 in a mutually exclusive manner (Luo et al, 2002; Sironi et al, 2002). This C-terminal region of Mad2, also called the 'safety-belt', undergoes a strong conformational change when O-Mad2 transforms into C-Mad2 (Luo et al, 2002; Luo et al, 2004; Sironi et al, 2002) and in the process entraps either Mad1 or Cdc20. The Mad2-binding motif of Mad1 and Cdc20 has been shown to integrate into the beta-sheets of the Mad2 HORMA domain (Luo et al, 2002; Luo et al, 2004; Sironi et al, 2001) by also adopting a beta-sheet fold (Luo et al, 2002; Luo et al, 2004). This mode of binding can only be resolved by partial unfolding, and coincides with an exceptional stability of the Mad1:C-Mad2 complex (Chen et al, 1999; Sironi et al, 2001), which confers resistance to harsh treatments like 5 M NaCl, 2 M Guanidine or 2 M Urea for the budding yeast complex (Chen et al, 1999) and 4 M NaCl and 4 M Urea for the human complex (Sironi et al, 2001). The complex assembles with a 2:2 ratio as a hetero-tetramer *in vitro* (Sironi et al, 2002), an arrangement also suggested to form the functional Mad1:C-Mad2 species *in vivo* (Sironi et al, 2002). The Mad1:C-Mad2 complex can form independently of other checkpoint components (Chen et al, 1999), persists throughout the cell cycle (Brady & Hardwick, 2000; Chen et al, 1999).
A view on the dimerization between C-Mad2 and O-Mad2 was obtained by crystallography (Mapelli et al, 2007) and supports the asymmetric binding mode of two Mad2 molecules proposed by the 'template model'. The interaction has to be asymmetric, as neither O-Mad2-O-Mad2 interactions nor C-Mad2-C-Mad2 interactions are possible due to sterical clashes in the crystal structures (Mapelli et al, 2007) and based on *in vitro* binding experiments (DeAntoni et al, 2005). Although a structure between C-Mad2 and C-Mad2 has also been solved (Yang et al, 2008), the existence of this homotypic dimerization *in vivo* is put into question because the cells used by Yang et al. (2008) still seem to express the wild type copy of Mad2 in addition a constitutive closed form of Mad2 (Mad2-L13A), thereby potentially allowing C-Mad2:O-Mad2 formation. Mad2 dimerization requires two highly conserved residues, Arg133 and Gln134 (Arg126, Gln127 in *S. cerevisiae*), in the third alpha-helix of Mad2 (Mapelli et al, 2007). Single or double point mutants of these residues interfere with Mad2 dimerization *in vitro* (De Antoni et al, 2005; DeAntoni et al, 2005; Mapelli et al, 2007; Nezi et al, 2006) and *in vivo* (Nezi et al, 2006) and abolish checkpoint signaling (Nezi et al, 2006). As dimerization-deficient Mad2 is still able to undergo a conformational change from O-Mad2 to C-Mad2, the interaction with Mad1 is not affected *in vitro* and *in vivo* (Nezi et al, 2006; Sironi et al, 2001). *In vitro*, the Mad2 dimerization mutants are also able to bind Cdc20 (Nezi et al, 2006; Sironi et al, 2001), but with very slow kinetics (Simonetta et al, 2009; Sironi et al, 2001). *In vivo* studies could not

detect an interaction of dimerization-deficient Mad2 with Cdc20 (Nezi et al, 2006), which explains the checkpoint defect seen with these mutants and supports the view that Mad2 dimerization is essential to ensure rapid sequestration of Cdc20 by C-Mad2 at the kinetochore for effective SAC signaling. The C-Mad2:Cdc20 complex has also been suggested to provide a platform for free O-Mad2 and to serve as a 'template' for creating new C-Mad2:Cdc20 complexes away from the kinetochore, thereby amplifying the checkpoint signal. However, recent experiments do not support this notion as they show that the dimerization surface of Mad2 in the C-Mad2:Cdc20 complex away from kinetochores is blocked by Mad3 (Chao et al, 2012; Mariani et al, 2012). In human cells, Mps1 has been shown to influence O-Mad2 recruitment to the Mad1:C-Mad2 complex at kinetochores. Inhibition of Mps1 kinase activity only affected kinetochore localization of the dynamic O-Mad2 pool, but left the stably bound Mad1:C-Mad2 at kinetochores unaffected, suggesting that Mps1 activity is required for Mad2 dimerization at kinetochores (Hewitt et al, 2010).

To allow for O-Mad2 to bind to a stable Mad1:C-Mad2 complex, Mad2 has to be in excess over Mad1. As a prerequisite all Mad1 has to be bound by Mad2, which has been shown for human cells (Shah et al, 2004). A large-scale study in budding yeast found a 2-fold higher cellular abundance of Mad2 compared to Mad1 (Ghaemmaghami et al, 2003). Sucrose gradients of budding yeast cell extracts suggest a Mad1-bound and a Mad1-free pool of Mad2 (Chen et al, 1999). This finding has been supported by gel filtration analysis of mitotic cell extracts from *X. laevis* (Chung & Chen, 2002) and human cells (Fava et al, 2011). Co-immunoprecipitation assays in *X. laevis* extracts also indicate that only a fraction of Mad2 (ca. 20-40%) is in complex with Mad1 (Chen et al, 1998), resulting in a Mad1-free pool of Mad2. In addition, the dynamics of both Mad1 and Mad2 turnover at kinetochores in mitotically arrested cells have been measured using FRAP and shed light on the different Mad2 pools present at kinetochores (Howell et al, 2000; Howell et al, 2004; Shah et al, 2004; Vink et al, 2006). Mad1 is a very stable protein at the kinetochore, with ~ 70% of the kinetochore-bound pool showing no exchange with the cytoplasmic pool (Howell et al, 2004; Shah et al, 2004). Conversely, Mad2 turnover is faster and comprises 2 populations: one stably bound pool, which is approximately 50% of the total Mad2 at kinetochores and presumably corresponds to the Mad1:C-Mad2 complex, as well as an additional, dynamic pool that transiently localizes to kinetochores and likely represents the fraction of O-Mad2 being recruited to the Mad1:C-Mad2 complex (Howell et al, 2004; Shah et al, 2004; Vink et al, 2006). Anion exchange chromatography of pre-fractionated human cell extracts indicated that the Mad1-free, monomeric pool of Mad2 exists

exclusively in the O-Mad2 conformation both in interphase and mitosis (Luo et al, 2004), again consistent with the template model.

1.6.3 Formation of the mitotic checkpoint complex (MCC)

To block cells from prematurely progressing into anaphase, the presence of C-Mad2:Cdc20 is not sufficient as cells depleted of the checkpoint component Mad3/BubR1 fail to arrest in mitosis despite being able to form the C-Mad2:Cdc20 complex (Chen, 2002; Hardwick et al, 2000; Li et al, 2010; Nilsson et al, 2008). Hence, Mad3/BubR1 is an essential part of the SAC signaling cascade and acts downstream of Mad1 and Mad2. Both Mad3 and BubR1 contain two KEN boxes (KEN1 and KEN2; KEN standing for the amino acids Lys, Glu, Asn) that have been shown to be required for checkpoint activity (Burton & Solomon, 2007; King et al, 2007; Sczaniecka et al, 2008). However, only the first, N-terminal KEN box, KEN1, is required for MCC formation and binding to the APC/C (King et al, 2007; Lara-Gonzalez et al, 2011; Sczaniecka et al, 2008), while the second KEN box, KEN2, blocks substrate recruitment to the APC/C, potentially by interfering with binding of the Cdc20-bound substrate with the APC/C subunit Apc10 (Chao et al, 2012; Lara-Gonzalez et al, 2011). The region between the two KEN boxes folds into a TPR domain similar to Bub1 (D'Arcy et al, 2010), which has been shown to crystallize with KNL1 *in vitro* (Krenn et al, 2012) and to interact with the N-terminus of KNL1 in a yeast-two-hybrid assay (Kiyomitsu et al, 2011), suggesting a direct interaction with the kinetochore. In addition, both Mad3 and BubR1 contain a GLEBS motif for interaction with Bub3 (Larsen et al, 2007). This motif is truncated in *S. pombe* Mad3 and supposedly lacks the capability to interact with Bub3 (Sczaniecka et al, 2008). The difference between BubR1 and Mad3 arises from the presence or absence of an additional C-terminal kinase domain. Organisms like *S. cerevisiae* or *S. pombe* that lost the kinase domain express Mad3-like proteins, whereas organisms such as *D. melanogaster, X. laevis* or *H. sapiens* express BubR1-like proteins (Suijkerbuijk et al, 2012a). Both proteins, together with Bub1, share a common ancestor called Madbub, which contains both the KEN boxes for checkpoint signaling (as seen in Mad3 and BubR1) as well as a functional kinase domain (as seen in Bub1) (Suijkerbuijk et al, 2012a). The kinase domain in BubR1 has been shown to be a non-functional ‘pseudo-kinase’ due to several inactivating mutations (Suijkerbuijk et al, 2012a). Although the BubR1 kinase domain is inactive and does not contribute to checkpoint signaling, it has been shown to enhance protein stability (Lara-Gonzalez et al, 2011; Suijkerbuijk et al, 2012a; Suijkerbuijk et al, 2012b).

To ultimately block APC/C activity, the mitotic checkpoint complex (MCC) is assembled by binding of Mad3/BubR1 and Bub3 to the pre-formed C-Mad2:Cdc20 complex (Sudakin et al, 2001) (Figure 2–3). Mad2-Cdc20 interaction is a prerequisite for binding of Mad3/BubR1 to form the MCC (Kulukian et al, 2009; Nilsson et al, 2008; Sczaniecka et al, 2008). The MCC complex can form away from the kinetochore (Kulukian et al, 2009) and has been found to directly bind to cytosolic APC/C (Herzog et al, 2009), thereby blocking its activity (Figure 2–3). APC/C inhibition by the MCC has been shown to be more potent than by Mad2 alone (Fang, 2002; Kulukian et al, 2009; Sudakin et al, 2001). The MCC has been suggested to be a hetero-tetrameric complex with Mad3/BubR1, Bub3, C-Mad2 and Cdc20 present in a 1:1:1:1 ratio (Sudakin et al, 2001). However, the exact stoichiometry of the MCC is still under debate and different forms of the MCC might exist. Recent studies indicate that Mad2 is present in sub-stoichiometric amounts in the APC/C:MCC complex and may play a catalytic role (Han et al, 2013; Kulukian et al, 2009; Nilsson et al, 2008). Thus, the BubR1:Cdc20 complex has been proposed to be the final inhibitor of the APC/C (Han et al, 2013). The role of Bub3 in the MCC is unclear. Although Bub3 forms a complex with Mad3 (Fraschini et al, 2001; Hardwick et al, 2000; Larsen et al, 2007), neither *in vitro* nor *in vivo* studies could find a synergistic effect of Bub3 with Mad2 and/or Mad3/BubR1 in APC/C inhibition (Fang, 2002; Kulukian et al, 2009; Sczaniecka et al, 2008; Windecker et al, 2009). Fission yeast MCC, which only comprises C-Mad2, Cdc20 (Slp1 in *S. pombe*) and Mad3, but lacks Bub3 (Sczaniecka et al, 2008), has recently been crystallized (Chao et al, 2012). The crystal structure showed the interaction sites both between C-Mad2 and Cdc20 as well as Mad3 and Cdc20. C-Mad2 bound the N-terminus of Cdc20 in the expected manner. The interaction between Cdc20 and Mad3 is more complex. First, the Mad3 N-terminal KEN1 box required for MCC formation shows a direct interaction with both Mad2 and Cdc20 in the crystal structure. The Mad2–Mad3 interaction facilitates the optimal positioning of the Mad3 KEN1 box towards the KEN-box receptor on top of the WD40 propeller of Cdc20, underlining the necessity of Mad2 for Mad3-Cdc20 interaction and MCC formation (Chao et al, 2012; Tipton et al, 2011). The Mad2–Mad3 interaction also shields the Mad2 dimerization surface, which blocks O-Mad2 from accessing Cdc20-bound C-Mad2 and therefore presumably does not serve as a 'template' for further C-Mad2:Cdc20 sequestration (Mariani et al, 2012). Second, a region between the TPR repeats and the second KEN box, termed the 'D-box mimic', can directly interact with the WD40 repeats of Cdc20 in the crystal structure, thereby potentially blocking the D-box recognition site in Cdc20 required for substrate binding. This mode of action has been termed 'pseudo-substrate inhibition',

as BubR1 blocks access of the APC/C to its substrates by competing with these substrates for Cdc20 binding (Burton & Solomon, 2007). Third, when the MCC binds the APC/C, Cdc20 takes a different position than in the APC/C:Cdc20 complex. When Cdc20 acts as an activator, it positions opposite to the D-box co-receptor Apc10. However, within the MCC, Cdc20 is shifted away from Apc10, which will also hinder substrate binding to the APC/C (Chao et al, 2012; Lara-Gonzalez et al, 2011). In addition, the displacement of Cdc20 brings it closer to the catalytic center of the APC/C, which might allow the ubiquitination and subsequent proteolysis of Cdc20, thus turning the APC/C co-activator into an APC/C substrate. Indeed, Cdc20 abundance fluctuates during the cell cycle and the protein has been shown to be ubiquitinated and subsequently degraded both at exit from mitosis by the APC/C (Sullivan & Morgan, 2007) as well as in an MCC-dependent manner during an active checkpoint (Foster & Morgan, 2012; Mansfeld et al, 2011; Reddy et al, 2007; Uzunova et al, 2012). Degradation of Cdc20 counteracts Cdc20 synthesis in mitosis and reduces the amount of Cdc20 that needs to be inactivated by the checkpoint. Cdc20 ubiquitination also releases Mad2 and Mad3 from the APC/C, which is beneficial for inactivating the checkpoint if the upstream signaling is discontinued. When the MCC disassembles, Mad2 has to be actively converted from C-Mad2, the form it takes in the MCC, to O-Mad2, the prevalent form of unbound Mad2 in the cytoplasm (Fava et al, 2011; Luo et al, 2004). This conversion ensures that O-Mad2 remains available for Cdc20 binding. The molecular mechanism underlying the ‘re-cycling’ of Mad2 is currently unknown.

1.7 Checkpoint silencing

Once kinetochores have been properly attached to microtubules from the mitotic spindle, the checkpoint signal has to be quickly and robustly silenced. How the signal is turned off once the checkpoint has been satisfied is only partially understood. Checkpoint silencing mechanisms include protein delocalization from kinetochores, inhibitory protein-protein interactions, MCC disassembly and removal of mitosis-specific phosphorylations. Checkpoint protein delocalization from kinetochores in metaphase seems to be a necessary step in checkpoint inactivation as artificial tethering of Mps1 (Jelluma et al, 2010) or Mad1 (Maldonado & Kapoor, 2011) to bi-oriented chromosomes prolongs a checkpoint-dependent mitotic arrest after chromosomes have become attached. In addition, dynein-dependent delocalization of Mad1 and Mad2 from kinetochores to the

minus-ends of microtubules helps to antagonize checkpoint signaling (Howell et al, 2001), while additional dynein-independent (and potentially KMN-dependent) de-localization of Mad1 and Mad2 has been observed both in human cells and in fission yeast (Courtheoux et al, 2007; Gassmann et al, 2010).

Another inhibitory protein that counteracts the SAC is p31^{comet}. p31^{comet} blocks Mad2 dimerization as well as MCC formation through a mechanism called 'structural mimicry', in which p31^{comet} adopts a very similar fold as Mad2 and prevents binding of an O-Mad2 molecule to C-Mad2 by blocking the Mad2–Mad2 dimerization interface (Mapelli et al, 2006; Teichner et al, 2011; Westhorpe et al, 2011; Xia et al, 2004; Yang et al, 2007). p31^{comet} seems to act predominantly on the C-Mad2 in the MCC downstream of kinetochores, as O-Mad2 recruitment to Mad1:C-Mad2 complexes at kinetochores is unaffected in cells with reduced or increased p31^{comet} levels (Westhorpe et al, 2011). How these two C-Mad2 pools are distinguished by p31^{comet} is unknown. The p31^{comet}-dependent extraction of C-Mad2 from the MCC has also been suggested to aid in Mad2 re-cycling in an active checkpoint, potentially by supporting the transition from C-Mad2 to O-Mad2 (Westhorpe et al, 2011).

MCC disassembly is also important to silence the checkpoint (Mansfeld et al, 2011; Uzunova et al, 2012). Upon inactivation of the upstream SAC signal, APC/C-free MCCs are disassembled, which is followed by the disassembly of APC/C:MCC complexes (Ma & Poon, 2011). Both MCC disassembly and MCC extraction from the APC/C are ATP-dependent processes (Miniowitz-Shemtov et al, 2010; Teichner et al, 2011). Moreover, MCC-dependent Cdc20 ubiquitination by the APC/C aids efficient MCC disassembly during SAC silencing as it reduces the Cdc20 pool available for APC/C binding and re-cycles the other MCC components (Foster & Morgan, 2012; Mansfeld et al, 2011; Reddy et al, 2007; Uzunova et al, 2012). The turnover of MCC components at the APC/C depends on the APC/C subunit Apc15 (Mansfeld et al, 2011; Uzunova et al, 2012). The absence of Apc15 delays exit from mitosis in both human cells and budding yeast (Foster & Morgan, 2012; Mansfeld et al, 2011; Uzunova et al, 2012). In human cells depleted of Apc15, MCC components and ubiquitinated Cdc20 remain locked on the APC/C. This in turn prevents crucial substrate ubiquitination by the APC/C at the metaphase-to-anaphase transition once the SAC has been satisfied (Mansfeld et al, 2011; Uzunova et al, 2012). Both Cdc20 ubiquitination as well as p31^{comet}-dependent Mad2 inhibition have been shown to act redundantly in checkpoint silencing (Jia et al, 2011).

Another regulatory mechanism contributing to checkpoint silencing is the de-phosphorylation of kinase substrates by counteracting phosphatases such as PP1 (protein

phosphatase 1). PP1 inhibition delays mitotic exit (Pinsky et al, 2009; Vanoosthuyse & Hardwick, 2009) and PP1 recruitment to the N-terminus of KNL1 has been shown to be required for counteracting Aurora B function and facilitate checkpoint inactivation (Meadows et al, 2011; Rosenberg et al, 2011). This places KNL1 as a bridge between checkpoint activation (via Bub1) and checkpoint inactivation (via PP1), but how these two forces are balanced remains unclear.

The dynein-dependent Mad1-Mad2 stripping mechanism and the Mad2-interactor p31^{comet} are not conserved in yeast. However, SAC silencing mechanisms involving checkpoint protein delocalization from kinetochores, Apc15-dependent checkpoint inactivation through MCC disassembly and Cdc20 ubiquitination and kinase-counteracting phosphatases have also been found in yeast and might be the more general mechanism of checkpoint inactivation (Lara-Gonzalez et al, 2012).

1.8 Robustness and fragility of checkpoint signaling

For the checkpoint to work reliably, it has to respond to different numbers of unattached kinetochores and needs to tolerate stochastic fluctuations in checkpoint protein abundances, implying a dynamic and potentially quantitative nature of signaling. One single unattached kinetochore can delay the onset of anaphase for several hours (Rieder et al, 1994). In turn, if the last unattached kinetochore is removed by laser ablation, cells quickly exit mitosis (Rieder et al, 1995). Rieder et al. (1994) showed that one unattached kinetochore can delay mitotic exit to a similar extent as several unattached kinetochores, which suggested that the checkpoint creates an ‘all-or-none’ signal independently of the number of unattached kinetochores. Others have argued that the checkpoint signal is of quantitative nature (Kops et al, 2005). Indeed, a recent report challenged the view of an ‘all-or-none’ signal as they showed that APC/C activity gradually increases with progressing kinetochore attachment, arguing for a graded checkpoint response (Dick & Gerlich, 2013). In addition, cells treated with different types of microtubule drugs, which differentially affect microtubule formation and/or dynamics, activate the checkpoint to different extents. Cells arrested in nocodazole, which depolymerizes microtubules and therefore creates fully unattached kinetochores, can arrest for longer than cells arrested in taxol, which stabilizes microtubules and does not allow tension at the kinetochore necessary to silence the checkpoint (Andreassen & Margolis, 1994; Collin et al, 2013; Yang et al, 2009). The strength of the SAC signal correlates with the amount of MCC

formed, which is lower in taxol-treated cells and higher in nocodazole-treated cells (Collin et al, 2013; Westhorpe et al, 2011). In addition, checkpoint inactivation takes longer in nocodazole-treated cells compared to taxol-treated cells, potentially because it takes longer to disassemble larger amounts of MCC complexes (Collin et al, 2013). Partial inactivation of the checkpoint by specifically inhibiting the kinase activity of either Aurora B or Mps1 using small molecule inhibitors also resulted in a gradual decline of checkpoint activity (Saurin et al, 2011), further substantiating the quantitative nature of the checkpoint signal.

In addition to working reliably even if one or only a few kinetochores are unattached, the checkpoint needs to work robustly despite naturally occurring variations in protein abundance. Studies in budding yeast and mammalian cells report protein concentrations of a subset of checkpoint proteins determined from cell extracts, which are all in the low nanomolar range (Ghaemmaghami et al, 2003; Howell et al, 2000; Nilsson et al, 2008; Poddar et al, 2005). Low abundant proteins typically tend to be very 'noisy', i.e. their expression shows a high cell-to-cell variability (Bar-Even et al, 2006; Newman et al, 2006). It is unknown if this is also true for checkpoint proteins and if these naturally occurring fluctuations have any influence on the robustness of the checkpoint. Strong variations in checkpoint protein abundance can cause problems in checkpoint signaling. Mad1 over-expression can titrate out the pool of free Mad2 and causes a checkpoint defect (Chung & Chen, 2002). In turn, strong Mad2 overexpression causes a mitotic arrest (Chen et al, 1998; Essex et al, 2009; Fang et al, 1998; He et al, 1997; Kim et al, 1998; Rossio et al, 2010; Sotillo et al, 2007) and in *X. laevis* and *S. pombe* bypasses the requirement for Mad1 in SAC signaling, indicating that an overabundance of Mad2 triggers Mad2-Cdc20 formation independently of Mad1 (Chen et al, 1998; Millband & Hardwick, 2002). Mad1 was still necessary for a mitotic arrest induced by over-expression of Mad2 in budding yeast, *C. elegans* and human cells (Essex et al, 2009; Rossio et al, 2010; Sironi et al, 2001). However, if budding yeast Mad2 was artificially tethered to Cdc20, Mad1 was no longer necessary to maintain a checkpoint arrest (Lau & Murray, 2012). How effectively a Mad1 overexpression can counteract a Mad2 overexpression might therefore rely on the relative abundance of Mad1 to Mad2 and potentially the strength of the Mad2–Cdc20 interaction. Conversely, reducing the abundance of checkpoint components has been shown to negatively affect SAC signaling. Both Mad2 and BubR1 in human and murine systems are haploinsufficient, which means that expression from only one instead of two functional gene copies is not enough to retain checkpoint functionality. This leads to an increase in chromosome mis-segregation in both human cells and mouse

embryonic fibroblasts, and enhances tumor development in mice (Dai et al, 2004; Michel et al, 2001). For Mad2, expression from only one gene locus instead of two reduces the protein abundance to ~70% of the wild type (Michel et al, 2001). The reduction is even more drastic for BubR1, where only ~25% of the wild type protein amount can be detected (Dai et al, 2004). Conversely, BubR1 hypomorphic mice with slightly higher BubR1 abundance (29% or 42%) behave like wild type (Baker et al, 2004). In diploid budding yeast, heterozygote *mad2+/mad2Δ* cells expressing ~50 % of Mad2 compared to *mad2+/mad2+* cells show a slightly elevated chromosome loss rate, which can be rescued by concomitant reduction of Mad1 abundance, potentially by increasing the free pool of Mad2 not bound to Mad1 (Barnhart et al, 2011). This mirrors data from *X. laevis* where an change in the Mad1:Mad2 ratio towards Mad2 positively affects checkpoint signaling (Chung & Chen, 2002). For Bub1, only a very strong reduction to < 5 % of its wild type abundance has been shown to cause a checkpoint defect (Meraldi & Sorger, 2005), which could hint towards a catalytic rather than stoichiometric role of Bub1 in the checkpoint. Taken together, changes in the abundance of checkpoint proteins affect SAC signaling. How these changes relate to each other in terms of absolute molecule numbers and if this differs in different organisms is not understood.

Cells with an active SAC can arrest in mitosis for a long period of time, but eventually exit from mitosis despite continued SAC signaling from unattached kinetochores. This highly asynchronous process is called ‘mitotic slippage’. Mitotic slippage may occur in cancer cells that escape treatment with spindle drugs (Gascoigne & Taylor, 2008; Gascoigne & Taylor, 2009; Orth et al, 2008; Rieder & Maiato, 2004). Mitotic slippage in vertebrates has been attributed to a slow decrease of cyclin B abundance over time during a mitotic arrest (Brito & Rieder, 2006). It was suggested that cells could at some point reach a critical threshold for CDK activity and eventually slip out of mitosis if CDK activity is below this threshold. A recent study in budding yeast argued against a slow decline in cyclin B abundance. Single cell analysis of cyclin B abundance (Clb2 in *S. cerevisiae*) in cells that undergo mitotic slippage showed that cyclin B levels increase shortly before slippage and only then sharply decline (Vernieri et al, 2013). Therefore, it was suggested that, at least in budding yeast, the sudden activation of the APC/C rather than a ‘residual’ activity in arrested cells causes the metaphase-to-anaphase transition in cells that slip out of the checkpoint-mediated mitotic arrest.

1.9 Aim of this study

The spindle assembly checkpoint is a highly conserved, essential signaling pathway that ensures faithful genome inheritance during mitosis. Although substantial cell biological and biochemical data on individual checkpoint components exist, the complex *in vivo* signaling mechanism remains poorly understood. One crucial aspect that is not fully understood is the necessity of checkpoint component enrichment at unattached kinetochores as a qualitative criterion for checkpoint function. Kinetochore recruitment has been shown to be a hallmark of SAC signaling. Nevertheless, fission yeast *bub3Δ* cells fail to enrich Bub1, Mad1, Mad2 and Mad3 at kinetochores, but still exhibit wild type-like checkpoint activity, which questioned whether kinetochore recruitment is an essential prerequisite for checkpoint signaling. It remained unclear if cells lacking *bub3* were still able to localize the upstream checkpoint components Ark1 and Mph1 or if a checkpoint signal can be established with none of the checkpoint components enriching at kinetochores. I therefore wanted to dissect the hierarchical organization of checkpoint protein recruitment to kinetochores in *S. pombe* with a focus on the interdependencies of Ark1 and Mph1 for kinetochore localization as well as the requirement for Ark1 and Mph1 to be recruited to kinetochores in cells lacking *bub3*.

Another fragmentarily characterized aspect of SAC signaling is the connection between the Bub1–Bub3 complex and the downstream checkpoint components, especially Mad1. Co-immunoprecipitations have linked Mad1 and Bub1 *in vivo*, but a more detailed understanding of the connection is missing. To determine if the interaction is conserved across species, I introduced Bub1 and Mad1 mutations, which have been described to abolish the Bub1-Mad1 interaction in *S. cerevisiae*, into the fission yeast proteins. As the specific mutations in Mad1 lie in the structured C-terminus of the protein, which had not been characterized, I additionally wanted to dissect the role of the Mad1 C-terminus in checkpoint signaling.

Equally important for a functional checkpoint is its ability to always operate reliably, despite stochastic intracellular fluctuations and environmental perturbations. The extent and mechanisms of this robustness have not been studied. I therefore wanted to systematically probe checkpoint signaling *in vivo* in single cells after modulating checkpoint protein abundance and nutrient conditions in fission yeast. I planned to investigate whether these perturbations resulted in different patterns of checkpoint functionality for each SAC protein and correlated this with their respective functions. To be able to compare and interpret these patterns, I wanted to determine relative and absolute

abundances of SAC proteins, and to correlate both the abundance and cell-to-cell variability of fission yeast checkpoint proteins with their capability to ensure robust checkpoint signaling.

2 Results

2.1 Mph1 kinetochore localization is crucial and upstream in the hierarchy of spindle assembly checkpoint protein recruitment to kinetochores

Stephanie Heinrich[1], Hanna Windecker[1,2], Nicole Hustedt[1,3], Silke Hauf[1]

[1]Friedrich Miescher Laboratory of the Max Planck Society, 72076 Tübingen, Germany
[2]Present address: IMB (Institute of Molecular Biology), Ackermannweg 4, 55128 Mainz, Germany
[3]Present address: Friedrich Miescher Institute, Maulbeerstrasse 66, CH-4058 Basel, Switzerland

Correspondence: silke.hauf@tuebingen.mpg.de

Published in **Journal of Cell Science**, Volume 125, p.4720–4727 (2012)
DOI: 10.1242/jcs.110387

Author contributions:

I carried out strain construction, live-cell imaging and data analysis of experiments shown in Fig. 1E – H; Fig. 2A,D; Fig. 3A – D (except for the immunoblot in Fig. 3B); Fig. S1B,C; Fig. S2, Fig. S3; Fig. S5A – E; Fig. S6A – E,G; Fig. S7A – E; Fig. S8A – E; Fig. S9A – E. I analysed the data from imaging experiments shown in Fig. 3E, Fig. 4B,C, Fig. S10 and assembled information on kinetochore localization dependencies in the different model organisms (Fig. 4A, Fig. S11). In addition, I contributed to writing the manuscript together with Silke Hauf and input by Hanna Windecker and Nicole Hustedt.

Hanna Windecker performed experiments and analysed the data shown in Fig. 1B – D; Fig. 2B,C; Fig. S1A, and she performed the imaging experiments shown in Fig. 3E, Fig. 4B,C, Fig. S10.

Nicole Hustedt performed the immunoblotting experiment shown in Fig. 3B, and experiments shown in Fig. S1D; Fig. S5F,G; Fig. S6F; Fig. S7F,G; Fig. S8F; Fig. S9F.

Silke Hauf supervised the study. She performed experiments shown in Fig. S4 and analysed all GFP signal intensities in mitotically arrested cells using the *nda3-KM311* mutant.

Mph1 kinetochore localization is crucial and upstream in the hierarchy of spindle assembly checkpoint protein recruitment to kinetochores

Stephanie Heinrich[1], Hanna Windecker[1,2], Nicole Hustedt[1,3] and Silke Hauf[1,*]

[1]Friedrich Miescher Laboratory of the Max Planck Society, Spemannstrasse 39, D-72076 Tuebingen, Germany
[2]Present address: Septomics Research Centre, Albert-Einstein-Strasse 10, D-07745 Jena, Germany
[3]Present address: Friedrich Miescher Institute, Maulbeerstrasse 66, CH-4058 Basel, Switzerland
*Author for correspondence (silke.hauf@tuebingen.mpg.de)

Accepted 7 June 2012
Journal of Cell Science 125, 4720–4727

doi: 10.1242/jcs.110387

Summary

The spindle assembly checkpoint (SAC) blocks entry into anaphase until all chromosomes have stably attached to the mitotic spindle through their kinetochores. The checkpoint signal originates from unattached kinetochores, where there is an enrichment of SAC proteins. Whether the enrichment of all SAC proteins is crucial for SAC signaling is unclear. Here, we provide evidence that, in fission yeast, recruitment of the kinase Mph1 is of vital importance for a stable SAC arrest. An Mph1 mutant that eliminates kinetochore enrichment abolishes SAC signaling, whereas forced recruitment of this mutant to kinetochores restores SAC signaling. In *bub3Δ* cells, the SAC is functional when only Mph1 and the Aurora kinase Ark1, but no other SAC proteins, are enriched at kinetochores. We analyzed the network of dependencies for SAC protein localization to kinetochores and identify a three-layered hierarchy with Ark1 and Mph1 on top, Bub1 and Bub3 in the middle, and Mad3 as well as the Mad1–Mad2 complex at the lower end of the hierarchy. If Mph1 is artificially recruited to kinetochores, Ark1 becomes dispensable for SAC activity. Our results highlight the crucial role of Mph1 at kinetochores and suggest that the Mad1–Mad2 complex does not necessarily need to be enriched at kinetochores for functional SAC signaling.

Key words: Mph1, Mitosis, Spindle assembly checkpoint, Kinetochore

Introduction

During cell division, chromosomes are segregated to the two daughter cells by microtubules of the mitotic spindle (Walczak et al., 2010). The spindle assembly checkpoint (SAC; also called mitotic checkpoint) is a signaling pathway that surveys chromosome attachment to the spindle and prevents anaphase as long as any of the chromosomes remains unattached (Musacchio and Salmon, 2007). The conserved SAC signaling network comprises the proteins Mps1 (Mph1 in fission yeast), Mad1, Mad2, Mad3 (BubR1 in some organisms), Bub1, and Bub3 (Musacchio and Salmon, 2007). In addition, the Aurora B kinase (Ark1 in fission yeast) is required for a functional SAC (Kallio et al., 2002; Petersen and Hagan, 2003; Maldonado and Kapoor, 2011; Santaguida et al., 2011; Saurin et al., 2011). The SAC prevents anaphase by inhibiting the activity of the anaphase-promoting complex or cyclosome (APC/C) (Peters, 2006) through binding of Mad2 and Mad3 to the APC/C-activator Cdc20 (Slp1 in fission yeast). The checkpoint signal originates from unattached kinetochores (Rieder et al., 1995) and functional kinetochores are essential for the production of a SAC signal (Fraschini et al., 2001; Gardner et al., 2001; Nabetani et al., 2001; McCleland et al., 2003; Meraldi et al., 2004). Most SAC proteins are enriched at unattached kinetochores (Musacchio and Hardwick, 2002; Burke and Stukenberg, 2008), but how they are recruited and whether the enrichment of all SAC proteins at unattached kinetochores is required for SAC signaling is largely unclear.

The dependencies among SAC proteins for their recruitment to kinetochores may reveal which proteins respond directly to the attachment state of the kinetochore. However, the available information is incomplete and often controversial, possibly as a result of varying degrees of protein depletion or inhibition in different experiments (Meraldi et al., 2004). We analyzed the network of kinetochore recruitment dependencies in the genetically amenable unicellular eukaryote *Schizosaccharomyces pombe*, where SAC genes can be entirely deleted to study the functional consequences. We find a hierarchical organization with the Aurora kinase Ark1 and the kinase Mph1 on top, and Mad2 at the bottom. Kinetochore enrichment of Mph1 is vital for SAC signaling and for kinetochore enrichment of other SAC proteins. Recruiting Mph1 to kinetochores seems the only crucial function of Ark1 in SAC signaling. In *bub3*-deleted fission yeast cells, SAC signaling is functional with Ark1 and Mph1 being the only SAC proteins that are visibly enriched at kinetochores. This demonstrates the central importance of Aurora and Mph1 as upstream factors at the kinetochore and suggests that activation of Mad2, which is ultimately required for inhibition of the APC/C, can happen away from kinetochores.

Results and Discussion

N-terminal truncation of Mph1 abolishes kinetochore enrichment and SAC signaling

It has been proposed that kinetochore localization of the SAC kinase Mps1 is essential for SAC signaling in vertebrates (Liu et al., 2003; Zhao and Chen, 2006; Hached et al., 2011), but more recent results have challenged this view (Maciejowski et al., 2010). To assess the importance of fission yeast Mph1 localization to

unattached kinetochores, we truncated the Mph1 protein N-terminally, leaving the kinase domain intact (Fig. 1A). Expression of the truncated versions from the endogenous locus resulted in protein abundance similar to wild type Mph1 (Fig. 1B). The shorter truncation (Mph1-Δ1-150) maintained kinetochore localization and SAC signaling, whereas the longer truncation

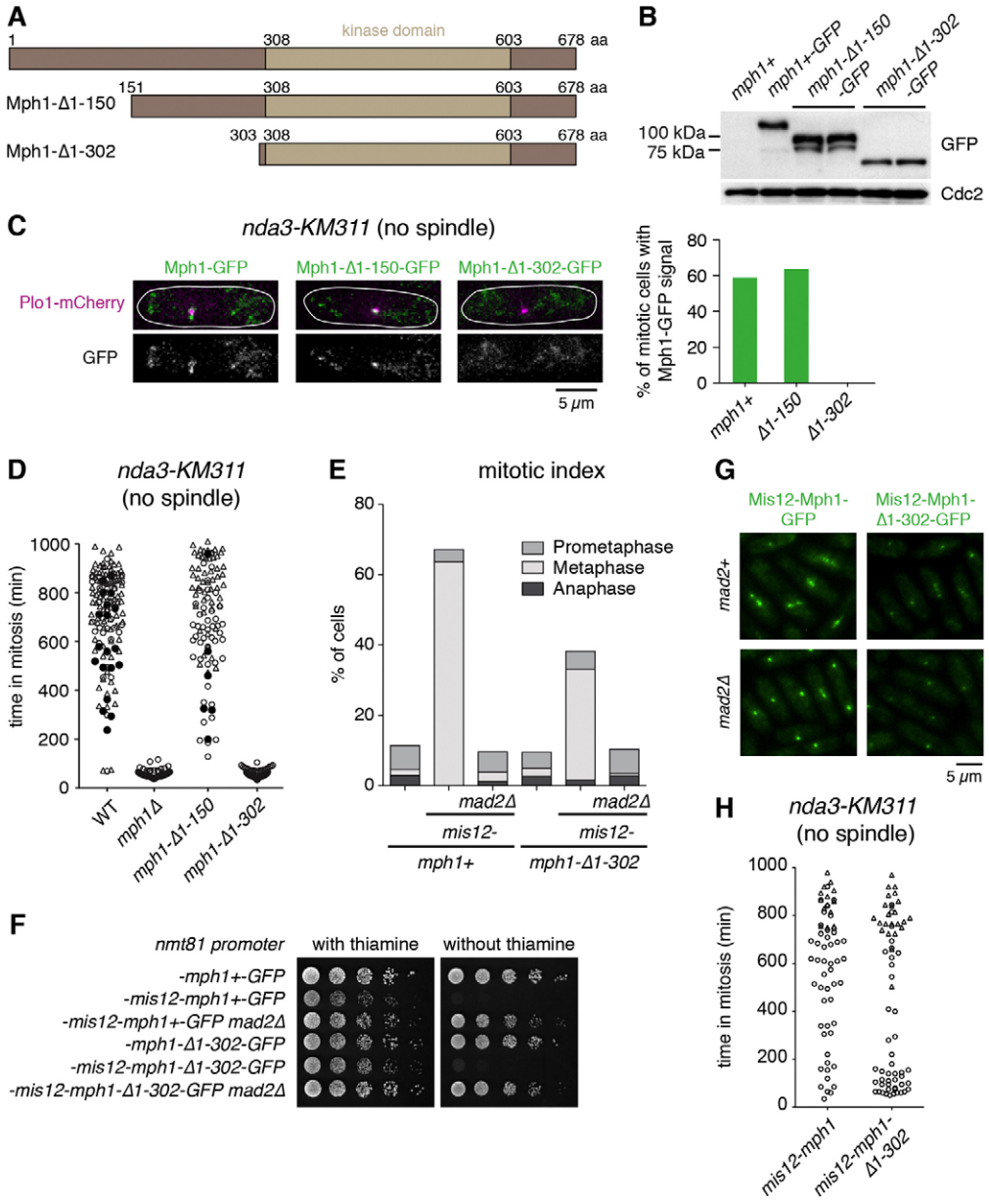

Fig. 1. Mph1 localization to kinetochores is required for SAC activity. (**A**) Schematic of the N-terminal Mph1 truncations. (**B**) Extracts from asynchronous cultures of the indicated strains were analyzed by immunoblotting. Cdc2 serves as a loading control. (**C**) Cells expressing *nda3-KM311*, *plo1+–mCherry* and the indicated *mph1* alleles were followed by live-cell imaging at the restrictive temperature for *nda3-KM311* (Hiraoka et al., 1984), which prevents microtubule formation. Plo1 localization at spindle pole bodies (SPBs) was used as a marker for mitotic cells (Mulvihill et al., 1999). Representative cells and the percentage of mitotic cells with localized Mph1 signal are shown (n>30 cells). (**D**) Cells were followed by live-cell imaging at the restrictive temperature for *nda3-KM311*. The duration of prometaphase was determined by the presence of Plo1–mCherry at SPBs. Circles indicate cells in which the entire mitosis was recorded, triangles indicate cells in which entry into mitosis but not exit from mitosis was recorded, filled circles indicate cells that died in mitosis. (**E**) Expression of the indicated Mph1 constructs from the thiamine-regulatable *nmt81* promoter (Basi et al., 1993) was induced by the depletion of thiamine. Mitotic cells were identified by the presence of Plo1–mCherry at SPBs and classified according to spindle length: <2 μm, prometaphase; between 2 and 2.5 μm, metaphase; >2.5 μm, anaphase; n>200 cells. (**F**) Serial dilutions of the strains used in E were grown on rich medium (with thiamine, *nmt81* promoter repressed) or minimal medium lacking thiamine (without thiamine, *nmt81* promoter induced). (**G**) Representative cells from the experiment shown in E. GFP signals were recorded under identical conditions. (**H**) The indicated *mis12–mph1* fusions were weakly expressed from the thiamine-repressible *nmt81* promoter and cells were followed by live-cell imaging at the restrictive temperature for *nda3-KM311*. The duration of prometaphase was determined by the presence of Plo1–mCherry at SPBs. Symbols are as in D.

(Mph1-Δ1-302) abolished both kinetochore localization and SAC signaling (Fig. 1C,D), suggesting that kinetochore localization is crucial for SAC activity.

To determine whether the SAC defect resulted from impaired kinetochore localization or whether the Mph1-Δ1-302 protein was generally dysfunctional, we artificially recruited the truncated protein to kinetochores by fusion to the kinetochore protein Mis12. Forced recruitment of wild-type Mph1 to kinetochores lead to a pronounced delay in mitosis and a growth defect (Fig. 1E,F), as has been seen before (Ito et al., 2012). The phenotypes were rescued by deletion of *mad2*, which indicates that forced recruitment of Mph1 artificially promoted SAC signaling and that the fusion to Mis12 did not impair kinetochore function. Forced recruitment of Mph1-Δ1-302 mimicked those of wild-type Mph1 (Fig. 1E,F). The slightly weaker phenotype when recruiting Mph1-Δ1-302 can be explained by the reduced presence of this protein at kinetochores compared to wild-type Mph1 (Fig. 1G). When both fusion proteins were expressed at very low levels, they were both able to support a mitotic delay in response to microtubule depolymerisation (Fig. 1H). These data indicate that Mph1-Δ1-302 retains the ability for SAC signaling and that the SAC failure in *mph1-Δ1-302* cells is a consequence of eliminating kinetochore enrichment of Mph1. Hence, kinetochore enrichment of Mph1 is a crucial prerequisite for SAC signaling in fission yeast.

Enrichment of Mph1 at unattached kinetochores in *bub3Δ* cells is necessary for SAC signaling

Others and we previously reported that the SAC is functional in *bub3*-deleted fission yeast cells despite the failure of these cells to enrich Mad1, Mad2, Mad3, and Bub1 at unattached kinetochores (Millband and Hardwick, 2002; Vanoosthuyse et al., 2009; Windecker et al., 2009). Since the kinetochore localization of Mph1 seems obligatory for SAC signaling (Fig. 1), we analyzed whether the enrichment of this SAC protein at kinetochores is

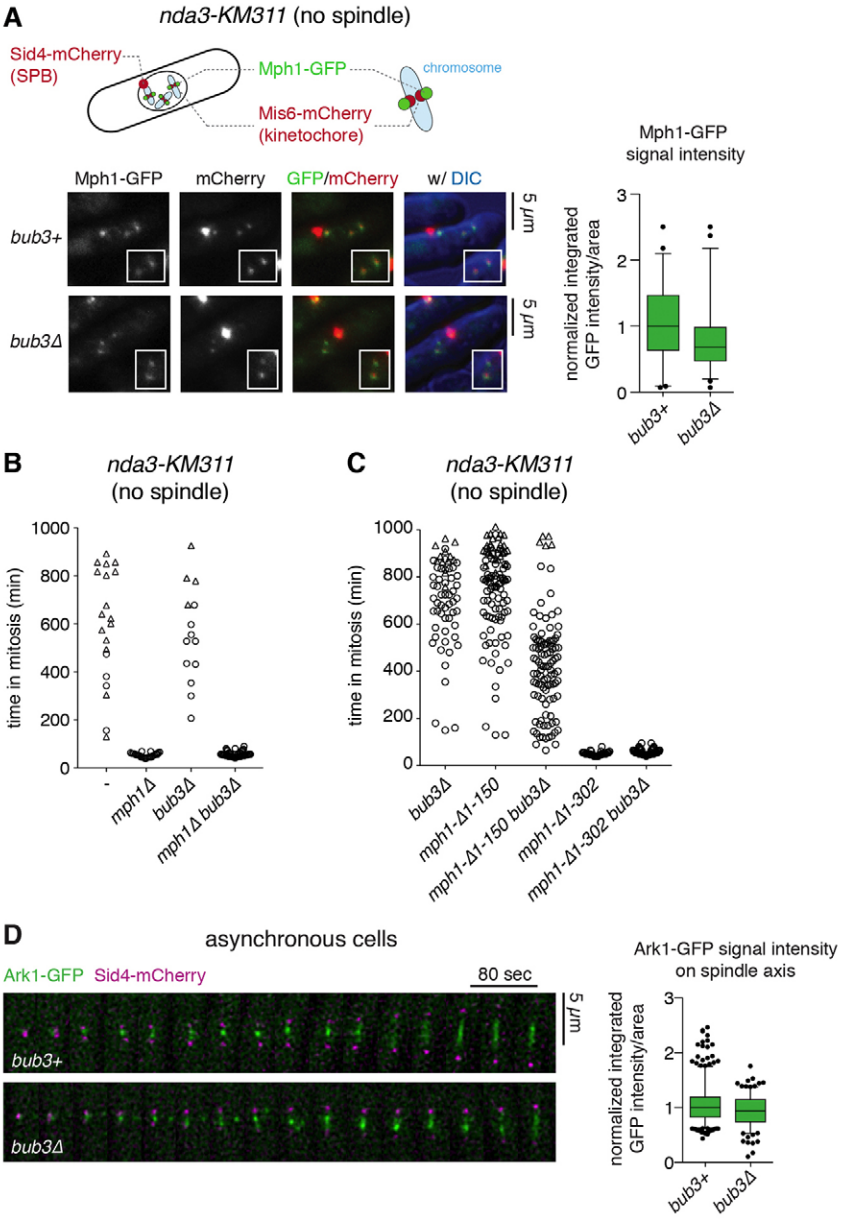

Fig. 2. Mph1 localization to kinetochores is required for SAC activity in *bub3Δ* cells. (**A**) Cells expressing the indicated markers were grown at the restrictive temperature for *nda3-KM311* and fixed with methanol. Insets are 1.4-times magnified relative to the main picture. DIC, differential interference contrast. Mph1–GFP signal intensity was quantified (n>48 cells; box plot with whiskers from 5th to 95th percentile; data normalized to median of *bub3+* cells). (**B**,**C**) The indicated strains were followed by live-cell imaging at the restrictive temperature for *nda3-KM311*. The duration of prometaphase was determined by the presence of Plo1–GFP at SPBs. Circles indicate cells in which the entire mitosis was recorded, triangles indicate cells in which entry into mitosis but not exit from mitosis was recorded. (**D**) Cells were followed by live-cell imaging with Sid4–mCherry as an SPB marker. Representative kymographs of the spindle region throughout mitosis are shown. The total signal intensity of Ark1–GFP on the spindle axis was determined for several time points in early mitosis (n>17 cells; box plot and normalization as in A).

preserved in *bub3Δ* cells. Indeed, Mph1 localizes to unattached kinetochores in *bub3Δ* cells (Fig. 2A). The intensity of Mph1 at unattached kinetochores (Fig. 2A) and the fraction of cells, in which a signal could be detected (supplementary material Fig. S1), were similar between *bub3+* and *bub3Δ* cells, as was the total abundance of Mph1 (supplementary material Fig. S1). Deletion of *mph1* abolished the SAC-mediated delay in *bub3Δ* cells (Fig. 2B), confirming that Mph1 is needed in *bub3Δ* cells to generate the SAC signal. To test whether localization of Mph1 to kinetochores is required, we combined deletion of *bub3* with the Mph1 N-terminal truncations. In the presence of Mph1-Δ1-150, the SAC was still functional in *bub3Δ* cells, although the mitotic delay was shorter than in *mph1-Δ1-150* or *bub3Δ* cells (Fig. 2C). In the presence of Mph1-Δ1-302, the SAC response in *bub3Δ* cells was abrogated (Fig. 2C), demonstrating that recruitment of Mph1 to kinetochores is necessary for SAC function in *bub3Δ* cells. This raises the possibility that activation of Mph1 at unattached kinetochores in *bub3Δ* cells is sufficient to transmit the SAC signal to the nucleoplasm and challenges the idea that the enrichment of the Mad1–Mad2 complex at kinetochores is crucial (Kulukian et al., 2009).

A localization feedback loop between Ark1 and Mph1

In addition to preserving the localization of Mph1 (Fig. 2A), *bub3Δ* cells largely preserve localization of the Aurora kinase Ark1 (Fig. 2D; supplementary material Fig. S2). Hence, Ark1 and Mph1 are the only SAC proteins that still display enrichment at the centromere/kinetochore region in *bub3Δ* cells. Whereas in budding yeast Aurora (Ipl1) and Mps1 seem to localize independently (Maure et al., 2007), metazoan Mps1 localization to kinetochores has been shown to depend on Aurora B kinase activity (Vigneron et al., 2004; Santaguida et al., 2010; Saurin et al., 2011). We find that kinetochore localization of fission yeast Mph1 crucially depends on Ark1 kinase activity (Fig. 3A,B). When proper chromosome attachment was prevented by a conditional mutation in kinesin-5 (*cut7-446*), Mph1 localized to kinetochores, but the enrichment was abrogated by chemical genetic inhibition of Ark1 with the small molecule 1NM-PP1 (Fig. 3A). When we inhibited Ark1 in mitotic cells lacking microtubules, the localized Mph1 signals largely disappeared within 5 minutes of Ark1 inhibition (Fig. 3B), although the mitosis-specific slower migration of Mph1–GFP in SDS-PAGE was preserved and cells maintained high CDK1 activity, as indicated by the continued presence of Plo1 at SPBs (Fig. 3B) (Dischinger et al., 2008). The loss of Mph1 from kinetochores cannot be attributed to side effects of the inhibitor (supplementary material Figs S1, S3). Together this suggests that Ark1 is directly and continuously required to maintain Mph1 localization to kinetochores. When Mph1 was artificially recruited to the kinetochore, inhibition of Ark1 did not shorten the mitotic delay in the absence of microtubules (Fig. 3C; supplementary material Fig. S4). In agreement with data from human cells (Jelluma et al., 2010), this suggests that localization of Mph1 may be the only crucial function of Ark1 in the SAC.

In contrast to the pronounced effect of Ark1 on Mph1 localization, Mph1 is only partially and largely indirectly required for localizing Ark1 (Fig. 3D,E; supplementary material Fig. S2). Ark1 concentration at centromeres is slightly reduced by deletion of *mph1* both in an otherwise unperturbed mitosis (Fig. 3D) and when microtubule formation was prevented (Fig. 3E; supplementary material Fig. S2). Mph1 is required for the kinetochore localization of Bub1 (Vanoosthuyse et al., 2004) (supplementary material Fig. S5) and Bub1 is known to aid efficient recruitment of Ark1 to centromeres through phosphorylation of histone H2A-S121 (Kawashima et al., 2007; Kawashima et al., 2010; Tsukahara et al., 2010). This suggests that Mph1 is indirectly required for Ark1 localization through promoting the kinetochore enrichment of Bub1. Indeed, deletion of *bub3*, which also abrogates the kinetochore enrichment of Bub1 (Vanoosthuyse et al., 2004), leads to a similar defect in Ark1 localization as deletion of *mph1* (supplementary material Fig. S2). No further enhancement is seen in the *mph1Δ bub3Δ* double deletion (supplementary material Fig. S2), indicating that Mph1 and Bub3 act in the same pathway. Deletion of *bub1* impairs Ark1 localization more strongly than deletion of *mph1* or *bub3* (supplementary material Fig. S2), suggesting that Bub1 partially promotes Ark1 localization even when delocalized. Additional deletion of *mph1* in *bub1Δ* cells further diminishes Ark1 centromere localization slightly, suggesting that Mph1 may also promote Ark1 localization independently of Bub1, but this effect is weak (supplementary material Fig. S2). Taken together, these results suggest that Ark1 is required for the kinetochore localization of Mph1, and recruitment of Mph1 reinforces localization of Ark1 to centromeres, presumably through localization of Bub1 and enhanced centromeric H2A-S121 phosphorylation. In *bub3Δ* cells, this feedback loop is broken, but some Ark1 still localizes to centromeres and is sufficient to recruit Mph1 to unattached kinetochores (Fig. 2).

The network of SAC protein localization dependencies

The preserved localization of Ark1 and Mph1 in *bub3Δ* cells indicates that these two proteins can be recruited independently of all other SAC proteins and are on top of the kinetochore localization hierarchy. Indeed, Ark1 and Mph1 are fully or partially required for the kinetochore enrichment of all other SAC proteins (Fig. 4A; supplementary material Figs S5–S10). For Mph1, its kinetochore localization is important, because recruitment of Bub1, Mad1 (Fig. 4B,C) and Ark1 (supplementary material Fig. S10) is equally defective upon deletion of *mph1* or expression of *mph1-Δ1-302*.

We systematically analyzed the kinetochore localization dependencies for all other SAC proteins and find that Bub1 and Bub3, which depend on each other for their kinetochore enrichment, form the second layer of the hierarchy (Fig. 4A). Deletion of *bub1* or *bub3* abolishes kinetochore enrichment of Mad1, Mad2, and Mad3 (supplementary material Figs S7, S8) (Millband and Hardwick, 2002; Windecker et al., 2009), but deletion of *bub3* leaves localization of Mph1 and Ark1 largely intact (Fig. 2; supplementary material Figs S1, S2). In the third layer of the hierarchy, Mad3 has a very slight effect on the localization of Mad1 and Mad2 (supplementary material Figs S7, S8), whereas neither deletion of *mad1* nor *mad2* affects the localization of Mad3 (supplementary material Fig. S9) (Millband and Hardwick, 2002). Kinetochore enrichment of Mad2 depends on Mad1, but not vice versa (supplementary material Figs S7, S8), putting Mad2 lowest in the kinetochore localization hierarchy.

Although the data on SAC protein kinetochore localization dependencies from other organisms are fragmentary and sometimes contradictory (supplementary material Fig. S11), the principal hierarchy seems conserved. Vertebrate Aurora B is

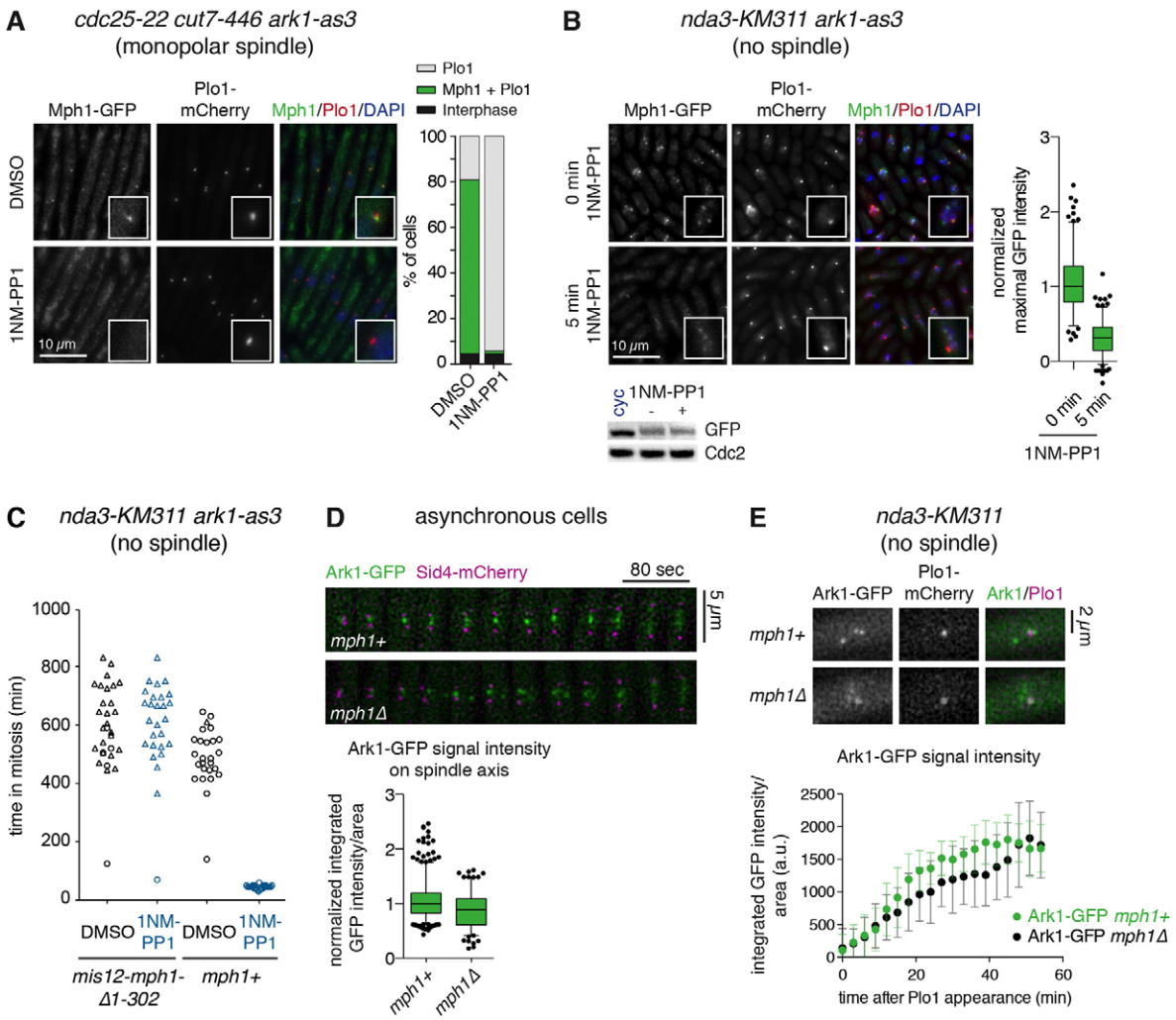

Fig. 3. Interdependent kinetochore localization of Mph1 and Ark1. (**A**) Cells were arrested in late G2 using the conditional *cdc25-22* mutation (Moreno et al., 1989) and released into mitosis in the presence of 5 μM of the Ark1-as3 inhibitor 1NM-PP1 (Hauf et al., 2007) or an equivalent amount of the solvent DMSO. The *cut7-446* allele leads to monopolar spindles (Hagan and Yanagida, 1990). Mitotic cells were fixed with methanol, and DNA was stained with DAPI. Insets are 2.5-times magnified relative to the main picture. The presence of a localized Plo1 signal indicates that cells are in mitosis. The percentage of cells with Plo1 and Mph1 signal was determined (n>100 cells). (**B**) Cells were grown at the restrictive temperature for *nda3-KM311*, treated with 1NM-PP1 and fixed with methanol after 0 min and 5 min. DNA was stained with DAPI. Insets are 2.5-times magnified relative to the main picture. Maximal Mph1–GFP signal intensity in mitotic cells was quantified (n>170 cells, box plot with whiskers from 5th to 95th percentile; data normalized to median of cells treated for 0 min). Protein abundance of Mph1–GFP in cycling cells (cyc) and mitotically arrested cells treated with (+) or without (−) 1NM-PP1 was determined by immunoblotting using anti-GFP and anti-Cdc2 (loading control) antibodies. (**C**) Cells expressing *ark1-as3* and *mph1+* or the *mis12-mph1-Δ1-302* fusion construct were followed by live-cell imaging at the restrictive temperature for *nda3-KM311* in the presence of 10 μM of the Ark1-as3 inhibitor 1NM-PP1 or an equivalent amount of the solvent DMSO. The duration of prometaphase was determined by the presence of Plo1–mCherry at SPBs. Symbols are as in Fig. 2B. (**D**) Cells were followed by live-cell imaging with Sid4–mCherry as the SPB marker. Representative kymographs of the spindle region are shown. The total signal intensity of Ark1–GFP on the spindle axis was determined for several time points in early mitosis (n>12 cells; box plot as in B; data normalized to median of *mph1+* cells). (**E**) Cells were followed by live-cell imaging at the restrictive temperature for *nda3-KM311*. Representative cells in early mitosis are shown. The Ark1–GFP signal was measured over time as cells entered mitosis (n>23 cells; ±s.d.).

required for efficient localization of Mps1 (Vigneron et al., 2004; Santaguida et al., 2010; Saurin et al., 2011), and Aurora B and Mps1 are required for the localization of other SAC proteins. In all organisms examined, Bub1 is upstream of Mad1 and Mad2 (Sharp-Baker and Chen, 2001; Gillett et al., 2004; Meraldi et al., 2004; Essex et al., 2009). Most variable in the hierarchy are Mad3 and BubR1, which coincides with the stronger evolutionary divergence compared to other SAC proteins (Musacchio and Salmon, 2007).

Our experiments and published results now suggest a general model for SAC protein recruitment to the kinetochore (Fig. 4D–F). Ark1 (Aurora B), whose localization to centromeres is largely independent of other SAC proteins, is the most upstream component. Aurora B phosphorylates kinetochore proteins dependent on the chromosome attachment state (Liu et al., 2009), which may provide a binding platform for the Mph1 (Mps1) kinase. Mph1 (Mps1) can then recruit additional SAC proteins through phosphorylation of kinetochore components

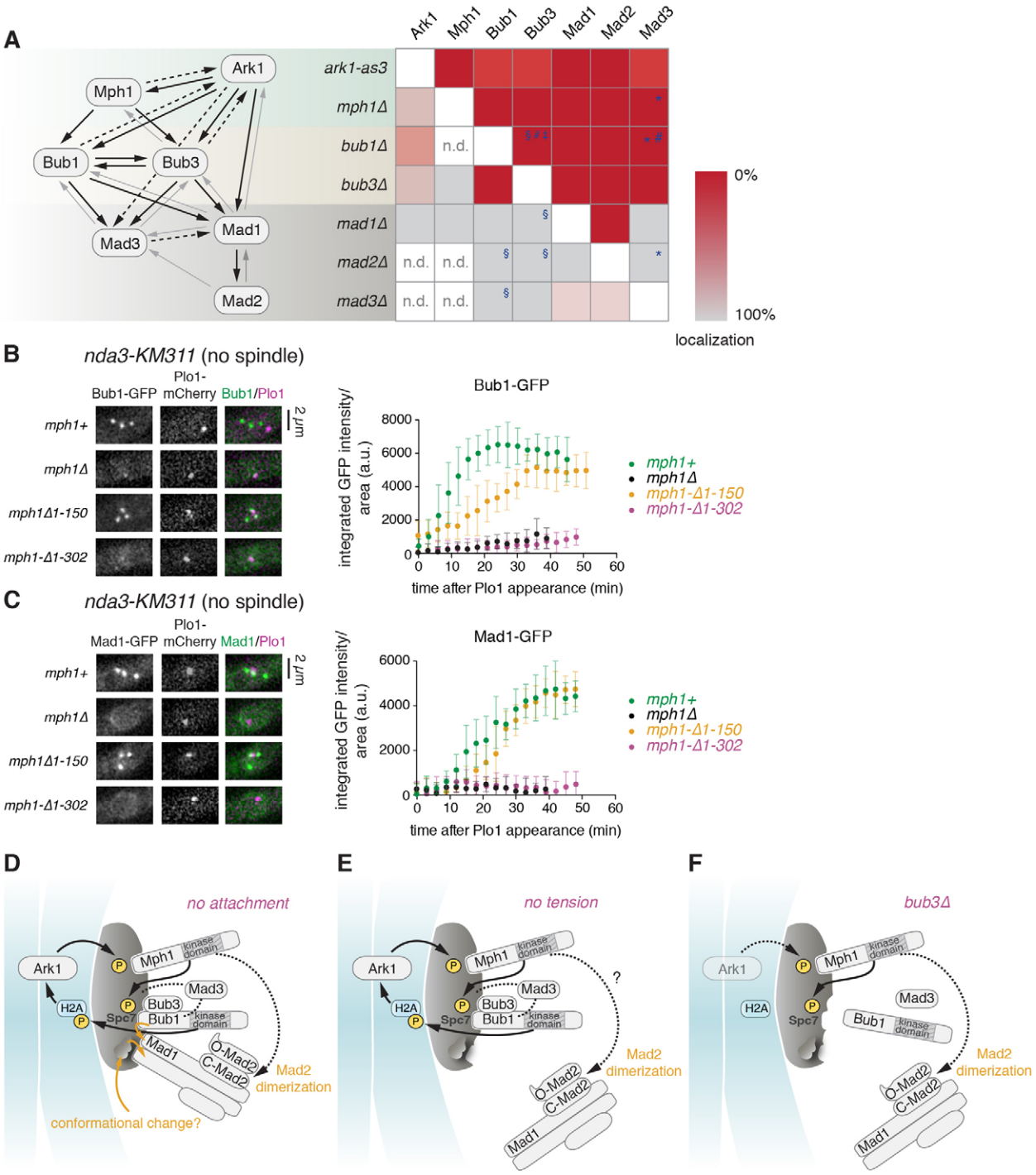

Fig. 4. The hierarchy of SAC protein localization dependencies. (**A**) Schematic of SAC protein localization dependencies. Black arrows indicate a dependency, dashed arrows a partial dependency and gray arrows the absence of dependency. Dependencies were determined in this study (Figs 2, 3; supplementary material Figs S2, S5–S9), except for those indicated by symbols (‡, Windecker et al., 2009; §, Vanoosthuyse et al., 2004; #, Kadura et al., 2005; *, Millband and Hardwick, 2002). n.d., not determined. (**B**,**C**) The indicated strains were followed by live-cell imaging at the restrictive temperature for *nda3-KM311*. The GFP signal was measured over time as cells entered mitosis ($n>7$ cells; ±s.d.). Representative nuclei in early mitosis are shown. (**D**–**F**) General scheme for SAC protein localization dependencies at unattached kinetochores (D), kinetochores not under tension (E) or kinetochores of *bub3Δ* cells (F). See text for details. *P*, phosphorylation; O-Mad2, Mad2 in the ‘open’ conformation; C-Mad2, Mad2 in the ‘closed’ conformation (Mapelli and Musacchio, 2007).

(Kemmler et al., 2009; London et al., 2012; Shepperd et al., 2012; Yamagishi et al., 2012) or SAC proteins (Hardwick et al., 1996). Recruitment of Bub1 and Bub3, probably to the outer kinetochore protein Spc7 (KNL-1, Blinkin) (Kiyomitsu et al., 2007; Bolanos-Garcia et al., 2011; Kiyomitsu et al., 2011; Krenn et al., 2012), may initiate a feedback loop with Ark1 (Aurora B) to strengthen the

interactions. Bub1 and Bub3 may provide a direct physical recruitment platform for Mad1 at the kinetochore. In addition, recruitment of Mad1 may require CDK1 activity (Vázquez-Novelle and Petronczki, 2010; Ito et al., 2012) or conformational changes at the kinetochore that signal the absence of microtubule attachment (Garcia et al., 2002). Mad1 co-recruits Mad2 and the Mad1–Mad2 complex activates additional Mad2 molecules, which then inhibit Cdc20 (De Antoni et al., 2005) (Fig. 4D).

It remains controversial whether kinetochores that contact microtubules but do not come under tension create a SAC signal (Nezi and Musacchio, 2009; Maresca and Salmon, 2010). We note that the upper two layers of the SAC protein localization hierarchy are recruited to 'tension-less' kinetochores (Skoufias et al., 2001; Garcia et al., 2002; Gillett et al., 2004; Howell et al., 2004) (Fig. 4E). In contrast, Mad1 and Mad2 are only enriched at kinetochores lacking attachment (Skoufias et al., 2001; Garcia et al., 2002; Gillett et al., 2004) (Fig. 4D). Because the SAC is functional in *bub3*-deleted fission yeast cells, although Mad1 and Mad2 are undetectable at kinetochores, Mph1 may in principle have the capacity to activate the Mad1–Mad2 complex even if the latter is away from kinetochores (Fig. 4F). Whether this is also possible in wild-type cells with kinetochores that are attached but not under tension is an open question (Fig. 4E). Additional recruitment of Mad1–Mad2 may additionally boost SAC signaling at unattached kinetochores (Fig. 4D). Mph1 localization to kinetochores is central for all aspects of SAC signaling at kinetochores, and it will be interesting to determine how Mph1 is recruited.

Materials and Methods

S. pombe strains

Strains are listed in supplementary material Table S1. GFP tagging was performed by PCR-based gene targeting (Bähler et al., 1998). To generate Mph1 truncation mutants, the bases corresponding to amino acids 2 to 150 (SKRN…NKTP) and 2 to 302 (SKRN…TPIP) were deleted by PCR and the modified *mph1* genes were integrated into the endogenous locus by replacing *ura4+* in an *mph1Δ::ura4+* strain. For fusion of Mph1 to Mis12, the *hygR* ≪ *Pnmt81* and *mis12+-(GGSG)2* fragments were connected by PCR and integrated into the genomic locus of the *mph1-S(GGGGS)3-GFP* ≪ *kanR* strain.

Culture conditions

Strains harbouring the *cdc25-22 cut7-446* alleles were grown in EMM (Moreno et al., 1991) at 25℃ until log phase. Cells were shifted to 36℃ for 4.5 hours. DMSO or 5 μM 1NM-PP1 {(4-amino-1-tertbutyl-3-(1′-naphthylmethyl)pyrazolo[3,4-d] pyrimidine; Toronto Research Chemicals} was added and cells were incubated for another 30 minutes at 36℃. Cells were released by shifting to 25℃ and were harvested after 10 min. Strains with the *nda3-KM311* mutation were grown at 30℃ in YE (Moreno et al., 1991) supplemented with Adenine, and shifted to 16℃ for 6 hours.

Microscopy

Live-cell imaging was performed on a DeltaVision microscope (Applied Precision) as previously described (Windecker et al., 2009). Imaging of fixed cells was performed on a Zeiss AxioImager microscope with a charged-coupled device camera and MetaMorph software (Molecular Devices Corporation). Typically, a *Z*-stack of 3 μm thickness with single planes spaced by 0.3 μm was acquired and subsequently projected to a single image.

Immunoblotting

Synchronization of cells (Windecker et al., 2009) and protein extraction (Koch et al., 2012) were performed as previously described. Mouse anti-GFP (Roche, 11814460001), mouse anti-Cdc13 (GeneTex/Acris, GTX10873) or rabbit anti-Cdc2 (Santa Cruz, SC-53) were used as primary antibodies.

Acknowledgements

We thank Julia Binder, Eva-Maria Illgen, Maria Langegger and Eva-Maria Schwoerzer for excellent technical support, Julia Kamenz, André Koch, and Yoshinori Watanabe for comments on the manuscript, and Yoshinori Watanabe for communicating unpublished results. We are grateful to Mitsuhiro Yanagida, Masayuki Yamamoto and the Yeast Genetic Resource Center (YGRC) for yeast strains.

Funding

The work was funded by the Max Planck Society. S. Heinrich was supported by the Ernst Schering Foundation.

Supplementary material available online at
http://jcs.biologists.org/lookup/suppl/doi:10.1242/jcs.110387/-/DC1

References

Abrieu, A., Magnaghi-Jaulin, L., Kahana, J. A., Peter, M., Castro, A., Vigneron, S., Lorca, T., Cleveland, D. W. and Labbé, J. C. (2001). Mps1 is a kinetochore-associated kinase essential for the vertebrate mitotic checkpoint. *Cell* **106**, 83-93.

Bähler, J., Wu, J. Q., Longtine, M. S., Shah, N. G., McKenzie, A., 3rd, Steever, A. B., Wach, A., Philippsen, P. and Pringle, J. R. (1998). Heterologous modules for efficient and versatile PCR-based gene targeting in *Schizosaccharomyces pombe*. *Yeast* **14**, 943-951.

Basi, G., Schmid, E. and Maundrell, K. (1993). TATA box mutations in the *Schizosaccharomyces pombe* nmt1 promoter affect transcription efficiency but not the transcription start point or thiamine repressibility. *Gene* **123**, 131-136.

Bolanos-Garcia, V. M., Lischetti, T., Matak-Vinković, D., Cota, E., Simpson, P. J., Chirgadze, D. Y., Spring, D. R., Robinson, C. V., Nilsson, J. and Blundell, T. L. (2011). Structure of a Blinkin-BUBR1 complex reveals an interaction crucial for kinetochore-mitotic checkpoint regulation via an unanticipated binding site. *Structure* **19**, 1691-1700.

Burke, D. J. and Stukenberg, P. T. (2008). Linking kinetochore-microtubule binding to the spindle checkpoint. *Dev. Cell* **14**, 474-479.

Chen, R. H. (2002). BubR1 is essential for kinetochore localization of other spindle checkpoint proteins and its phosphorylation requires Mad1. *J. Cell Biol.* **158**, 487-496.

De Antoni, A., Pearson, C. G., Cimini, D., Canman, J. C., Sala, V., Nezi, L., Mapelli, M., Sironi, L., Faretta, M., Salmon, E. D. et al. (2005). The Mad1/Mad2 complex as a template for Mad2 activation in the spindle assembly checkpoint. *Curr. Biol.* **15**, 214-225.

Dischinger, S., Krapp, A., Xie, L., Paulson, J. R. and Simanis, V. (2008). Chemical genetic analysis of the regulatory role of Cdc2p in the S. pombe septation initiation network. *J. Cell Sci.* **121**, 843-853.

Essex, A., Dammermann, A., Lewellyn, L., Oegema, K. and Desai, A. (2009). Systematic analysis in *Caenorhabditis elegans* reveals that the spindle checkpoint is composed of two largely independent branches. *Mol. Biol. Cell* **20**, 1252-1267.

Fraschini, R., Beretta, A., Lucchini, G. and Piatti, S. (2001). Role of the kinetochore protein Ndc10 in mitotic checkpoint activation in Saccharomyces cerevisiae. *Mol. Genet. Genomics* **266**, 115-125.

Garcia, M. A., Koonrugsa, N. and Toda, T. (2002). Spindle-kinetochore attachment requires the combined action of Kin I-like Klp5/6 and Alp14/Dis1-MAPs in fission yeast. *EMBO J.* **21**, 6015-6024.

Gardner, R. D., Poddar, A., Yellman, C., Tavormina, P. A., Monteagudo, M. C. and Burke, D. J. (2001). The spindle checkpoint of the yeast Saccharomyces cerevisiae requires kinetochore function and maps to the CBF3 domain. *Genetics* **157**, 1493-1502.

Gillett, E. S., Espelin, C. W. and Sorger, P. K. (2004). Spindle checkpoint proteins and chromosome-microtubule attachment in budding yeast. *J. Cell Biol.* **164**, 535-546.

Hached, K., Xie, S. Z., Buffin, E., Cladière, D., Rachez, C., Sacras, M., Sorger, P. K. and Wassmann, K. (2011). Mps1 at kinetochores is essential for female mouse meiosis I. *Development* **138**, 2261-2271.

Hagan, I. and Yanagida, M. (1990). Novel potential mitotic motor protein encoded by the fission yeast cut7+ gene. *Nature* **347**, 563-566.

Hardwick, K. G., Weiss, E., Luca, F. C., Winey, M. and Murray, A. W. (1996). Activation of the budding yeast spindle assembly checkpoint without mitotic spindle disruption. *Science* **273**, 953-956.

Hauf, S., Biswas, A., Langegger, M., Kawashima, S. A., Tsukahara, T. and Watanabe, Y. (2007). Aurora controls sister kinetochore mono-orientation and homolog bi-orientation in meiosis-I. *EMBO J.* **26**, 4475-4486.

Hiraoka, Y., Toda, T. and Yanagida, M. (1984). The NDA3 gene of fission yeast encodes beta-tubulin: a cold-sensitive nda3 mutation reversibly blocks spindle formation and chromosome movement in mitosis. *Cell* **39**, 349-358.

Howell, B. J., Moree, B., Farrar, E. M., Stewart, S., Fang, G. and Salmon, E. D. (2004). Spindle checkpoint protein dynamics at kinetochores in living cells. *Curr. Biol.* **14**, 953-964.

Ito, D., Saito, Y. and Matsumoto, T. (2012). Centromere-tethered Mps1 pombe homolog (Mph1) kinase is a sufficient marker for recruitment of the spindle checkpoint protein Bub1, but not Mad1. *Proc. Natl. Acad. Sci. USA* **109**, 209-214.

Jelluma, N., Dansen, T. B., Sliedrecht, T., Kwiatkowski, N. P. and Kops, G. J. (2010). Release of Mps1 from kinetochores is crucial for timely anaphase onset. *J. Cell Biol.* **191**, 281-290.

Kadura, S., He, X., Vanoosthuyse, V., Hardwick, K. G. and Sazer, S. (2005). The A78V mutation in the Mad3-like domain of *Schizosaccharomyces pombe* Bub1p

perturbs nuclear accumulation and kinetochore targeting of Bub1p, Bub3p, and Mad3p and spindle assembly checkpoint function. *Mol. Biol. Cell* **16**, 385-395.

Kallio, M. J., McCleland, M. L., Stukenberg, P. T. and Gorbsky, G. J. (2002). Inhibition of aurora B kinase blocks chromosome segregation, overrides the spindle checkpoint, and perturbs microtubule dynamics in mitosis. *Curr. Biol.* **12**, 900-905.

Kawashima, S. A., Tsukahara, T., Langegger, M., Hauf, S., Kitajima, T. S. and Watanabe, Y. (2007). Shugoshin enables tension-generating attachment of kinetochores by loading Aurora to centromeres. *Genes Dev.* **21**, 420-435.

Kawashima, S. A., Yamagishi, Y., Honda, T., Ishiguro, K. and Watanabe, Y. (2010). Phosphorylation of H2A by Bub1 prevents chromosomal instability through localizing shugoshin. *Science* **327**, 172-177.

Kemmler, S., Stach, M., Knapp, M., Ortiz, J., Pfannstiel, J., Ruppert, T. and Lechner, J. (2009). Mimicking Ndc80 phosphorylation triggers spindle assembly checkpoint signalling. *EMBO J.* **28**, 1099-1110.

Kerscher, O., Crotti, L. B. and Basrai, M. A. (2003). Recognizing chromosomes in trouble: association of the spindle checkpoint protein Bub3p with altered kinetochores and a unique defective centromere. *Mol. Cell. Biol.* **23**, 6406-6418.

Kiyomitsu, T., Obuse, C. and Yanagida, M. (2007). Human Blinkin/AF15q14 is required for chromosome alignment and the mitotic checkpoint through direct interaction with Bub1 and BubR1. *Dev. Cell* **13**, 663-676.

Kiyomitsu, T., Murakami, H. and Yanagida, M. (2011). Protein interaction domain mapping of human kinetochore protein Blinkin reveals a consensus motif for binding of spindle assembly checkpoint proteins Bub1 and BubR1. *Mol. Cell. Biol.* **31**, 998-1011.

Klebig, C., Korinth, D. and Meraldi, P. (2009). Bub1 regulates chromosome segregation in a kinetochore-independent manner. *J. Cell Biol.* **185**, 841-858.

Koch, A., Rode, H. B., Richters, A., Rauh, D. and Hauf, S. (2012). A chemical genetic approach for covalent inhibition of analogue-sensitive aurora kinase. *ACS Chem. Biol.* **7**, 723-731.

Krenn, V., Wehenkel, A., Li, X., Santaguida, S. and Musacchio, A. (2012). Structural analysis reveals features of the spindle checkpoint kinase Bub1-kinetochore subunit Knl1 interaction. *J. Cell Biol.* **196**, 451-467.

Kulukian, A., Han, J. S. and Cleveland, D. W. (2009). Unattached kinetochores catalyze production of an anaphase inhibitor that requires a Mad2 template to prime Cdc20 for BubR1 binding. *Dev. Cell* **16**, 105-117.

Liu, S. T., Chan, G. K., Hittle, J. C., Fujii, G., Lees, E. and Yen, T. J. (2003). Human MPS1 kinase is required for mitotic arrest induced by the loss of CENP-E from kinetochores. *Mol. Biol. Cell* **14**, 1638-1651.

Liu, D., Vader, G., Vromans, M. J., Lampson, M. A. and Lens, S. M. (2009). Sensing chromosome bi-orientation by spatial separation of aurora B kinase from kinetochore substrates. *Science* **323**, 1350-1353.

London, N., Ceto, S., Ranish, J. A. and Biggins, S. (2012). Phosphoregulation of Spc105 by Mps1 and PP1 regulates Bub1 localization to kinetochores. *Curr. Biol.* **22**, 900-906.

Maciejowski, J., George, K. A., Terret, M. E., Zhang, C., Shokat, K. M. and Jallepalli, P. V. (2010). Mps1 directs the assembly of Cdc20 inhibitory complexes during interphase and mitosis to control M phase timing and spindle checkpoint signaling. *J. Cell Biol.* **190**, 89-100.

Maldonado, M. and Kapoor, T. M. (2011). Constitutive Mad1 targeting to kinetochores uncouples checkpoint signalling from chromosome biorientation. *Nat. Cell Biol.* **13**, 475-482.

Mapelli, M. and Musacchio, A. (2007). MAD contortions: conformational dimerization boosts spindle checkpoint signaling. *Curr. Opin. Struct. Biol.* **17**, 716-725.

Maresca, T. J. and Salmon, E. D. (2010). Welcome to a new kind of tension: translating kinetochore mechanics into a wait-anaphase signal. *J. Cell Sci.* **123**, 825-835.

Martin-Lluesma, S., Stucke, V. M. and Nigg, E. A. (2002). Role of Hec1 in spindle checkpoint signaling and kinetochore recruitment of Mad1/Mad2. *Science* **297**, 2267-2270.

Maure, J. F., Kitamura, E. and Tanaka, T. U. (2007). Mps1 kinase promotes sister-kinetochore bi-orientation by a tension-dependent mechanism. *Curr. Biol.* **17**, 2175-2182.

McCleland, M. L., Gardner, R. D., Kallio, M. J., Daum, J. R., Gorbsky, G. J., Burke, D. J. and Stukenberg, P. T. (2003). The highly conserved Ndc80 complex is required for kinetochore assembly, chromosome congression, and spindle checkpoint activity. *Genes Dev.* **17**, 101-114.

Meraldi, P., Draviam, V. M. and Sorger, P. K. (2004). Timing and checkpoints in the regulation of mitotic progression. *Dev. Cell* **7**, 45-60.

Millband, D. N. and Hardwick, K. G. (2002). Fission yeast Mad3p is required for Mad2p to inhibit the anaphase-promoting complex and localizes to kinetochores in a Bub1p-, Bub3p-, and Mph1p-dependent manner. *Mol. Cell. Biol.* **22**, 2728-2742.

Moreno, S., Hayles, J. and Nurse, P. (1989). Regulation of p34cdc2 protein kinase during mitosis. *Cell* **58**, 361-372.

Moreno, S., Klar, A. and Nurse, P. (1991). Molecular genetic analysis of fission yeast *Schizosaccharomyces pombe*. *Methods Enzymol.* **194**, 795-823.

Mulvihill, D. P., Petersen, J., Ohkura, H., Glover, D. M. and Hagan, I. M. (1999). Plo1 kinase recruitment to the spindle pole body and its role in cell division in *Schizosaccharomyces pombe*. *Mol. Biol. Cell* **10**, 2771-2785.

Musacchio, A. and Hardwick, K. G. (2002). The spindle checkpoint: structural insights into dynamic signalling. *Nat. Rev. Mol. Cell Biol.* **3**, 731-741.

Musacchio, A. and Salmon, E. D. (2007). The spindle-assembly checkpoint in space and time. *Nat. Rev. Mol. Cell Biol.* **8**, 379-393.

Nabetani, A., Koujin, T., Tsutsumi, C., Haraguchi, T. and Hiraoka, Y. (2001). A conserved protein, Nuf2, is implicated in connecting the centromere to the spindle during chromosome segregation: a link between the kinetochore function and the spindle checkpoint. *Chromosoma* **110**, 322-334.

Nezi, L. and Musacchio, A. (2009). Sister chromatid tension and the spindle assembly checkpoint. *Curr. Opin. Cell Biol.* **21**, 785-795.

Peters, J. M. (2006). The anaphase promoting complex/cyclosome: a machine designed to destroy. *Nat. Rev. Mol. Cell Biol.* **7**, 644-656.

Petersen, J. and Hagan, I. M. (2003). S. pombe aurora kinase/survivin is required for chromosome condensation and the spindle checkpoint attachment response. *Curr. Biol.* **13**, 590-597.

Rieder, C. L., Cole, R. W., Khodjakov, A. and Sluder, G. (1995). The checkpoint delaying anaphase in response to chromosome monoorientation is mediated by an inhibitory signal produced by unattached kinetochores. *J. Cell Biol.* **130**, 941-948.

Santaguida, S., Tighe, A., D'Alise, A. M., Taylor, S. S. and Musacchio, A. (2010). Dissecting the role of MPS1 in chromosome biorientation and the spindle checkpoint through the small molecule inhibitor reversine. *J. Cell Biol.* **190**, 73-87.

Santaguida, S., Vernieri, C., Villa, F., Ciliberto, A. and Musacchio, A. (2011). Evidence that Aurora B is implicated in spindle checkpoint signalling independently of error correction. *EMBO J.* **30**, 1508-1519.

Saurin, A. T., van der Waal, M. S., Medema, R. H., Lens, S. M. and Kops, G. J. (2011). Aurora B potentiates Mps1 activation to ensure rapid checkpoint establishment at the onset of mitosis. *Nat. Commun.* **2**, 316.

Sharp-Baker, H. and Chen, R. H. (2001). Spindle checkpoint protein Bub1 is required for kinetochore localization of Mad1, Mad2, Bub3, and CENP-E, independently of its kinase activity. *J. Cell Biol.* **153**, 1239-1250.

Shepperd, L. A., Meadows, J. C., Sochaj, A. M., Lancaster, T. C., Zou, J., Buttrick, G. J., Rappsilber, J., Hardwick, K. G. and Millar, J. B. (2012). Phosphodependent recruitment of Bub1 and Bub3 to Spc7/KNL1 by Mph1 kinase maintains the spindle checkpoint. *Curr. Biol.* **22**, 891-899.

Skoufias, D. A., Andreassen, P. R., Lacroix, F. B., Wilson, L. and Margolis, R. L. (2001). Mammalian mad2 and bub1/bubR1 recognize distinct spindle-attachment and kinetochore-tension checkpoints. *Proc. Natl. Acad. Sci. USA* **98**, 4492-4497.

Sliedrecht, T., Zhang, C., Shokat, K. M. and Kops, G. J. (2010). Chemical genetic inhibition of Mps1 in stable human cell lines reveals novel aspects of Mps1 function in mitosis. *PLoS ONE* **5**, e10251.

Tsukahara, T., Tanno, Y. and Watanabe, Y. (2010). Phosphorylation of the CPC by Cdk1 promotes chromosome bi-orientation. *Nature* **467**, 719-723.

Vanoosthuyse, V., Valsdottir, R., Javerzat, J. P. and Hardwick, K. G. (2004). Kinetochore targeting of fission yeast Mad and Bub proteins is essential for spindle checkpoint function but not for all chromosome segregation roles of Bub1p. *Mol. Cell. Biol.* **24**, 9786-9801.

Vanoosthuyse, V., Meadows, J. C., van der Sar, S. J., Millar, J. B. and Hardwick, K. G. (2009). Bub3p facilitates spindle checkpoint silencing in fission yeast. *Mol. Biol. Cell* **20**, 5096-5105.

Vázquez-Novelle, M. D. and Petronczki, M. (2010). Relocation of the chromosomal passenger complex prevents mitotic checkpoint engagement at anaphase. *Curr. Biol.* **20**, 1402-1407.

Vigneron, S., Prieto, S., Bernis, C., Labbé, J. C., Castro, A. and Lorca, T. (2004). Kinetochore localization of spindle checkpoint proteins: who controls whom? *Mol. Biol. Cell* **15**, 4584-4596.

Walczak, C. E., Cai, S. and Khodjakov, A. (2010). Mechanisms of chromosome behaviour during mitosis. *Nat. Rev. Mol. Cell Biol.* **11**, 91-102.

Weiss, E. and Winey, M. (1996). The Saccharomyces cerevisiae spindle pole body duplication gene MPS1 is part of a mitotic checkpoint. *J. Cell Biol.* **132**, 111-123.

Windecker, H., Langegger, M., Heinrich, S. and Hauf, S. (2009). Bub1 and Bub3 promote the conversion from monopolar to bipolar chromosome attachment independently of shugoshin. *EMBO Rep.* **10**, 1022-1028.

Yamagishi, Y., Yang, C. H., Tanno, Y. and Watanabe, Y. (2012). MPS1/Mph1 phosphorylates the kinetochore protein KNL1/Spc7 to recruit SAC components. *Nat. Cell Biol.* **14**, 746-752.

Zhao, Y. and Chen, R. H. (2006). Mps1 phosphorylation by MAP kinase is required for kinetochore localization of spindle-checkpoint proteins. *Curr. Biol.* **16**, 1764-1769.

Supplementary Information

Supplementary Figure 1 Mph1-GFP localization to unattached kinetochores in *bub3Δ* cells

Supplementary Figure 2 Kinetochore localization requirements for Ark1-GFP

Supplementary Figure 3 Effect of 1NM-PP1 on mitotically arrested *ark1+* and *ark1-as3* cells

Supplementary Figure 4 Ark1 inhibition in strains with Mph1 artificially tethered to the kinetochore by fusion to Mis12.

Supplementary Figure 5 Kinetochore localization requirements for Bub1-GFP

Supplementary Figure 6 Kinetochore localization requirements for Bub3-GFP

Supplementary Figure 7 Kinetochore localization requirements for Mad1-GFP

Supplementary Figure 8 Kinetochore localization requirements for Mad2-GFP

Supplementary Figure 9 Kinetochore localization requirements for Mad3-GFP

Supplementary Figure 10 Ark1-GFP localization in strains with N-terminally truncated Mph1

Supplementary Figure 11 Kinetochore localization dependencies of SAC proteins in other eukaryotes

Supplementary Table 1 *S. pombe* strains

Figure S1

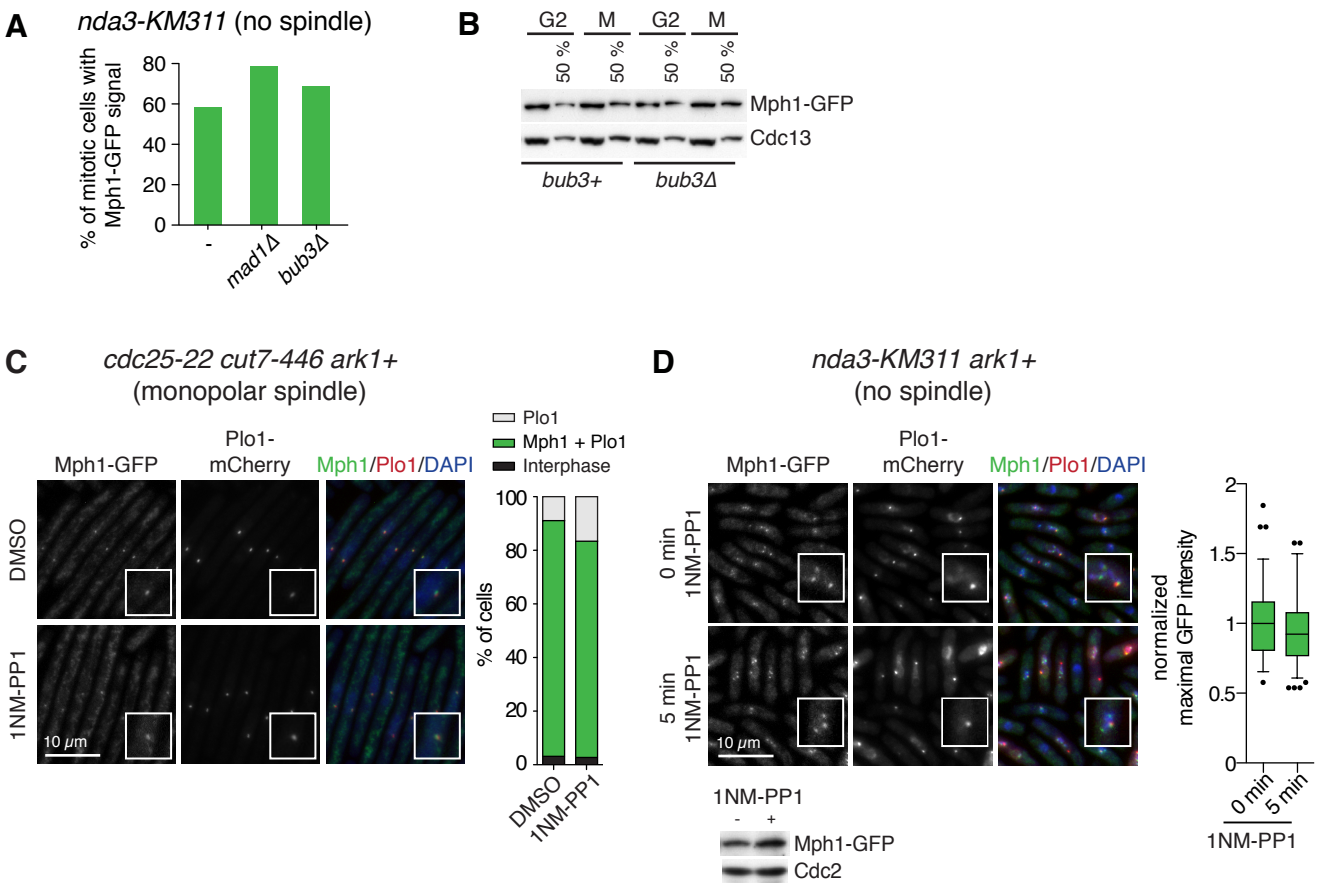
A
nda3-KM311 (no spindle)
% of mitotic cells with Mph1-GFP signal
80
60
40
20
0
-
mad1Δ
bub3Δ
B
G2
M
G2
M
50 %
50 %
50 %
50 %
Mph1-GFP
Cdc13
bub3+
bub3Δ
C
cdc25-22 cut7-446 ark1+
(monopolar spindle)
Mph1-GFP
Plo1-mCherry
Mph1/Plo1/DAPI
DMSO
1NM-PP1
10 μm
Plo1
Mph1 + Plo1
Interphase
% of cells
100
80
60
40
20
0
DMSO
1NM-PP1
D
nda3-KM311 ark1+
(no spindle)
Mph1-GFP
Plo1-mCherry
Mph1/Plo1/DAPI
0 min 1NM-PP1
5 min 1NM-PP1
10 μm
1NM-PP1
-
+
Mph1-GFP
Cdc2
normalized maximal GFP intensity
2
1.5
1
0.5
0
0 min
5 min
1NM-PP1

Figure S1 I Mph1-GFP localization to unattached kinetochores in *bub3Δ* cells

A Mph1 localization to kinetochores is preserved in *mad1Δ* and *bub3Δ* cells. Mph1-GFP strains expressing *nda3-KM311*, *plo1+-mCherry* and the indicated SAC gene deletions were followed by live cell imaging at the restrictive temperature for *nda3-KM311,* which prevents microtubule formation. The percentage of cells with localized Mph1 signal in early mitosis is shown (n > 30 cells).

B Mph1 abundance is unchanged by *bub3* deletion. The indicated strains were harvested in G2 and mitosis (M) and analysed by immunoblotting using anti-GFP and anti-Cdc13 antibodies. In every second lane, half the amount of sample (50 %) was loaded.

C 1NM-PP1 treatment of *ark1+* cells does not lead to loss of Mph1 localization. Cells expressing *ark1+* were arrested in late G2 using the conditional *cdc25-22* mutation and released into mitosis in the presence of 5 μM of the Ark1-as3 inhibitor 1NM-PP1 or an equivalent amount of the solvent DMSO. The presence of the *cut7-446* allele leads to monopolar spindles. Mitotic cells were fixed with methanol, and DNA was stained with DAPI. Insets are 2.5-times magnified relative to the main picture. The presence of a localized Plo1 signal indicates that cells are in mitosis. The percentage of cells with Plo1 and Mph1 signal was determined (n > 100 cells).

D 1NM-PP1 treatment of *ark1+* cells does not lead to loss of Mph1 localization. Cells expressing *ark1+* were grown at the restrictive temperature for *nda3-KM311*, which prevents microtubule formation. Cells were treated with 1NM-PP1 and fixed with methanol after 0 min and 5 min. DNA was stained with DAPI. Insets are 2.5-times magnified relative to the main picture. Maximal Mph1-GFP signal intensity in mitotic cells was quantified (n > 170 cells, box plot with whiskers from 5^{th} to 95^{th} percentile; data normalized to median of cells treated for 0 min). Protein abundance of Mph1-GFP in mitotically arrested cells treated with (+) or without (-) 1NM-PP1 was determined by immunoblotting using anti-GFP and anti-Cdc2 (loading control) antibodies.

Figure S2

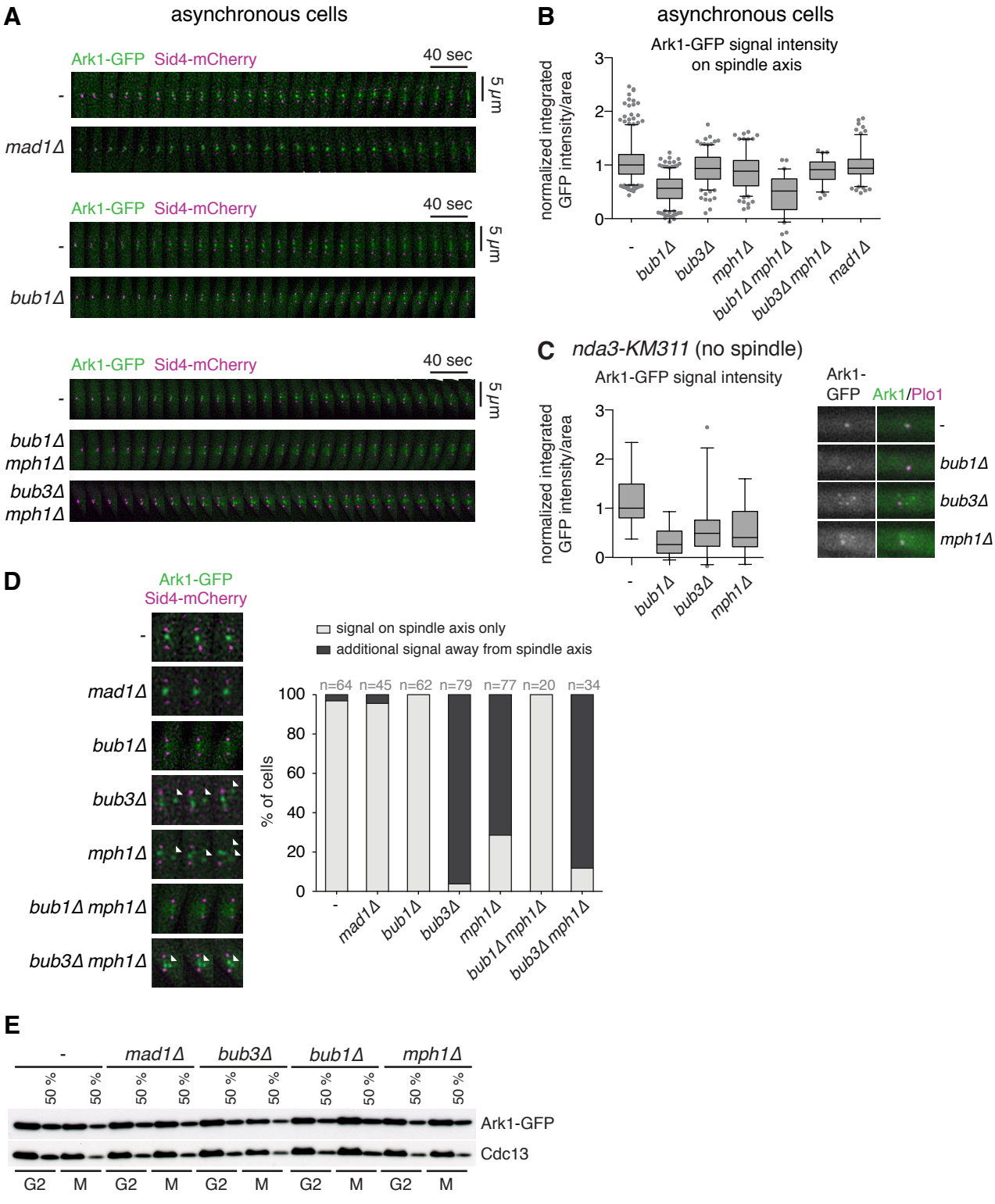
A
asynchronous cells
Ark1-GFP Sid4-mCherry
40 sec
5 μm
-
mad1Δ
bub1Δ
bub1Δ mph1Δ
bub3Δ mph1Δ
B
asynchronous cells
Ark1-GFP signal intensity on spindle axis
normalized integrated GFP intensity/area
bub1Δ
bub3Δ
mph1Δ
bub1Δ mph1Δ
bub3Δ mph1Δ
mad1Δ
C
nda3-KM311 (no spindle)
Ark1-GFP signal intensity
Ark1-GFP
Ark1/Plo1
D
Ark1-GFP
Sid4-mCherry
signal on spindle axis only
additional signal away from spindle axis
n=64 n=45 n=62 n=79 n=77 n=20 n=34
% of cells
E
50 %
Ark1-GFP
Cdc13
G2
M

Figure S2 | Kinetochore localization requirements for Ark1-GFP

A Mitotic localization of Ark1 in strains deleted of SAC genes. Cells were followed by live cell imaging with Sid4-mCherry as spindle pole body (SPB) marker. Exemplary kymographs of the spindle region are shown.

B Centromere localization of Ark1 is strongly impaired by deletion of *bub1.* The signal intensity of Ark1-GFP on the spindle axis was determined for several time points in early mitosis. Background was measured in the nucleoplasm and subtracted ($n > 17$ cells; box plot with whiskers from 5^{th} to 95^{th} percentile; data normalized to median of wild type cells (-)). The data for wild type and *bub3Δ* are also shown in Fig. 2D, the data for wild type and *mph1Δ* are also shown in Fig. 3D.

C Centromere localization of Ark1 is strongly impaired by deletion of *bub1* and slightly impaired by deletion of *mph1* or *bub3.* Cells were followed by live cell imaging at the restrictive temperature for *nda3-KM311*, which prevents microtubule formation. Ark1-GFP signals close to the SPB were assumed to result from centromeric localization and were quantified at 35 min after cells had entered mitosis. Background was measured in the nucleoplasm, avoiding localized Ark1 signals in the nucleoplasm, and was subtracted ($n > 13$ cells; box plot with whiskers from 5^{th} to 95^{th} percentile; data normalized to median of wild type cells). Exemplary nuclei are shown on the right.

D Ark1-GFP localizes to additional spots away from the spindle axis in *bub3Δ, mph1Δ* and *bub3Δ mph1Δ* cells. Shown are magnified regions from the kymographs in (A) and Fig. 2D and 3D. Arrowheads indicate signals away from the spindle axis. The frequency of occurrence of such signals is shown on the right. We attribute the occurrence of these signals to subtelomeric localization of Ark1. In interphase, Sgo2 enriches at subtelomeric regions, and this localization depends on Bub1 and H2A phosphorylation (Kawashima et al., 2010). It is conceivable that in *mph1Δ* and *bub3Δ* cells H2A phosphorylation at this region persists into mitosis, leading to the recruitment of the Ark1 complex by Sgo2. In *bub1Δ* cells, H2A phosphorylation, and therefore Ark1 localization at this region, is missing.

E Ark1 abundance is unchanged in SAC gene deletion strains. The indicated strains were harvested in G2 and mitosis (M) and analysed by immunoblotting using anti-GFP and anti-Cdc13 antibodies. In every second lane, half the amount of sample (50 %) was loaded.

Figure S3

A

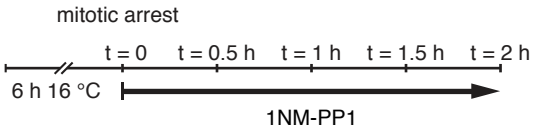
mitotic arrest
t = 0
t = 0.5 h
t = 1 h
t = 1.5 h
t = 2 h
6 h 16 °C
1NM-PP1

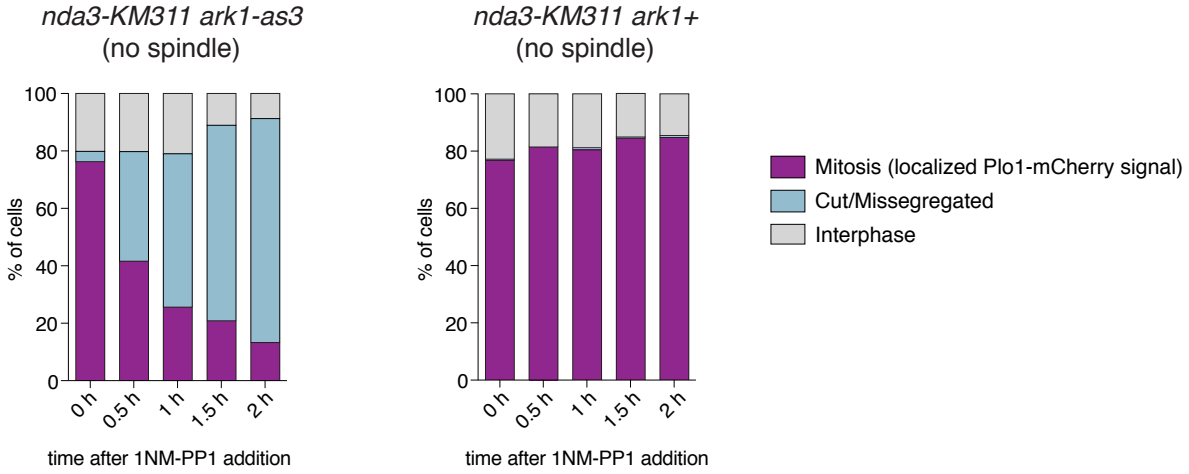
nda3-KM311 ark1-as3
(no spindle)
nda3-KM311 ark1+
(no spindle)
% of cells
100
80
60
40
20
0
0 h
0.5 h
1 h
1.5 h
2 h
time after 1NM-PP1 addition
Mitosis (localized Plo1-mCherry signal)
Cut/Missegregated
Interphase

B

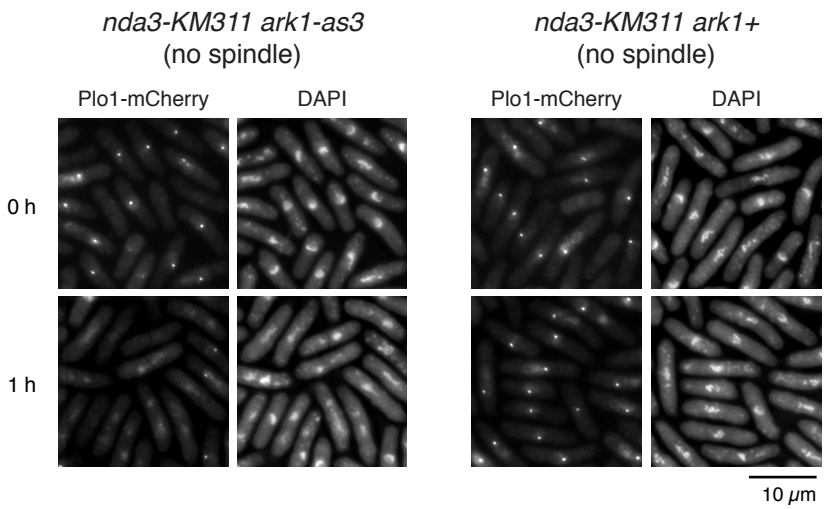
nda3-KM311 ark1-as3
(no spindle)
nda3-KM311 ark1+
(no spindle)
Plo1-mCherry
DAPI
0 h
1 h
10 μm

Figure S3 | Effect of 1NM-PP1 on mitotically arrested *ark1+* and *ark1-as3* cells

A 1NM-PP1 induces mitotic exit in *nda3-KM311 ark1-as3*, but not in *ark1+* cells. Schematic outline of the experiment is shown on top. Cells were arrested in mitosis by incubation at the restrictive temperature for *nda3-KM311* (16 °C) for 6 h. While maintaining 16 °C, cells were treated with 1NM-PP1 and fixed with methanol at the indicated time points. Mitotic cells were identified by the presence of Plo1-mCherry at SPBs, cut or missegregation phenotypes were scored based on DAPI.

B Representative pictures of the experiment shown in (A).

Figure S4

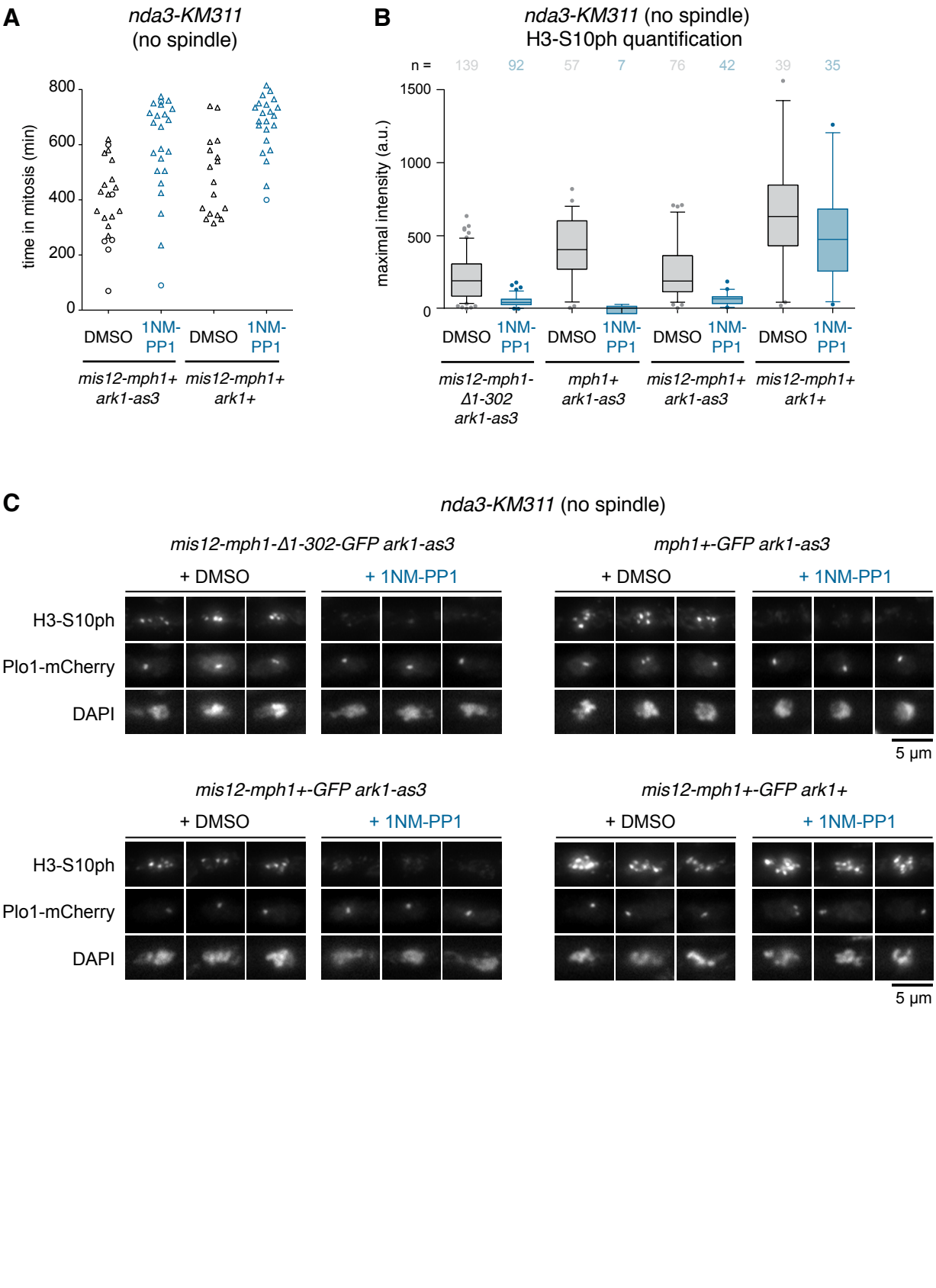
A
nda3-KM311
(no spindle)
time in mitosis (min)
800
600
400
200
0
DMSO
1NM-PP1
DMSO
1NM-PP1
mis12-mph1+ ark1-as3
mis12-mph1+ ark1+
B
nda3-KM311 (no spindle)
H3-S10ph quantification
n = 139 92 57 7 76 42 39 35
maximal intensity (a.u.)
1500
1000
500
0
DMSO
1NM-PP1
mis12-mph1-Δ1-302 ark1-as3
mph1+ ark1-as3
mis12-mph1+ ark1-as3
mis12-mph1+ ark1+
C
nda3-KM311 (no spindle)
mis12-mph1-Δ1-302-GFP ark1-as3
mph1+-GFP ark1-as3
+ DMSO
+ 1NM-PP1
H3-S10ph
Plo1-mCherry
DAPI
5 μm
mis12-mph1+-GFP ark1-as3
mis12-mph1+-GFP ark1+

Figure S4 | Ark1 inhibition in strains with Mph1 artificially tethered to the kinetochore by fusion to Mis12.

A Inhibition of Ark1 does not shorten the mitotic delay in cells expressing *mis12-mph1+*. Cells expressing the indicated *mis12-mph1+* fusion constructs and either wild type *ark1+* or the analog-sensitive allele *ark1-as3* were followed by live cell imaging at the restrictive temperature for *nda3-KM311* (preventing the formation of microtubules) in the presence of 10 μM of the Ark1-as3 inhibitor 1NM-PP1 or an equivalent amount of the solvent DMSO. The duration of prometaphase was determined by the presence of Plo1-mCherry at SPBs. Circles indicate cells in which the entire mitosis was recorded, triangles indicate cells in which entry into mitosis but not exit from mitosis was recorded.

B 1NM-PP1 treatment strongly impairs histone H3-Serine10 phosphorylation in cells expressing *ark1-as3*, indicating that Ark1 was efficiently inhibited. Strains shown in Fig. 3C and (A) were cultured as in (A). Samples were fixed with paraformaldehyde after 5 h at the restrictive temperature for *nda3-KM311* and immunostained for Histone H3 Serine10 phosphorylation (H3-S10ph; upstate antibody 06-570). Maximal signal intensity in the nucleus was quantified and maximal signal intensity measured in the cytoplasm was subtracted as background (n between 7 and 139 cells; box plot with whiskers from 5^{th} to 95^{th} percentile; a. u. = arbitrary units).

C Exemplary nuclei of the experiment shown in (B). DNA was stained with DAPI.

Figure S5

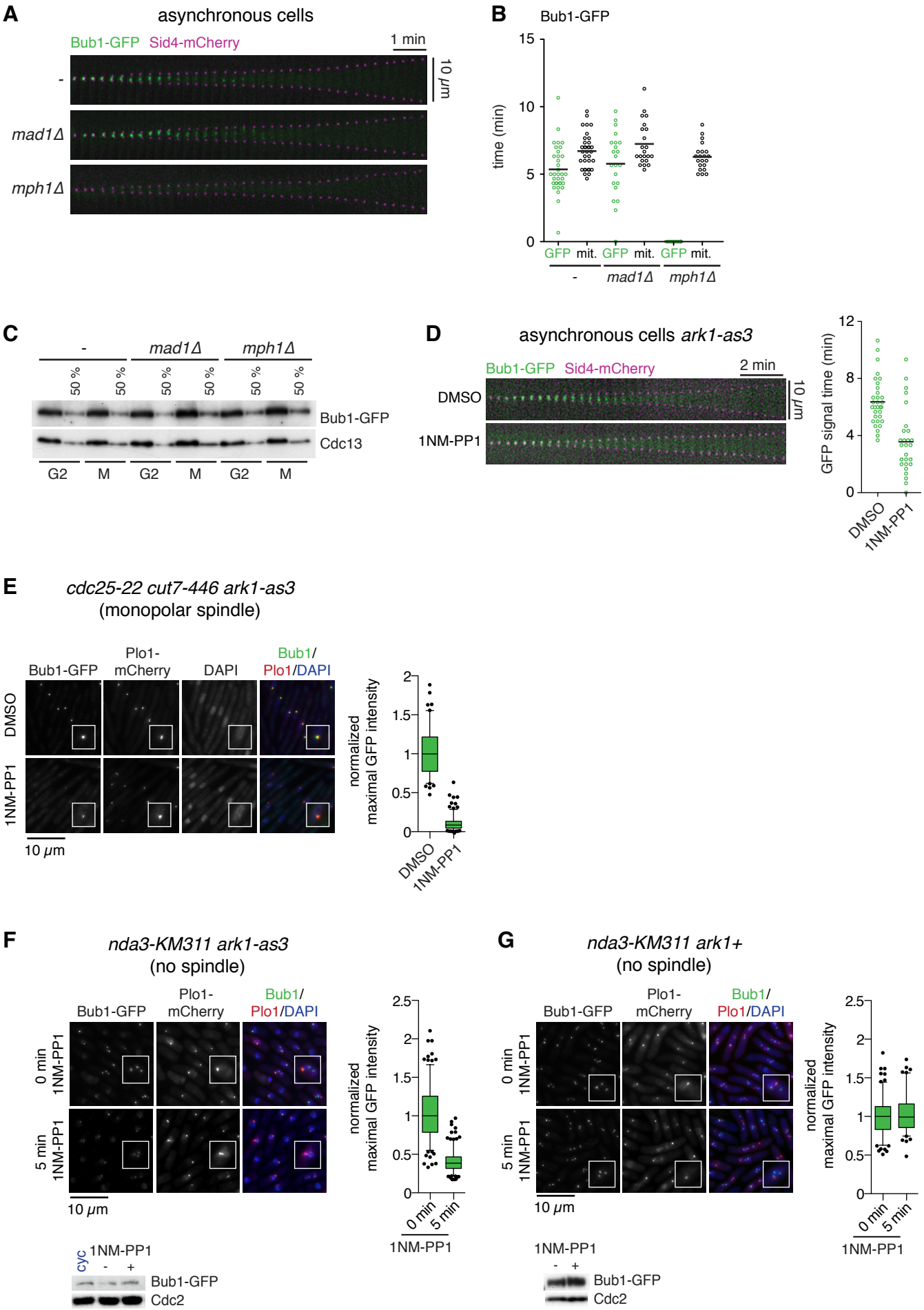
A
asynchronous cells
Bub1-GFP Sid4-mCherry
1 min
10 μm
-
mad1Δ
mph1Δ
B
Bub1-GFP
time (min)
15
10
5
0
GFP mit. GFP mit. GFP mit.
-
mad1Δ
mph1Δ
C
-
mad1Δ
mph1Δ
50 %
Bub1-GFP
Cdc13
G2 M G2 M G2 M
D
asynchronous cells ark1-as3
Bub1-GFP Sid4-mCherry
2 min
10 μm
DMSO
1NM-PP1
GFP signal time (min)
12
8
4
0
DMSO
1NM-PP1
E
cdc25-22 cut7-446 ark1-as3
(monopolar spindle)
Bub1-GFP
Plo1-mCherry
DAPI
Bub1/Plo1/DAPI
DMSO
1NM-PP1
10 μm
normalized maximal GFP intensity
2
1.5
1
0.5
0
DMSO
1NM-PP1
F
nda3-KM311 ark1-as3
(no spindle)
Bub1-GFP
Plo1-mCherry
Bub1/Plo1/DAPI
0 min 1NM-PP1
5 min 1NM-PP1
10 μm
normalized maximal GFP intensity
2.5
2
1.5
1
0.5
0
0 min
5 min
1NM-PP1
cyc 1NM-PP1
- +
Bub1-GFP
Cdc2
G
nda3-KM311 ark1+
(no spindle)
Bub1-GFP
Plo1-mCherry
Bub1/Plo1/DAPI
0 min 1NM-PP1
5 min 1NM-PP1
10 μm
normalized maximal GFP intensity
2.5
2
1.5
1
0.5
0
0 min
5 min
1NM-PP1
1NM-PP1
- +
Bub1-GFP
Cdc2

Figure S5 | Kinetochore localization requirements for Bub1-GFP

A Mitotic localization of Bub1 in *mad1Δ* and *mph1Δ* cells. Cells were followed by live cell imaging with Sid4-mCherry as SPB marker. Exemplary kymographs of the spindle region are shown. In an unperturbed mitosis, Bub1-GFP is unable to localize to kinetochores in the absence of *mph1*.

B Quantitative analysis of the experiment in (A). The graph shows the time in mitosis, during which a localized GFP signal was observed (GFP), and the time in mitosis (mit.) from SPB separation to anaphase (SPB distance > 2.5 μm). Horizontal bars indicate the mean.

C Bub1 abundance is unchanged by deletion of *mad1* or *mph1.* The indicated strains were harvested in G2 and mitosis (M) and analysed by immunoblotting using anti-GFP and anti-Cdc13 antibodies. In every second lane, half the amount of sample (50 %) was loaded.

D Inhibition of Ark1 reduces kinetochore localization of Bub1. Cells were grown in the absence (DMSO) or presence of 1NM-PP1 to inhibit Ark1-as3, and were followed by live cell imaging. Exemplary kymographs of the spindle region are shown. The graph shows the time in mitosis, during which a localized GFP signal was observed. Horizontal bars indicate the mean.

E Ark1 is required for Bub1 localization in cells with monopolar spindles. Cells were arrested in G2 and released into mitosis in the absence (DMSO) or presence of 1NM-PP1 to inhibit Ark1-as3. The presence of the *cut7-446* allele leads to monopolar spindles. Mitotic cells were fixed with methanol. DNA was stained with DAPI. Insets are 2.5-times magnified relative to the main picture. The maximal GFP intensity in mitotic cells was determined and corrected for background signal (n > 100 cells, box plot with whiskers from 5^{th} to 95^{th} percentile; data normalized to median of DMSO-treated cells).

F, G Ark1 is required to maintain Bub1 localization in cells lacking microtubules. Cells were grown at the restrictive temperature for *nda3-KM311,* which prevents microtubule formation, so that cells are halted in mitosis. Cells were treated with 1NM-PP1 and samples were fixed with methanol after 0 min and 5 min. DNA was stained with DAPI. Insets are 2.5-times magnified relative to the main picture. Maximal Bub1-GFP signal intensity in mitotic cells was quantified and corrected for

background signal (n > 190 cells, box plot with whiskers from 5th to 95th percentile; data normalized to median of cells treated for 0 min). Protein abundance of Bub1-GFP in cycling cells (cyc) and mitotically arrested cells treated with (+) or without (-) 1NM-PP1 was determined by immunoblotting using anti-GFP and anti-Cdc2 (loading control) antibodies. Unlike in *ark1-as3* cells (F), 1NM-PP1 treatment does not show any effect on Bub1 localization in *ark1+* cells (G). This suggests that the observed effect results from Ark1 inhibition rather than from side effects of the inhibitor 1NM-PP1.

Figure S6

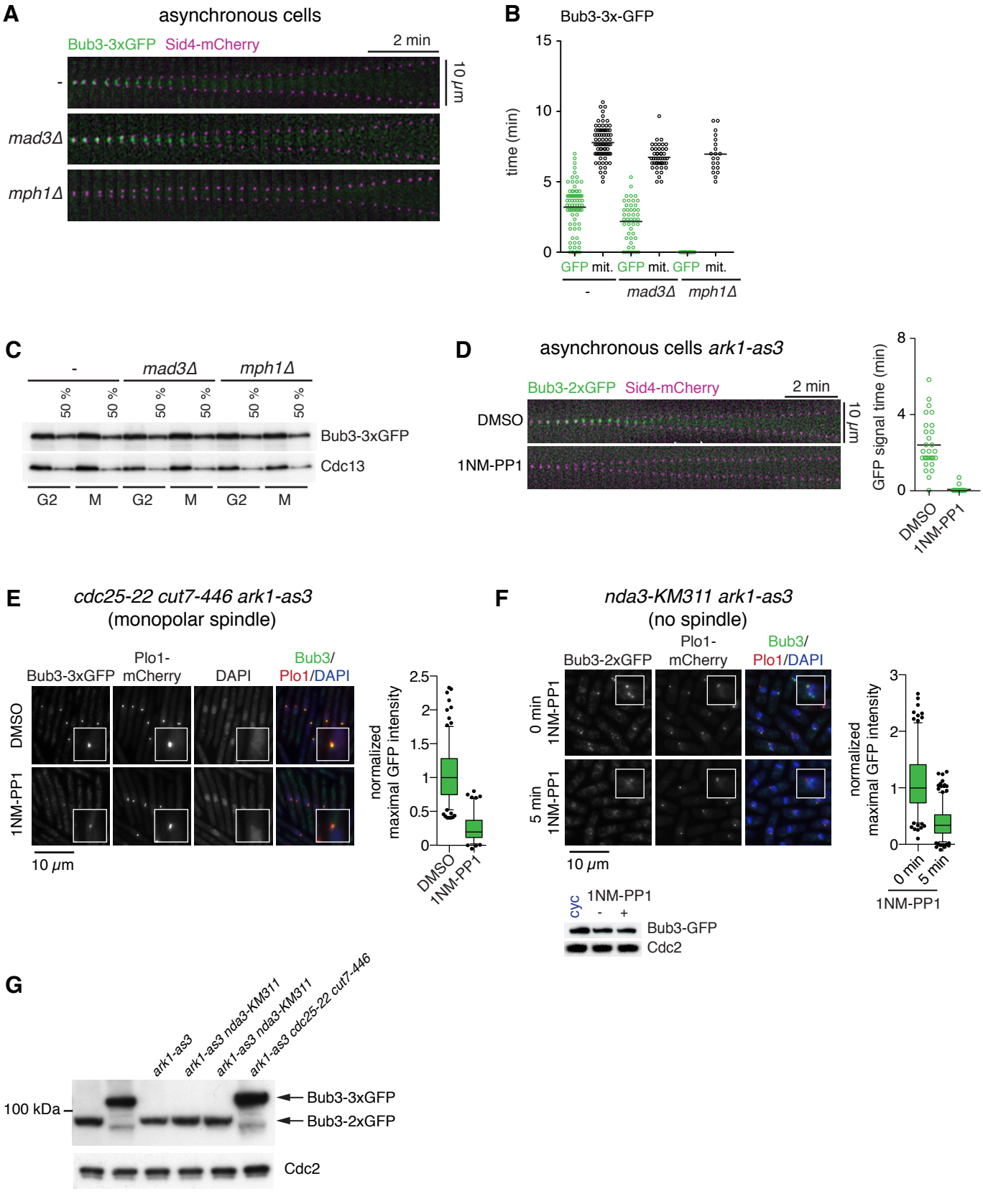
A
asynchronous cells
Bub3-3xGFP Sid4-mCherry
2 min
10 µm
-
mad3Δ
mph1Δ
B
Bub3-3x-GFP
time (min)
15
10
5
0
GFP mit. GFP mit. GFP mit.
-
mad3Δ
mph1Δ
C
-
mad3Δ
mph1Δ
50 %
50 %
50 %
50 %
50 %
50 %
Bub3-3xGFP
Cdc13
G2
M
G2
M
G2
M
D
asynchronous cells ark1-as3
Bub3-2xGFP Sid4-mCherry
2 min
10 µm
DMSO
1NM-PP1
GFP signal time (min)
8
4
0
DMSO
1NM-PP1
E
cdc25-22 cut7-446 ark1-as3
(monopolar spindle)
Bub3-3xGFP
Plo1-mCherry
DAPI
Bub3/Plo1/DAPI
DMSO
1NM-PP1
10 µm
normalized maximal GFP intensity
2.5
2
1.5
1
0.5
0
DMSO
1NM-PP1
F
nda3-KM311 ark1-as3
(no spindle)
Bub3-2xGFP
Plo1-mCherry
Bub3/Plo1/DAPI
0 min 1NM-PP1
5 min 1NM-PP1
10 µm
normalized maximal GFP intensity
3
2
1
0
0 min
5 min
1NM-PP1
cyc
1NM-PP1
-
+
Bub3-GFP
Cdc2
G
ark1-as3
ark1-as3 nda3-KM311
ark1-as3 nda3-KM311
ark1-as3 cdc25-22 cut7-446
100 kDa
Bub3-3xGFP
Bub3-2xGFP
Cdc2

Figure S6 | Kinetochore localization requirements for Bub3-GFP

A Mitotic localization of Bub3 in *mad3Δ* and *mph1Δ* cells. Cells were followed by live cell imaging with Sid4-mCherry as SPB marker. Exemplary kymographs of the spindle region are shown. In an unperturbed mitosis, Bub3-GFP is unable to localize to kinetochores in the absence of *mph1*.

B Quantitative analysis of the experiment in (A). The graph shows the time in mitosis, during which a localized GFP signal was observed (GFP), and the time in mitosis (mit.) from SPB separation to anaphase (SPB distance > 2.5 μm). Horizontal bars indicate the mean.

C Bub3 abundance is unchanged by deletion of *mad3* or *mph1.* The indicated strains were harvested in G2 and mitosis (M) and analysed by immunoblotting using anti-GFP and anti-Cdc13 antibodies. In every second lane, half the amount of sample (50 %) was loaded.

D Inhibition of Ark1 reduces kinetochore localization of Bub3. Cells were grown in the absence (DMSO) or presence of 1NM-PP1 to inhibit Ark1-as3, and were followed by live cell imaging. Exemplary kymographs of the spindle region are shown. The graph shows the time in mitosis, during which a localized GFP signal was observed. Horizontal bars indicate the mean.

E Ark1 is required for Bub3 localization in cells with monopolar spindles. Cells were arrested in G2 and released into mitosis in the absence (DMSO) or presence of 1NM-PP1 to inhibit Ark1-as3. The presence of the *cut7-446* allele leads to monopolar spindles. Mitotic cells were fixed with methanol. DNA was stained with DAPI. Insets are 2.5-times magnified relative to the main picture. The maximal GFP intensity in mitotic cells was determined and corrected for background signal (n > 100 cells, box plot with whiskers from 5^{th} to 95^{th} percentile; data normalized to median of DMSO-treated cells).

F Ark1 is required to maintain Bub3 localization in cells lacking microtubules. Cells were grown at the restrictive temperature for *nda3-KM311,* which prevents microtubule formation, so that cells are halted in mitosis. Cells were treated with 1NM-PP1 and samples were fixed with methanol after 0 min and 5 min. DNA was stained with DAPI. Insets are 2.5-times magnified relative to the main picture. Maximal Bub3-GFP signal intensity in mitotic cells was quantified and corrected for

background signal (n > 180 cells, box plot with whiskers from 5th to 95th percentile; data normalized to median of cells treated for 0 min). Protein abundance of Bub3-GFP in cycling cells (cyc) and mitotically arrested cells treated with (+) or without (-) 1NM-PP1 was determined by immunoblotting using anti-GFP and anti-Cdc2 (loading control) antibodies.

G Extracts from asynchronous cultures of the indicated strains (used in S6A-F) were analysed by immunoblotting using anti-GFP and anti-Cdc2 (loading control) antibodies.

Figure S7

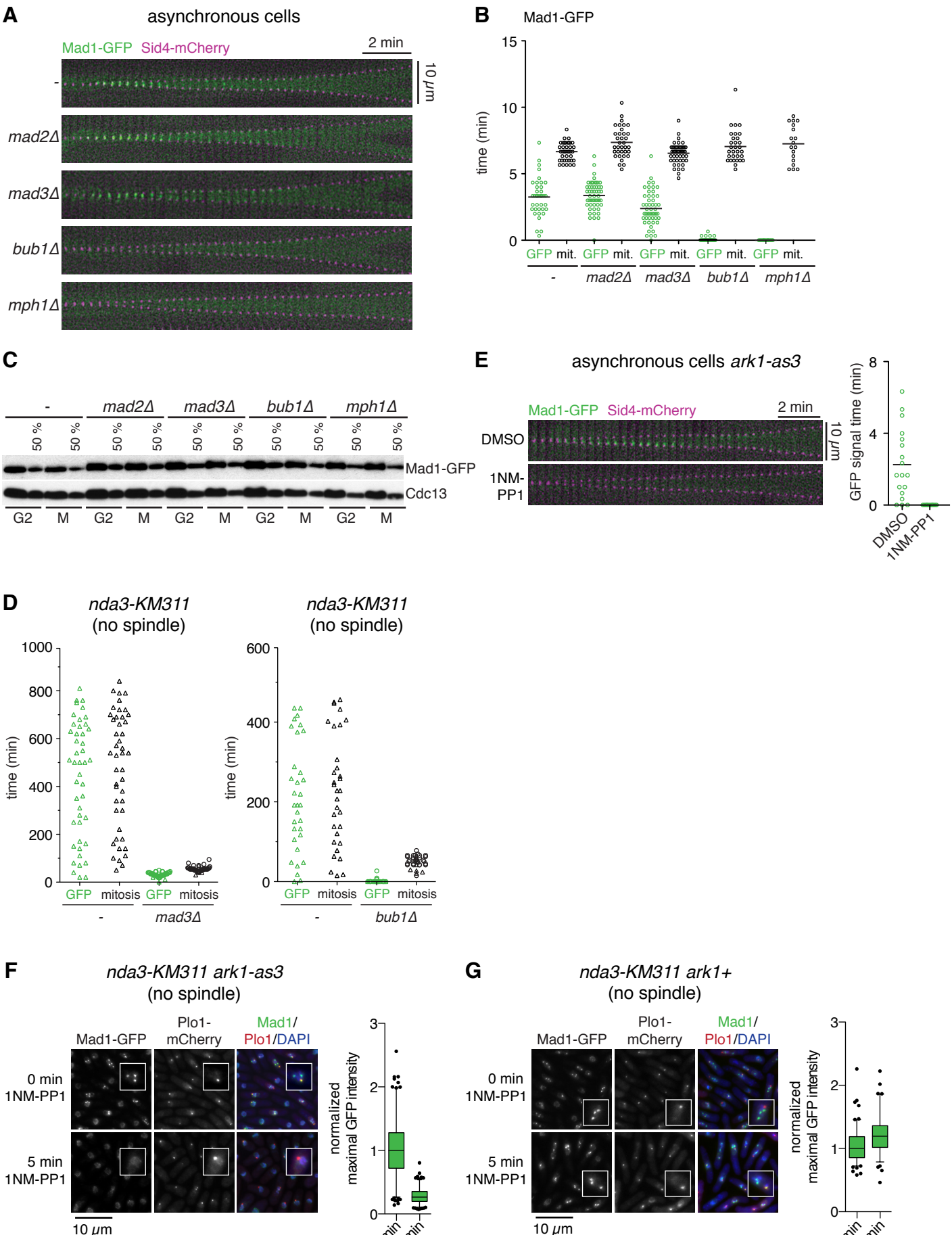
A
asynchronous cells
Mad1-GFP Sid4-mCherry
2 min
10 μm
-
mad2Δ
mad3Δ
bub1Δ
mph1Δ
B
Mad1-GFP
time (min)
15
10
5
0
GFP mit. GFP mit. GFP mit. GFP mit. GFP mit.
-
mad2Δ
mad3Δ
bub1Δ
mph1Δ
C
-
mad2Δ
mad3Δ
bub1Δ
mph1Δ
50 %
Mad1-GFP
Cdc13
G2 M G2 M G2 M G2 M G2 M
D
nda3-KM311
(no spindle)
time (min)
1000
800
600
400
200
0
GFP mitosis GFP mitosis
-
mad3Δ
nda3-KM311
(no spindle)
600
400
200
0
GFP mitosis GFP mitosis
-
bub1Δ
E
asynchronous cells ark1-as3
Mad1-GFP Sid4-mCherry
2 min
10 μm
DMSO
1NM-PP1
GFP signal time (min)
8
4
0
DMSO
1NM-PP1
F
nda3-KM311 ark1-as3
(no spindle)
Mad1-GFP
Plo1-mCherry
Mad1/Plo1/DAPI
0 min 1NM-PP1
5 min 1NM-PP1
10 μm
normalized maximal GFP intensity
3
2
1
0
0 min
5 min
1NM-PP1
cyc
1NM-PP1
- +
Mad1-GFP
Cdc2
G
nda3-KM311 ark1+
(no spindle)
Mad1-GFP
Plo1-mCherry
Mad1/Plo1/DAPI
0 min 1NM-PP1
5 min 1NM-PP1
10 μm
normalized maximal GFP intensity
3
2
1
0
0 min
5 min
1NM-PP1
1NM-PP1
- +
Mad1-GFP
Cdc2

Figure S7 | Kinetochore localization requirements for Mad1-GFP

A Mitotic localization of Mad1 in strains deleted of SAC genes. Cells were followed by live cell imaging with Sid4-mCherry as SPB marker. Exemplary kymographs of the spindle region are shown. In an unperturbed mitosis, Mad1-GFP is unable to localize to kinetochores in the absence of *bub1* or *mph1*.

B Quantitative analysis of the experiment in (A). The graph shows the time in mitosis, during which a localized GFP signal was observed (GFP), and the time in mitosis (mit.) from SPB separation to anaphase (SPB distance > 2.5 μm). Horizontal bars indicate the mean. Deletion of *bub1* or *mph1* prevents localization of Mad1, whereas deletion of *mad3* seems to slightly shorten the time during which a signal is observed.

C Mad1 abundance is unchanged by deletion of *mad2, mad3, bub1* or *mph1.* The indicated strains were harvested in G2 and mitosis (M) and analysed by immunoblotting using anti-GFP and anti-Cdc13 antibodies. In every second lane, half the amount of sample (50 %) was loaded.

D Bub1 is required for Mad1 localization in cells lacking microtubules. Cells were grown at the restrictive temperature for *nda3-KM311*, which prevents microtubule formation, and were followed by live cell imaging. The graph shows the time in mitosis, during which a localized GFP signal was observed (GFP), and the duration of prometaphase (mitosis) as determined by the presence of Plo1-mCherry at SPBs. Circles indicate cells in which the entire mitosis was recorded, triangles indicate cells in which entry into mitosis but not exit from mitosis was recorded. Mad1 was unable to localize to unattached kinetochores in the absence of *bub1*, but was still able to localize in the absence of *mad3*. The mitotic delay was abrogated by deletion of either *mad3* or *bub1*.

E Inhibition of Ark1 abolishes kinetochore localization of Mad1. Cells were grown in the absence (DMSO) or presence of 1NM-PP1 to inhibit Ark1-as3, and were followed by live cell imaging. Exemplary kymographs of the spindle region are shown. The graph shows the time in mitosis, during which a localized GFP signal was observed. Horizontal bars indicate the mean.

F, G Ark1 is required to maintain Mad1 localization in cells lacking microtubules. Cells were grown at the restrictive temperature for *nda3-KM311,* which prevents

microtubule formation, so that cells are halted in mitosis. Cells were treated with 1NM-PP1 and samples were fixed with methanol after 0 min and 5 min. DNA was stained with DAPI. Insets are 2.5-times magnified relative to the main picture. Maximal Mad1-GFP signal intensity in mitotic cells was quantified and corrected for background signal ($n > 160$ cells, box plot with whiskers from 5^{th} to 95^{th} percentile; data normalized to median of cells treated for 0 min). Protein abundance of Mad1-GFP in cycling cells (cyc) and mitotically arrested cells treated with (+) or without (-) 1NM-PP1 was determined by immunoblotting using anti-GFP and anti-Cdc2 (loading control) antibodies. Unlike in *ark1-as3* cells (F), 1NM-PP1 treatment does not show any effect on Mad1 localization in *ark1+* cells (G). This suggests that the observed effect results from Ark1 inhibition rather than from side effects of the inhibitor 1NM-PP1.

Figure S8

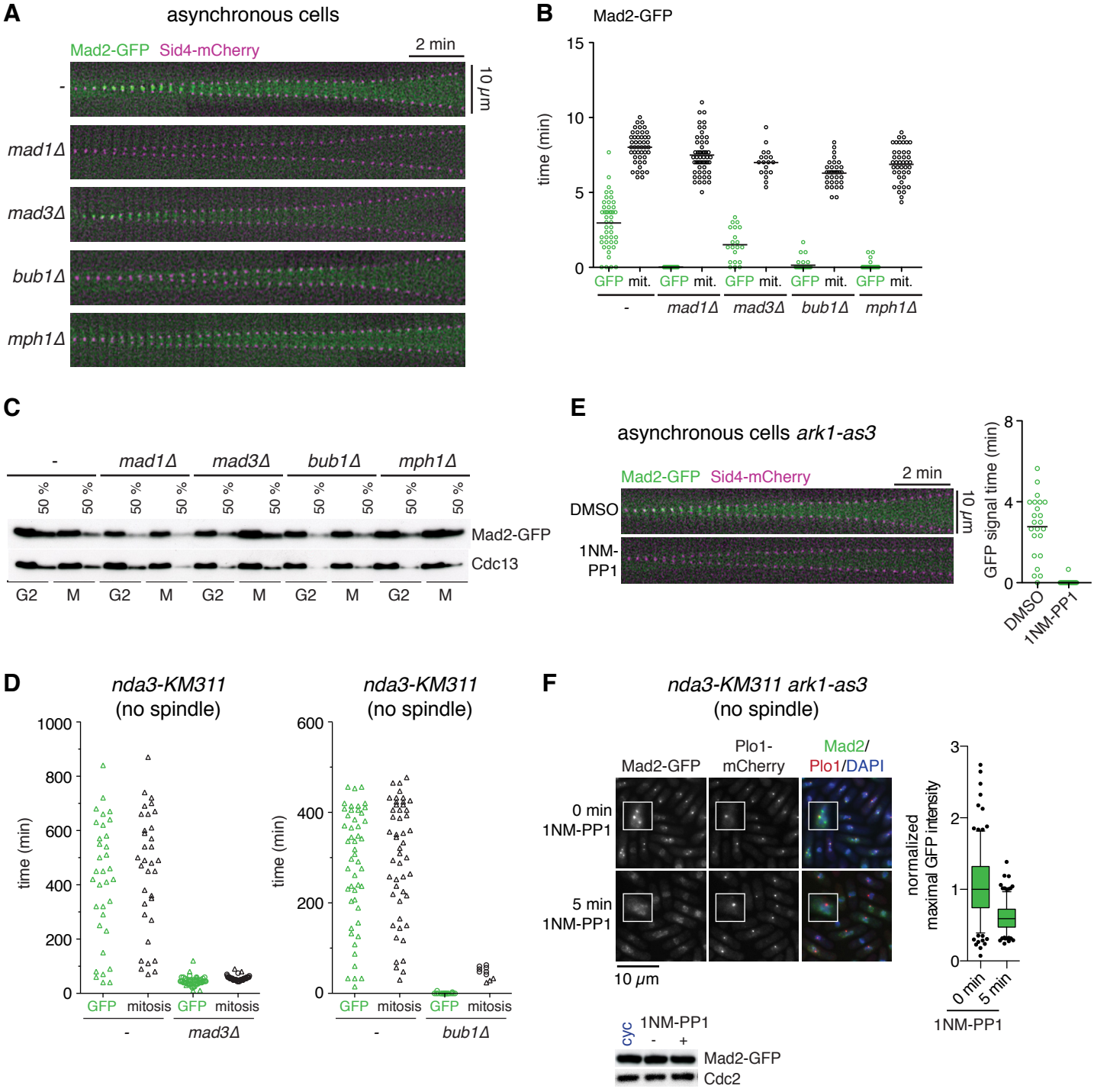
A
asynchronous cells
Mad2-GFP Sid4-mCherry
2 min
10 μm
-
mad1Δ
mad3Δ
bub1Δ
mph1Δ
B
Mad2-GFP
time (min)
15
10
5
0
GFP mit. GFP mit. GFP mit. GFP mit. GFP mit.
-
mad1Δ
mad3Δ
bub1Δ
mph1Δ
C
-
mad1Δ
mad3Δ
bub1Δ
mph1Δ
50 %
Mad2-GFP
Cdc13
G2 M G2 M G2 M G2 M G2 M
E
asynchronous cells ark1-as3
Mad2-GFP Sid4-mCherry
2 min
10 μm
DMSO
1NM-PP1
GFP signal time (min)
8
4
0
DMSO
1NM-PP1
D
nda3-KM311
(no spindle)
time (min)
1000
800
600
400
200
0
GFP mitosis GFP mitosis
-
mad3Δ
nda3-KM311
(no spindle)
600
400
200
0
GFP mitosis GFP mitosis
-
bub1Δ
F
nda3-KM311 ark1-as3
(no spindle)
Mad2-GFP
Plo1-mCherry
Mad2/Plo1/DAPI
0 min 1NM-PP1
5 min 1NM-PP1
10 μm
normalized maximal GFP intensity
3
2
1
0
0 min
5 min
1NM-PP1
cyc 1NM-PP1
- +
Mad2-GFP
Cdc2

Figure S8 | Kinetochore localization requirements for Mad2-GFP

A Mitotic localization of Mad2 in strains deleted of SAC genes. Cells were followed by live cell imaging with Sid4-mCherry as SPB marker. Exemplary kymographs of the spindle region are shown. In an unperturbed mitosis, Mad2-GFP is unable to localize to kinetochores in the absence of *mad1, bub1* or *mph1*.

B Quantitative analysis of the experiment in (A). The graph shows the time in mitosis, during which a localized GFP signal was observed (GFP), and the time in mitosis (mit.) from SPB separation to anaphase (SPB distance > 2.5 μm). Horizontal bars indicate the mean. Deletion of *mad1, bub1* or *mph1* impairs localization of Mad2, whereas deletion of *mad3* seems to slightly shorten the time during which a signal is observed. The signals observed in *bub1Δ* and *mph1Δ* cells may reflect localization of Mad2 to SPBs or the nuclear envelope, which cannot always be distinguished from kinetochore localization.

C Mad2 abundance is unchanged by deletion of *mad1, mad3, bub1* or *mph1.* The indicated strains were harvested in G2 and mitosis (M) and analysed by immunoblotting using anti-GFP and anti-Cdc13 antibodies. In every second lane, half the amount of sample (50 %) was loaded.

D Bub1 is required for Mad2 localization in cells lacking microtubules. Cells were grown at the restrictive temperature for *nda3-KM311*, which prevents microtubule formation, and were followed by live cell imaging. The graph shows the time in mitosis, during which a localized GFP signal was observed (GFP), and the duration of prometaphase (mitosis) as determined by the presence of Plo1-mCherry at SPBs. Circles indicate cells in which the entire mitosis was recorded, triangles indicate cells in which entry into mitosis but not exit from mitosis was recorded. Mad2 was unable to localize to unattached kinetochores in the absence of *bub1*, but was still able to localize in the absence of *mad3*. The mitotic delay was abrogated by deletion of either *mad3* or *bub1*.

E Inhibition of Ark1 abolishes kinetochore localization of Mad2. Cells were grown in the absence (DMSO) or presence of 1NM-PP1 to inhibit Ark1-as3, and were followed by live cell imaging. Exemplary kymographs of the spindle region are shown. The graph shows the time in mitosis, during which a localized GFP signal was observed. Horizontal bars indicate the mean.

F Ark1 is required to maintain Mad2 localization in cells lacking microtubules. Cells were grown at the restrictive temperature for *nda3-KM311,* which prevents microtubule formation, so that cells are halted in mitosis. Cells were treated with 1NM-PP1 and samples were fixed with methanol after 0 min and 5 min. DNA was stained with DAPI. Insets are 2.5-times magnified relative to the main picture. Maximal Mad2-GFP signal intensity in mitotic cells was quantified and corrected for background signal ($n > 210$ cells, box plot with whiskers from 5^{th} to 95^{th} percentile; data normalized to median of cells treated for 0 min). Protein abundance of Mad2-GFP in cycling cells (cyc) and mitotically arrested cells treated with (+) or without (-) 1NM-PP1 was determined by immunoblotting using anti-GFP and anti-Cdc2 (loading control) antibodies.

Figure S9

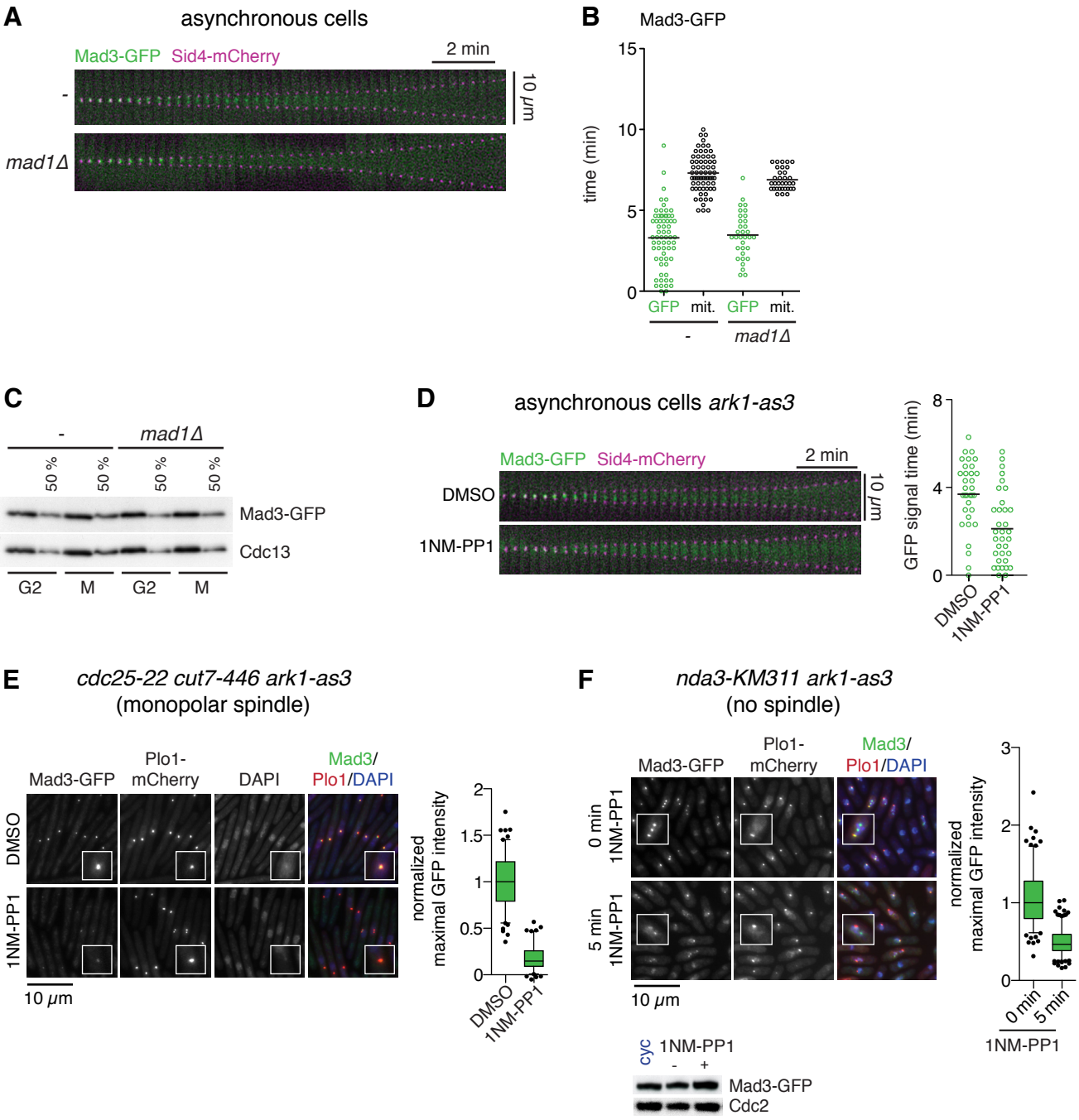
A
asynchronous cells
Mad3-GFP Sid4-mCherry
2 min
10 µm
-
mad1Δ
B
Mad3-GFP
time (min)
15
10
5
0
GFP mit. GFP mit.
-
mad1Δ
C
-
mad1Δ
50 %
50 %
50 %
50 %
Mad3-GFP
Cdc13
G2 M G2 M
D
asynchronous cells ark1-as3
Mad3-GFP Sid4-mCherry
2 min
10 µm
DMSO
1NM-PP1
GFP signal time (min)
8
4
0
DMSO
1NM-PP1
E
cdc25-22 cut7-446 ark1-as3
(monopolar spindle)
Mad3-GFP
Plo1-mCherry
DAPI
Mad3/Plo1/DAPI
DMSO
1NM-PP1
10 µm
normalized maximal GFP intensity
2
1.5
1
0.5
0
DMSO
1NM-PP1
F
nda3-KM311 ark1-as3
(no spindle)
Mad3-GFP
Plo1-mCherry
Mad3/Plo1/DAPI
0 min 1NM-PP1
5 min 1NM-PP1
10 µm
normalized maximal GFP intensity
3
2
1
0
0 min
5 min
1NM-PP1
cyc
1NM-PP1
-
+
Mad3-GFP
Cdc2

Figure S9 | Kinetochore localization requirements for Mad3-GFP

A Mitotic localization of Mad3 is preserved in *mad1Δ* cells. Cells were followed by live cell imaging with Sid4-mCherry as SPB marker. Exemplary kymographs of the spindle region are shown.

B Quantitative analysis of the experiment in (A). The graph shows the time in mitosis, during which a localized GFP signal was observed (GFP), and the time in mitosis (mit.) from SPB separation to anaphase (SPB distance > 2.5 μm). Horizontal bars indicate the mean.

C Mad3 abundance is unchanged by deletion of *mad1.* The indicated strains were harvested in G2 and mitosis (M) and analysed by immunoblotting using anti-GFP and anti-Cdc13 antibodies. In every second lane, half the amount of sample (50 %) was loaded.

D Inhibition of Ark1 reduces kinetochore localization of Mad3. Cells were grown in the absence (DMSO) or presence of 1NM-PP1 to inhibit Ark1-as3, and were followed by live cell imaging. Exemplary kymographs of the spindle region are shown. The graph shows the time in mitosis, during which a localized GFP signal was observed. Horizontal bars indicate the mean.

E Ark1 is required for Mad3 localization in cells with monopolar spindles. Cells were arrested in G2 and released into mitosis in the absence (DMSO) or presence of 1NM-PP1 to inhibit Ark1-as3. The presence of the *cut7-446* allele leads to monopolar spindles. Mitotic cells were fixed with methanol. DNA was stained with DAPI. Insets are 2.5-times magnified relative to the main picture. The maximal GFP intensity in mitotic cells was determined and corrected for background signal (n > 100 cells, box plot with whiskers from 5th to 95th percentile; data normalized to median of DMSO-treated cells).

F Ark1 is required to maintain Mad3 localization in cells lacking microtubules. Cells were grown at the restrictive temperature for *nda3-KM311,* which prevents microtubule formation, so that cells are halted in mitosis. Cells were treated with 1NM-PP1 and samples were fixed with methanol after 0 min and 5 min. DNA was stained with DAPI. Insets are 2.5-times magnified relative to the main picture. Maximal Mad3-GFP signal intensity in mitotic cells was quantified and corrected for background signal (n > 170 cells, box plot with whiskers from 5th to 95th percentile;

data normalized to median of cells treated for 0 min). Protein abundance of Mad3-GFP in cycling cells (cyc) and mitotically arrested cells treated with (+) or without (-) 1NM-PP1 was determined by immunoblotting using anti-GFP and anti-Cdc2 (loading control) antibodies.

Figure S10

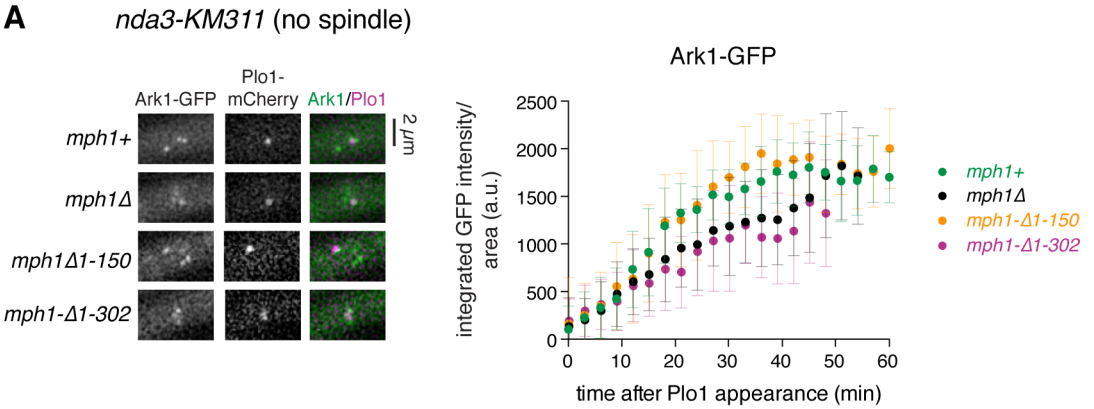

Figure S10 | Ark1-GFP localization in strains with N-terminally truncated Mph1

A Deletion of *mph1* or expression of *mph1-Δ1-302* impairs Ark1 centromere localization to a similar extent. Cells were followed by live cell imaging at the restrictive temperature for *nda3-KM311*. The graph on the right shows Ark1-GFP signals over time corrected for background (11 to 35 cells; error bars: s.d.; a.u. = arbitrary units). Both *mph1Δ* and *mph1-Δ1-302* slightly impair Ark1-GFP accumulation at centromeres, whereas Ark1-GFP accumulation in *mph1-Δ1-150* cells is similar to wild type (*mph1+*). Representative pictures of prometaphase nuclei are shown on the left. The data for *mph1+* and *mph1Δ* is also shown in Fig. 3E.

Figure S11 Kinetochore localization dependencies

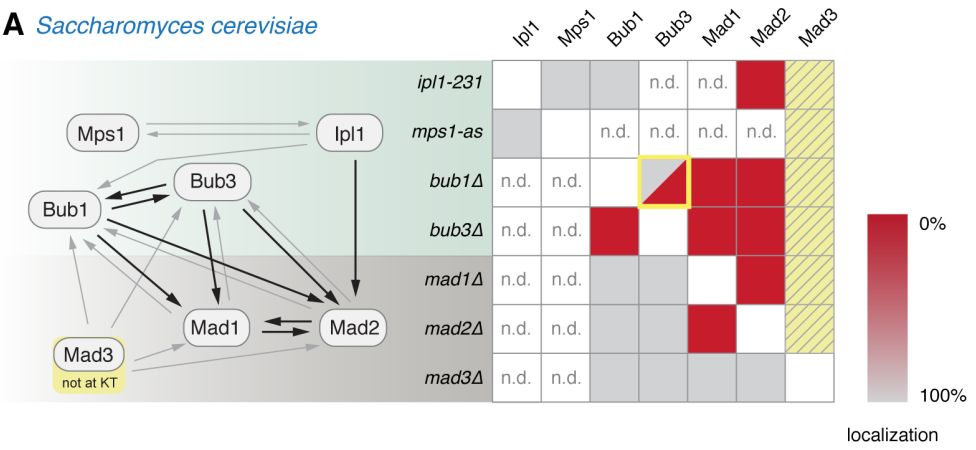

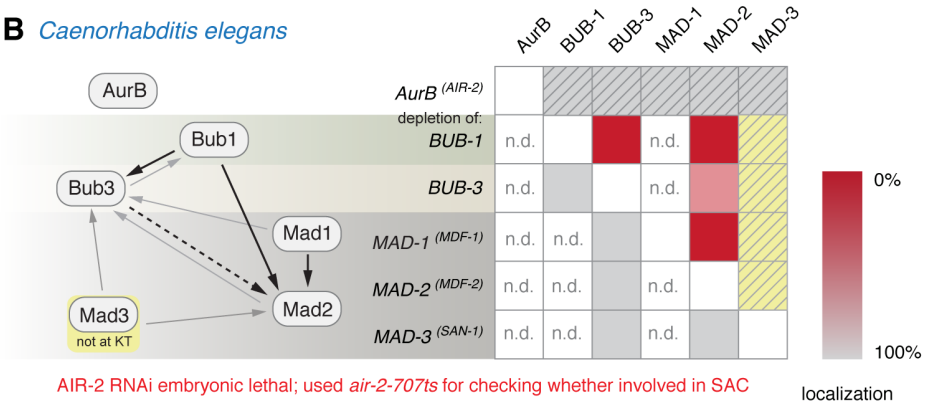

AIR-2 RNAi embryonic lethal; used *air-2-707ts* for checking whether involved in SAC

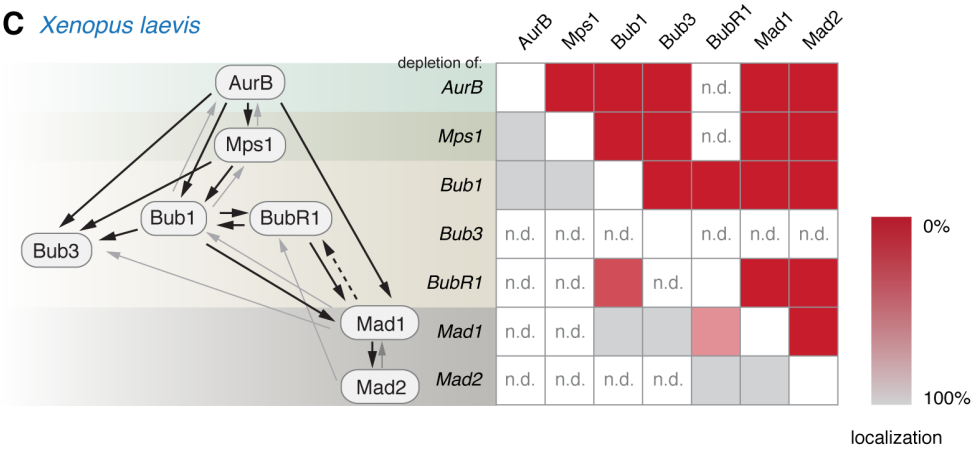

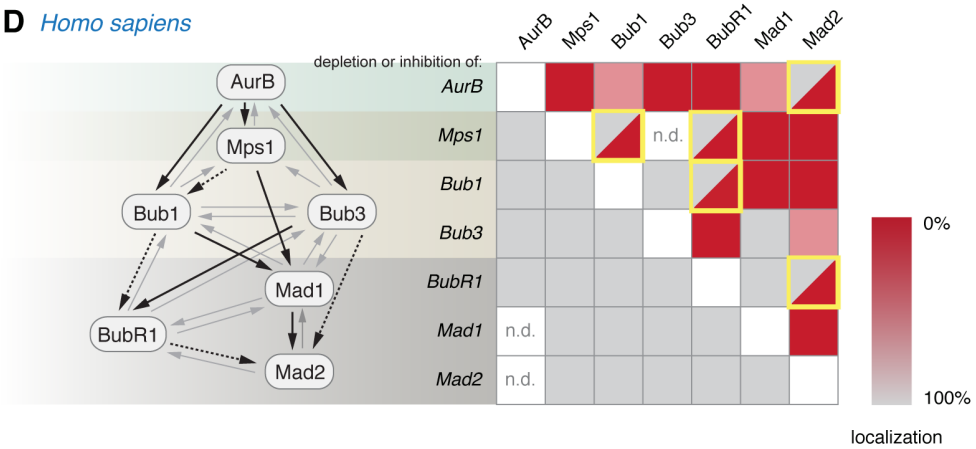

= contradiction in literature

= not at kinetochore

= no SAC defect if impaired

Figure S11 | Kinetochore localization dependencies of SAC proteins in other eukaryotes

A In *S. cerevisiae* Mad3 is not seen at kinetochores (Gillett et al., 2004). Mps1 and the Aurora kinase (Ipl1) have been reported to localize independently of each other (Maure et al., 2007). The influence of Mps1 on kinetochore localization of SAC proteins remains unclear, although *S. cerevisiae* Mps1 is required for the SAC (Weiss and Winey, 1996) and some data suggest that phosphorylation of the kinetochore protein Ndc80 by Mps1 contributes to SAC activity (Kemmler et al., 2009). Bub1 and Bub3 seem to depend on each other, and are required for the localization of Mad1 and Mad2 (Kerscher et al., 2003; Gillett et al., 2004).

B In *C. elegans* an Mps1 kinase has not been identified and Mad3 does not localize to kinetochores. Bub1 seems to be upstream of Bub3 and Mad2, but the role of Aurora B and other details are unclear (Essex et al., 2009).

C In *X. laevis* Aurora B is required for Mps1 localization, but not vice versa (Vigneron et al., 2004). Like in fission yeast, Aurora B and Mps1 are required for the localization of other downstream components, and there is feedback in localization between Mps1 and Bub1, as well as Bub1 and BubR1 (Abrieu et al., 2001; Chen, 2002; Vigneron et al., 2004). Mad1 localization requires Bub1, but not Mad2 (Sharp-Baker and Chen, 2001; Chen, 2002). Unlike in other organisms, BubR1 is at least partially required for Mad1 localization, which in turn reinforces BubR1 localization (Chen, 2002). As in fission yeast, Aurora B is most upstream and Mad2 most downstream.

D In human cells, Aurora B seems to be required for the efficient localization of Mps1 (Santaguida et al., 2010; Saurin et al., 2011). Whether Mps1 is required for the localization of Bub1 and BubR1 is not entirely clear ((Maciejowski et al., 2010) and references therein), but more recent data support a requirement for Mps1 (Maciejowski et al., 2010; Santaguida et al., 2010; Sliedrecht et al., 2010; Yamagishi et al., 2012). Bub1 is required for Mad1 localization, and Mad1 is required for Mad2 localization, but not vice versa (Martin-Lluesma et al., 2002; Meraldi et al., 2004; Klebig et al., 2009).

Supplementary Table 1 | *S. pombe* strains

Figure 1B

JY002	*h+*	*wild type*
SK820	*h-*	*leu1 mph1+-S(GGGGS)3-GFP<<kanR*
SL333	*h-*	*leu1-32 ade6-M216 ura4-D18 mph1Δ::mph1-Δ1-150-S(GGGGS)3-GFP<<kanR*
SL334	*h-*	*leu1-32 ade6-M216 ura4-D18 mph1Δ::mph1-Δ1-150-S(GGGGS)3-GFP<<kanR*
SL335	*h-*	*leu1-32 ade6-M216 ura4-D18 mph1Δ::mph1-Δ1-302-S(GGGGS)3-GFP<<kanR*
SL336	*h-*	*leu1-32 ade6-M216 ura4-D18 mph1Δ::mph1-Δ1-302-S(GGGGS)3-GFP<<kanR*

Figure 1C

SK847	*h-*	*leu1 mph1+-S(GGGGS)3-GFP<<kanR plo1+-mCherry<<natR nda3-KM311*
SL339	*h+*	*leu1 (ade6-M216?) mph1::mph1-Δ1-150-S(GGGGS)3-GFP<<kanR plo1+-mCherry<<natR nda3-KM311*
SL348'	*h+*	*leu1 (ade6-M216?) mph1::mph1-Δ1-302-S(GGGGS)3-GFP<<kanR plo1+-mCherry<<natR nda3-KM311*

Figure 1D

SH511	*h-*	*leu1 ade6-M216 nda3-KM311 plo1+-GFP<<kanR*
SH211	*h+*	*leu1 ade6-M216 nda3-KM311 plo1+-GFP<<kanR*
SK197	*h-*	*leu1 (ura4-D18?) ade6-M216 mph1Δ::ura4+ nda3-KM311 plo1+-GFP<<kanR*
SK197'	*h-*	*leu1 (ura4-D18?) ade6-M216 mph1Δ::ura4+ nda3-KM311 plo1+-GFP<<kanR*
SK191	*h+*	*leu1 ade6-M216 nda3-KM311 mph1Δ::mph1-Δ1-150 plo1+-GFP<<kanR*
SK193	*h-*	*leu1 ade6-M216 nda3-KM311 mph1Δ::mph1-Δ1-150 plo1+-GFP<<kanR*
SK198	*h+*	*leu1 ade6-M216 nda3-KM311 mph1Δ::mph1-Δ1-302 plo1+-GFP<<kanR*
SL305	*h-*	*leu1 ade6-M216 nda3-KM311 mph1Δ::mph1-Δ1-302 plo1+-GFP-kanR*

Figure 1E and 1G

SM751	*h-*	*leu1 (ade6-M216?) hygR<<Pnmt81<<mph1+-S(GGGGS)3-GFP<<kanR plo1+-mCherry<<natR*
SP211	*h-*	*leu1 ade6-M216 hygR<<Pnmt81<<mis12-(GGSG)2-mph1+-S(GGGGS)3-GFP<<kanR plo1+-mCherry<<natR*
SP213	*h-*	*leu1 hygR<<Pnmt81<<mis12-(GGSG)2-mph1+-S(GGGGS)3-GFP<<kanR mad2Δ::hygR plo1+-mCherry<<natR*
SM755	*h-*	*leu1 (ade6-M216?) hygR<<Pnmt81<<mph1-Δ1-302-S(GGGGS)3-GFP<<kanR plo1+-mCherry<<natR*
SP207	*h+*	*leu1 (ade6-M216?) hygR<<Pnmt81<<mis12-mph1-Δ1-302-S(GGGGS)3-GFP<<kanR plo1+-mCherry<<natR*
SP208	*h+*	*leu1 (ade6-M216?) hygR<<Pnmt81<<mis12-mph1-Δ1-302-S(GGGGS)3-GFP<<kanR mad2Δ::hygR plo1+-mCherry<<natR*

Figure 1F

SM751	*h-*	*leu1 (ade6-M216?) hygR<<Pnmt81<<mph1+-S(GGGGS)3-GFP<<kanR plo1+-mCherry<<natR*
SP211	*h-*	*leu1 ade6-M216 hygR<<Pnmt81<<mis12-(GGSG)2-mph1+-S(GGGGS)3-GFP<<kanR plo1+-mCherry<<natR*
SP213	*h-*	*leu1 hygR<<Pnmt81<<mis12-(GGSG)2-mph1+-S(GGGGS)3-GFP<<kanR mad2Δ::hygR plo1+-mCherry<<natR*
SM755	*h-*	*leu1 (ade6-M216?) hygR<<Pnmt81<<mph1-Δ1-302-S(GGGGS)3-GFP<<kanR plo1+-mCherry<<natR*
SP204	*h+*	*leu1 (ade6-M216?) hygR<<Pnmt81<<mis12-mph1-Δ1-302-S(GGGGS)3-GFP<<kanR plo1+-mCherry<<natR*
SP203	*h+*	*leu1 (ade6-M216?) hygR<<Pnmt81<<mis12-mph1-Δ1-302-S(GGGGS)3-GFP<<kanR mad2Δ::hygR plo1+-mCherry<<natR*

Figure 1H

SM760	*h+*	*leu1 (ade6-M216?) ura4-D18 nda3-KM311 hygR<<Pnmt81<<mis12-(GGSG)2-mph1-Δ1-302-S(GGGGS)3-GFP<<kanR plo1+-mCherry<<natR*

SM766	*h-*	*leu1 nda3-KM311 hygR<<Pnmt81<<mis12-(GGSG)2-mph1+-S(GGGGS)3-GFP<<kanR plo1+-mCherry<<natR*

Figure 2A

SM020	*h-*	*mph1+-S(GGGGS)3-GFP<<kanR mis6+-mCherry<<kanR sid4+-mCherry<<natR nda3-KM311*
SM021	*h-*	*ade6-M216 mph1+-S(GGGGS)3-GFP<<kanR mis6+-mCherry<<kanR sid4+-mCherry<<natR nda3-KM311*
SM022	*h+*	*leu1 mph1+-S(GGGGS)3-GFP<<kanR mis6+-mCherry<<kanR sid4+-mCherry<<natR nda3-KM311 bub3Δ::ura4+*
SM022'	*h+*	*leu1 mph1+-S(GGGGS)3-GFP<<kanR mis6+-mCherry<<kanR sid4+-mCherry<<natR nda3-KM311 bub3Δ::ura4+*

Figure 2B

SH511	*h-*	*leu1 ade6-M216 nda3-KM311 plo1+-GFP<<kanR*
SH211	*h+*	*leu1 ade6-M216 nda3-KM311 plo1+-GFP<<kanR*
SI438	*h-*	*leu1 ade6-M216 (ura4-D18?) bub3Δ::ura4+ nda3-KM311 plo1+-GFP<<kanR*
SL302	*h-*	*leu1 ade6-M216 (ura4-D18?) bub3Δ::ura4+ mph1Δ::ura4+ nda3-KM311 plo1+-GFP<<kanR*
SK197	*h-*	*leu1 (ura4-D18?) ade6-M216 mph1Δ::ura4+ nda3-KM311 plo1+-GFP<<kanR*
SK195	*h-*	*leu1 (ura4-D18?) ade6-M216 bub3Δ::ura4+ bub1Δ::ura4+ nda3-KM311 plo1+-GFP<<kanR*

Figure 2C

SI438	*h-*	*leu1 ade6-M216 (ura4-D18?) bub3Δ::ura4+ nda3-KM311 plo1-GFP<<kanR*
SK191	*h+*	*leu1 ade6-M216 nda3-KM311 mph1Δ::mph1-Δ1-150 plo1+-GFP<<kanR*
SK198	*h+*	*leu1 ade6-M216 mph1Δ::mph1-Δ1-302 nda3-KM311 plo1+-GFP<<kanR*
SP128	*h?*	*leu1 ade6-M216 (ura4-D18?) nda3-KM311 mph1Δ::mph1-Δ1-150 bubΔ3::ura4+ plo1+-GFP<<kanR*
SP132	*h+*	*leu1 ade6-M216 (ura4-D18?) mph1Δ::mph1-Δ1-302 bub3Δ::ura4+ nda3-KM311 plo1+-GFP<<kanR*
SP132'	*h+*	*leu1 ade6-M216 (ura4-D18?) mph1Δ::mph1-Δ1-302 bub3Δ::ura4+ nda3-KM311 plo1+-GFP<<kanR*

Figure 2D

SK402	*h+*	*ark1+-GFP<<kanR sid4+-mCherry<<natR*
SK523	*h+*	*ark1+-GFP<<kanR sid4+-mCherry<<natR bub3Δ::ura4+*

Figure 3A

SM128	*h+*	*hygR<<ark1-as3 plo1+-mCherry<<natR mph1+-GFP<<kanR cut7-446 cdc25-22*

Figure 3B

SK697	*h+*	*nda3-KM311 hygR<<ark1-as3 plo1+-mCherry<<natR mph1+-GFP<<kanR*

Figure 3C

SP165	*h-*	*leu1 ade6-M216 hygR<<ark1-as3 hygR>>Pnmt81>>mis12-(GGSG)2-mph1-Δ1-302-S(GGGGS)3-GFP<<kanR plo1+-mCherry<<natR nda3-KM311*
SK698	*h-*	*leu1 hygR<<ark1-as3 mph1+-GFP<<kanR plo1+-mCherry<<natR nda3-KM311*

Figure 3D

SK402	*h+*	*ark1+-GFP<<kanR sid4+-mCherry<<natR*
SK555	*h-*	*leu1 ark1+-GFP<<kanR sid4+-mCherry<<natR mph1Δ::ura4+*

Figure 3E

SL894	*h+*	*leu1 ade6-M210 nda3-KM311 plo1+-mCherry<<natR ark1+-GFP<<kanR*
SL895	*h-*	*leu1 ade6-M210 nda3-KM311 plo1+-mCherry<<natR ark1+-GFP<<kanR*
SL400	*h+*	*leu1 (ura4-D18?) ade6-M216 nda3-KM311 plo1+-mCherry<<natR ark1+-GFP<<kanR mph1Δ::ura4+*
SM701	*h-*	*leu1 (ura4-D18?) ade6-M210 nda3-KM311 plo1+-mCherry<<natR ark1+-GFP<<kanR mph1Δ::ura4+*

Figure 4B

SL389	*h+*	*leu1 nda3-KM311 plo1+-mCherry<<natR bub1+-GFP<<kanR*
SL901	*h+*	*leu1 nda3-KM311 plo1+-mCherry<<natR bub1+-GFP<<kanR*
SL399	*h-*	*leu1 (ura4-D18?) mph1Δ::ura4+ nda3-KM311 plo1+-mCherry<<natR bub1+-GFP<<kanR*
SL374	*h-*	*leu1 mph1Δ::mph1-Δ1-150 nda3-KM311 plo1+-mCherry<<natR bub1+-GFP<<kanR*

SL380	*h+*	*leu1 mph1Δ::mph1-Δ1-302 nda3-KM311 plo1+-mCherry<<natR bub1+-GFP<<kanR*
SL381	*h-*	*leu1 mph1Δ::mph1-Δ1-302 nda3-KM311 plo1+-mCherry<<natR bub1+-GFP<<kanR*

Figure 4C

SK891	*h+*	*leu1 mad1+-GFP<<kanR plo1+-mCherry<<natR nda3-KM311*
SL386	*h+*	*leu1 (ura4-D18?) mph1Δ::ura4+ nda3-KM311 plo1+-mCherry<<natR mad1+-GFP<<kanR*
SL383	*h+*	*leu1 mph1Δ::mph1-Δ1-302 nda3-KM311 plo1+-mCherry<<natR mad1+-GFP<<kanR*
SL384	*h-*	*leu1 ade6-M216 mph1Δ::mph1-Δ1-302 nda3-KM311 plo1+-mCherry<<natR mad1+-GFP<<kanR*
SL377	*h-*	*leu1 ade6-M216 mph1Δ::mph1-Δ1-150 nda3-KM311 plo1+-mCherry<<natR mad1+-GFP<<kanR*
SL378	*h+*	*leu1 mph1::mph1Δ-Δ1-150 nda3-KM311 plo1+-mCherry<<natR mad1+-GFP<<kanR*

Figure S1A

SK846	*h+*	*leu1 mph1+-S(GGGGS)3-GFP<<kanR plo1+-mCherry<<natR nda3-KM311*
SK847	*h-*	*leu1 mph1+-S(GGGGS)3-GFP<<kanR plo1+-mCherry<<natR nda3-KM311*
SK882	*h+*	*leu1 (ura4-D18?) mph1+-S(GGGGS)3-GFP<<kanR plo1+-mCherry<<natR nda3-KM311 bub3Δ::ura4+*
SK883	*h-*	*leu1 (ura4-D18?) mph1+-S(GGGGS)3-GFP<<kanR plo1+-mCherry<<natR nda3-KM311 bub3Δ::ura4+*
SM709	*h+*	*leu1 ade6-M216 nda3-KM311 plo1+-mCherry<<natR mph1+-GFP<<kanR mad1Δ::ura4+*
SM709'	*h+*	*leu1 ade6-M216 nda3-KM311 plo1+-mCherry<<natR mph1+-GFP<<kanR mad1Δ::ura4+*

Figure S1B

SK847	*h-*	*leu1 mph1+-S(GGGGS)3-GFP<<kanR plo1+-mCherry<<natR nda3-KM311*
SK882	*h+*	*leu1 (ura4-D18?) mph1+-S(GGGGS)3-GFP<<kanR plo1+-mCherry<<natR nda3-KM311 bub3Δ::ura4+*

Figure S1C

SP434'	*h+*	*mph1+-GFP<<kanR plo1+-mCherry<<natR cdc25-22 cut7-446*

Figure S1D

SK699	*h+*	*mph1+-GFP<<kanR plo1+-mCherry<<natR nda3-KM311*

Figure S2A

SK402	*h+*	*ark1+-GFP<<kanR sid4+-mCherry<<natR*
SK526	*h-*	*leu1 (ura4-D18?) ark1+-GFP<<kanR sid4+-mCherry<<natR mad1Δ::ura4+*
SM031	*h+?*	*leu1 ade6-M216 (ura4-D18?) his1-102 ark1+-GFP<<kanR sid4+-mCherry<<natR bub1Δ::ura4+*
SP225	*h+*	*ade6-M210/M216 ark1+-GFP<<kanR sid4+-mCherry<<natR mph1Δ::ura4+ bub1Δ::natR*
SP227	*h+*	*ark1+-GFP<<kanR sid4+-mCherry<<natR mph1Δ::ura4+ bub3Δ::ura4+*

Figure S2B

SK402	*h+*	*ark1+-GFP<<kanR sid4+-mCherry<<natR*
SM031	*h+?*	*leu1 ade6-M216 (ura4-D18?) his1-102 ark1+-GFP<<kanR sid4+-mCherry<<natR bub1Δ::ura4+*
SK523	*h+*	*ark1+-GFP<<kanR sid4+-mCherry<<natR bub3Δ::ura4+*
SK555	*h-*	*leu1 ark1+-GFP<<kanR sid4+-mCherry<<natR mph1Δ::ura4+*
SP225	*h+*	*ade6-M210/M216 ark1+-GFP<<kanR sid4+-mCherry<<natR mph1Δ::ura4+ bub1Δ::natR*
SP227	*h+*	*ark1+-GFP<<kanR sid4+-mCherry<<natR mph1Δ::ura4+ bub3Δ::ura4+*
SK526	*h-*	*leu1 (ura4-D18?) ark1+-GFP<<kanR sid4+-mCherry<<natR mad1Δ::ura4+*

Figure S2C

SL896	*h-*	*leu1 ark1+-GFP<<kanR plo1+-mCherry<<natR nda3-KM311*
SP170	*h+*	*leu1 ade6-M210 ark1+-GFP<<kanR plo1+-mCherry<<natR nda3-KM311 bub1Δ::ura4+*
SP157	*h-*	*leu1 ark1+-GFP<<kanR plo1+-mCherry<<natR nda3-KM311 bub3Δ::ura4+*
SP158	*h+*	*leu1 ade6-M210 ark1+-GFP<<kanR plo1+-mCherry<<natR nda3-KM311 bub3Δ::ura4+*
SL400	*h+*	*leu1 (ura4-D18?) ade6-M216 ark1+-GFP<<kanR plo1+-mCherry<<natR nda3-KM311 mph1Δ::ura4+*

Figure S2D

SK402	*h+*	*ark1+-GFP<<kanR sid4+-mCherry<<natR*
SK526	*h-*	*leu1 (ura4-D18?) ark1+-GFP<<kanR sid4+-mCherry<<natR mad1Δ::ura4+*
SK527	*h+*	*(ura4-D18?) ark1+-GFP<<kanR sid4+-mCherry<<natR mad1Δ::ura4+*

SM031	*h+?*	*leu1 ade6-M216 (ura4-D18?) his1-102 ark1+-GFP<<kanR sid4+-mCherry<<natR bub1Δ::ura4+*
SK523	*h+*	*ark1+-GFP<<kanR sid4+-mCherry<<natR bub3Δ::ura4+*
SK524	*h-*	*leu1 ark1+-GFP<<kanR sid4+-mCherry<<natR bub3Δ::ura4+*
SK555	*h-*	*leu1 ark1+-GFP<<kanR sid4+-mCherry<<natR mph1Δ::ura4+*
SK555'	*h-*	*leu1 ark1+-GFP<<kanR sid4+-mCherry<<natR mph1Δ::ura4+*
SP225	*h+*	*ade6-M210/M216 ark1+-GFP<<kanR sid4+-mCherry<<natR mph1Δ::ura4+ bub1Δ::natR*
SP227	*h+*	*ark1+-GFP<<kanR sid4+-mCherry<<natR mph1Δ::ura4+ bub3Δ::ura4+*

Figure S2E

SK402	*h+*	*ark1+-GFP<<kanR sid4+-mCherry<<natR*
SK526	*h-*	*leu1 (ura4-D18?) ark1+-GFP<<kanR sid4+-mCherry<<natR mad1Δ::ura4+*
SK523	*h+*	*ark1+-GFP<<kanR sid4+-mCherry<<natR bub3Δ::ura4+*
SM031	*h+?*	*leu1 ade6-M216 (ura4-D18?) his1-102 ark1+-GFP<<kanR sid4+-mCherry<<natR bub1Δ::ura4+*
SK555	*h-*	*leu1 ark1+-GFP<<kanR sid4+-mCherry<<natR mph1Δ::ura4+*

Figure S3

SK671	*h-*	*lys1 hygR<<ark1-as3 plo1+-mCherry<<natR mad1+-GFP<<kanR nda3-KM311*
SK891	*h+*	*leu1 mad1+-GFP<<kanR plo1+-mCherry<<natR nda3-KM311*

Figure S4A

SP168	*h-*	*leu1 hygR<<ark1-as3 hygR>>Pnmt81>>mis12-(GGSG)2-mph1+-S(GGGGS)3-GFP<<kanR plo1+-mCherry<<natR nda3-KM311*
SM766	*h-*	*leu1 hygR>>Pnmt81>>mis12-(GGSG)2-mph1+-S(GGGGS)3-GFP<<kanR plo1+-mCherry<<natR nda3-KM311*

Figure S4B and S4C

SP165	*h-*	*leu1 ade6-M216 hygR<<ark1-as3 hygR>>Pnmt81>>mis12-(GGSG)2-mph1-Δ1-302-S(GGGGS)3-GFP<<kanR plo1+-mCherry<<natR nda3-KM311*
SK698	*h-*	*leu1 hygR<<ark1-as3 mph1+-GFP<<kanR plo1+-mCherry<<natR nda3-KM311*
SP168	*h-*	*leu1 hygR<<ark1-as3 hygR>>Pnmt81>>mis12-(GGSG)2-mph1+-S(GGGGS)3-GFP<<kanR plo1+-mCherry<<natR nda3-KM311*
SM766	*h-*	*leu1 hygR>>Pnmt81>>mis12-(GGSG)2-mph1+-S(GGGGS)3-GFP<<kanR plo1+-mCherry<<natR nda3-KM311*

Figure S5A – S5C

SK415	*h+*	*bub1+-GFP<<kanR sid4+-mCherry<<natR*
SL712	*h-*	*leu1 (ura4-D18?) bub1+-GFP<<kanR sid4+-mCherry<<natR mad1Δ::ura4+*
SL714	*h-*	*leu1 (ura4-D18?) bub1+-GFP<<kanR sid4+-mCherry<<natR mph1Δ::ura4+*

Figure S5D

SK607	*h+*	*leu1 bub1+-GFP<<kanR sid4+-mCherry<<natR hygR<<ark1-as3*
SK608	*h-*	*bub1+-GFP<<kanR sid4+-mCherry<<natR hygR<<ark1-as3*

Figure S5E

SL544	*h+*	*hygR<<ark1-as3 plo1+-mCherry<<natR bub1+-GFP<<kanR cut7-446 cdc25-22*

Figure S5F

SK676	*h-*	*lys1 hygR<<ark1-as3 plo1+-mCherry<<natR bub1+-GFP<<kanR nda3-KM311*

Figure S5G

SM520	*h+*	*leu1 bub1+-GFP<<kanR plo1+-mCherry<<natR nda3-KM311*

Figure S6A – S6C

SK010'	*h-*	*leu1 ade6-M216 sid4+-mCherry<<natR bub3+-S(GGGGS)3-3xmyeGFP<<kanR*
SK517	*h+*	*(ade6-M210?) bub3+-S(GGGGS)3-3xmyeGFP<<kanR sid4+-mCherry<<natR mad3Δ::ura4+*
SK517'	*h+*	*(ade6-M210?) bub3+-S(GGGGS)3-3xmyeGFP<<kanR sid4+-mCherry<<natR mad3Δ::ura4+*
SL716	*h-*	*leu1 (ura4-D18?) sid4+-mCherry<<natR bub3+-S(GGGGS)3-3xmyeGFP<<kanR mph1Δ::ura4+*

Figure S6D

SK609	*h-*	*leu1 ade6-M210 bub3+-S(GGGGS)3-2xmyeGFP<<kanR sid4+-mCherry<<natR hygR<<ark1-as3*

Figure S6E

SL546	*h+*	*hygR<<ark1-as3 plo1+-mCherry<<natR bub3+-S(GGGGS)3-3xmyeGFP<<kanR cdc25-22 cut7-446*

Figure S6F

SK678	*h+*	*lys1 hygR<<ark1-as3 plo1+-mCherry<<natR bub3+-S(GGGGS)3-2xmye-GFP<<kanR nda3-KM311*

Figure S6G

SK410	*h-*	*leu1 ade6-M216 bub3+-S(GGGGS)3-2xmyeGFP<<kanR sid4+-mCherry<<natR*
SK010'	*h-*	*leu1 ade6-M216 sid4+-mCherry<<natR bub3-S(GGGGS)3-3xmyeGFP<<kanR*
SK609	*h-*	*leu1 ade6-M210 hygR<<ark1-as3 sid4+-mCherry<<natR bub3+-S(GGGGS)3-2xmyeGFP<<kanR*
SK678	*h+*	*lys1 hygR<<ark1-as3 plo1+-mCherry<<natR bub3+-S(GGGGS)3-2xmye-GFP<<kanR nda3-KM311*
SK679	*h-*	*lys1 hygR<<ark1-as3 plo1+-mCherry<<natR bub3+-S(GGGGS)3-2xmye-GFP<<kanR nda3-KM311*
SL546	*h+*	*hygR<<ark1-as3 plo1+-mCherry<<natR bub3+-S(GGGGS)3-3xmyeGFP<<kanR cdc25-22 cut7-446*

Figure S7A – S7C

SK094	*h+*	*mad1+-GFP<<kanR sid4+-mCherry<<natR*
SK461	*h-*	*mad1+-GFP<<kanR sid4+-mCherry<<natR mad2Δ::ura4+*
SK462	*h-*	*leu1 mad1+-GFP<<kanR sid4+-mCherry<<natR mad2Δ::ura4+*
SK487	*h+*	*mad1+-GFP<<kanR sid4+-mCherry<<natR mad3Δ::ura4+*
SK488	*h-*	*leu1 ade6-M210 mad1+-GFP<<kanR sid4+-mCherry<<natR mad3Δ::ura4+*
SK507	*h+*	*ade6-M216 mad1+-GFP<<kanR sid4+-mCherry<<natR bub1Δ::ura4+*
SK456	*h-*	*leu1 ade6-M216 mad1+-GFP<<kanR sid4+-mCherry<<natR mph1Δ::ura4+*
SK456'	*h-*	*leu1 ade6-M216 mad1+-GFP<<kanR sid4+-mCherry<<natR mph1Δ::ura4+*

Figure S7D

SK891	*h+*	*leu1 mad1+-GFP<<kanR plo1+-mCherry<<natR nda3-KM311*
SM025	*h+*	*leu1 ade6-M210 mad1+-GFP<<kanR plo1+-mCherry<<natR nda3-KM311 mad3Δ::ura4+*
SM025'	*h+*	*leu1 ade6-M210 mad1+-GFP<<kanR plo1+-mCherry<<natR nda3-KM311 mad3Δ::ura4+*
SL777	*h+*	*leu1 (ura4-D18?) (his2-102?) ade6-M216 plo1+-mCherry<<natR mad1+-GFP<<kanR bub1Δ::ura4+ nda3-KM311*

Figure S7E

SK601	*h-*	*leu1 mad1+-GFP<<kanR sid4+-mCherry<<natR hygR<<ark1-as3*

Figure S7F

SK671	*h-*	*lys1 hygR<<ark1-as3 plo1+-mCherry<<natR mad1+-GFP<<kanR nda3-KM311*

Figure S7G

SK891	*h+*	*leu1 mad1+-GFP<<kanR plo1+-mCherry<<natR nda3-KM311*

Figure S8A – S8C

SK100	*h+*	*mad2+-GFP<<kanR sid4+-mCherry<<natR*
SK458	*h+*	*leu1 (ura4-D18?) mad2+-GFP<<kanR sid4+-mCherry<<natR mad1Δ::ura4+*
SK459	*h+*	*(ura4-D18?) mad2+-GFP<<kanR sid4+-mCherry<<natR mad1Δ::ura4+*
SK510	*h+*	*ade6-M216 mad2+-GFP<<kanR sid4+-mCherry<<natR mad3Δ::ura4+*
SK511	*h-*	*leu1 mad2+-GFP<<kanR sid4+-mCherry<<natR mad3Δ::ura4+*
SK508	*h-*	*leu1 ade6-M216 mad2+-GFP<<kanR sid4+-mCherry<<natR bub1Δ::ura4+*
SK509	*h+*	*ade6-M216 mad2+-GFP<<kanR sid4+-mCherry<<natR bub1Δ::ura4+*
SK483	*h-*	*leu1 mad2+-GFP<<kanR sid4+-mCherry<<natR mph1Δ::ura4+*
SK483'	*h-*	*leu1 mad2+-GFP<<kanR sid4+-mCherry<<natR mph1Δ::ura4+*

Figure S8D

SK842	*h+*	*leu1 mad2+-GFP<<kanR plo1+-mCherry<<natR nda3-KM311*
SM027	*h-*	*leu1 ade6-M210 mad2+-GFP<<kanR plo1+-mCherry<<natR nda3-KM311 mad3Δ::ura4+*

SM028	*h+*	*leu1 ade6-M210 mad2+-GFP<<kanR plo1+-mCherry<<natR nda3-KM311 mad3Δ::ura4+*
SL724	*h+*	*leu1 ade6-M216 his2? mad2+-GFP<<kanR plo1+-mCherry<<natR nda3-KM311 bub1Δ::ura4+*

Figure S8E

SK603	*h+*	*mad2+-GFP<<kanR sid4+-mCherry<<natR hygR<<ark1-as3*

Figure S8F

SK673	*h-*	*lys1 hygR<<ark1-as3 plo1+-mCherry<<natR mad2+-GFP<<kanR nda3-KM311*

Figure S9A – S9C

SK404	*h+*	*leu1 mad3+-GFP<<kanR sid4+-mCherry<<natR*
SM029	*h+*	*leu1 (ura4-D18?) mad3+-GFP<<kanR sid4+-mCherry<<natR mad1Δ::ura4+*
SM029'	*h+*	*leu1 (ura4-D18?) mad3+-GFP<<kanR sid4+-mCherry<<natR mad1Δ::ura4+*

Figure S9D

SK605	*h+*	*leu1 mad3+-GFP<<kanR sid4+-mCherry<<natR hygR<<ark1-as3*
SK605'	*h+*	*leu1 mad3+-GFP<<kanR sid4+-mCherry<<natR hygR<<ark1-as3*

Figure S9E

SL552'	*h+*	*lys1 hygR<<ark1-as3 plo1+-mCherry<<natR mad3+-GFP<<kanR cdc25-22 cut7-446*

Figure S9F

SK675	*h-*	*lys1 hygR<<ark1-as3 plo1+-mCherry<<natR mad3+-GFP<<kanR nda3-KM311*

Figure S10A

SL894	*h+*	*leu1 ade6-M210 nda3-KM311 plo1+-mCherry<<natR ark1+-GFP<<kanR*
SL895	*h-*	*leu1 ade6-M210 nda3-KM311 plo1+-mCherry<<natR ark1+-GFP<<kanR*
SL400	*h+*	*leu1 (ura4-D18?) ade6-M216 mph1Δ::ura4+ nda3-KM311 plo1+-mCherry<<natR ark1+-GFP<<kanR*
SM701	*h-*	*leu1 (ura4-D18?) ade6-M210 mph1Δ::ura4+ nda3-KM311 plo1+-mCherry<<natR ark1+-GFP<<kanR*
SL375	*h-*	*leu1 ade6-M210 mph1Δ::mph1-Δ1-150 nda3-KM311 plo1+-mCherry<<natR ark1+-GFP<<kanR*
SL376	*h+*	*leu1 ade6-M216 mph1Δ::mph1-Δ1-150 nda3-KM311 plo1+-mCherry<<natR ark1+-GFP<<kanR*
SL382'	*h-*	*leu1 ade6-M216 mph1Δ::mph1-Δ1-302 nda3-KM311 plo1+-mCherry<<natR ark1+-GFP<<kanR*

S. pombe strains with the following mutations or modifications have been described previously: *nda3-KM311* (PMID: 6094012) *cdc25-22 (*PMID: 3955656*), cut7-446 (*PMID: 2145514*), plo1+-GFP<<kanR (*PMID: 17322402*), mad1+-GFP<<kanR, mad2+-GFP<<kanR, mad3+-GFP<<kanR, bub3+-S(GGGGS)3-2xGFP<<kanR (*PMID: 19680287*), mad1Δ::ura4+*, *mad3Δ::ura4+* (PMID: 15509783), *mad2Δ::ura4+ (*PMID: 9223296, 9461438*), bub1Δ::ura4+ (*PMID: 9864354*), bub3Δ::ura4+ (*PMID: 11909965*), mph1Δ::ura4+ (*PMID: 9601094*), bub1+-GFP<<kanR (*PMID: 12606573*), hphR<<ark1-as3 (*PMID: 17932486*), gtb1-93 (*PMID: 15280226*), fin1Δ::ura4+ (*PMID: 9490640*), mal3Δ (*PMID: 9348288*).*

2.2 Mad1 actively promotes checkpoint signalling in addition to recruiting Mad1:Mad2 to kinetochores

Stephanie Heinrich[1], Katharina Sewart[1], Hanna Windecker[1,2], Maria Langegger[1], Nadine Schmidt[1], Silke Hauf[1]

[1]Friedrich Miescher Laboratory of the Max Planck Society, 72076 Tübingen, Germany
[2]Present address: IMB (Institute of Molecular Biology), Ackermannweg 4, 55128 Mainz, Germany

Correspondence: silke.hauf@tuebingen.mpg.de

Submitted as manuscript to **EMBO Reports**

Author contributions:

I performed experiments and analysed the data shown in Fig. 1B,C,E; Fig. 2A – C,D(left); Fig. 3B,D; Fig. S1A,B,E,F; Fig. S2C–E and Fig. S3A(left). I analysed the data from imaging experiments shown in Fig. 3C,G and Fig. S4B,C (experiments have been performed by **Katharina Sewart**). In addition, I contributed to writing the manuscript together with Silke Hauf and input by Katharina Sewart, Maria Langegger and Nadine Schmidt.

Katharina Sewart performed experiments and analysed the data shown in Fig. 1F,G; Fig. 2D(right); Fig. 3E,F,G,H; Fig. S1D; Fig. S2B; Fig. S3A(right),B and Fig. S4D,E.

Hanna Windecker constructed the Mad1-RLK/AAA mutant, and performed experiments in Fig. 1D and Fig. S1C.

Maria Langegger performed the experiments and analysed the data shown in Fig. 1E (Mad1-RLK/ALA mutant); Fig. S2F and Fig. S4A.

Nadine Schmidt performed experiments and analysed the data shown in Fig. 1 H–K and Fig. S1G–J.

Silke Hauf supervised the study.

Mad1 actively promotes checkpoint signalling in addition to recruiting Mad1:Mad2 to kinetochores

Stephanie Heinrich, Katharina Sewart, Hanna Windecker[#], Maria Langegger, Nadine Schmidt, and Silke Hauf*

Friedrich Miescher Laboratory of the Max Planck Society, Spemannstrasse 39, 72076 Tübingen, Germany

[#]*current address: IMB (Institute of Molecular Biology), Ackermannweg 4, 55128 Mainz, Germany*

*Correspondence: silke.hauf@tuebingen.mpg.de

Running title: Mad1 C-terminus promotes checkpoint activity

Abstract

The spindle assembly checkpoint inhibits anaphase until chromosomes have become attached to the mitotic spindle. The checkpoint protein Mad1 binds Mad2 and provides a platform for Mad2:Mad2 dimerization at unattached kinetochores, which enables Mad2 to delay anaphase. Here, we show that Mad1 has a crucial role in signalling beyond presenting Mad2. Mutations within the Mad1 C-terminal domain (CTD) that impair kinetochore localization fail to provide checkpoint activity when artificially tethered to kinetochores, despite recruiting Mad2. Furthermore, specific mutations within the CTD head preserve Mad1:Mad2 kinetochore localization, but abolish checkpoint activity. Hence, the Mad1-CTD has a previously unrecognized, active role in checkpoint signalling.

Keywords: spindle assembly checkpoint / kinetochore / Mad1 / mitosis / fission yeast

Introduction

Mad1 is part of the spindle assembly checkpoint, a conserved mitotic signalling pathway that protects genome integrity. The checkpoint monitors chromosome attachment to the mitotic spindle and delays anaphase until all chromosomes have achieved proper attachment [1]. Checkpoint proteins, including Mad1, localize to unattached kinetochores, and initiate a signalling cascade that leads to the inhibition of Cdc20 (Slp1 in *S. pombe*). Cdc20 is an essential co-activator of the anaphase-promoting complex/cyclosome (APC/C) and its inhibition prevents anaphase [2].

Mad1 forms a tetrameric complex with the checkpoint protein Mad2 [3]. At unattached kinetochores, Mad1-bound Mad2 dimerizes with soluble Mad2 to induce binding of the latter to Cdc20 [1, 4]. This enables additional binding of Mad3 (BubR1 in many organisms) to Cdc20 to form the mitotic checkpoint complex (MCC), which is a potent inhibitor of the APC/C [2, 5, 6]. In *S. pombe*, the Aurora B kinase Ark1, the checkpoint kinase Mph1 (Mps1 in other species), Bub1 and Bub3, are required to bring Mad1:Mad2 to unattached kinetochores [7]. Similar dependencies exist in other organisms [1]. Human Mps1 is also required to allow dimerization between Mad1-bound and soluble Mad2 at kinetochores [8]. Consistent with the important role of the Mad1:Mad2 complex in initiating Cdc20 inhibition, preventing the Mad1:Mad2 interaction abolishes checkpoint activity ([9, 10], Kruse *et al.*, accompanying manuscript, Heinrich *et al.*, in press). Hence, Mad1 is important to present Mad2 at unattached kinetochores.

Mad1 is a protein of approx. 80 kDa; the stretch that binds Mad2 is less than 20 amino acids long. This raises the question whether the remaining parts only have a structural role or contribute to checkpoint signalling. The Mad1 part that lies N-terminal to the Mad2-binding site is predicted to form a long coiled-coil. The structure of the C-terminal end of this coiled-coil (α1) together with the Mad2-binding site bound to Mad2 as well as a C-terminal helix (α2) has been solved and indicates that the N-terminal coiled-coil mediates Mad1 dimerization [3]. A more recent structure of the part of Mad1 following α2 showed another intermolecular coiled-coil (α3) and a globular head [11] (see Fig 1A and 4A). The Mad1 C-terminus has repeatedly been implicated in kinetochore binding [12, 13], whereas some studies have suggested a role for the N-terminus [14, 15]. These observations indicate that the structured parts of Mad1 are required to bring the Mad1:Mad2 complex to kinetochores.

Here, we show that the Mad1 C-terminus promotes checkpoint activity in addition to its role in kinetochore localization. Artificial tethering of kinetochore-binding deficient C-terminal mutants does not restore checkpoint activity, although Mad2 is co-recruited. Furthermore, specific mutations within the Mad1 C-terminal head leave kinetochore localization and Mad1:Mad2 interaction intact, but do not provide checkpoint activity. Hence, the Mad1 C-terminus is not only required for bringing Mad2 to kinetochores, but has an additional, previously unrecognized role in promoting checkpoint activity.

Results and Discussion

Mad1-RLK motif and Bub1-conserved motif 1 are required for kinetochore localization of Mad1 and checkpoint activity

To assess potential functions of Mad1, we initially focused on the highly conserved RLK motif (amino acid (aa) 580-582) within α3 [16]. In budding yeast, mutation of this motif abolished checkpoint function [16]; in human cells, mutation abolished Mad1 kinetochore localization with unknown effects on checkpoint activity [11]. When we mutated all motif residues to alanine in *S. pombe*, kinetochore localization of both Mad1 and Mad2 was impaired (Fig 1A-D), whereas localization to the nuclear envelope stayed intact (supplementary Fig S1A,E). Checkpoint activity was lost in the Mad1-RLK/AAA mutant (Fig 1E), although kinetochore localization of Ark1, Bub1, Bub3 and Mad3 was preserved (Fig 1D, supplementary Fig S1C), and although the protein was present at normal levels (Fig 1F) and the Mad1:Mad2 interaction was intact (Fig 1G). This suggests that the failure to bring Mad1:Mad2 to kinetochores could cause the checkpoint defect. A similar concomitant loss of Mad1 localization and checkpoint activity occurred when only the outward facing amino acids R and K of the RLK motif were mutated or when fragments of the C-terminus were truncated (Fig 1). The latter supports results from budding yeast [17]. Like RLK/AAA, the RLK/ALA mutation preserved Mad2 interaction, whereas truncation of the C-terminus led to a gradual loss of Mad1:Mad2 interaction (Fig 1G). Although the Mad1 C-terminus was necessary for kinetochore binding (Fig 1B,C), it did not seem sufficient (supplementary Fig S2). In contrast to the C-terminus, the Mad1 N-terminus was required for nuclear envelope localisation, but at least partly dispensable for kinetochore localisation (supplementary Fig S2). The RLK motif has been implicated in binding to Bub1 in budding yeast [16, 18], which involves a region of Bub1 that contains the 'conserved motif 1' (cm1; [19]). Interestingly, mutation of Bub1-cm1 phenocopied Mad1-RLK mutants (Fig 1H-K). Bub1 itself still localized to kinetochores, but Mad2 (and therefore presumably Mad1 [7]) was strongly reduced (Fig 1I,J) and cells lacked checkpoint activity (Fig 1K). We conclude that the C-terminus of Mad1 (with the RLK motif) and Bub1-cm1 are involved in recruiting Mad1 to kinetochores and both regions are important for checkpoint function.

The Mad1 C-terminus promotes checkpoint activity independently of its role in kinetochore localization

The inability of Mad1-RLK mutants to support checkpoint activity (Fig 1E) could be due to a failure to bring Mad1 to kinetochores or could reflect an additional function. We therefore tested checkpoint activity after artificially recruiting Mad1-RLK/AAA to kinetochores by fusion to the kinetochore protein Mis12 (Fig 2). Although the levels of tethered Mad1 at unattached kinetochores were slightly lower than for wild type Mad1 (Fig 2D), tethering of wild type Mad1 provided checkpoint activity (Fig 2B). In contrast, tethering of Mad1-RLK/AAA did not, although the levels of tethered wild type Mad1 and Mad1-RLK/AAA and of co-recruited Mad2 were similar (Fig 2D, supplementary Fig S3B). This indicated that the Mad1 C-terminus has an additional role within the spindle assembly checkpoint, apart from recruiting Mad1 and Mad2 to kinetochores.

To confirm this, we screened for mutations that preserve Mad1 kinetochore localization, but abolish checkpoint activity. An initial screen narrowed down the region of interest to the very C-terminus (supplementary Fig S4A). We noticed a conserved, negatively charged surface patch on 'top' of the Mad1-CTD head, which we either mutated (EDD/QNN) or which we removed by truncating the protein before the last α helix (Δhelix) (Fig 3A). Both mutants maintained Mad1 kinetochore localization (Fig 3B,C), but strongly or entirely lost checkpoint activity (Fig 3D), despite similar levels as wild type Mad1 (Fig 3E). Importantly, both immunoprecipitation (Fig 3F) and co-recruitment to the kinetochore (Fig 3G, supplementary Fig S4D) demonstrated that the interaction with Mad2 was preserved.

The C-terminal part of Mad1 (α3 and head) has been proposed to fold back onto Mad1-α2 [3], which would bring the Mad1 head in close vicinity to Mad2. Because Mad1-bound Mad2 needs to dimerize with additional Mad2 to support checkpoint function [4, 20], we suspected that the Mad1 C-terminal head promotes this dimerization. Confirming results from human cells [8], the Mad2 to Mad1 ratio at kinetochores is reduced in a dimerization-deficient Mad2 mutant (Mad2-R133A [21]; Fig 3G), presumably because Mad2 cannot be recruited to the kinetochore through Mad2:Mad2 dimerization, but only through binding to Mad1. In contrast to Mad2-R133A, the (wild type) Mad2 to Mad1 ratio was not obviously reduced in the Mad1-EDD/QNN or -Δhelix mutant (Fig 3G). Similarly, the tethered Mad1-RLK/AAA mutant recruited similar levels of Mad2 as tethered wild type Mad1 (Fig 3H). Hence, the Mad1 C-terminal head and the RLK motif promote checkpoint function, but seemingly

not through facilitating Mad2 dimerization. Together, our data indicate that the C-terminal head of Mad1 has a previously unrecognized role in checkpoint signalling, which is neither related to the requirement for the C-terminus to bring Mad1 to kinetochores (Fig 1) nor related to the role of Mad1 in recruiting Mad2, either directly or through Mad2:Mad2 dimerization (Fig 2, 3). Since very similar findings have been made in human cells (Kruse *et al.*, accompanying manuscript), this function of Mad1 is probably conserved across eukaryotes.

Current models for the spindle assembly checkpoint see Mad1 as a mere platform for presenting Mad2 at kinetochores. Our findings revise this picture and make Mad1 an active player in checkpoint signalling (Fig 4). How the Mad1 C-terminus promotes checkpoint activity remains unclear. Although we find Mad2 dimerization apparently intact in the Mad1-EDD/QNN, Mad1-Δhelix or Mad1-RLK/AAA mutant (Fig 3), it remains possible that these regions are involved in promoting the conformational change of Mad2 (Fig 4C) that is required for binding of free Mad2 to Cdc20 [22, 23]. We strongly suspect that the Mad1 head, like similar folds in other kinetochore proteins [24-27], mediates a protein-protein interaction. The interacting partner could be Mad2 or another (checkpoint) protein. Particularly puzzling is the effect of the RLK/AAA and RLK/ALA mutations. Despite being restricted to a small region, these mutations abrogate both functions of the C-terminus, kinetochore recruitment (Fig 1) and the enigmatic other role (Fig 2). Given that the α3 helices can interact in an intermolecular fashion [11], but have also been suggested to fold back onto α2 [3] (Fig 4), it is possible that the Mad1 C-terminus undergoes a conformational change that is important for its function in promoting checkpoint activity. The development of viable hypotheses for the new Mad1 function will require mapping the interactions of the Mad1 C-terminus both intra- and intermolecularly.

Methods

S. pombe strains

Strains are listed in Supplementary Table S1. For the amino acid (aa) numbering of Mad1, please note that we corrected the annotation of the start codon, which shifted by 13 aa (see Supplementary Information). In general, mutants were integrated into endogenous locus using PCR-based gene targeting [28] and replaced the wild type allele. *P(nmt81)-(mis12-)mad1-(AAA)-GFP* constructs were integrated into the *leu1* locus using the pDUAL system [29] and the endogenous *mad1+* gene was deleted. *S. pombe* strains with the following mutations or modifications have been described: *nda3-KM311* [30], *mad1+-GFP<<kanR, mad2+-GFP<<kanR, mad3+-GFP<<kanR*, *plo1+-mCherry*, *ark1+*-GFP [7]*, bub1+-GFP<<kanR* [31]*, mad1Δ::ura4+* [32], *bub1Δ::ura4+* [33].

Culture conditions

For live cell imaging, cells were grown at 30 °C in either rich medium (YEA) or Edinburgh minimal medium (EMM) containing the necessary supplements. Mad1 constructs expressed from *P(nmt81)* at the *leu1* locus were cultured for 19 h in EMM without thiamine to induce expression, then washed three times with EMM containing 16 μM thiamine and resuspended in EMM containing 16 μM thiamine before shifting to 16 °C for imaging.

Live cell imaging to assess checkpoint functionality

Live-cell imaging was performed on a DeltaVision microscope (Applied Precision/GE Healthcare) as previously described [7].

Quantification of GFP and mCherry signals in the nucleus and at the kinetochore

To determine the intensity of checkpoint protein-GFP or -mCherry signals at the kinetochores, mitotic cells were identified by the appearance of localized Plo1-mCherry signal at SPBs, or by localized Mad1-GFP or Mad2-mCherry signal at kinetochores. In those mitotic cells, an area was placed around kinetochores (for checkpoint protein-GFP or -mCherry strains) or SPBs (for Plo1-mCherry strains). Because kinetochores cluster at the SPB in early mitosis, this captures the signal at kinetochores. The GFP or mCherry signal in this area was traced over time. To determine signal intensity at the kinetochore, the total signal intensity per area of a similarly sized region in the nucleoplasm was subtracted from the total signal intensity per area around the kinetochore. A third, similarly sized region in the medium surrounding the cell was used to determine the nucleoplasmic signal by

subtracting the signal intensity per area of the medium from the total signal intensity per area in the nucleoplasm. For cells expressing constitutive kinetochore-tethered Mad1 (Mis12-Mad1), where entry into mitosis could not be judged, signals were measured for 50 min before the kinetochores unclustered, which is typical for cells in late stages of mitosis.

Fluorescence microscopy of asynchronous cell cultures

Images of living cells were acquired with a CoolSnap EZ (Roper) camera using a 63x/1.4 Plan Apochromat oil objective on a Zeiss AxioImager microscope, and were processed with MetaMorph software (Molecular Devices Corporation). Typically, a Z-stack of about 3-µm thickness, with single planes spaced by 0.3 µm, was acquired and subsequently projected. Shown are sum intensity projections of the Z-stack for checkpoint proteins and maximum intensity projections of the Z-stack for Plo1.

Co-immunoprecipitation

Co-immunoprecipitation was performed as previously described (Heinrich *et al.*, in press) using rabbit anti-Mad1 (Heinrich *et al.*, in press) or mouse anti-GFP (Roche, 11814460001) antibodies and protein A-coated magnetic beads (Dynabeads, Invitrogen 10002D).

Cell extracts, SDS-PAGE and immunoblotting

Protein extraction was performed as previously described [7]. Mouse anti-GFP (Roche, 11814460001), rabbit anti-Mad1 (Heinrich *et al.*, in press), rabbit anti-Mad2 [34], or rabbit anti-Cdc2 (Santa Cruz, SC-53) were used as primary antibodies. Secondary antibodies were anti-mouse or anti-rabbit HRP-conjugates (Dianova, 115-035-003, 111-035-003) and were read out using chemiluminescence.

Acknowledgments

We thank Katrin Bertram, Holda Anagho, Eva Illgen, Julia Binder, Julia Sauerwald, Alexandra Dudek and Philipp Spät for excellent technical help, Andrei Lupas for advice on coiled-coil truncations, Nicole Hustedt and the Proteome Center of the University of Tübingen for mass spectrometric analysis, and Jakob Nilsson and his group for communicating unpublished results. We are grateful for funding by the Max Planck Society; St.H. was additionally supported by the Ernst Schering Foundation.

Author contributions

St.H. (Fig 1-3, S1-S4), K.S. (Fig 1-3, S1-S4), H.W. (Fig 1), M.L. (Fig 1, 3), and N.S. (Fig 1, S1) designed and performed experiments; S.H. devised the project and wrote the manuscript together with St.H. and input from all other authors.

Conflict of Interest

None declared.

References

1. Lara-Gonzalez P, Westhorpe FG, Taylor SS (2012) The spindle assembly checkpoint. *Current biology : CB* **22:** R966-980

2. Primorac I, Musacchio A (2013) Panta rhei: the APC/C at steady state. *The Journal of cell biology* **201:** 177-189

3. Sironi L, Mapelli M, Knapp S, De Antoni A, Jeang KT, Musacchio A (2002) Crystal structure of the tetrameric Mad1-Mad2 core complex: implications of a 'safety belt' binding mechanism for the spindle checkpoint. *The EMBO journal* **21:** 2496-2506

4. De Antoni A *et al* (2005) The Mad1/Mad2 complex as a template for Mad2 activation in the spindle assembly checkpoint. *Current biology : CB* **15:** 214-225

5. Chao WC, Kulkarni K, Zhang Z, Kong EH, Barford D (2012) Structure of the mitotic checkpoint complex. *Nature* **484:** 208-213

6. Jia L, Kim S, Yu H (2013) Tracking spindle checkpoint signals from kinetochores to APC/C. *Trends Biochem Sci* **38:** 302-311

7. Heinrich S, Windecker H, Hustedt N, Hauf S (2012) Mph1 kinetochore localization is crucial and upstream in the hierarchy of spindle assembly checkpoint protein recruitment to kinetochores. *Journal of cell science*, 10.1242/jcs.110387

8. Hewitt L, Tighe A, Santaguida S, White AM, Jones CD, Musacchio A, Green S, Taylor SS (2010) Sustained Mps1 activity is required in mitosis to recruit O-Mad2 to the Mad1-C-Mad2 core complex. *J Cell Biol* **190:** 25-34

9. Emre D, Terracol R, Poncet A, Rahmani Z, Karess RE (2011) A mitotic role for Mad1 beyond the spindle checkpoint. *J Cell Sci* **124:** 1664-1671

10. Mariani L, Chiroli E, Nezi L, Muller H, Piatti S, Musacchio A, Ciliberto A (2012) Role of the Mad2 dimerization interface in the spindle assembly checkpoint independent of kinetochores. *Current biology : CB* **22:** 1900-1908

11. Kim S, Sun H, Tomchick DR, Yu H, Luo X (2012) Structure of human Mad1 C-terminal domain reveals its involvement in kinetochore targeting. *Proceedings of the National Academy of Sciences of the United States of America* **109:** 6549-6554

12. Kastenmayer JP, Lee MS, Hong AL, Spencer FA, Basrai MA (2005) The C-terminal half of Saccharomyces cerevisiae Mad1p mediates spindle checkpoint function, chromosome transmission fidelity and CEN association. *Genetics* **170:** 509-517

13. Scott RJ, Lusk CP, Dilworth DJ, Aitchison JD, Wozniak RW (2005) Interactions between Mad1p and the nuclear transport machinery in the yeast Saccharomyces cerevisiae. *Molecular biology of the cell* **16:** 4362-4374

14. Chung E, Chen RH (2002) Spindle checkpoint requires Mad1-bound and Mad1-free Mad2. *Molecular biology of the cell* **13:** 1501-1511

15. Martin-Lluesma S, Stucke VM, Nigg EA (2002) Role of Hec1 in spindle checkpoint signaling and kinetochore recruitment of Mad1/Mad2. *Science* **297:** 2267-2270

16. Brady DM, Hardwick KG (2000) Complex formation between Mad1p, Bub1p and Bub3p is crucial for spindle checkpoint function. *Current biology : CB* **10:** 675-678

17. Chen RH, Brady DM, Smith D, Murray AW, Hardwick KG (1999) The spindle checkpoint of budding yeast depends on a tight complex between the Mad1 and Mad2 proteins. *Molecular biology of the cell* **10:** 2607-2618

18. Warren CD, Brady DM, Johnston RC, Hanna JS, Hardwick KG, Spencer FA (2002) Distinct chromosome segregation roles for spindle checkpoint proteins. *Molecular biology of the cell* **13:** 3029-3041

19. Klebig C, Korinth D, Meraldi P (2009) Bub1 regulates chromosome segregation in a kinetochore-independent manner. *The Journal of cell biology* **185:** 841-858

20. Nezi L, Rancati G, De Antoni A, Pasqualato S, Piatti S, Musacchio A (2006) Accumulation of Mad2-Cdc20 complex during spindle checkpoint activation requires binding of open and closed conformers of Mad2 in Saccharomyces cerevisiae. *The Journal of cell biology* **174:** 39-51

21. Sironi L, Melixetian M, Faretta M, Prosperini E, Helin K, Musacchio A (2001) Mad2 binding to Mad1 and Cdc20, rather than oligomerization, is required for the spindle checkpoint. *The EMBO journal* **20:** 6371-6382

22. Luo X, Yu H (2008) Protein metamorphosis: the two-state behavior of Mad2. *Structure* **16:** 1616-1625

23. Mapelli M, Musacchio A (2007) MAD contortions: conformational dimerization boosts spindle checkpoint signaling. *Curr Opin Struct Biol* **17:** 716-725

24. Wei RR, Schnell JR, Larsen NA, Sorger PK, Chou JJ, Harrison SC (2006) Structure of a central component of the yeast kinetochore: the Spc24p/Spc25p globular domain. *Structure* **14:** 1003-1009

25. Ciferri C *et al* (2008) Implications for kinetochore-microtubule attachment from the structure of an engineered Ndc80 complex. *Cell* **133:** 427-439

26. Corbett KD, Yip CK, Ee LS, Walz T, Amon A, Harrison SC (2010) The monopolin complex crosslinks kinetochore components to regulate chromosome-microtubule attachments. *Cell* **142:** 556-567

27. Schmitzberger F, Harrison SC (2012) RWD domain: a recurring module in kinetochore architecture shown by a Ctf19-Mcm21 complex structure. *EMBO reports* **13:** 216-222
28. Bahler J, Wu JQ, Longtine MS, Shah NG, McKenzie A, 3rd, Steever AB, Wach A, Philippsen P, Pringle JR (1998) Heterologous modules for efficient and versatile PCR-based gene targeting in Schizosaccharomyces pombe. *Yeast* **14:** 943-951

29. Matsuyama A, Shirai A, Yashiroda Y, Kamata A, Horinouchi S, Yoshida M (2004) pDUAL, a multipurpose, multicopy vector capable of chromosomal integration in fission yeast. *Yeast* **21:** 1289-1305

30. Hiraoka Y, Toda T, Yanagida M (1984) The NDA3 gene of fission yeast encodes beta-tubulin: a cold-sensitive nda3 mutation reversibly blocks spindle formation and chromosome movement in mitosis. *Cell* **39:** 349-358

31. Yamaguchi S, Decottignies A, Nurse P (2003) Function of Cdc2p-dependent Bub1p phosphorylation and Bub1p kinase activity in the mitotic and meiotic spindle checkpoint. *The EMBO journal* **22:** 1075-1087

32. Vanoosthuyse V, Valsdottir R, Javerzat JP, Hardwick KG (2004) Kinetochore targeting of fission yeast Mad and Bub proteins is essential for spindle checkpoint function but not for all chromosome segregation roles of Bub1p. *Molecular and cellular biology* **24:** 9786-9801

33. Bernard P, Hardwick K, Javerzat JP (1998) Fission yeast bub1 is a mitotic centromere protein essential for the spindle checkpoint and the preservation of correct ploidy through mitosis. *The Journal of cell biology* **143:** 1775-1787

34. Yamada HY, Matsumoto S, Matsumoto T (2000) High dosage expression of a zinc finger protein, Grt1, suppresses a mutant of fission yeast slp1(+), a homolog of CDC20/p55CDC/Fizzy. *Journal of cell science* **113 (Pt 22):** 3989-3999

35. Mulvihill DP, Petersen J, Ohkura H, Glover DM, Hagan IM (1999) Plo1 kinase recruitment to the spindle pole body and its role in cell division in Schizosaccharomyces pombe. *Molecular biology of the cell* **10:** 2771-2785

Figure Legends

Figure 1 The Mad1 C-terminus is required for kinetochore localization and checkpoint activity

A Domain structure of Mad1, and point mutations and truncations employed in this study. The dimer of two α3 helices and heads has been termed Mad1 C-terminal domain (CTD) [11]. It remains unclear whether the folding unit *in vivo* includes α2 [3].

B Cells expressing *plo1+-mCherry*, the conditional tubulin mutant *nda3-KM311* and the indicated Mad1-GFP fusion proteins were grown at the permissive temperature for the *nda3-KM311* mutant (30 °C). A localized Plo1 signal was used as marker for mitosis [35]; representative nuclei of mitotic cells are shown (scale bar: 2 μm; see supplementary Fig S1A for a larger field of view).

C The same strains as in (B) were analysed at the restrictive temperature for *nda3-KM311* (16 °C), which prevents microtubule formation. Mad1-GFP signals were quantified at the kinetochore and in the nucleoplasm (supplementary Fig S1B) as cells entered mitosis (a.u. = arbitrary units; error bars = s.d.; n ≥ 20 cells)

D Cells expressing *plo1+-mCherry*, *nda3-KM311* and the indicated GFP fusion proteins were analysed at 16 °C as in (C). Representative nuclei of mitotic cells are shown (scale bar: 2 μm).

E Cells expressing *plo1+-mCherry* and *nda3-KM311* were analysed at 16 °C as in (C). The time that each cell spent in prometaphase was determined by the localized Plo1-mCherry signal at spindle pole bodies (SPBs) (circle). Cells that had not yet exited mitosis when filming stopped are indicated by triangles.

F Immunoblotting of cell extracts using anti-GFP and anti-Cdc2 (loading control) antibodies. A dilution series was loaded for each strain to compare intensities.

G Anti-Mad1 immunoprecipitations of the indicated strains were analysed for the presence of Mad1 and Mad2 using anti-GFP (left), anti-Mad1 (right) and anti-Mad2 antibodies. Input and flow through are shown in supplementary Fig S1D.

H Domain structure of Bub1 (TPR: tetratricopeptide repeats; Bub3 binding: Bub3-binding motif, also called GLEBS; cm1: conserved motif 1; kinase: kinase domain).

I Cells expressing *mad2+-mCherry*, *nda3-KM311* and the indicated *bub1-GFP* fusions were imaged at 30 °C as in (B). Representative nuclei of mitotic cells are shown (scale bar: 2 μm; see supplementary Fig S1H for a larger field of view). The Bub1-cm1 mutant (cm1-mut) contains aa changes S381A, T383A and T386A. The total cellular abundance of wild type and mutant Bub1-GFP was similar (supplementary Fig S1F).

J Bub1-GFP or Mad2-mCherry signals were quantified at the kinetochore and in the nucleoplasm (supplementary Figure S1I,J) as in (C) (a.u. = arbitrary units; error bars = s.d.; n ≥ 24 cells for Bub1-GFP, n ≥ 22 cells for Mad2-mCherry)

K Checkpoint function of the indicated strains was analysed as in (E).

Figure 2 The Mad1 C-terminus has a role in signalling beyond its role in kinetochore localization

A Representative images of cells expressing *plo1+-mCherry*, *nda3-KM311* and the indicated GFP fusion proteins. Cells were imaged at the permissive temperature for the *nda3-KM311* mutant (30 °C). *P(nmt81)* indicates expression from the *nmt81* promoter. The endogenous *mad1* gene is deleted in these strains. Scale bar: 2 *μ*m

B Checkpoint function of the indicated strains was analysed as in Fig 1E.

C Immunoblotting of cell extracts using anti-GFP and anti-Cdc2 (loading control) antibodies. Strains are the same as in (B). The asterisk indicates a cross-reaction of the antibody.

D Mad1-GFP (from cells in (B)) or Mad2-mCherry signals were quantified both at the kinetochore and in the nucleoplasm (supplementary Fig S4A) as cells entered mitosis (a.u. = arbitrary units; error bars = s.d.; n ≥ 20 cells). Representative nuclei are shown on the right. (Scale bar: 2 *μ*m; see supplementary Fig S4B for a larger field of view).

Figure 3 The top of the globular head of the Mad1 C-terminus is required for checkpoint signalling, but not for kinetochore localization of Mad1:Mad2

A Position of the C-terminal head mutations. The inset shows a homology model of the C-terminus of *S. pombe* (aa562-676) based on the crystal structure of the dimeric *H. sapiens* Mad1 C-terminal domain (PDB code: 4ZDO, [11]). (black: RLK motif (aa580-582); blue: last helix of the C-terminal head (aa662-676); purple: aaE670/D673/D676)

B The indicated strains were imaged as in Fig 1B. Representative nuclei of mitotic cells are shown (scale bar: 2 *μ*m; see supplementary Fig S4B for a larger field of view).

C The same strains as in (B) were analysed at the restrictive temperature for *nda3-KM311* (16 °C) as in Fig 1C. Mad1-GFP signals were quantified at the kinetochore and in the nucleoplasm (supplementary Fig S4C) as cells entered mitosis (a.u. = arbitrary units; error bars = s.d.; n ≥ 22 cells).

D Checkpoint function of the indicated strains was analysed as in Fig 1E.

E Immunoblotting of cell extracts using anti-GFP and anti-Cdc2 (loading control) antibodies. A dilution series was loaded for each strain to compare intensities.

F Anti-Mad1 immunoprecipitations of the indicated strains were analysed for the presence of Mad1 and Mad2 using anti-GFP and anti-Mad2 antibodies. Input and flow through of the immunoprecipitation are shown in supplementary Fig S4E.

G Cells expressing *nda3-KM311*, the indicated *mad1-GFP* constructs and either *mad2+-mCherry* or *mad2-R133A-mCherry* were followed by live-cell imaging at 16 °C. The Mad2-mCherry to Mad1-GFP ratio at kinetochores was determined as cells entered mitosis. (a.u. = arbitrary units; error bars = s.d.; n ≥ 7 cells)

H Strains were followed by live-cell imaging as in (G). Mad2-mCherry signals were quantified at the kinetochore in mitotic cells. (a.u. = arbitrary units; error bars = s.d.; n ≥ 20 cells). Representative nuclei are shown on the right (scale bar: 2 μm).

Figure 4 Functions of the Mad1 C-terminus

A Domain structure of the Mad1 C-terminus [3, 11].

B Summary of our findings. The RLK motif is required for kinetochore localization. If kinetochore localization is bypassed by artificial recruitment (Fig 2), the RLK motif is still required for proper checkpoint activity. Hence, the RLK motif has a dual role. The top of the Mad1 C-terminal head is required for checkpoint activity, although not required for Mad1:Mad2 kinetochore localization and Mad2 dimerization (Fig 3).

C Hypotheses and questions about the function of the Mad1 C-terminus.

Figure 1

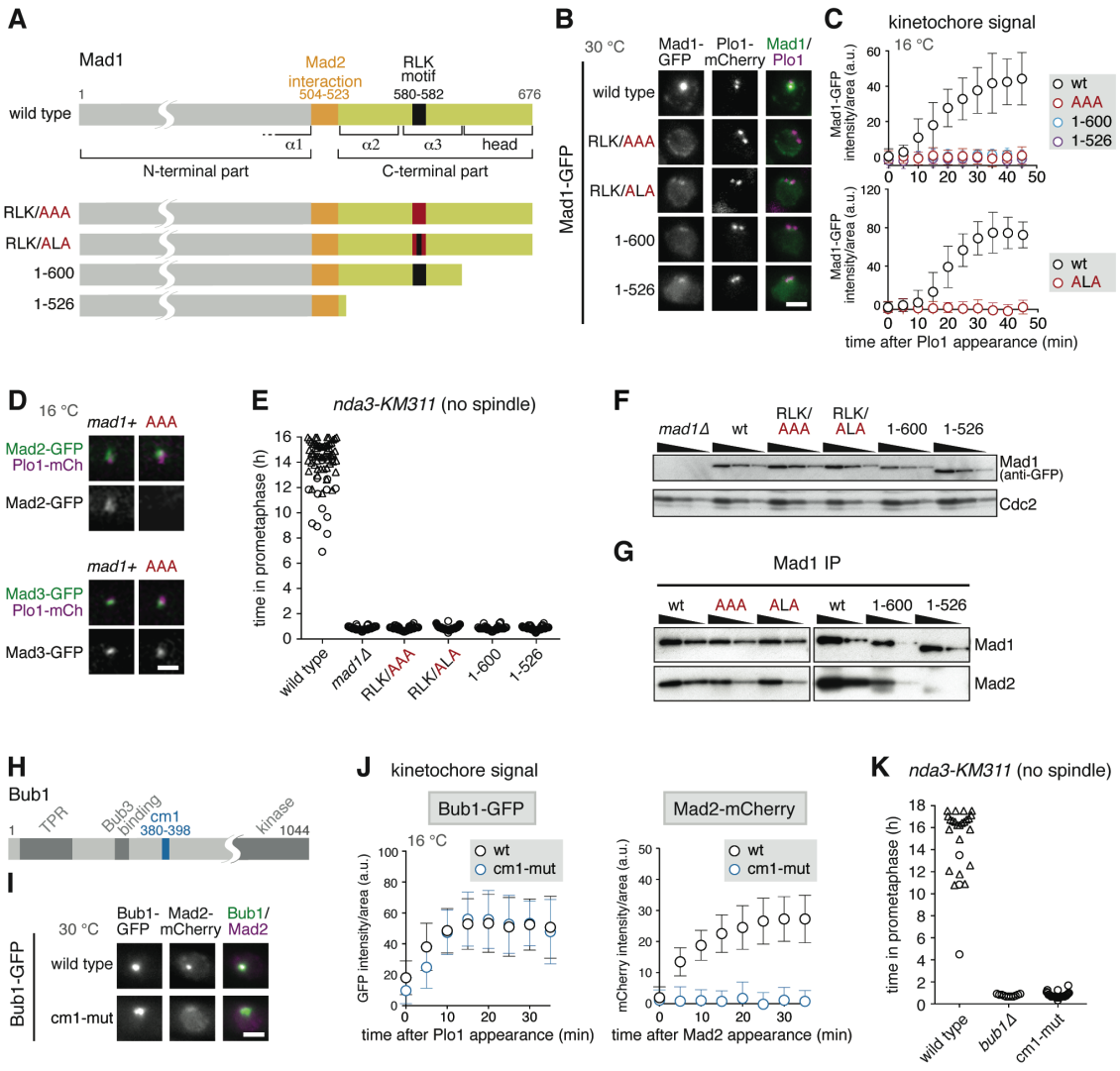
A
Mad1
Mad2 interaction 504-523
RLK motif 580-582
1
676
wild type
α1
α2
α3
head
N-terminal part
C-terminal part
RLK/AAA
RLK/ALA
1-600
1-526
B
30 °C
Mad1-GFP
Plo1-mCherry
Mad1/Plo1
Mad1-GFP
wild type
RLK/AAA
RLK/ALA
1-600
1-526
C
kinetochore signal
16 °C
Mad1-GFP intensity/area (a.u.)
wt
AAA
1-600
1-526
ALA
time after Plo1 appearance (min)
D
16 °C
mad1+ AAA
Mad2-GFP Plo1-mCh
Mad2-GFP
Mad3-GFP Plo1-mCh
Mad3-GFP
E
nda3-KM311 (no spindle)
time in prometaphase (h)
wild type
mad1Δ
RLK/AAA
RLK/ALA
1-600
1-526
F
mad1Δ
wt
RLK/AAA
RLK/ALA
1-600
1-526
Mad1 (anti-GFP)
Cdc2
G
Mad1 IP
wt
AAA
ALA
wt
1-600
1-526
Mad1
Mad2
H
Bub1
TPR
Bub3 binding
cm1 380-398
kinase
1
1044
I
30 °C
Bub1-GFP
Mad2-mCherry
Bub1/Mad2
Bub1-GFP
wild type
cm1-mut
J
kinetochore signal
Bub1-GFP
16 °C
wt
cm1-mut
GFP intensity/area (a.u.)
time after Plo1 appearance (min)
Mad2-mCherry
mCherry intensity/area (a.u.)
time after Mad2 appearance (min)
K
nda3-KM311 (no spindle)
time in prometaphase (h)
wild type
bub1Δ
cm1-mut

Figure 2

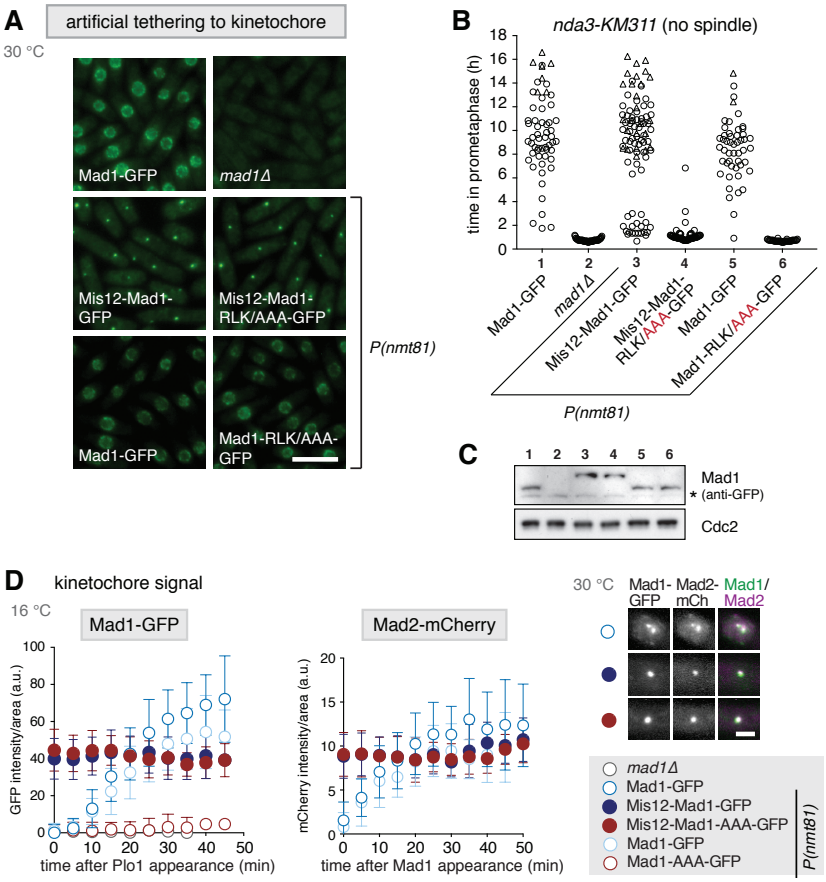
A
artificial tethering to kinetochore
30 °C
Mad1-GFP
mad1Δ
Mis12-Mad1-GFP
Mis12-Mad1-RLK/AAA-GFP
Mad1-GFP
Mad1-RLK/AAA-GFP
P(nmt81)
B
nda3-KM311 (no spindle)
time in prometaphase (h)
Mad1-GFP
mad1Δ
Mis12-Mad1-GFP
Mis12-Mad1-RLK/AAA-GFP
Mad1-GFP
Mad1-RLK/AAA-GFP
P(nmt81)
C
Mad1
* (anti-GFP)
Cdc2
D
kinetochore signal
16 °C
Mad1-GFP
Mad2-mCherry
GFP intensity/area (a.u.)
mCherry intensity/area (a.u.)
time after Plo1 appearance (min)
time after Mad1 appearance (min)
30 °C
Mad1-GFP
Mad2-mCh
Mad1/Mad2
mad1Δ
Mad1-GFP
Mis12-Mad1-GFP
Mis12-Mad1-AAA-GFP
Mad1-GFP
Mad1-AAA-GFP
P(nmt81)

Figure 3

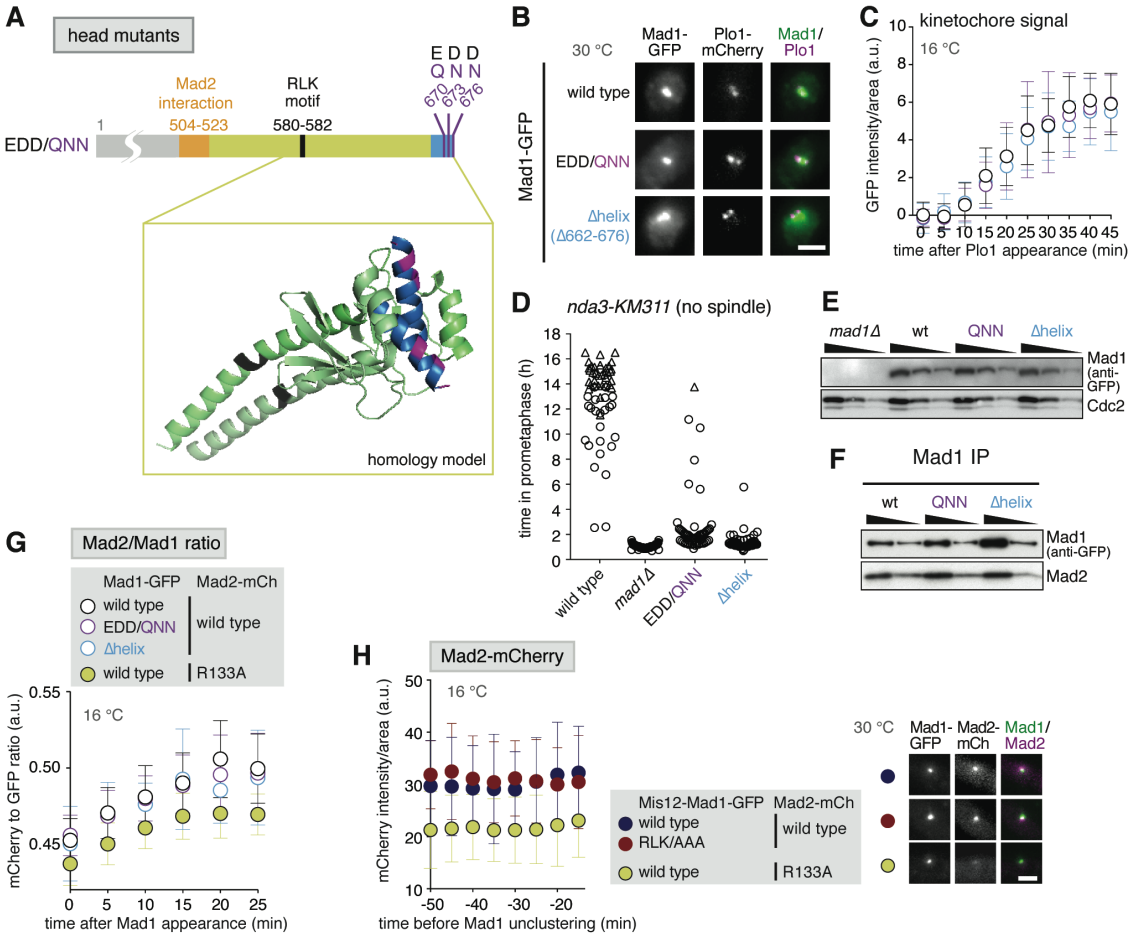
A
head mutants
Mad2 interaction 504-523
RLK motif 580-582
E D D Q N N 670 673 676
EDD/QNN
1
homology model
B
30 °C
Mad1-GFP
Plo1-mCherry
Mad1/Plo1
wild type
EDD/QNN
Δhelix (Δ662-676)
C
kinetochore signal
16 °C
GFP intensity/area (a.u.)
time after Plo1 appearance (min)
D
nda3-KM311 (no spindle)
time in prometaphase (h)
wild type
mad1Δ
EDD/QNN
Δhelix
E
mad1Δ
wt
QNN
Δhelix
Mad1 (anti-GFP)
Cdc2
F
Mad1 IP
wt
QNN
Δhelix
Mad1 (anti-GFP)
Mad2
G
Mad2/Mad1 ratio
Mad1-GFP
Mad2-mCh
wild type
EDD/QNN
Δhelix
wild type
wild type
R133A
16 °C
mCherry to GFP ratio (a.u.)
time after Mad1 appearance (min)
H
Mad2-mCherry
16 °C
mCherry intensity/area (a.u.)
time before Mad1 unclustering (min)
Mis12-Mad1-GFP
Mad2-mCh
wild type
RLK/AAA
wild type
wild type
R133A
30 °C
Mad1-GFP
Mad2-mCh
Mad1/Mad2

Figure 4

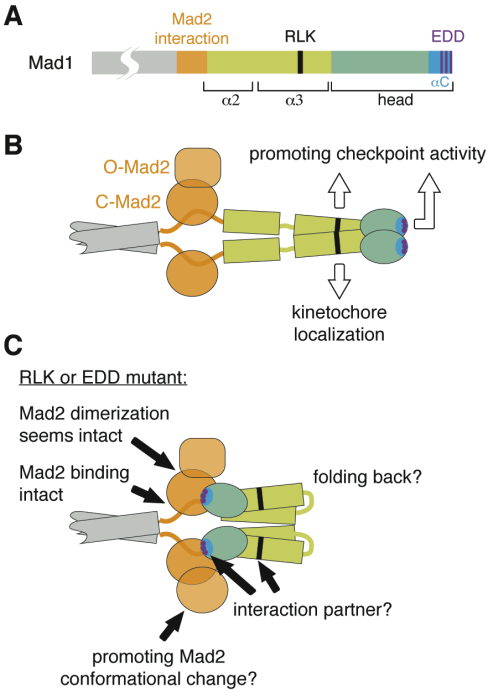
A
Mad2
interaction
RLK
EDD
Mad1
αC
α2
α3
head
B
O-Mad2
C-Mad2
promoting checkpoint activity
kinetochore
localization
C
RLK or EDD mutant:
Mad2 dimerization
seems intact
Mad2 binding
intact
folding back?
interaction partner?
promoting Mad2
conformational change?

Supplementary Information

Supplementary Figure 1 Supplementary data related to Figure 1

Supplementary Figure 2 The Mad1 N-terminal part is not required for kinetochore localization, the C-terminal part is not sufficient

Supplementary Figure 3 Supplementary data related to Figure 2

Supplementary Figure 4 Supplementary data related to Figure 3

Supplementary Information Re-annotation of the Mad1 start codon

Supplementary Table 1 *S. pombe* strains

Figure S1

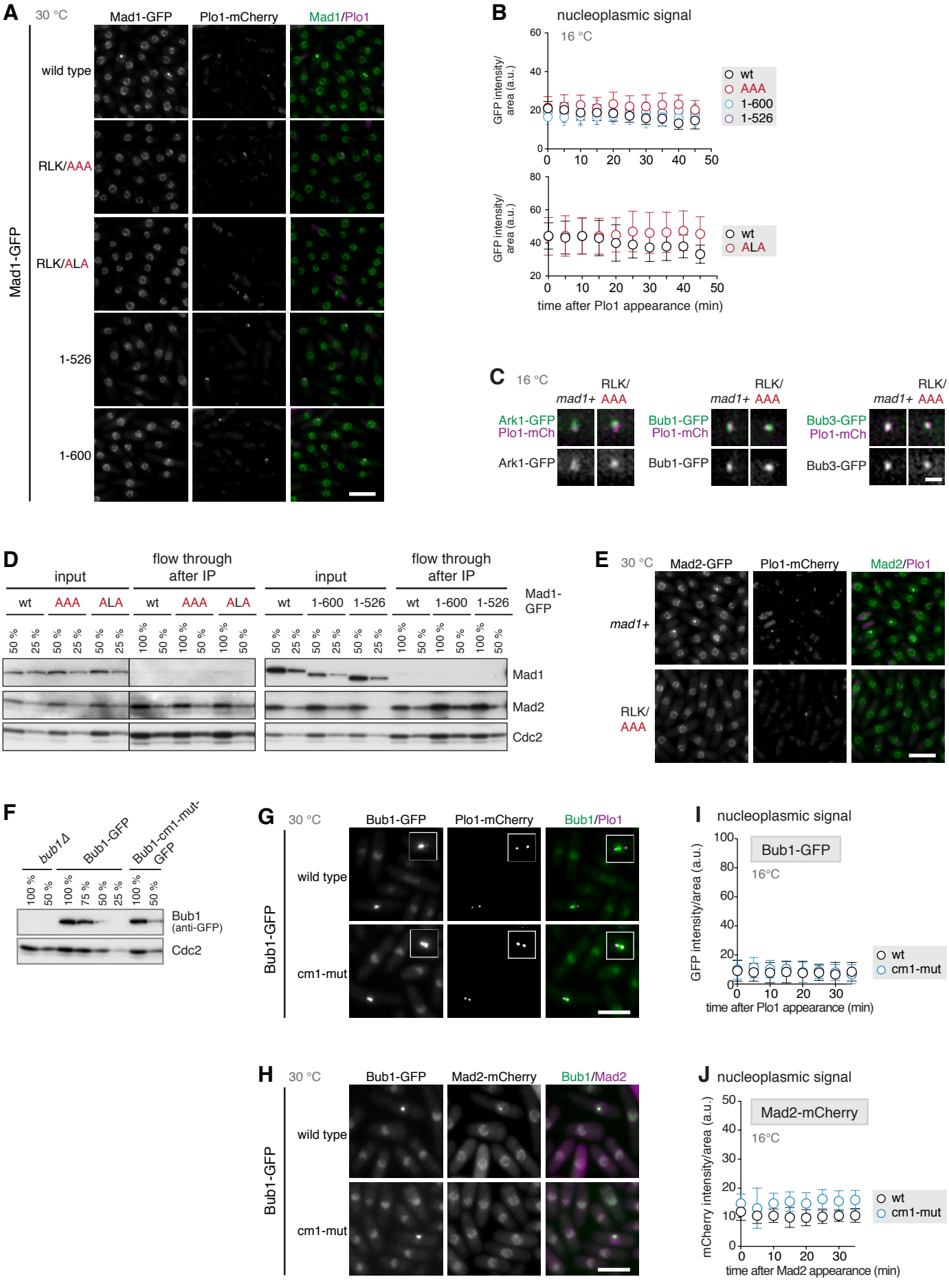
A
30 °C
Mad1-GFP
Plo1-mCherry
Mad1/Plo1
Mad1-GFP
wild type
RLK/AAA
RLK/ALA
1-526
1-600
B
nucleoplasmic signal
16 °C
GFP intensity/ area (a.u.)
wt
AAA
1-600
1-526
ALA
time after Plo1 appearance (min)
C
16 °C
mad1+
RLK/ AAA
Ark1-GFP Plo1-mCh
Ark1-GFP
Bub1-GFP Plo1-mCh
Bub1-GFP
Bub3-GFP Plo1-mCh
Bub3-GFP
D
input
flow through after IP
wt
AAA
ALA
1-600
1-526
Mad1-GFP
Mad1
Mad2
Cdc2
E
30 °C
Mad2-GFP
Plo1-mCherry
Mad2/Plo1
mad1+
RLK/ AAA
F
bub1Δ
Bub1-GFP
Bub1-cm1-mut-GFP
Bub1 (anti-GFP)
Cdc2
G
30 °C
Bub1-GFP
Plo1-mCherry
Bub1/Plo1
Bub1-GFP
wild type
cm1-mut
I
nucleoplasmic signal
Bub1-GFP
16°C
GFP intensity/area (a.u.)
wt
cm1-mut
time after Plo1 appearance (min)
H
30 °C
Bub1-GFP
Mad2-mCherry
Bub1/Mad2
Bub1-GFP
wild type
cm1-mut
J
nucleoplasmic signal
Mad2-mCherry
16°C
mCherry intensity/area (a.u.)
wt
cm1-mut
time after Mad2 appearance (min)

Figure S1 Supplementary data related to Figure 1

A Mad1-RLK mutants and C-terminal truncations localize to the nuclear rim

Representative images of cells expressing *plo1+-mCherry*, the conditional tubulin mutant *nda3-KM311* and the indicated *mad1-GFP* fusions. Cells were grown at permissive temperature for the *nda3-KM311* mutant (30 °C). A localized Plo1-mCherry signal indicates that cells are in mitosis. Scale bar: 10 *µ*m

B Nucleoplasmic Mad1-GFP signals of strains analysed in Fig. 1C.

C Ark1, Bub1 and Bub3 localise to kinetochores in the *mad1-RLK/AAA* mutant

Cells expressing *plo1+-mCherry*, *nda3-KM311* and the indicated GFP fusion proteins were analysed at 16 °C as in Fig. 1C. Representative nuclei of mitotic cells are shown (scale bar: 2 *µ*m).

D Mad1 is efficiently depleted by immunoprecipitation

Input and flow through of the anti-Mad1 immunoprecipitation shown in Fig. 1G. To detect the Mad1-RLK mutants, anti-GFP antibody was used; to detect the Mad1 truncations, anti-Mad1 antibody was used. Cdc2 serves as loading control. The C-terminal truncations Mad1-1-600 and Mad1-1-526 contain more Mad2 in the flow through, in agreement with inefficient binding of Mad2 to Mad1 (Fig. 1G).

E Mad2 localisation to kinetochores is strongly reduced in *mad1+-RLK/AAA* mutant

Representative images of cells expressing *mad1+* or *mad1-RLK/AAA*, as well as *mad2+-GFP*, *plo1+-mCherry* and *nda3-KM311*. Cells were grown at permissive temperature for the *nda3-KM311* mutant (30 °C). Mad2-GFP localisation to the nuclear rim in interphase is similar between wild type and *mad1+-RLK/AAA* cells, but localisation to the kinetochore in mitosis is impaired in the *mad1-RLK/AAA* mutant. Scale bar: 10 *µ*m.

F Bub1-cm1 mutant is present at similar levels as wild type Bub1

Extracts were analysed by immunoblotting using anti-GFP and anti-Cdc2 (loading control) antibodies. Percentages on top indicate how much of the extract was loaded.

G Bub1-cm1 mutant is enriched in the nucleus and localizes to kinetochores

Representative images of cells expressing *bub1-GFP* (wild type or cm1 mutant), *plo1+-mCherry* and *nda3-KM311*. Cells were grown at permissive temperature for the *nda3-KM311* mutant (30 °C). Both wild type Bub1 and Bub1-cm1 enrich in the nucleus in interphase. Inset: Plo1-mCherry marks mitotic spindle pole bodies, and both Bub1 and Bub1-cm1 localize to the region of the mitotic spindle (most likely by localizing to kinetochores). Scale bar: 10 *µ*m. Insets are additionally magnified 1.87-fold.

H Mad2-mCherry localisation to the nuclear rim is not impaired by the *bub1-cm1* mutation Representative images of cells expressing *bub1-GFP* (wild type or cm1 mutant), *mad2+-mCherry* and *nda3-KM311*. Cells were grown at permissive temperature for the *nda3-KM311* mutant (30 °C). Nuclei of mitotic cells with localized Bub1-GFP signal from these panels are shown in Fig. 1I. Scale bar: 10 μm

I,J Nucleoplasmic Bub1-GFP (I) or Mad2-mCherry (J) signals of strains analysed in Fig. 1J.

Figure S2

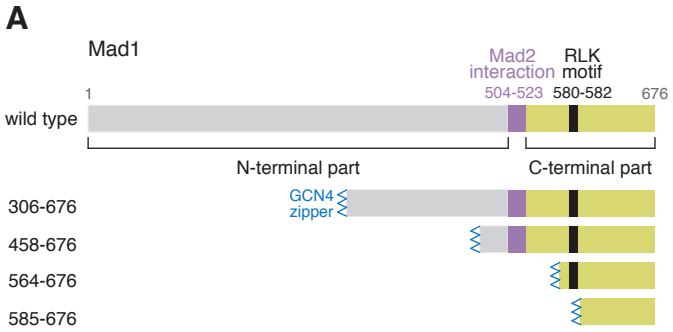
A
Mad1
Mad2 interaction
RLK motif
1
504-523
580-582
676
wild type
N-terminal part
C-terminal part
GCN4 zipper
306-676
458-676
564-676
585-676

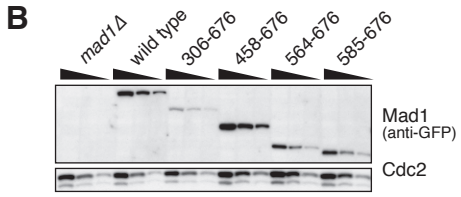
B
mad1Δ
wild type
306-676
458-676
564-676
585-676
Mad1 (anti-GFP)
Cdc2

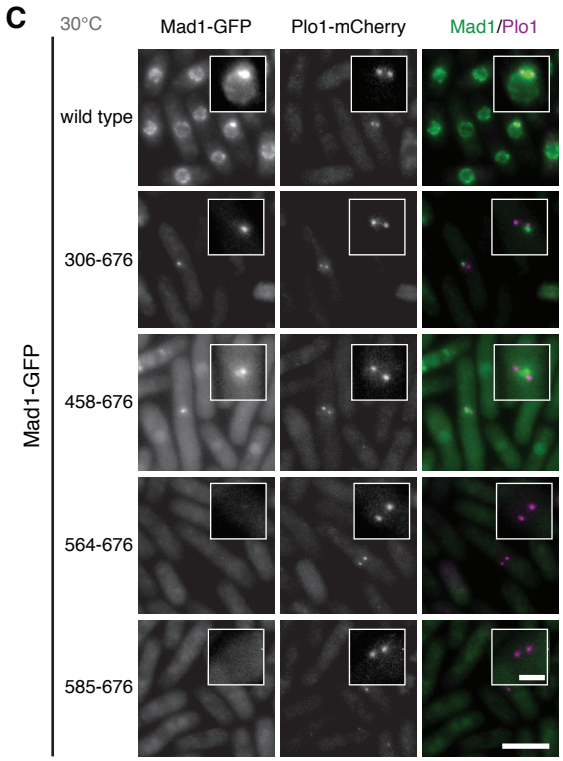
C
30°C
Mad1-GFP
Plo1-mCherry
Mad1/Plo1
wild type
306-676
458-676
564-676
585-676
Mad1-GFP

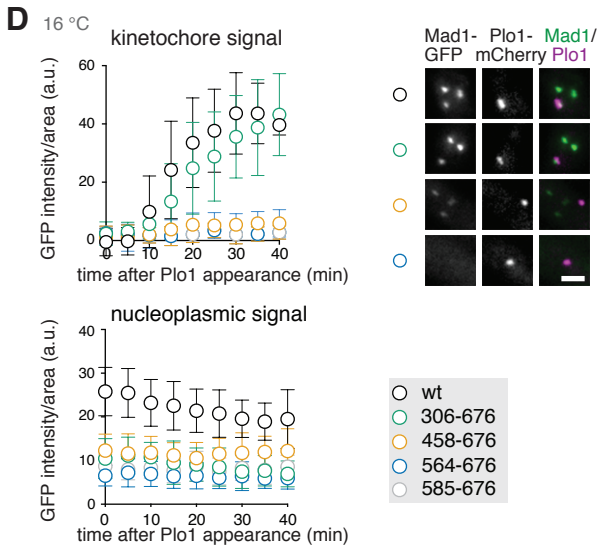
D
16 °C
kinetochore signal
GFP intensity/area (a.u.)
time after Plo1 appearance (min)
Mad1-GFP
Plo1-mCherry
Mad1/Plo1
nucleoplasmic signal
wt
306-676
458-676
564-676
585-676

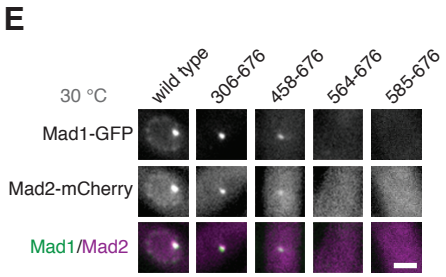
E
30 °C
wild type
306-676
458-676
564-676
585-676
Mad1-GFP
Mad2-mCherry
Mad1/Mad2

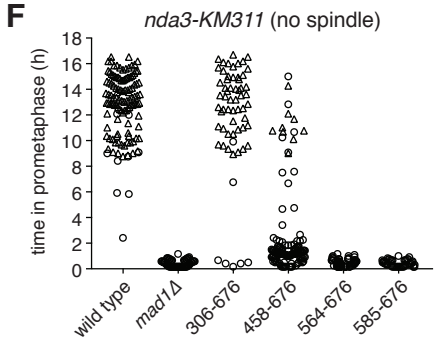
F
nda3-KM311 (no spindle)
time in prometaphase (h)
wild type
mad1Δ
306-676
458-676
564-676
585-676

Figure S2 The Mad1 N-terminal part is not required for kinetochore localisation, the C-terminal part is not sufficient

A Domain structure of the Mad1 protein and N-terminal truncations. A fragment of *S. cerevisiae* Gcn4p (aa250-277; GCN4 zipper) was used to aid coiled-coil formation of the remaining alpha-helical parts and dimerization [1, 2].

B N-terminal truncation mutants of Mad1 are expressed

Immunoblotting of cell extracts using anti-GFP and anti-Cdc2 (loading control) antibodies. A dilution series was loaded for each strain to compare intensities. The N-terminal Mad1 truncations were expressed, but not all to the same level as wild type Mad1-GFP (also see (C)).

C Truncation of the Mad1 N-terminus abolishes nuclear rim localisation

Representative images of cells expressing *plo1+-mCherry*, *nda3-KM311* and the indicated *mad1-GFP* fusions. Cells were grown at permissive temperature for the *nda3-KM311* mutant (30 °C). Scale bar: 10 μm; scale bar in inset: 2 μm. Nuclear rim localisation was lost in all N-terminal truncations, whereas kinetochore localisation was at least partly preserved in mutants that retained parts of the N-terminal coiled-coil. The C-terminal part of Mad1 was not sufficient for kinetochore localisation.

D The same strains as in (C) were shifted to the restrictive temperature for *nda3-KM311* (16 °C) and imaged as in Fig. 1C. Mad1-GFP signals were quantified at the kinetochore and in the nucleoplasm as cells entered mitosis (a.u. = arbitrary units; error bars = s.d.; n ≥ 20 cells). The kinetochore localization of Mad1-458-676 was almost undetectable in live cell imaging (upper left panel), but was visible at 16 °C when the same image acquisition settings as in (C) were used (upper right panel).

E Cells expressing *mad2+-mCherry*, *nda3-KM311* and the indicated *mad1-GFP* fusions were imaged at 30 °C. Representative nuclei of cells in mitosis are shown. Scale bar: 2 μm. Mad1-306-676 and Mad1-458-676 co-recruit Mad2 to the kinetochore, indicating that the interaction with Mad2 is preserved.

F The shorter N-terminal Mad1 truncation (Mad1-306-676) largely preserves checkpoint activity.

Checkpoint function in the indicated strains was analysed as in Fig. 1E. Checkpoint activity in Mad1-306-676 was largely preserved (although the abundance seemed lower than wild type Mad1 (B,C)). Checkpoint activity in Mad1-458-676 was impaired, which coincided with an impairment of localisation to the kinetochore that was more pronounced at 16 °C (C,D,E). The two shortest Mad1 fragments (Mad1-564-676 and 585-676) were checkpoint-deficient, which was expected from the lack of the Mad2-interaction motif.

Figure S3

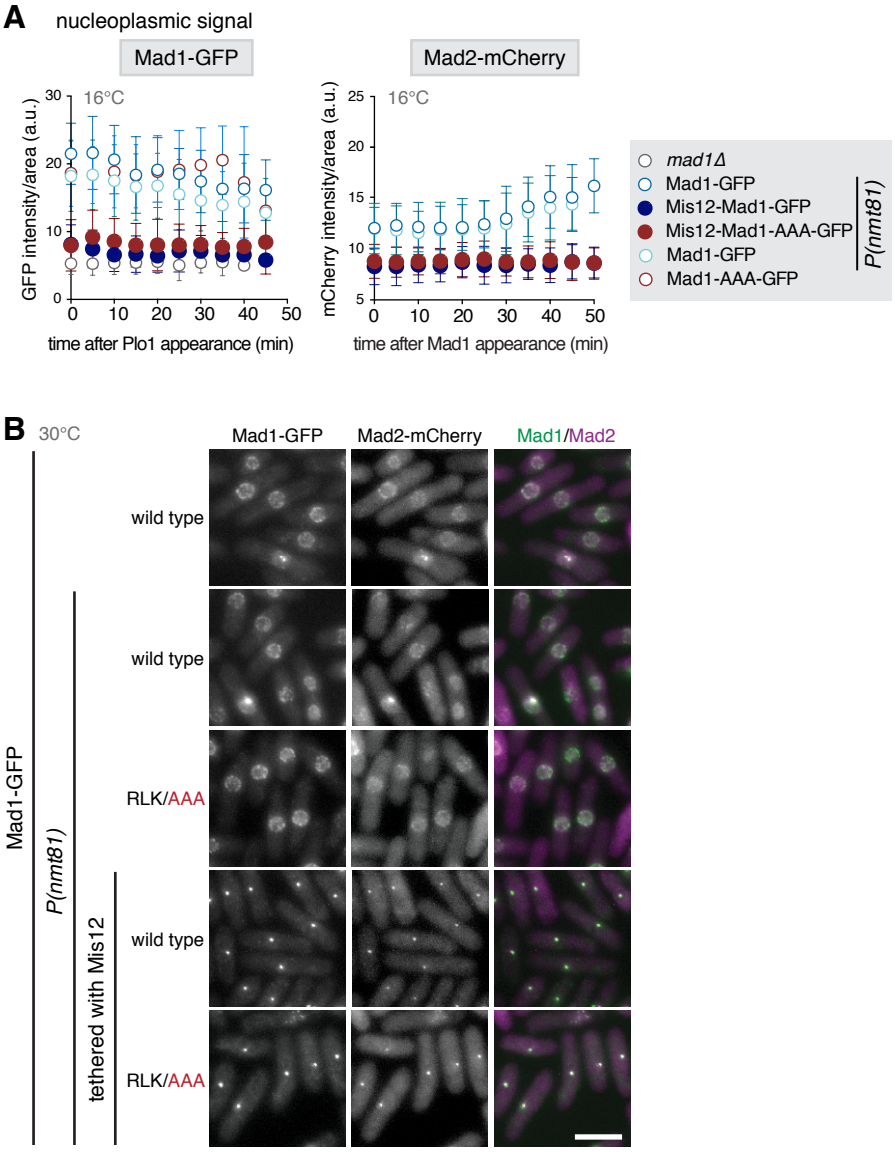

Figure S3 Supplementary data related to Figure 2

A Nucleoplasmic Mad1-GFP (left) and Mad2-mCherry (right) signals of strains analysed in Fig. 2D.

B Representative images of cells expressing *mad2+-mCherry*, *nda3-KM311* and the indicated Mad1 wild type or RLK/AAA GFP fusion proteins. Cells were grown at permissive temperature for the *nda3-KM311* mutant (30 °C). *P(nmt81)* indicates expression of the construct from the *nmt81* promoter rather than from the endogenous *mad1* promoter. Scale bar: 10 μm

Figure S4

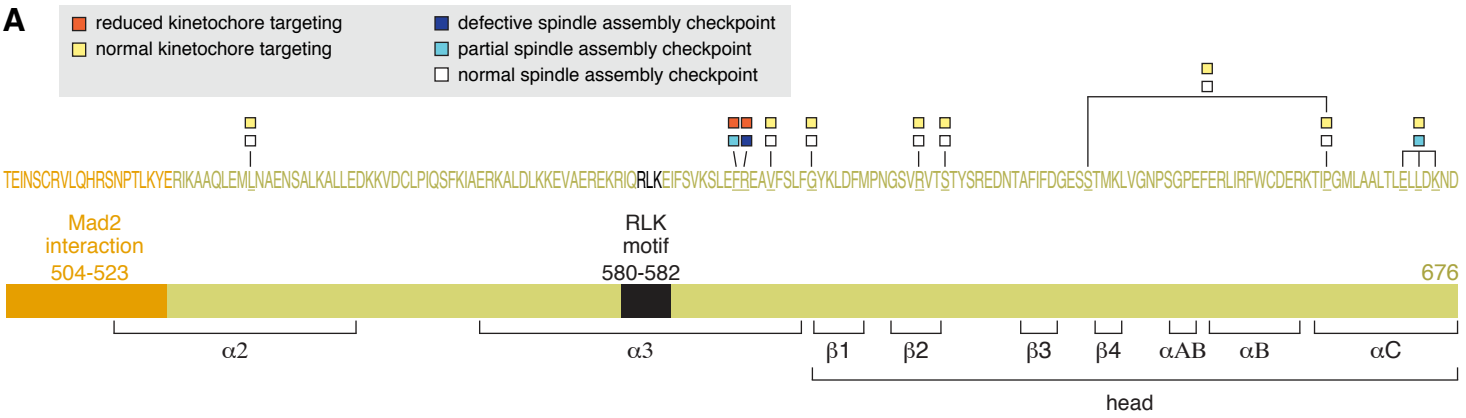
A
reduced kinetochore targeting
normal kinetochore targeting
defective spindle assembly checkpoint
partial spindle assembly checkpoint
normal spindle assembly checkpoint
TEINSCRVLQHRSNPTLKYERIKAAQLEMLNAENSALKALLEDKKVDCLPIQSFKIAERKALDLKKEVAEREKRIQRLKEIFSVKSLEFREAVFSLFGYKLDFMPNGSVRVTSTYSREDNTAFIFDGESSTMKLVGNPSGPEFERLIRFWCDERKTIPGMLAALTLELLDKND
Mad2 interaction 504-523
RLK motif 580-582
676
α2
α3
β1
β2
β3
β4
αAB
αB
αC
head

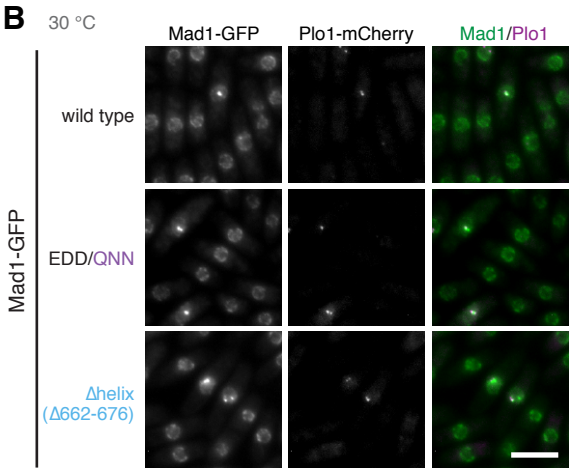
B
30 °C
Mad1-GFP
Plo1-mCherry
Mad1/Plo1
wild type
EDD/QNN
Δhelix (Δ662-676)
Mad1-GFP

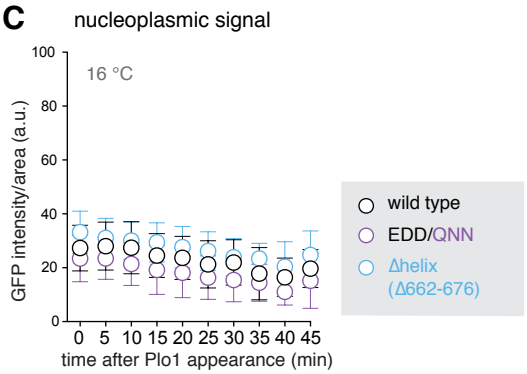
C
nucleoplasmic signal
16 °C
GFP intensity/area (a.u.)
100
80
60
40
20
0
0 5 10 15 20 25 30 35 40 45
time after Plo1 appearance (min)
wild type
EDD/QNN
Δhelix (Δ662-676)

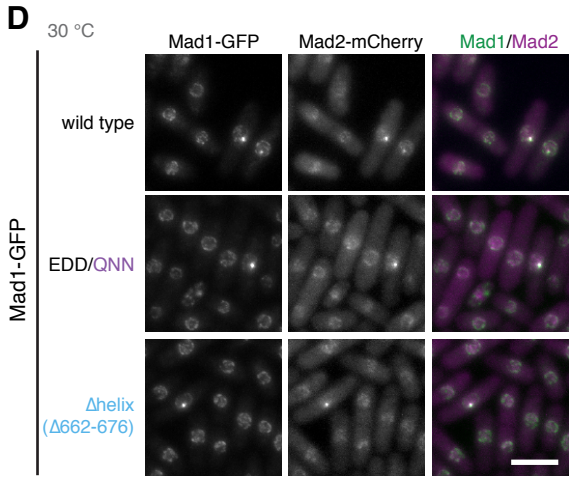
D
30 °C
Mad1-GFP
Mad2-mCherry
Mad1/Mad2
wild type
EDD/QNN
Δhelix (Δ662-676)
Mad1-GFP

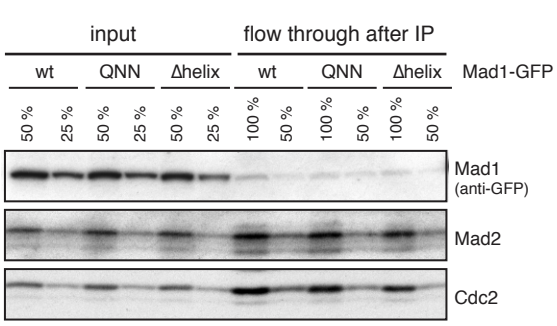
E
input
flow through after IP
wt
QNN
Δhelix
wt
QNN
Δhelix
Mad1-GFP
50 %
25 %
50 %
25 %
50 %
25 %
100 %
50 %
100 %
50 %
100 %
50 %
Mad1 (anti-GFP)
Mad2
Cdc2

Figure S4 Supplementary data related to Figure 3

A Additional Mad1 mutants screened for kinetochore targeting ability and spindle assembly checkpoint activity

Individual residues in Mad1 were mutated to alanine, with the exception of S633, which was mutated to glycine. Checkpoint activity was assayed in cells expressing *plo1+-mCherry* and *nda3-KM311* as in Fig. 1E. Mad1 localisation to kinetochores was scored as cells entered mitosis.

B Mad1-EDD/QNN and Mad1-Δhelix show similar localisation to wild type Mad1

Representative images of cells expressing *plo1+-mCherry*, *nda3-KM311* and the indicated *mad1-GFP* fusions. Cells were grown at permissive temperature for the *nda3-KM311* mutant (30 °C). Scale bar: 10 μm

C Nucleoplasmic Mad1-GFP signals of strains analysed in Fig. 3C.

D Mad2-mCherry localisation is not perturbed by *mad1-EDD/QNN* or *mad1-Δhelix*

Representative images of cells expressing *mad2+-mCherry*, *nda3-KM311* and the indicated *mad1-GFP* fusions. Cells were grown at permissive temperature for the *nda3-KM311* mutant (30 °C). Scale bar: 10 μm

E Input and flow through of the anti-Mad1 immunoprecipitation shown in Fig. 3F. Cdc2 was used as loading control.

Supplementary Information

Re-annotation of the Mad1 start codon

In the *Schizosaccharomyces pombe* genome database (www.pombase.org), the *mad1+* coding sequence is annotated to start at position 1,277,098 on chromosome II. Alignment with the sequence of other *Schizosaccharomyces* species [3] indicates that the first 13 amino acids (MSSKLTVYQATTS) are not conserved and that it is likely that the start codon is amino acid 14, another Methionine. To corroborate this notion, we performed mass spectrometric analysis of immunopurified Mad1, digested with trypsin. We did not find any peptide corresponding to the first 13 presumed amino acids, but identified a peptide (ADSPRDPFQSR (amino acid 15 – 25), containing N-terminal acetylation), which supports start at amino acid 14 (spectrum below). The *mad1+* coding sequence therefore likely starts at position 1,277,059 on chromosome II, and the *S. pombe* Mad1 protein has 676 amino acids. We are in the process of requesting correction of the start codon in PomBase.

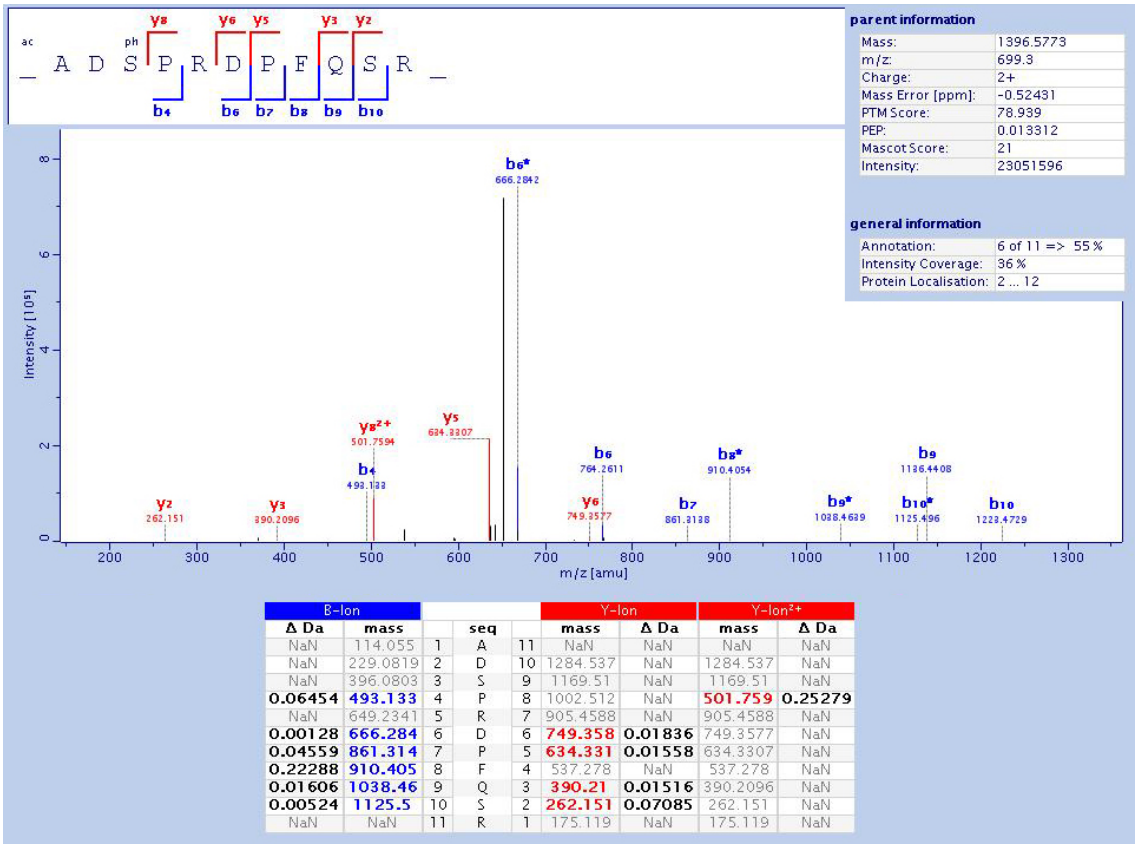

Supplementary References

1. Kammerer RA, Schulthess T, Landwehr R, Lustig A, Engel J, Aebi U, Steinmetz MO (1998) An autonomous folding unit mediates the assembly of two-stranded coiled coils. *Proceedings of the National Academy of Sciences of the United States of America* **95:** 13419-13424

2. O'Shea EK, Klemm JD, Kim PS, Alber T (1991) X-ray structure of the GCN4 leucine zipper, a two-stranded, parallel coiled coil. *Science* **254:** 539-544

3. Rhind N *et al* (2011) Comparative functional genomics of the fission yeasts. *Science* **332:** 930-936

Supplementary Table 1 | S. pombe strains

Figure 1B,C		
SK891	*h+*	*leu1 mad1+-GFP<<kanR plo1+-mCherry<<natR nda3-KM311*
SM001	*h-*	*leu1 mad1-RLK/AAA(R580A/L581A/K582A)-GFP<<kanR plo1+-mCherry<<natR nda3-KM311*
ST146	*h+*	*leu1 mad1-RLK/ALA(R580A/K582A)-GFP<<kanR plo1+-mCherry<<natR nda3-KM311*
SM090	*h+*	*mad1-1-600-GFP<<kanNT3 plo1+-mCherry<<natR nda3-KM311*
SM091	*h+*	*mad1-1-526-GFP<<kanNT3 plo1+-mCherry<<natR nda3-KM311*
Figure 1D		
SK842	*h+*	*leu1 mad2+-GFP<<kanR plo1+-mCherry<<natR nda3-KM311*
SL905	*h-*	*leu1 mad2+-GFP<<kanR plo1+-mCherry<<natR nda3-KM311 mad1-RLK/AAA*
SL759	*h-*	*leu1 mad3+-GFP<<kanR plo1+-mCherry<<natR nda3-KM311*
SL907	*h-*	*leu1 mad3+-GFP<<kanR plo1+-mCherry<<natR nda3-KM311 mad1-RLK/AAA*
Figure 1E,F		
SK891	*h+*	*leu1 mad1+-GFP<<kanR plo1+-mCherry<<natR nda3-KM311*
SK893	*h+*	*leu1 ade6-M216 mad1Δ::ura4+ plo1+-mCherry<<natR nda3-KM311*
SM001	*h-*	*leu1 mad1-RLK/AAA-GFP<<kanR plo1+-mCherry<<natR nda3-KM311*
ST146	*h+*	*leu1 mad1-RLK/ALA-GFP<<kanR plo1+-mCherry<<natR nda3-KM311*
SM090	*h+*	*mad1-1-600-GFP<<kanNT3 plo1+-mCherry<<natR nda3-KM311*
SM091	*h+*	*mad1-1-526-GFP<<kanNT3 plo1+-mCherry<<natR nda3-KM311*
Figure 1G		
SK891	*h+*	*leu1 mad1+-GFP<<kanR plo1+-mCherry<<natR nda3-KM311*
SM001	*h-*	*leu1 mad1-RLK/AAA-GFP<<kanR plo1+-mCherry<<natR nda3-KM311*
ST146	*h+*	*leu1 mad1-RLK/ALA-GFP<<kanR plo1+-mCherry<<natR nda3-KM311*
SM090	*h+*	*mad1-1-600-GFP<<kanNT3 plo1+-mCherry<<natR nda3-KM311*
SM091	*h+*	*mad1-1-526-GFP<<kanNT3 plo1+-mCherry<<natR nda3-KM311*
Figure 1I		
ST038	*h+*	*leu1 bub1+-GFP<<kanR mad2+-mCherry<<natR nda3-KM311*
ST035	*h+*	*leu1 bub1-STT/AAA(cm1-mut;S381A/T383A/T386A)-GFP<<kanR mad2+-mCherry<<natR nda3-KM311*
Figure 1J		
SL901	*h+*	*leu1 bub1+-GFP<<kanR plo1+-mCherry<<natR nda3-KM311*
SP705	*h-*	*leu1 bub1-STT/AAA-GFP<<kanR plo1+-mCherry<<natR nda3-KM311*
ST038	*h+*	*leu1 bub1+-GFP<<kanR mad2+-mCherry<<natR nda3-KM311*
ST035	*h+*	*leu1 bub1-STT/AAA-GFP<<kanR mad2+-mCherry<<natR nda3-KM311*
Figure 1K		
SL901	*h+*	*leu1 bub1+-GFP<<kanR plo1+-mCherry<<natR nda3-KM311*
SI437	*h+*	*leu1 ade6-M216 (ura4DS/E?) bub1::ura4+ plo1+-GFP<<kanR nda3-KM311*
SP705	*h-*	*leu1 bub1-STT/AAA-GFP<<kanR plo1+-mCherry<<natR nda3-KM311*
Figure 2A,B,C		
SK891	*h+*	*leu1 mad1+-GFP<<kanR plo1+-mCherry<<natR nda3-KM311*
SK893	*h+*	*leu1 ade6-M216 mad1Δ::ura4+ plo1+-mCherry<<natR nda3-KM311*
SM814	*h+*	*ade6-M216 mad1Δ::ura4+ pDUAL-Pnmt81-mis12-mad1+-GFP<<leu1+ plo1+-mCherry<<natR nda3-KM311*
SM815	*h+*	*ade6-M216 mad1Δ::ura4+ pDUAL-Pnmt81-mis12-mad1-RLK/AAA-GFP<<leu1+ plo1+-mCherry<<natR nda3-KM311*
SM827	*h+*	*(ade6-M216?) mad1Δ::ura4+ pDUAL-Pnmt81-mad1+-GFP<<leu1+ plo1+-mCherry<<natR nda3-KM311*
SM828	*h+*	*(ade6-M216?) mad1Δ::ura4+ pDUAL-Pnmt81-mad1-RLK/AAA-GFP<<leu1+ plo1+-mCherry<<natR nda3-KM311*
Figure 2D		
SK891	*h+*	*leu1 mad1+-GFP<<kanR plo1+-mCherry<<natR nda3-KM311*
SK893	*h+*	*leu1 ade6-M216 mad1Δ::ura4+ plo1+-mCherry<<natR nda3-KM311*
SM814	*h+*	*ade6-M216 mad1Δ::ura4+ pDUAL-Pnmt81-mis12-mad1+-GFP<<leu1+ plo1+-mCherry<<natR nda3-KM311*
SM815	*h+*	*ade6-M216 mad1Δ::ura4+ pDUAL-Pnmt81-mis12-mad1-RLK/AAA-GFP<<leu1+ plo1+-mCherry<<natR nda3-KM311*
SM827	*h+*	*(ade6-M216?) mad1Δ::ura4+ pDUAL-Pnmt81-mad1+-GFP<<leu1+ plo1+-mCherry<<natR nda3-KM311*
SM828	*h+*	*(ade6-M216?) mad1Δ::ura4+ pDUAL-Pnmt81-mad1-RLK/AAA-GFP<<leu1+ plo1+-mCherry<<natR nda3-KM311*
ST162	*h-*	*mad1+-GFP<<kanR mad2+-mCherry<<natR nda3-KM311*
ST167	*h-*	*(ura4-D18?) mad2+-mCherry<<natR mad1Δ::ura4+ pDUAL-Pnmt81-mis12-mad1+-GFP<<leu1+ nda3-KM311*
ST168	*h-*	*(ura4-D18?) mad2+-mCherry<<natR mad1Δ::ura4+ pDUAL-Pnmt81-mis12-mad1-RLK/AAA-GFP<<leu1+ nda3-KM311*
ST170	*h-*	*(ura4-D18?) mad2+-mCherry<<natR mad1Δ::ura4+ pDUAL-Pnmt81-mad1+-GFP<<leu1+ nda3-KM311*
Figure 3B,C,F		
SK891	*h+*	*leu1 mad1+-GFP<<kanR plo1+-mCherry<<natR nda3-KM311*
ST174	*h-*	*leu1 mad1-EDD/QNN(E670Q/D673N/D676N)-GFP<<kanR plo1+-mCherry<<natR nda3-KM311*
ST190"	*h-*	*leu1 mad1-1-661-GFP<<kanR plo1+-mCherry<<natR nda3-KM311*
Figure 3D,E		
SK891	*h+*	*leu1 mad1+-GFP<<kanR plo1+-mCherry<<natR nda3-KM311*
SK893	*h+*	*leu1 ade6-M216 mad1Δ::ura4+ plo1+-mCherry<<natR nda3-KM311*
ST174	*h-*	*leu1 mad1-EDD/QNN-GFP<<kanR plo1+-mCherry<<natR nda3-KM311*
ST190"	*h-*	*leu1 mad1-1-661-GFP<<kanR plo1+-mCherry<<natR nda3-KM311*
Figure 3G		
ST162	*h-*	*mad1+-GFP<<kanR mad2+-mCherry<<natR nda3-KM311*
ST443	*h+*	*leu1 mad1-EDD/QNN-GFP<<kanR mad2+-mCherry<<natR nda3-KM311*
ST448	*h-*	*leu1 mad1+-GFP<<kanR mad2-R133A-mCherry<<natR nda3-KM311*
ST460	*h+*	*ade6-M216 leu1 mad1-1-661-GFP<<kanR mad2+-mCherry<<natR nda3-KM311*
Figure 3H		
ST167	*h-*	*(ura4-D18?) mad2+-mCherry<<natR mad1Δ::ura4+ pDUAL-Pnmt81-mis12-mad1+-GFP<<leu1+ nda3-KM311*
ST168	*h-*	*(ura4-D18?) mad2+-mCherry<<natR mad1Δ::ura4+ pDUAL-Pnmt81-mis12-mad1-RLK/AAA-GFP<<leu1+ nda3-KM311*
ST447	*h+*	*ade6-M216 mad1Δ::ura4+ pDUAL-Pnmt81-mis12-mad1+-GFP<<leu1+ mad2-R133A-mCherry<<natR nda3-KM311*
Figure S1A,B,D		
SK891	*h+*	*leu1 mad1+-GFP<<kanR plo1+-mCherry<<natR nda3-KM311*
SM001	*h-*	*leu1 mad1-RLK/AAA-GFP<<kanR plo1+-mCherry<<natR nda3-KM311*
ST146	*h+*	*leu1 mad1-RLK/ALA-GFP<<kanR plo1+-mCherry<<natR nda3-KM311*
SM090	*h+*	*mad1-1-600-GFP<<kanNT3 plo1+-mCherry<<natR nda3-KM311*
SM091	*h+*	*mad1-1-526-GFP<<kanNT3 plo1+-mCherry<<natR nda3-KM311*
Figure S1C		
SL894	*h+*	*leu1 ade6-M210 ark1+-GFP<<kanR plo1+-mCherry<<natR nda3-KM311*
SL891	*h+*	*leu1 ark1+-GFP<<kanR plo1+-mCherry<<natR nda3-KM311 mad1-RLK/AAA*
SL900	*h-*	*leu1 bub1+-GFP<<kanR plo1+-mCherry<<natR nda3-KM311*
SL898	*h-*	*leu1 bub1+-GFP<<kanR plo1+-mCherry<<natR nda3-KM311 mad1-RLK/AAA*
SM092	*h-*	*leu1 ade6-M216 bub3+-S(GGGGS)3-GFP<<kanR plo1+-mCherry<<natR nda3-KM311*
SL358	*h-*	*leu1 bub3+-S(GGGGS)3-GFP<<kanR plo1+-mCherry<<natR nda3-KM311 mad1-RLK/AAA*

Figure S1E

SK842	*h+*	*leu1 mad2+-GFP<<kanR plo1+-mCherry<<natR nda3-KM311*
SL905	*h-*	*leu1 mad1Δ::mad1-RLK/AAA mad2+-GFP<<kanR plo1+-mCherry<<natR nda3-KM311*

Figure S1F

SP784	*h+*	*leu1 rpl42::cyhR(sP56Q) bub1Δ::rpl42+hphNT1*
PX938	*h-*	*leu1 bub1+-GFP<<kanR*
SP297	*h-*	*leu1 bub1-STT/AAA-GFP<<kanR*

Figure S1G,I

SK442	*h+*	*leu1 bub1+-GFP<<kanR plo1+-mCherry<<natR*
SP705	*h-*	*leu1 bub1-STT/AAA-GFP<<kanR plo1+-mCherry<<natR nda3-KM311*

Figure S1H,J

ST038	*h+*	*leu1 bub1+-GFP<<kanR mad2+-mCherry<<natR nda3-KM311*
ST035	*h+*	*leu1 bub1-STT/AAA-GFP<<kanR mad2+-mCherry<<natR nda3-KM311*

Figure S2B

SK891	*h+*	*leu1 mad1+-GFP<<kanR plo1+-mCherry<<natR nda3-KM311*
SK893	*h+*	*leu1 ade6-M216 mad1Δ::ura4+ plo1+-mCherry<<natR nda3-KM311*
ST141	*h+*	*leu1 ade6-M216 GCN4(250-277)-mad1-306-676-GFP<<kanR plo1+-mCherry<<natR nda3-KM311*
ST441	*h+*	*leu1 GCN4(250-277)-mad1-458-676-GFP<<kanR plo1+-mCherry<<natR nda3-KM311*
ST408	*h-*	*leu1 GCN4(250-277)-mad1-564-676-GFP<<kanR plo1+-mCherry<<natR nda3-KM311*
ST417	*h+*	*leu1 ade6-M216 GCN4(250-277)-mad1-585-676-GFP<<kanR plo1+-mCherry<<natR nda3-KM311*

Figure S2C,D

SK891	*h+*	*leu1 mad1+-GFP<<kanR plo1+-mCherry<<natR nda3-KM311*
ST141	*h+*	*leu1 ade6-M216 GCN4(250-277)-mad1-306-676-GFP<<kanR plo1+-mCherry<<natR nda3-KM311*
ST442	*h+*	*leu1 GCN4(250-277)-mad1-458-676-GFP<<kanR plo1+-mCherry<<natR nda3-KM311*
ST408	*h-*	*leu1 GCN4(250-277)-mad1-564-676-GFP<<kanR plo1+-mCherry<<natR nda3-KM311*
ST417	*h+*	*leu1 ade6-M216 GCN4(250-277)-mad1-585-676-GFP<<kanR plo1+-mCherry<<natR nda3-KM311*

Figure S2E

ST162	*h-*	*mad1+-GFP<<kanR mad2+-mCherry<<natR nda3-KM311*
ST748	*h-*	*leu1 (ade6-M216?) GCN4(250-277)-mad1-306-676-GFP<<kanR mad2+-mCherry<<natR nda3-KM311*
ST750	*h+*	*leu1 (ade6-M216?) GCN4(250-277)-mad1-458-676-GFP<<kanR mad2+-mCherry<<natR nda3-KM311*
ST752	*h-*	*leu1 (ade6-M216?) GCN4(250-277)-mad1-564-676-GFP<<kanR mad2+-mCherry<<natR nda3-KM311*
ST754	*h+*	*leu1 (ade6-M216?) GCN4(250-277)-mad1-585-676-GFP<<kanR mad2+-mCherry<<natR nda3-KM311*

Figure S2F

SK891	*h+*	*leu1 mad1+-GFP<<kanR plo1+-mCherry<<natR nda3-KM311*
SK893	*h+*	*leu1 ade6-M216 mad1Δ::ura4+ plo1+-mCherry<<natR nda3-KM311*
ST141	*h+*	*leu1 ade6-M216 GCN4(250-277)-mad1-306-676-GFP<<kanR plo1+-mCherry<<natR nda3-KM311*
ST142	*h+*	*leu1 ade6-M216 GCN4(250-277)-mad1-306-676-GFP<<kanR plo1+-mCherry<<natR nda3-KM311*
ST441	*h+*	*leu1 GCN4(250-277)-mad1-458-676-GFP<<kanR plo1+-mCherry<<natR nda3-KM311*
ST442	*h+*	*leu1 GCN4(250-277)-mad1-458-676-GFP<<kanR plo1+-mCherry<<natR nda3-KM311*
ST408	*h-*	*leu1 GCN4(250-277)-mad1-564-676-GFP<<kanR plo1+-mCherry<<natR nda3-KM311*
ST409	*h-*	*leu1 ade6-M216 GCN4(250-277)-mad1-564-676-GFP<<kanR plo1+-mCherry<<natR nda3-KM311*
ST417	*h+*	*leu1 ade6-M216 GCN4(250-277)-mad1-585-676-GFP<<kanR plo1+-mCherry<<natR nda3-KM311*
ST419	*h-*	*leu1 ade6-M216 GCN4(250-277)-mad1-585-676-GFP<<kanR plo1+-mCherry<<natR nda3-KM311*

Figure S3A

SK891	*h+*	*leu1 mad1+-GFP<<kanR plo1+-mCherry<<natR nda3-KM311*
SK893	*h+*	*leu1 ade6-M216 mad1Δ::ura4+ plo1+-mCherry<<natR nda3-KM311*
SM814	*h+*	*ade6-M216 mad1Δ::ura4+ pDUAL-Pnmt81-mis12-mad1+-GFP<<leu1+ plo1+-mCherry<<natR nda3-KM311*
SM815	*h+*	*ade6-M216 mad1Δ::ura4+ pDUAL-Pnmt81-mis12-mad1-RLK/AAA-GFP<<leu1+ plo1+-mCherry<<natR nda3-KM311*
SM827	*h+*	*(ade6-M216?) mad1Δ::ura4+ pDUAL-Pnmt81-mad1+-GFP<<leu1+ plo1+-mCherry<<natR nda3-KM311*
SM828	*h+*	*(ade6-M216?) mad1Δ::ura4+ pDUAL-Pnmt81-mad1-RLK/AAA-GFP<<leu1+ plo1+-mCherry<<natR nda3-KM311*
ST162	*h-*	*mad2+-mCherry<<natR mad1+-GFP<<kanR nda3-KM311*
ST167	*h-*	*(ura4-D18?) mad2+-mCherry<<natR mad1Δ::ura4+ pDUAL-Pnmt81-mis12-mad1+-GFP<<leu1+ nda3-KM311*
ST168	*h-*	*(ura4-D18?) mad2+-mCherry<<natR mad1Δ::ura4+ pDUAL-Pnmt81-mis12-mad1-RLK/AAA-GFP<<leu1+ nda3-KM311*
ST170	*h-*	*(ura4-D18?) mad2+-mCherry<<natR mad1Δ::ura4+ pDUAL-Pnmt81-mad1+-GFP<<leu1+ nda3-KM311*

Figure S3B

ST162	*h-*	*mad2+-mCherry<<natR mad1+-GFP<<kanR nda3-KM311*
ST167	*h-*	*(ura4-D18?) mad2+-mCherry<<natR mad1Δ::ura4+ pDUAL-Pnmt81-mis12-mad1+-GFP<<leu1+ nda3-KM311*
ST168	*h-*	*(ura4-D18?) mad2+-mCherry<<natR mad1Δ::ura4+ pDUAL-Pnmt81-mis12-mad1-RLK/AAA-GFP<<leu1+ nda3-KM311*
ST170	*h-*	*(ura4-D18?) mad2+-mCherry<<natR mad1Δ::ura4+ pDUAL-Pnmt81-mad1+-GFP<<leu1+ nda3-KM311*
ST171	*h-*	*(ura4-D18?) mad2+-mCherry<<natR mad1Δ::ura4+ pDUAL-Pnmt81-mad1-RLK/AAA-GFP<<leu1+ nda3-KM311*

Figure S4A

SP903	*h-*	*leu1 mad1-L533A-GFP<<kanR plo1+-mCherry<<natR nda3-KM311*
SP965	*h?*	*leu1 ade6-M216 mad1-F592A-GFP<<kanR plo1+-mCherry<<natR nda3-KM311*
SP986	*h+*	*leu1 mad1-R593A-GFP<<kanR plo1+-mCherry<<natR nda3-KM311*
SP983	*h+*	*leu1 mad1-V596A-GFP<<kanR plo1+-mCherry<<natR nda3-KM311*
SP967	*h+*	*leu1 mad1-G601A-GFP<<kanR plo1+-mCherry<<natR nda3-KM311*
ST115	*h+*	*leu1 ade6-M216 mad1-R613A-GFP<<kanR plo1+-mCherry<<natR nda3-KM311*
SP476	*h+*	*leu1 ade6-M216 mad1-S616A-GFP<<kanR plo1+-mCherry<<natR nda3-KM311*
SP511	*h+*	*leu1 mad1-P661A-GFP<<kanR plo1+-mCherry<<natR nda3-KM311*
SP513	*h+*	*leu1 mad1-P661A/S633G-GFP<<kanR plo1+-mCherry<<natR nda3-KM311*
SP597	*h-*	*leu1 mad1-ELK/AAA(E670A/L672A/K674A)-GFP<<kanR plo1+-mCherry<<natR nda3-KM311*
ST148	*h-*	*leu1 mad1-ELK/AAA plo1+-mCherry<<natR nda3-KM311*

Figure S4B,C,E

SK891	*h+*	*leu1 mad1+-GFP<<kanR plo1+-mCherry<<natR nda3-KM311*
ST174	*h-*	*leu1 mad1-EDD/QNN-GFP<<kanR plo1+-mCherry<<natR nda3-KM311*
ST190"	*h-*	*leu1 mad1-1-661-GFP<<kanR plo1+-mCherry<<natR nda3-KM311*

Figure S4D

ST162	*h-*	*mad1-GFP<<kanR mad2+-mCherry<<natR nda3-KM311*
ST443	*h+*	*leu1 mad1-EDD/QNN-GFP<<kanR mad2+-mCherry<<natR nda3-KM311*
ST460	*h+*	*ade6-M216 leu1 mad1-1-661-GFP<<kanR mad2+-mCherry<<natR nda3-KM311*

2.3 Determinants of robustness in spindle assembly checkpoint signalling

Stephanie Heinrich[1], Eva-Maria Geissen[2], Julia Kamenz[1], Susanne Trautmann[3,8], Christian Widmer[1,4], Philipp Drewe[1,4], Michael Knop[3,5], Nicole Radde[2], Jan Hasenauer[6,7], Silke Hauf[1]

[1]Friedrich Miescher Laboratory of the Max Planck Society, 72076 Tübingen, Germany
[2]Institute for Systems Theory and Automatic Control, University of Stuttgart, Germany
[3]EMBL, Heidelberg, Germany
[4]Computational Biology Center, Memorial Sloan-Kettering Cancer Center, New York, USA
[5]ZMBH, University of Heidelberg, Germany
[6]Institute of Computational Biology, Helmholtz Zentrum München, Germany
[7]Department of Mathematics, Technische Universität München, Germany
[8]Present address: PicoQuant GmbH, Berlin, Germany

Correspondence: silke.hauf@tuebingen.mpg.de

Published in **Nature Cell Biology**, Volume 15, p.1328–1339 (2013)
DOI: 10.1038/ncb2864

Author contributions:

I designed and performed all experiments, with the exception of Slp1 quantification in EMM (performed by **Julia Kamenz**), characterization of the Mad1-RL/AG mutant (performed by **Julia Kamenz**) and fluorescence correlation spectroscopy (FCS, performed by **Susanne Trautmann** and **Michael Knop**). I constructed plasmids and strains with contributions by **Julia Kamenz.**

In addition, I contributed to writing the manuscript together with Silke Hauf, Eva-Maria Geissen, Jan Hasenauer and input from all other authors.

Eva-Maria Geissen, Jan Hasenauer, Nicole Radde and **Silke Hauf** performed modelling and statistical evaluation.

Christian Widmer developed the automated nuclear tracking approach with contributions from **Philipp Drewe.**

Silke Hauf supervised the study and performed modelling and statistical evaluation.

nature cell biology

Determinants of robustness in spindle assembly checkpoint signalling

Stephanie Heinrich[1], Eva-Maria Geissen[2], Julia Kamenz[1], Susanne Trautmann[3,8], Christian Widmer[1,4], Philipp Drewe[1,4], Michael Knop[3,5], Nicole Radde[2], Jan Hasenauer[6,7] and Silke Hauf[1,9]

The spindle assembly checkpoint is a conserved signalling pathway that protects genome integrity. Given its central importance, this checkpoint should withstand stochastic fluctuations and environmental perturbations, but the extent of and mechanisms underlying its robustness remain unknown. We probed spindle assembly checkpoint signalling by modulating checkpoint protein abundance and nutrient conditions in fission yeast. For core checkpoint proteins, a mere 20% reduction can suffice to impair signalling, revealing a surprising fragility. Quantification of protein abundance in single cells showed little variability (noise) of critical proteins, explaining why the checkpoint normally functions reliably. Checkpoint-mediated stoichiometric inhibition of the anaphase activator Cdc20 (Slp1 in *Schizosaccharomyces pombe*) can account for the tolerance towards small fluctuations in protein abundance and explains our observation that some perturbations lead to non-genetic variation in the checkpoint response. Our work highlights low gene expression noise as an important determinant of reliable checkpoint signalling.

Biological systems need to operate reliably under a variety of environmental conditions and need to buffer naturally occurring variations in the abundance of biomolecules (termed noise)[1,2]. The spindle assembly checkpoint (SAC) is a signalling pathway that protects genome integrity by detecting and responding to errors in chromosome attachment during mitosis[3,4]. The SAC is essential for the viability of mammals, and its function and components are conserved in eukaryotes[5]. As a guardian of genome integrity, the checkpoint should operate robustly. How this is accomplished is unknown.

SAC proteins accumulate on unattached kinetochores and start a signalling cascade that ultimately inhibits Cdc20 (called Slp1 in *S. pombe*), an essential cofactor of the anaphase-promoting complex/cyclosome (APC/C; refs 6,7). Mad1, Mad2, Mad3 (or BubR1, depending on the organism), Bub1, Bub3 and Mps1 (Mph1 in *S. pombe*) are considered the core components of the SAC. Mad1 and Mad2 form a complex, in which Mad2 adopts a closed conformation[8] (C-Mad2). According to the well-supported template model, Mad1-bound C-Mad2 dimerizes with a second molecule of Mad2 in the open (O-Mad2) conformation, and triggers binding of this second Mad2 molecule, now in the C-conformation, to Cdc20 (refs 9–11). Mad3 then binds C-Mad2:Cdc20. The proteins together form the mitotic checkpoint complex[12] (MCC), which is a potent inhibitor of the APC/C (Fig. 1b).

Requirements for robust checkpoint signalling have been evaluated theoretically[13], but not experimentally. We systematically probed SAC activity following changes in protein abundance or nutrient conditions in fission yeast. This allowed us to define the borders for reliable checkpoint function. Some alterations were tolerated well; other alterations shifted SAC signalling into one of two regimes: either the checkpoint failed entirely, or the cell population split into two genetically identical but phenotypically different populations with dissimilar SAC responses. As critical checkpoint proteins are kept within tight windows of abundance, cells normally do not reach these regimes.

RESULTS

Abundance of SAC proteins and APC/C subunits

SAC signalling involves a series of protein–protein interactions. Hence, signalling outcome should be affected by the abundance of SAC proteins. As a basis to assess how signalling varies with protein abundance, we measured the concentration of SAC proteins and APC/C subunits *in vivo* in single fission yeast cells. We expressed SAC genes as green

[1]Friedrich Miescher Laboratory of the Max Planck Society, 72076 Tübingen, Germany. [2]Institute for Systems Theory and Automatic Control, University of Stuttgart, 70550 Stuttgart, Germany. [3]EMBL, 69117 Heidelberg, Germany. [4]Computational Biology Center, Memorial Sloan-Kettering Cancer Center, New York 10065, USA. [5]Zentrum für Molekulare Biologie der Universität Heidelberg, Deutsches Krebsforschungszentrum, DKFZ-ZMBH Allianz, 69120 Heidelberg, Germany. [6]Institute of Computational Biology, Helmholtz Zentrum München, 85764 Neuherberg, Germany. [7]Department of Mathematics, Technische Universität München, 85748 Garching, Germany. [8]Present address: PicoQuant GmbH, 12849 Berlin, Germany.
[9]Correspondence should be addressed to S. Hauf (e-mail: silke.hauf@tuebingen.mpg.de)

Received 9 April 2013; accepted 20 September 2013; published online 27 October 2013; DOI: 10.1038/ncb2864

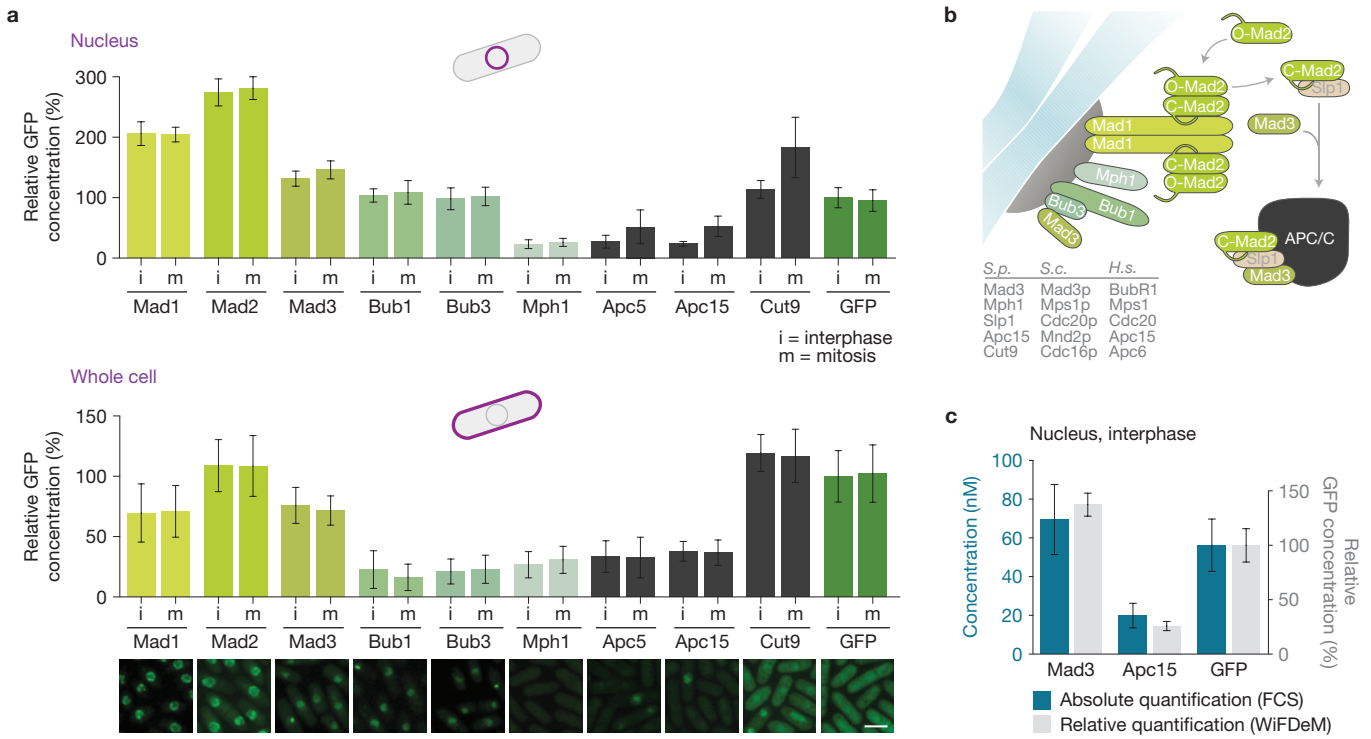

Figure 1 Abundance of SAC proteins and APC/C subunits. (**a**) Concentration of GFP-fusion proteins in the nucleus and the whole cell, normalized to the interphase concentration of free GFP expressed from the *mad3* promoter (GFP). Error bars, s.d. Statistics in Supplementary Table 1. Pictures show representative cells (scale bar, 5 μm). (**b**) Simplified schematic of the SAC signalling pathway. SAC proteins enrich at unattached kinetochores. Dimerization between Mad1-bound Mad2 and free Mad2 initiates binding of Mad2 to Cdc20 (*S. pombe* Slp1), followed by binding of Mad3 to form the mitotic checkpoint complex (MCC; template model[9]). When it is part of the MCC, Cdc20/Slp1 is unable to activate the APC/C. Protein names differ between organisms *(S.p., Schizosaccharomyces pombe; S.c., Saccharomyces cerevisiae; H.s., Homo sapiens).* (**c**) Average concentration of Mad3–GFP, Apc15–GFP and free GFP in the interphase nucleus determined by FCS (Supplementary Fig. 3). Relative abundances from **a** are shown for comparison.

fluorescent protein (GFP) fusions from the endogenous promoter at the endogenous locus, assessed their functionality (Supplementary Fig. 1) and quantified relative protein abundance both in the nucleus and in the entire cell by wide-field fluorescence deconvolution microscopy[14] (WiFDeM; Supplementary Fig. 2). SAC and APC/C protein abundances were similar between interphase and mitosis, but the APC/C became enriched in the nucleus during mitosis (Fig. 1a and Supplementary Table 1). The APC/C subunit Cut9 (Cdc16/Apc6 in other organisms) was more abundant than Apc5 and Apc15, presumably because it is present in the APC/C in two copies[15] and has an additional non-APC/C-bound pool[16]. According to the template model, Mad2 should be in excess over Mad1, which was the case (Fig. 1a). Bub1 and Bub3 showed similar abundances and nucleo-cytoplasmic distributions, fitting the complex formation between these proteins[17]. Furthermore, the low abundance of Mph1 was consistent with its catalytic role in the checkpoint[18,19]. Hence, our protein quantifications agree with existing knowledge on the molecular mechanisms of the SAC (Fig. 1b).

We measured absolute protein concentrations by fluorescence correlation spectroscopy (FCS) and quantitative immunoblotting in a strain that expresses freely diffusible GFP from the *mad3* promoter (*Pmad3–GFP*). FCS yielded a nuclear GFP concentration of 56 nM (Fig. 1c). On the basis of the relative quantification (Fig. 1a), this indicated nuclear concentrations between 13 nM (Mph1) and 154 nM (Mad2) for the SAC proteins (Supplementary Table 2). We also assessed the abundance of Mad3– and Apc15–GFP by FCS (Fig. 1c). FCS and WiFDeM found similar relative abundances between Mad3, Apc15 and free GFP, which cross-validates the methods. By quantitative immunoblotting, the free GFP concentration was 134 nM (Supplementary Fig. 3). Proteome-wide quantitative mass spectrometry determined values for SAC proteins that were lower or similar to those determined by FCS (Supplementary Table 2). We therefore consider the absolute concentrations derived from FCS of free GFP, in conjunction with relative abundance by WiFDeM, an adequate estimate.

SAC sensitivity to protein abundance changes

To determine which variations of checkpoint protein abundance are compatible with checkpoint activity, we modified the concentration of Mad1, Mad2 and Mad3 by promoter modifications (Supplementary Fig. 4 and Table 3). We assessed SAC activity by measuring mitosis time after preventing microtubule formation with a conditional tubulin mutation (*nda3-KM311*; ref. 20; Fig. 2a). Wild-type cells engage the SAC and remain in mitosis for longer than 5 h. Cells with a reduction of Mad1 to 30% of its wild-type level maintained a mitotic delay (Fig. 2b). Even reduction to about 10% of the original Mad1 level, which is hardly visible by fluorescence microscopy (Fig. 2e), did not fully abolish the SAC. As opposed to the strong reduction of Mad1 that was necessary to affect the SAC, already a slight reduction of Mad2 to 80% of the

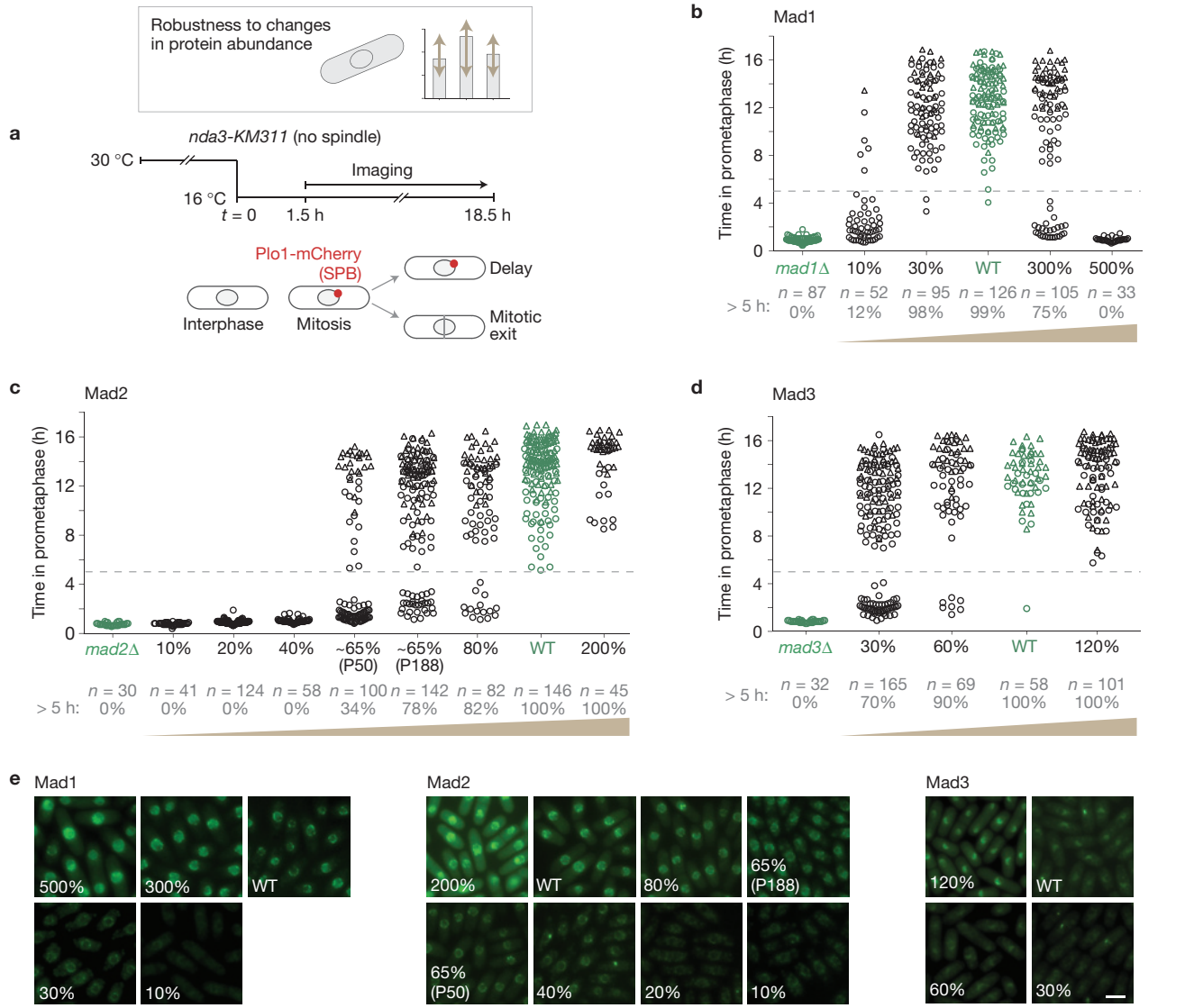

Figure 2 Sensitivity of the checkpoint to SAC protein abundance. (**a**) Cells expressing the tubulin mutant *nda3-KM311* and *plo1*$^{+}$*–mCherry* are shifted to the restrictive temperature for *nda3-KM311* to prevent microtubule formation, which is followed by live-cell imaging. The time in prometaphase, which indicates SAC functionality, is determined by the presence of Plo1–mCherry at spindle pole bodies (SPBs). (**b**–**d**) Mad1–GFP (**b**), Mad2–GFP (**c**) and Mad3–GFP (**d**) strains were followed by live-cell imaging as outlined in **a**. Percentages in black indicate the abundance of the respective protein relative to wild-type cells (Supplementary Fig. 4). Circles indicate cells in which the entire mitosis was recorded; triangles indicate cells that were still in mitosis when filming ended, so that only the lower bound of the mitosis time is known. Number of cells (*n*) and percentage of cells that delayed in mitosis for longer than 5 h are shown in grey. WT, wild type. (**e**) Representative GFP images from strains used in **b**–**d**. Imaging conditions and scaling are identical for strains expressing the same checkpoint protein, but differ between checkpoint proteins. Scale bar, 5 μm.

wild-type level impaired SAC function (Fig. 2c). Reduction to about 65% aggravated the effect, and at abundances of 40% or lower, cells lacked checkpoint activity. At about 65% of Mad2, the SAC response was noticeably different in two strains that had similar levels judged by immunoblotting (termed P188 and P50, Supplementary Fig. 4). This suggests a sharp decline in SAC activity at this level. Mad3 is required together with Mad2 to form the MCC and inhibit the APC/C (refs 12,21). Reduction of Mad3 to 60% slightly impaired the SAC, and reduction to 30% impaired the SAC roughly to a similar extent as 65% of Mad2 (Fig. 2d). Hence, the SAC exhibits distinct sensitivity to changes in the amounts of Mad1, Mad2 and Mad3, and the abundance of Mad2 is particularly critical.

Noise of SAC proteins and APC/C subunits

If a mere 20% reduction of Mad2 impairs SAC signalling (Fig. 2c), the cell-to-cell variability in Mad2 abundance must be small to ensure reliable signalling in wild-type cells. Our single-cell measurements (Fig. 1a) allowed us to estimate the protein noise (coefficient of variation (CV); standard deviation/mean×100(%)). The accuracy of the estimate increases with protein concentration (Supplementary Note). For nuclear Mad1 and Mad2, which have the highest concentration, we determine noise around 10% (Fig. 3a), which is low for proteins in this abundance range (Supplementary Note)[22,23]. Hence, it is indeed rare for wild-type cells to reach a level of 80% Mad2 relative to the population average that would perturb SAC signalling.

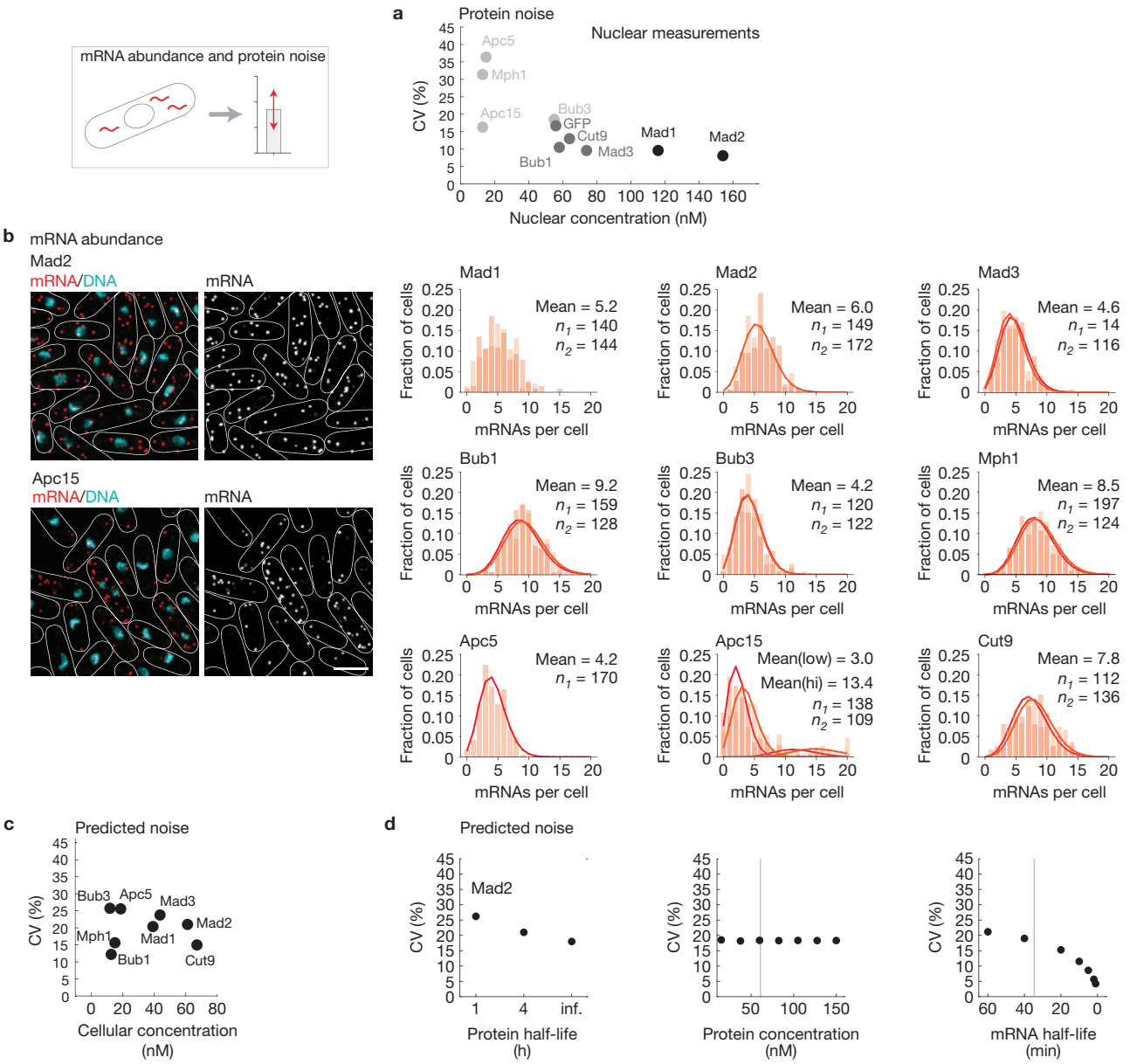

Figure 3 Expression noise of SAC proteins and APC/C subunits. (**a**) Protein noise (CV; standard deviation/mean×100 (%)) from nuclear measurements in Fig. 1a plotted against the nuclear concentration determined by FCS (Fig. 1c and Supplementary Table 2). Low GFP intensity leads to an overestimation of the noise (Supplementary Note). Darker grey indicates more reliable noise measurements. (**b**) Single-molecule FISH with probes against GFP mRNA in strains expressing fusions between the indicated proteins and GFP. Representative images for Mad2–GFP and Apc15–GFP mRNA are shown on the left (scale bar, 5 μm). The histograms show mRNA frequency distributions of two biological replicates (except for Apc5–GFP), and the corresponding fit assuming a Poisson distribution (curve), except for those samples where the *P* value determined from the statistics of the root-mean-square error between model and data, assessed using parametric bootstrapping, rejected the fit (n_1 or n_2 = number of cells in each replicate). Apc15 mRNA abundance fluctuated with cell cycle stage, in agreement with microarray analyses[60–62]; the mean for low and high (hi) expressing cells is given. (**c**) CVs for protein abundance were predicted by stochastic simulation assuming the measured protein concentration (Supplementary Table 2) and mRNA number (**b**), published mRNA half-life[25] and an estimate of 240 min for the protein half-life (Supplementary Note). CVs are plotted against the cellular protein concentration in interphase. (**d**) Protein half-life, protein synthesis rate and mRNA half-life were varied, and CVs were determined by stochastic simulation (Supplementary Note). Thin grey lines indicate measured values (Supplementary Table 2 and ref. 25).

Noise is influenced by messenger RNA number, protein concentration, and mRNA and protein degradation rate. Studies on cell populations determined an mRNA number of SAC genes of about 1 per cell[24] with half-lives between 15 and 35 min (refs 25,26). On the basis of these values, stochastic simulations predict noise of at least 45% for Mad1 and Mad2 (Supplementary Note), considerably higher than our measurement. We therefore assessed mRNA numbers for SAC proteins in single cells by fluorescence *in situ* hybridization[27] (FISH). We detected an average of 4–9 molecules (Fig. 3b), which decreases the expected checkpoint protein noise to 12–26% (Fig. 3c). However, for Mad2 the expected (21%) was still higher than the observed noise (8%). As all measurements that are required for the estimate are associated with uncertainty, we scanned a range of values (Fig. 3d). A longer protein half-life does not suffice for the observed noise, but a

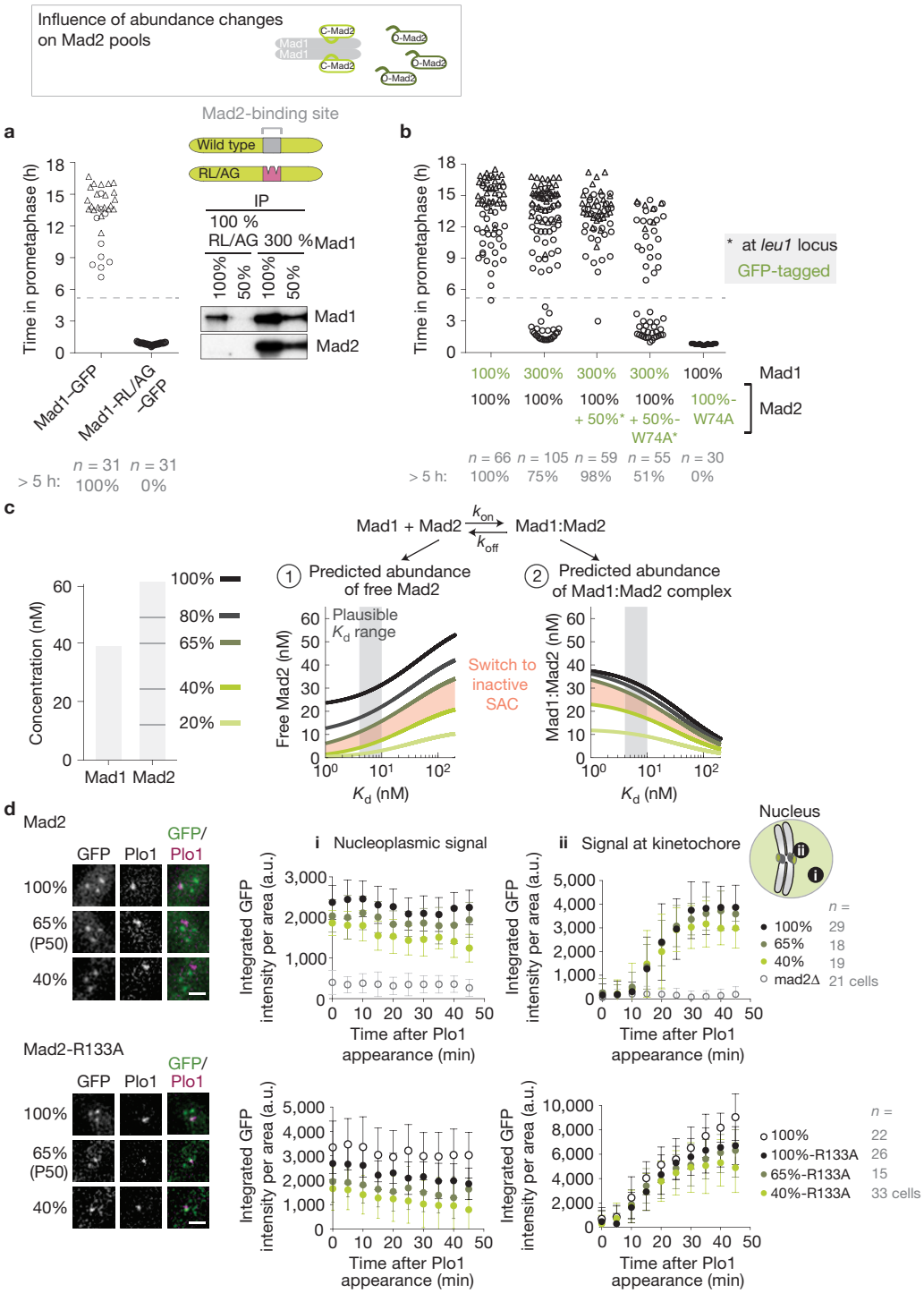

Figure 4 Influence of protein abundance changes on Mad1-bound and free pool of Mad2. (**a**) (Left) Strains were followed by live-cell imaging as in Fig. 2. Mad1-RL/AG contains two point mutations in the Mad2-binding site. (Right) Mad1 immunoprecipitations were analysed for the presence of Mad1 and Mad2. Input and flow through shown in Supplementary Fig. 5c. (**b**) Strains were followed by live-cell imaging as in Fig. 2. Protein abundances were determined by immunoblotting (Supplementary Figs 4a and 5f). Note that expression of 200% of Mad2–GFP is insufficient to delay mitosis or cause checkpoint activation in the absence of Mad1 (Supplementary Fig. 5h,i). Hence, the rescue is not due to artificial checkpoint activation by 150% Mad2. (**c**) Free Mad2 and Mad1:Mad2 abundance were computed from measured cellular concentrations of Mad1 and Mad2 in the wild type and in strains with altered protein abundance. Calculation was performed across a range of K_d values for Mad1:Mad2 complex formation. A plausible range of K_d values is indicated in grey (Supplementary Note). (**d**) The amount of Mad2–GFP or Mad2-R133A–GFP in the nucleoplasm (1) and at the kinetochore (2) was recorded as cells entered mitosis in the absence of microtubules (error bars, s.d.; statistical analysis: Supplementary Fig. 6f). Representative prometaphase nuclei are shown on the left. The dot-like GFP signals result from localization to the kinetochores of the three chromosomes. The dot-like Plo1 signal results from mitosis-specific localization to spindle pole bodies, which fail to separate in the absence of microtubules. Scale bars, 2 μm. Mad2-R133A has similar abundance as wild-type Mad2, but causes a checkpoint defect (Supplementary Fig. 6d,e). Uncropped images of blots are shown in Supplementary Fig. 9.

shorter mRNA half-life allows noise on the order of 10% (Fig. 3d). It is therefore possible that the discrepancy between measured (Fig. 3a) and predicted noise (Fig. 3c) is a consequence of inaccuracies in the existing measurements. Alternatively, yet undescribed feedback mechanisms control the abundance of checkpoint proteins and suppress noise.

SAC sensitivity to relative Mad1 and Mad2 abundance

The checkpoint is doubly sensitive to reduction of Mad2: even a slight reduction impairs checkpoint signalling; and reduction to 40%, which is still higher than the abundance of several other checkpoint proteins, abrogates checkpoint function (Fig. 2c). To address the molecular basis, we analysed the Mad1-bound and Mad1-unbound (free) pool of Mad2. Eliminating the Mad1-bound Mad2 pool by mutation of the binding site within Mad1 abolishes checkpoint signalling[28] (Fig. 4a), although the localization of Mad1 remains intact and Mad2 is present at normal levels (Supplementary Fig. 5). Overexpression of Mad1 to 300 and 500% reduces the free pool of Mad2 and impairs checkpoint signalling[29,30] (Figs 2b and 4b and Supplementary Fig. 5). Additional expression of wild-type Mad2 to about 150% re-increases the free Mad2 pool (Supplementary Fig. 5e) and rescues the checkpoint defect (Fig. 4b and Supplementary Fig. 5g), whereas additional expression of checkpoint-deficient Mad2 (Mad2-W74A; refs 31,32) does not (Fig. 4b). Together, these experiments confirm that both Mad2 pools are vital for checkpoint function.

We predicted the changes in the two Mad2 pools following reduction of Mad2, given the measured abundances of Mad1 and Mad2 (Fig. 4c). Lowering Mad2 to 80% or 65% should reduce the pool of free Mad2, but affect Mad1-bound Mad2 only little (Fig. 4c). Further reduction of Mad2 to 40 and 20% should continue to lower the pool of free Mad2, but should also decrease the abundance of Mad1:Mad2 (Fig. 4c). To test this prediction, we analysed the levels of Mad2 at kinetochores and in the nucleoplasm. As kinetochore localization of Mad2 crucially depends on Mad1 (ref. 33), the pool of Mad2 at kinetochores reflects the abundance of Mad1:Mad2. In contrast, the nucleoplasmic pool is additionally influenced by free Mad2. We measured wild-type Mad2 and the dimerization-deficient Mad2-R133A (ref. 34), which can be recruited to kinetochores only by direct binding to Mad1. Nucleoplasmic Mad2 decreased progressively as Mad2 was reduced to 65 and 40% Mad2 (Fig. 4d), which fitted our expectation for free Mad2. In contrast, the abundance of Mad2 at the kinetochore was less affected at 65% than at 40% (Fig. 4d) or 20% Mad2 (Supplementary Fig. 6a), in accordance with our prediction for Mad1:Mad2. To exclude that the reduction of Mad2 at kinetochores is influenced by the checkpoint failure in some strains, we tested Mad2 localization in cells lacking Mad3 or expressing Slp1 that is unable to bind Mad2 (*slp1-mr63*; ref. 35). Neither of these conditions reduced Mad2 kinetochore localization (Supplementary Fig. 6c). We conclude that reductions of Mad2 to 80 or 65% are likely to preferentially diminish the free pool of Mad2, leading to a partial checkpoint defect, mimicking the situation of 300% Mad1 (Supplementary Figs 5e and 6b). The checkpoint failure in cells with 40% or less Mad2 is unlikely to be solely due to the reduction of Mad1:Mad2, because cells with 30% Mad1 have less Mad1:Mad2 at kinetochores than cells with 40% Mad2 (Supplementary Fig. 6g), yet maintain checkpoint function (Fig. 2b). Instead, the checkpoint failure below 40% Mad2 could be due to either strong depletion of free Mad2 (Supplementary Fig. 6b), not leaving enough Mad2 to capture all Slp1, or could be due to a concomitant reduction of free Mad2 and Mad1:Mad2. Overall, the experiments underline the importance of appropriate relative levels between Mad1 and Mad2 (refs 29,36–39). Given this necessity, it is surprising that there is apparently no co-regulation of Mad1 and Mad2 abundance (Supplementary Figs 4–6).

SAC sensitivity to nutrient conditions

The checkpoint needs to be robust to fluctuations in intracellular conditions and to changes in the environment. We therefore probed SAC signalling in two different media (rich and minimal; Fig. 5). When chromosome attachment was prevented, wild-type cells delayed in mitosis in both media, suggesting robustness. In strains with altered SAC protein levels, however, the mitotic delay times differed between the two media (Fig. 5a). In cells with 30% Mad1, the checkpoint was markedly impaired in minimal medium, although largely functional in rich medium. This indicated that SAC signalling changes in response to nutrient conditions. We did not observe any difference in SAC protein or APC/C subunit abundance between the two media (Fig. 5b). However, the checkpoint target Slp1 accumulated to about twice the level in minimal compared with rich medium (Fig. 5c). This indicates that the environment alters SAC signalling, at least partly through changes in Slp1 abundance.

Tolerated Mad2 and Mad3 abundance set by Slp1 abundance

The SAC blocks APC/C activity by binding of Mad2 and Mad3 to Slp1, forming the MCC. The relative abundance between these proteins should therefore be an important determinant of checkpoint activity. As Slp1 (like other Cdc20 orthologues) has a short half-life[40,41] (Supplementary Fig. 3h), the comparably long maturation time of GFP (ref. 42) makes quantification through a GFP tag inaccurate. We therefore determined the abundance of endogenous Slp1 by quantitative immunoblotting (Fig. 6a and Supplementary Fig. 7). In cells synchronously undergoing mitosis, Slp1 accumulated to about 21 nM in rich medium (Fig. 6a) with slight enrichment (to about 30 nM) in the nucleus (Supplementary Fig. 7d). By single-molecule FISH, the number of Slp1 mRNAs varied between 0 (mean: 4.5) in interphase and up to more than 100 molecules in mitotic cells (Fig. 6b and Supplementary Fig. 7f). We confirmed that Slp1 is about twice as abundant in minimal medium (Supplementary Fig. 7). As we measured absolute Slp1 abundance by a different method from the absolute abundance of SAC proteins, we can compare the numbers only with some reservation. However, the amount of Mad3 (44 nM, Supplementary Table 2) and free Mad2 (around 30 nM, Fig. 4c) would be sufficient to capture 21 nM of Slp1.

To corroborate that the relative levels between Mad2, Mad3 and Slp1 matter, we decreased and increased Slp1. Decreasing Slp1 to about 40% fully rescued the checkpoint defect of cells with 30% Mad3, 65 or 40% Mad2, and of cells with both Mad2 and Mad3 reduced to 40 and 30%, respectively (Fig. 6c,d). Cells with 40% Slp1 and 20% Mad2 had an almost fully functional checkpoint, whereas the absence of Mad2 or Mad3 still caused a checkpoint failure. Increasing Slp1 abundance by inserting a second copy under its endogenous regulatory sequences (Fig. 6f) enhanced the effect of lowering Mad2 or Mad3, and the checkpoint was impaired even when Mad2 and Mad3 were unchanged (Fig. 6e). This was consistent with our abundance measurements, which suggested that Mad2 and Mad3 become limiting

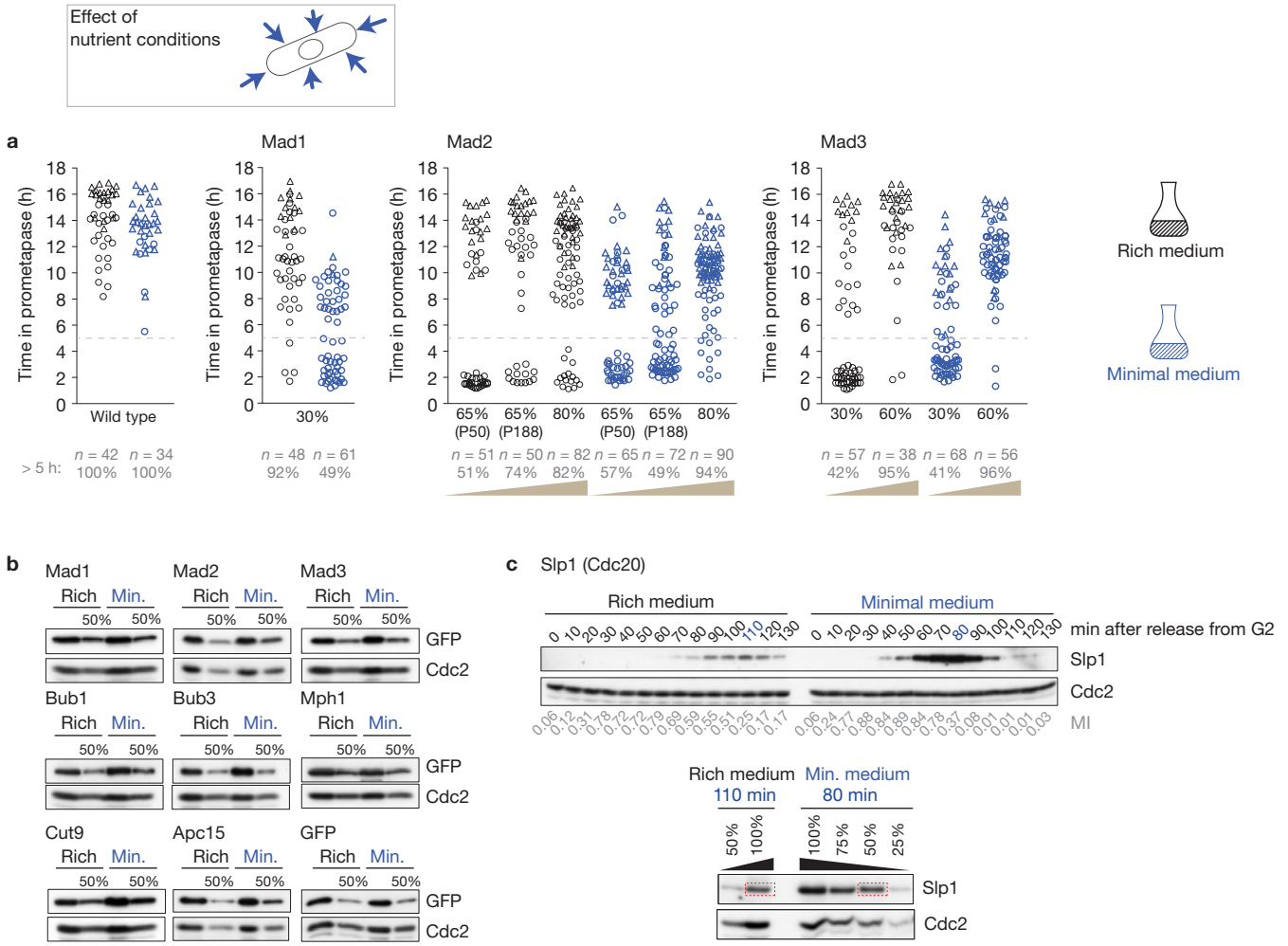

Figure 5 Alteration of the checkpoint response by growth medium. (**a**) Strains were followed by live-cell imaging as in Fig. 2 in either rich medium (black) or minimal medium (blue). (**b**) Strains expressing protein–GFP fusions from the endogenous locus were grown in rich or minimal (min.) medium. Extracts were analysed by immunoblotting using anti-GFP and anti-Cdc2 (loading control) antibodies. In every second lane, half the amount of extract was loaded (50%). (**c**) Cdc25-22 cells were cultured in rich or minimal medium, synchronized in G2 and released into mitosis at 16 °C. Samples were taken every 10 min and cell extracts were analysed for Slp1 abundance by immunoblotting with Cdc2 as the loading control. The mitotic index (MI; fraction of (pro)metaphase cells) is given below. The time point of maximal Slp1 signal was used to compare Slp1 abundance in rich and minimal medium (lower part). Percentages on top indicate how much of the extract was loaded. Dashed rectangles indicate bands with similar signal strength from which relative protein abundances were deduced. Uncropped images of blots are shown in Supplementary Fig. 9.

when Slp1 is increased to 200%, and with data from budding yeast showing that overexpression of the Slp1 orthologue by about threefold impaired the SAC (ref. 40). However, the result contrasted with the functional checkpoint observed in minimal medium for a similar abundance of Slp1 (Fig. 5). We suggest that additional, possibly post-translational modifications alter SAC signalling in minimal medium. Our experiments underline the importance of accurate relative levels both within checkpoint proteins and between checkpoint proteins and the checkpoint target Slp1.

Stoichiometric Slp1 inhibition as the cause of the population split

In several of our experiments the mitosis time of cells in a clonal population showed a bimodal distribution (for example, Fig. 2b–d), which we confirmed by statistical analysis (Fig. 7a and Supplementary Fig. 8a). We observed the split into two populations (which we call A and B (Fig. 7a)) when decreasing Mad2 or Mad3 (Fig. 2c,d) or increasing Slp1 (Fig. 6e). This hinted at a mechanism involving MCC formation. Stoichiometric binding reactions, such as MCC formation, can generate ultrasensitivity[43], which could be the source of the population split. To investigate this possibility, we analysed a model for MCC formation (model M1; Fig. 7b). In this model the amount of free Slp1 in the steady state can vary disproportionally with small changes (biological noise) in the Slp1 synthesis rate or the inhibitor concentration (Supplementary Note). We assumed that free Slp1 has to surpass a threshold to initiate anaphase and estimated the required parameters from the observed sizes of population A and B under different experimental conditions (Supplementary Note). Parameters within physiologically plausible boundaries reproduced our observations: free Slp1 stayed below the threshold in wild-type cells, despite varying levels of Slp1 synthesis and inhibitor (Fig. 7c), whereas in 30% Mad3 (Fig. 7c) or similar perturbations (Supplementary Note), Slp1 surpassed the threshold in the experimentally observed fraction of cells.

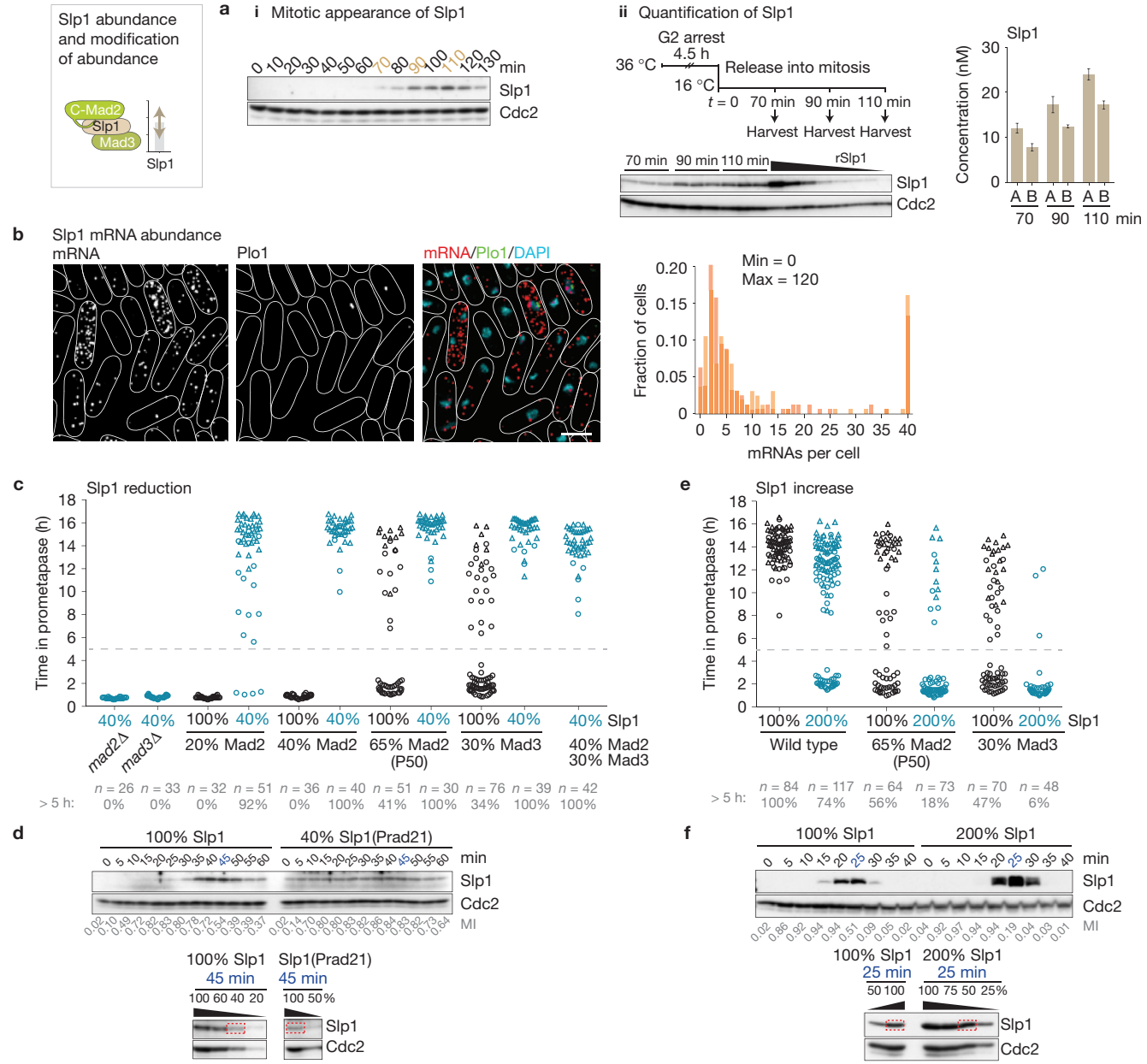

Figure 6 Influence of Slp1 abundance on the amount of Mad2 and Mad3 required for checkpoint function. (**a**) *Cdc25-22* cells were grown in rich medium, synchronized in G2 and released into mitosis at 16 °C. Immunoblotting shows an absence of Slp1 from G2 cells and accumulation in mitosis (**i**). To determine Slp1 concentration, three technical replicates were collected at the indicated time points and analysed by immunoblotting using anti-Slp1 and anti-Cdc2 (loading control) antibodies (**ii**). Recombinant His_6–Slp1 (rSlp1) was mixed with G2 extract and used as the standard for quantification. The graph on the right shows the average concentrations determined in two independent experiments (A, B; error bars, s.d. of technical replicates). (**b**) Single-molecule FISH of cells grown in rich medium with probes against Slp1 mRNA. A representative image is shown on the left (scale bar, 5 μm). Localized Plo1–GFP signals indicate cells in prometaphase. The histogram on the right depicts the mRNA frequency distribution of two replicates ($n = 158$ and 161 cells). (**c**–**f**) Slp1 abundance was altered and combined with changes in Mad2 or Mad3 abundance. (**c**,**e**) Strains were followed by live-cell imaging as in Fig. 2. (**d**,**f**) *Cdc25-22* cells were cultured in rich (**d**) or minimal (**f**) medium, synchronized in G2 and released into mitosis at 25 °C. Cell extracts taken at the indicated time points were analysed by immunoblotting using anti-Slp1 and anti-Cdc2 (loading control) antibodies. The mitotic index (MI; fraction of (pro)metaphase cells) is given below. The time point of maximal Slp1 signal was used to compare Slp1 abundances (lower part) as in Fig. 5c. Uncropped images of blots are shown in Supplementary Fig. 9.

The APC/C mediates MCC disassembly[44–46], which forms a double-negative feedback loop with the MCC-mediated inhibition of the APC/C. This could also cause ultrasensitivity and explain a population split. We therefore included the APC/C into the MCC formation model (model M2; Fig. 7d). Parameters within physiologically plausible boundaries could describe the population split through a bimodal distribution of the APC/C:Slp1 steady-state concentration; that is, although single cells differ only by typical protein noise, the resulting APC/C:Slp1 concentrations, and therefore the propensity to initiate anaphase, can show a bimodal distribution (Fig. 7e and Supplementary Note). Hence,

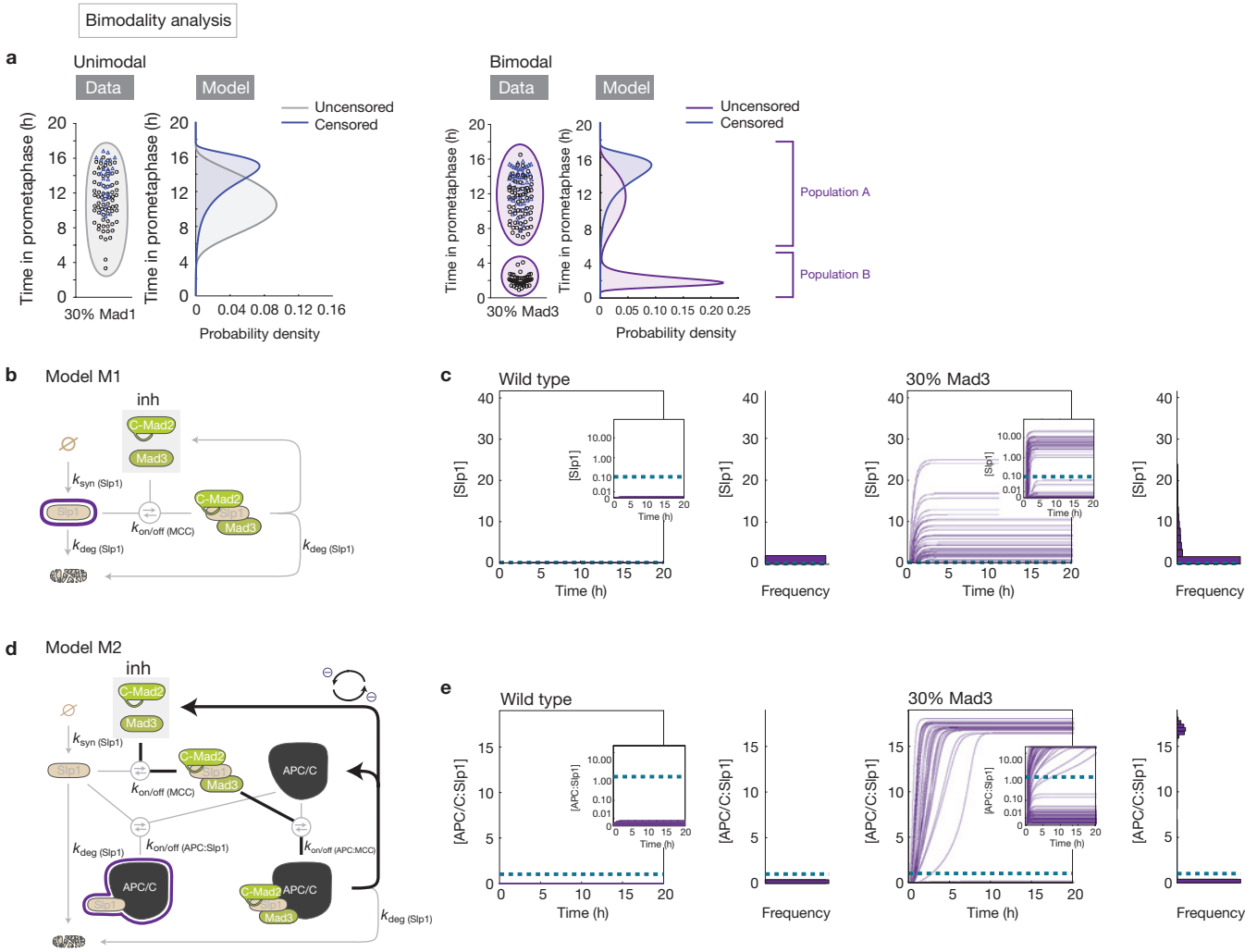

Figure 7 Models for core checkpoint reactions describing the occurrence of two populations. (**a**) Mitosis times were analysed by multi-experiment modelling for the occurrence of one or two subpopulations (Supplementary Fig. 8a). Examples for a unimodal (left, 30% Mad1) and a bimodal (right, 30% Mad3) distribution are shown. Uncensored (full mitosis time recorded) and censored mitosis times (recording stopped before mitosis ended) were modelled separately. (**b**) Reaction scheme for MCC formation. Slp1 is synthesized with rate $k_{syn(Slp1)}$ and degraded with rate $k_{deg(Slp1)}$. Mad2 and Mad3 act as stoichiometric inhibitors (inh) of Slp1 and bind with association rate $k_{on(MCC)}$ and dissociation rate $k_{off(MCC)}$. Slp1 within the complex is degraded with the same rate as free Slp1 (Supplementary Note). (**c**) The model in **b** was parameterized to fit the experimental data and simulated over time (Supplementary Note) for wild-type or 30% Mad3. Slp1 synthesis and inhibitor concentration are randomly sampled from log-normal distributions. The largest plot shows the concentration of free Slp1, [Slp1], over time (purple lines) with the frequency distribution at 20 h plotted on the right. The inset shows [Slp1] using a nonlinear *y* axis (Supplementary Note), which allows visualization of the trajectories around the threshold. When Slp1 stays below the threshold (dashed blue line), we consider this cell to arrest in mitosis (population A); when Slp1 passes the threshold, we assume that the cell exits mitosis (population B). (**d**) Reaction scheme for MCC formation and APC/C binding. In addition to the reactions in **b**, Slp1 binds the APC/C with $k_{on(APC:Slp1)}$ and $k_{off(APC:Slp1)}$, and MCC binds the APC/C with $k_{on(APC:MCC)}$ and $k_{off(APC:MCC)}$. Slp1 within the MCC bound to the APC/C is degraded with the same rate as Slp1, which leads to dissociation of Mad2 and Mad3 from the APC/C (Supplementary Note). APC/C inhibition by the MCC and MCC disassembly by the APC/C form a double-negative feedback loop (bold lines) that can lead to ultrasensitivity. (**e**) The model in **d** was parameterized to fit the experimental data and simulated over time as in **c**. The predicted concentration of APC/C:Slp1 in 30% Mad3 cells after 20 h shows a bimodal distribution.

our computational models suggest that known checkpoint reactions can explain the population split through protein noise.

Non-genetic variability in checkpoint signalling

To explore whether population A and B may indeed result from protein noise, we analysed the checkpoint activity of sister cells in situations where a population split was observed (Fig. 8a). As protein abundance in the mother cell is passed on to the daughter cells, sister cells resemble each other in protein abundance just after cell division but the similarity disappears over time owing to continuing noise[47–49]. We found that sister cells showed the same checkpoint behaviour more often than expected for unrelated cells (Fig. 8a). Hence, there is some correlation between sister cells, which is consistent with protein noise as the basis of the population split. About 20% of sister cell pairs differed in their checkpoint behaviour, which is strong evidence against a genetic cause. We conclude that non-genetic, stochastic variations in protein abundance may determine whether a cell shows the fate of population A or B.

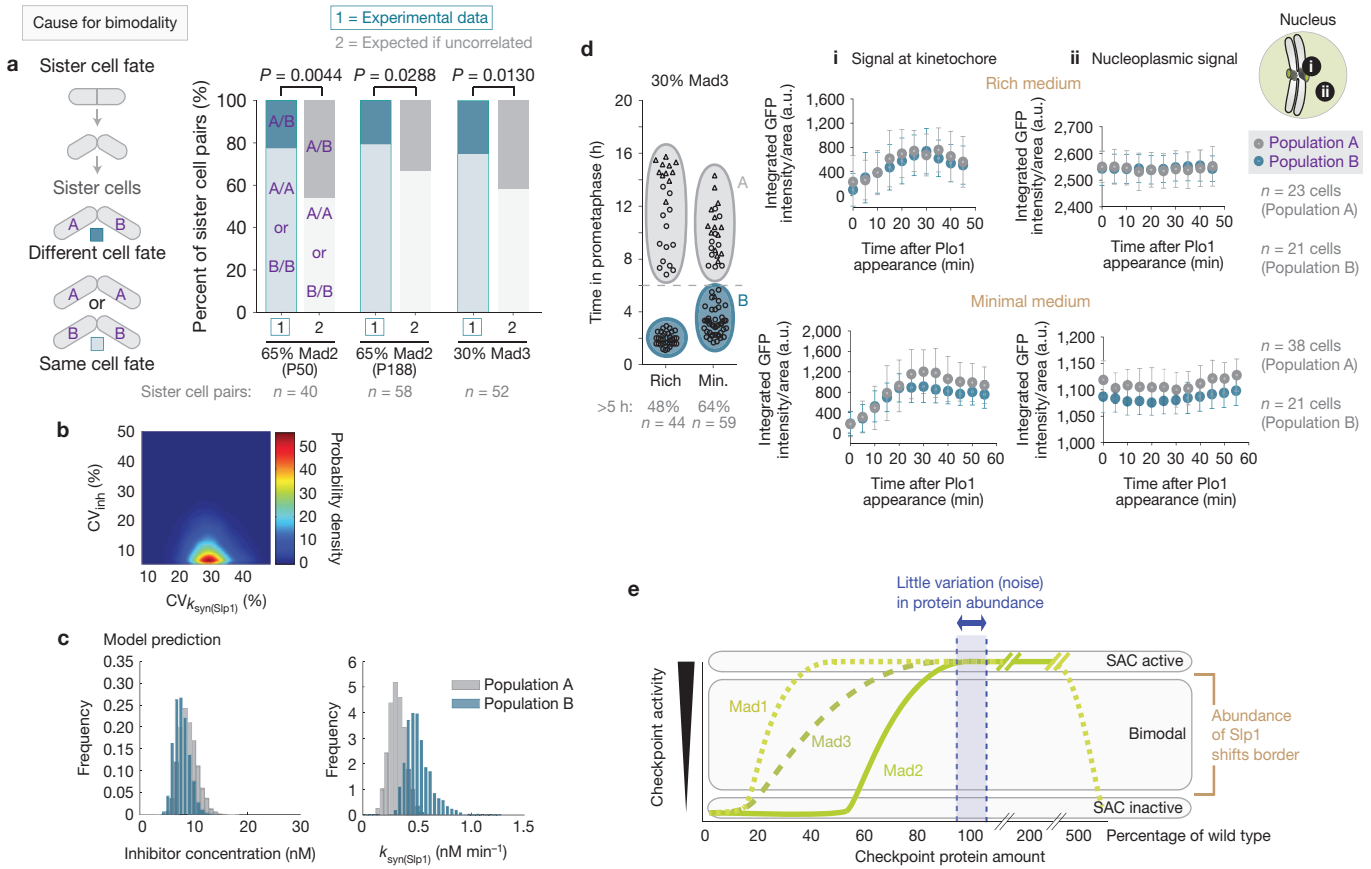

Figure 8 Non-genetic basis of the population split. (**a**) Sister cell pairs were followed by live-cell imaging as in Fig. 2. For each pair, we recorded whether it consisted of two cells with the same fate (A/A or B/B), or of two cells with different fates (A/B) (experimental data). The expected distribution for uncorrelated sister behaviour, which depends on the size of populations A and B, is shown in grey (expected if uncorrelated). Experimental result and expected outcome for uncorrelated behaviour were compared using a Chi-squared test. (**b**) The density distribution for the noise (CV) of Slp1 synthesis rate ($k_{syn(Slp1)}$) and inhibitor concentration was determined with model M1 (Supplementary Note). For wild-type cells, the model predicts lower noise in inhibitor concentration than in Slp1 synthesis. (**c**) The distributions of inhibitor concentration and Slp1 synthesis rate in populations A and B in cells with 30% Mad3 were predicted with model M2 (Supplementary Note). (**d**) Strains were followed by live-cell imaging as in Fig. 2 in either rich or minimal (min.) medium (left side). Mad3–GFP signals were quantified in each population (A and B) as cells entered mitosis (right side; a.u., arbitrary units; error bars, s.d). Statistical analysis: Supplementary Fig. 8d). Differences in Mad3 concentration between the two populations in minimal medium were statistically significant ($P < 0.05$). For rich medium, one representative out of two independent experiments is shown. (**e**) Sensitivity of the SAC to alterations in protein abundance. Checkpoint signalling is normally reliable, and all cells that encounter unattached chromosomes are delayed in mitosis (the SAC is active). Alterations in checkpoint protein abundance can shift checkpoint signalling into one of two other regimes: either only a fraction of cells responds reliably to unattached chromosomes (bimodal), or the checkpoint response is abolished in the entire population (SAC is inactive). To preserve reliable signalling, the abundance of some SAC proteins (for example, Mad2) can fluctuate only little. The abundance of Slp1 shifts the borders at which transition into another regime happens.

We used models M1 and M2 to investigate which extent of noise is required for the observed population split, while preserving a stable arrest in wild-type cells. Both models agreed that the noise for the inhibitor concentration in wild-type cells should be lower (CV: 5 and 9%, respectively) than for Slp1 synthesis (CV: 32 and 35%, respectively). An exhaustive exploration of the parameter space for model M1 confirmed this notion (Fig. 8b). This is consistent with the low noise of checkpoint proteins (Fig. 3), and we find it conceivable that the strong increase in transcription, and potentially translation, for Slp1 at the start of mitosis leads to a larger variability (Fig. 6). Model M2 indicated that the mean inhibitor concentration should differ little between population A and B, whereas the Slp1 synthesis rate should differ more (Fig. 8c). We cannot specifically measure the concentration of the active, inhibitory species of Mad2 and Mad3, but measured the total concentration as a substitute. The levels of Mad2 and Mad3 were highly similar between the two populations (Fig. 8d and Supplementary Fig. 8b–d). In minimal medium, we observed a slight tendency for higher Mad2 and Mad3 levels in the population of cells arresting for longer, consistent with the model prediction. When we vary Mad3 abundance in a strain with 65% Mad2, the fraction of cells in population A and B changes only little (Supplementary Fig. 8f), which confirms the relative insensitivity of the population split to changes in Mad3 abundance. As the pool of active Mad2 and Mad3 could be influenced by upstream checkpoint components, we analysed the amount of Bub1 in the two populations, but also found no significant difference (Supplementary Fig. 8e). Both experiments and model predictions therefore support that differences in the Slp1 synthesis rate play a stronger role in determining whether a cell is able to arrest following checkpoint activation or escapes the arrest. Overall, our results suggest that slight cell-to-cell variations can cause a

population split in the checkpoint response and that known checkpoint reactions can explain this split.

DISCUSSION

The SAC is crucial for genome integrity. How this checkpoint operates robustly is not understood. Here, we provide a comprehensive quantification of SAC proteins and perform an *in vivo* sensitivity analysis that evaluates checkpoint activity following changes in checkpoint protein abundance or nutrient conditions. We made several important observations: even small variations in checkpoint protein abundance can strongly impact signalling; the level of the relevant checkpoint proteins is kept within a narrow window; changes in protein abundance can cause non-genetic variability in the checkpoint response; and nutrient conditions influence the level of the checkpoint target Slp1, suggesting that cells modify SAC signalling in response to the environment.

Stoichiometric inhibition underlies robustness and fragility of SAC signalling

Robustness to perturbations is a key feature of many biological systems. Tight binding of an activator by an inhibitor can buffer variations in these components, as long as the inhibitor is in large enough excess[43]. A theoretical analysis of SAC signalling suggested that inhibition of the APC/C activator Slp1 (Cdc20) through sequestration by Mad2 and Mad3 provides robustness to fluctuations in Slp1 production[13]. Our experimental and theoretical analysis supports this mechanism (Figs 7 and 8). The robustness provided by stoichiometric inhibition, however, comes at a price. If the abundance of the inhibitor is reduced, the system output becomes variable, as is the case with 80% Mad2 or 60% Mad3. Hence, for the checkpoint to work reliably the abundance of these proteins should not fluctuate beyond certain borders, and indeed we observe low noise for Mad2 and Mad3 (Fig. 3). This level of noise is lower than is expected on the basis of measured protein and mRNA abundance and half-life (Supplementary Note). It remains an open question whether the discrepancy is due to incorrect measurements or whether yet undiscovered regulatory mechanisms, for example negative feedback between protein abundance and translation rate, control protein noise.

Reasons for narrow zone of reliable signalling

The fragility of the checkpoint to reduction of some of its components seems dangerous for cells and requires that these proteins are kept within tight windows of abundance (Fig. 8e). Slightly increasing the abundance of these proteins does not impair checkpoint signalling (Fig. 2), raising the question of why the level is not higher. The reason could be adaptability of the system. Alterations in the abundance of Slp1, as they are seen in different media, will not have a consequence on SAC signalling if the levels of critical SAC proteins are so high that these alterations are buffered. Hence, the system has to find a trade-off between reliable signalling in most situations, and the possibility to alter the system if needed. Alternatively, kinetic requirements may determine the levels. Higher levels of Mad2 or Mad3 may impair the ability to quickly and reliably silence the checkpoint. We expect that the levels of checkpoint proteins are under selection, and different organisms may operate with different relative and absolute levels. For example, for both budding yeast and vertebrate cells[29,50–56], there is evidence that the relative excess of Mad2 over Mad1 is higher than in fission yeast. Clearly, more work is needed to determine how different organisms regulate checkpoint levels and why certain levels are chosen.

Alteration of SAC signalling by changes in protein abundance

We show that SAC signalling can be both altered and abolished by changes in protein abundance. Such changes in abundance may occur in physiologic or pathologic situations. Modifications in checkpoint gene expression or protein abundance have been observed in different tissues (The Human Protein Atlas, ref. 57), during ageing[58], and in cancer cells (Oncomine database). In these situations, checkpoint signalling may be modified, and non-genetic variability in signalling could arise. Cancer cells show non-genetic variability in response to antimitotic drugs that activate the checkpoint[59]. Whether this is indeed related to altered checkpoint protein abundance remains to be examined. Overall, our results highlight both the robustness and the plasticity of SAC signalling and emphasize that checkpoint protein abundance is an important determinant in specifying the checkpoint response. □

METHODS

Methods and any associated references are available in the online version of the paper.

Note: Supplementary Information is available in the online version of the paper

ACKNOWLEDGEMENTS

We thank S. Umrania and G. Raetsch for help with developing image analysis software, M. Wachsmuth for FCS analysis software, D. Zenklusen and S-R. Imrazene for sharing their FISH protocol, B. Schwalb and A. Tresch for providing mRNA half-life measurements, N. Hustedt and J. Sauerwald for experiments, E. Illgen, E. Schwoerzer, J. Binder, F. Bolukbasi and W. Hauf for excellent technical help, T. Holder for data processing scripts, C. Liebig for advice on image processing, and F. Theis for support in developing the multi-experiment modelling. We are grateful to K. Gull and T. Matsumoto for antibodies, and to F. Bono, F. Herzog, M. Hothorn, S. Legewie and Y. Watanabe for comments on the manuscript. This work was supported by the Max Planck Society (S. Hauf, S. Heinrich, J.K., C.W. and P.D.), the Ernst Schering Foundation (fellowship to S. Heinrich), the Boehringer Ingelheim Fonds (fellowship to J.K.), the Memorial Sloan-Kettering Cancer Center (C.W. and P.D.), the Cluster of Excellence in Simulation Technology (EXC 310) of the German Research Foundation (DFG; N.R.), the Human Frontier Science Program (HFSP; postdoctoral fellowship to S.T.), the funding program for junior professors of the Ministry of Science, Research and Arts of Baden-Württemberg (E-M.G. and N.R.), and the Federal Ministry of Education and Research (BMBF) within the Virtual Liver project (Grant No. 0315766; J.H.).

AUTHOR CONTRIBUTIONS

S. Heinrich designed and performed all experiments, with the exception of FCS (by S.T. and M.K.), Slp1 quantification in EMM (J.K.), and characterization of the Mad1-RL/AG mutant (J.K.); S. Heinrich constructed plasmids and strains with contributions by J.K.; E-M.G., N.R., J.H. and S. Hauf performed modelling and statistical evaluation; C.W. developed the automated nuclear tracking approach with contributions from P.D.; S. Hauf devised the project and wrote the manuscript together with S. Heinrich and input from all authors.

COMPETING FINANCIAL INTERESTS

The authors declare no competing financial interests.

Published online at www.nature.com/doifinder/10.1038/ncb2864
Reprints and permissions information is available online at www.nature.com/reprints

1. Barkai, N. & Shilo, B. Z. Variability and robustness in biomolecular systems. *Mol. Cell* **28,** 755–760 (2007).
2. Raj, A. & van Oudenaarden, A. Nature, nurture, or chance: stochastic gene expression and its consequences. *Cell* **135,** 216–226 (2008).
3. Lara-Gonzalez, P., Westhorpe, F. G. & Taylor, S. S. The spindle assembly checkpoint. *Curr. Biol.* **22,** R966–R980 (2012).

4. Jia, L., Kim, S. & Yu, H. Tracking spindle checkpoint signals from kinetochores to APC/C. *Trends Biochem. Sci.* **38,** 302–311 (2013).
5. Vleugel, M., Hoogendoorn, E., Snel, B. & Kops, G. J. Evolution and function of the mitotic checkpoint. *Dev. Cell* **23,** 239–250 (2012).
6. Pines, J. Cubism and the cell cycle: the many faces of the APC/C. *Nat. Rev. Mol. Cell Biol.* **12,** 427–438 (2011).
7. Primorac, I. & Musacchio, A. Panta rhei: the APC/C at steady state. *J. Cell Biol.* **201,** 177–189 (2013).
8. Sironi, L. *et al.* Crystal structure of the tetrameric Mad1-Mad2 core complex: implications of a 'safety belt' binding mechanism for the spindle checkpoint. *EMBO J.* **21,** 2496–2506 (2002).
9. De Antoni, A. *et al.* The Mad1/Mad2 complex as a template for Mad2 activation in the spindle assembly checkpoint. *Curr. Biol.* **15,** 214–225 (2005).
10. Mapelli, M. & Musacchio, A. MAD contortions: conformational dimerization boosts spindle checkpoint signaling. *Curr. Opin. Struct. Biol.* **17,** 716–725 (2007).
11. Luo, X. & Yu, H. Protein metamorphosis: the two-state behavior of Mad2. *Structure* **16,** 1616–1625 (2008).
12. Chao, W. C., Kulkarni, K., Zhang, Z., Kong, E. H. & Barford, D. Structure of the mitotic checkpoint complex. *Nature* **484,** 208–213 (2012).
13. Doncic, A., Ben-Jacob, E. & Barkai, N. Noise resistance in the spindle assembly checkpoint. *Mol. Syst. Biol.* **2,** 1–6 (2006).
14. Wu, J. Q. & Pollard, T. D. Counting cytokinesis proteins globally and locally in fission yeast. *Science* **310,** 310–314 (2005).
15. Ohi, M. D. *et al.* Structural organization of the anaphase-promoting complex bound to the mitotic activator Slp1. *Mol. Cell* **28,** 871–885 (2007).
16. Yamashita, Y. M. *et al.* 20S cyclosome complex formation and proteolytic activity inhibited by the cAMP/PKA pathway. *Nature* **384,** 276–279 (1996).
17. Vanoosthuyse, V., Valsdottir, R., Javerzat, J. P. & Hardwick, K. G. Kinetochore targeting of fission yeast Mad and Bub proteins is essential for spindle checkpoint function but not for all chromosome segregation roles of Bub1p. *Mol. Cell Biol.* **24,** 9786–9801 (2004).
18. He, X., Jones, M. H., Winey, M. & Sazer, S. Mph1, a member of the Mps1-like family of dual specificity protein kinases, is required for the spindle checkpoint in *S. pombe*. *J. Cell Sci.* **111,** 1635–1647 (1998).
19. Zich, J. *et al.* Kinase activity of fission yeast Mph1 is required for Mad2 and Mad3 to stably bind the anaphase promoting complex. *Curr. Biol.* **22,** 296–301 (2012).
20. Hiraoka, Y., Toda, T. & Yanagida, M. The NDA3 gene of fission yeast encodes beta-tubulin: a cold-sensitive nda3 mutation reversibly blocks spindle formation and chromosome movement in mitosis. *Cell* **39,** 349–358 (1984).
21. Millband, D. N. & Hardwick, K. G. Fission yeast Mad3p is required for Mad2p to inhibit the anaphase-promoting complex and localizes to kinetochores in a Bub1p-, Bub3p-, and Mph1p-dependent manner. *Mol. Cell Biol.* **22,** 2728–2742 (2002).
22. Bar-Even, A. *et al.* Noise in protein expression scales with natural protein abundance. *Nat. Genet.* **38,** 636–643 (2006).
23. Newman, J. R. *et al.* Single-cell proteomic analysis of *S. cerevisiae* reveals the architecture of biological noise. *Nature* **441,** 840–846 (2006).
24. Marguerat, S. *et al.* Quantitative analysis of fission yeast transcriptomes and proteomes in proliferating and quiescent cells. *Cell* **151,** 671–683 (2012).
25. Amorim, M. J., Cotobal, C., Duncan, C. & Mata, J. Global coordination of transcriptional control and mRNA decay during cellular differentiation. *Mol. Syst. Biol.* **6,** 380 (2010).
26. Sun, M. *et al.* Comparative dynamic transcriptome analysis (cDTA) reveals mutual feedback between mRNA synthesis and degradation. *Genome Res.* **22,** 1350–1359 (2012).
27. Castelnuovo, M. *et al.* Bimodal expression of PHO84 is modulated by early termination of antisense transcription. *Nat. Struct. Mol. Biol.* **20,** 851–858 (2013).
28. Emre, D., Terracol, R., Poncet, A., Rahmani, Z. & Karess, R. E. A mitotic role for Mad1 beyond the spindle checkpoint. *J. Cell Sci.* **124,** 1664–1671 (2011).
29. Chung, E. & Chen, R. H. Spindle checkpoint requires Mad1-bound and Mad1-free Mad2. *Mol. Biol. Cell* **13,** 1501–1511 (2002).
30. Schuyler, S. C., Wu, Y. F. & Kuan, V. J. The Mad1-Mad2 balancing act—a damaged spindle checkpoint in chromosome instability and cancer. *J. Cell Sci.* **125,** 4197–4206 (2012).
31. Tipton, A. R. *et al.* BUBR1 and closed MAD2 (C-MAD2) interact directly to assemble a functional mitotic checkpoint complex. *J. Biol. Chem.* **286,** 21173–21179 (2011).
32. Yang, M. *et al.* Insights into mad2 regulation in the spindle checkpoint revealed by the crystal structure of the symmetric mad2 dimer. *PLoS Biol.* **6,** 643–655 (2008).
33. Heinrich, S., Windecker, H., Hustedt, N. & Hauf, S. Mph1 kinetochore localization is crucial and upstream in the hierarchy of spindle assembly checkpoint protein recruitment to kinetochores. *J. Cell Sci.* **125,** 4720–4727 (2012).
34. Sironi, L. *et al.* Mad2 binding to Mad1 and Cdc20, rather than oligomerization, is required for the spindle checkpoint. *EMBO J.* **20,** 6371–6382 (2001).
35. Kim, S. H., Lin, D. P., Matsumoto, S., Kitazono, A. & Matsumoto, T. Fission yeast Slp1: an effector of the Mad2-dependent spindle checkpoint. *Science* **279,** 1045–1047 (1998).
36. Barnhart, E. L., Dorer, R. K., Murray, A. W. & Schuyler, S. C. Reduced Mad2 expression keeps relaxed kinetochores from arresting budding yeast in mitosis. *Mol. Biol. Cell* **22,** 2448–2457 (2011).
37. Michel, L. S. *et al.* MAD2 haplo-insufficiency causes premature anaphase and chromosome instability in mammalian cells. *Nature* **409,** 355–359 (2001).
38. Iwanaga, Y. *et al.* Heterozygous deletion of mitotic arrest-deficient protein 1 (MAD1) increases the incidence of tumors in mice. *Cancer Res.* **67,** 160–166 (2007).
39. Ryan, S. D. *et al.* Up-regulation of the mitotic checkpoint component Mad1 causes chromosomal instability and resistance to microtubule poisons. *Proc. Natl Acad. Sci. USA* **109,** E2205–E2214 (2012).
40. Pan, J. & Chen, R. H. Spindle checkpoint regulates Cdc20p stability in *Saccharomyces cerevisiae*. *Genes Dev.* **18,** 1439–1451 (2004).
41. Sczaniecka, M. *et al.* The spindle checkpoint functions of Mad3 and Mad2 depend on a Mad3 KEN box-mediated interaction with Cdc20-anaphase-promoting complex (APC/C). *J. Biol. Chem.* **283,** 23039–23047 (2008).
42. Heim, R., Cubitt, A. B. & Tsien, R. Y. Improved green fluorescence. *Nature* **373,** 663–664 (1995).
43. Buchler, N. E. & Louis, M. Molecular titration and ultrasensitivity in regulatory networks. *J. Mol. Biol.* **384,** 1106–1119 (2008).
44. Reddy, S. K., Rape, M., Margansky, W. A. & Kirschner, M. W. Ubiquitination by the anaphase-promoting complex drives spindle checkpoint inactivation. *Nature* **446,** 921–925 (2007).
45. Mansfeld, J., Collin, P., Collins, M. O., Choudhary, J. S. & Pines, J. APC15 drives the turnover of MCC-CDC20 to make the spindle assembly checkpoint responsive to kinetochore attachment. *Nat. Cell Biol.* **13,** 1234–1243 (2011).
46. Uzunova, K. *et al.* APC15 mediates CDC20 autoubiquitylation by APC/C(MCC) and disassembly of the mitotic checkpoint complex. *Nat. Struct. Mol. Biol.* **19,** 1116–1123 (2012).
47. Sigal, A. *et al.* Variability and memory of protein levels in human cells. *Nature* **444,** 643–646 (2006).
48. Spencer, S. L., Gaudet, S., Albeck, J. G., Burke, J. M. & Sorger, P. K. Non-genetic origins of cell-to-cell variability in TRAIL-induced apoptosis. *Nature* **459,** 428–432 (2009).
49. Balazsi, G., van Oudenaarden, A. & Collins, J. J. Cellular decision making and biological noise: from microbes to mammals. *Cell* **144,** 910–925 (2011).
50. Chen, R. H., Brady, D. M., Smith, D., Murray, A. W. & Hardwick, K. G. The spindle checkpoint of budding yeast depends on a tight complex between the Mad1 and Mad2 proteins. *Mol. Biol. Cell* **10,** 2607–2618 (1999).
51. Fraschini, R. *et al.* Bub3 interaction with Mad2, Mad3 and Cdc20 is mediated by WD40 repeats and does not require intact kinetochores. *EMBO J.* **20,** 6648–6659 (2001).
52. Sudakin, V., Chan, G. K. & Yen, T. J. Checkpoint inhibition of the APC/C in HeLa cells is mediated by a complex of BUBR1, BUB3, CDC20, and MAD2. *J. Cell Biol.* **154,** 925–936 (2001).
53. Shah, J. V. *et al.* Dynamics of centromere and kinetochore proteins; implications for checkpoint signaling and silencing. *Curr. Biol.* **14,** 942–952 (2004).
54. Poddar, A., Stukenberg, P. T. & Burke, D. J. Two complexes of spindle checkpoint proteins containing Cdc20 and Mad2 assemble during mitosis independently of the kinetochore in *Saccharomyces cerevisiae*. *Eukaryot. Cell* **4,** 867–878 (2005).
55. Nilsson, J., Yekezare, M., Minshull, J. & Pines, J. The APC/C maintains the spindle assembly checkpoint by targeting Cdc20 for destruction. *Nat. Cell Biol.* **10,** 1411–1420 (2008).
56. Schwanhausser, B. *et al.* Global quantification of mammalian gene expression control. *Nature* **473,** 337–342 (2011).
57. Uhlen, M. *et al.* Towards a knowledge-based Human Protein Atlas. *Nat. Biotechnol.* **28,** 1248–1250 (2010).
58. Baker, D. J. *et al.* BubR1 insufficiency causes early onset of aging-associated phenotypes and infertility in mice. *Nat. Genet.* **36,** 744–749 (2004).
59. Gascoigne, K. E. & Taylor, S. S. Cancer cells display profound intra- and interline variation following prolonged exposure to antimitotic drugs. *Cancer Cell* **14,** 111–122 (2008).
60. Oliva, A. *et al.* The cell cycle-regulated genes of *Schizosaccharomyces pombe*. *PLoS Biol.* **3,** 1239–1260 (2005).
61. Rustici, G. *et al.* Periodic gene expression program of the fission yeast cell cycle. *Nat. Genet.* **36,** 809–817 (2004).
62. Peng, X. *et al.* Identification of cell cycle-regulated genes in fission yeast. *Mol. Biol. Cell* **16,** 1026–1042 (2005).

METHODS

***S. pombe* strains and culture conditions.** Strains are listed in Supplementary Table 4. The *bub3*$^{+}$*-S(GGGGS)3–GFP ≪ kanR*, *mad1–CRVLQHRS/CAV GQHRS (RL/AG)–GFP ≪ kanR*, *mad2-R133A–GFP ≪ kanR*, *mad2-W74A–GFP ≪ kanR* and *mad3*$^{+}$*–GFP–Y66L≪ kanR* strains were generated by PCR-based gene targeting[63]. GFP–Y66L is a non-fluorescent version[64]. To create a strain with doubled abundance of Slp1, the *slp1*$^{+}$ genomic region from 1,504 base pairs (bp) 5′ to 549 bp 3′ of the open reading frame was integrated into the *leu1* locus using the pDUAL system[65]. To create a strain with extra copies of *mad2*$^{+}$*–GFP–T(adh), mad2-W74A–GFP–T(adh)* or *mad2*$^{+}$*-T(mad2)*, the respective genomic region with 950 bp 5′ and 485 bp 3′ (for *mad2*$^{+}$*-Tmad2*) of the *mad2* open reading frame was integrated into the *leu1* locus using the pDUAL system[65]. Other *S. pombe* strains have been described previously: *nda3-KM311* (ref. 20), *cdc25-22* (ref. 66), *cut7-446* (ref. 67), *kanR ≪ Prad21-slp1*$^{+}$ (ref. 68), *mad1*$^{+}$*–GFP ≪ kanR, mad2*$^{+}$*–GFP ≪ kanR, mad3*$^{+}$*–GFP ≪ kanR, bub3*$^{+}$*-S(GGGGS)3–2xGFP ≪ kanR* (ref. 69), *mad1Δ::ura4*$^{+}$, *mad3Δ::ura4*$^{+}$ (ref. 17), *mad2Δ::ura4*$^{+}$ (refs 35,70), *gtb1-93* (ref. 71), *fin1Δ::ura4*$^{+}$ (refs 72,73) and *cut2-364* (refs 74,75).

Cells were grown in either YEA or EMM (ref. 76) containing the necessary supplements. Strains expressing *cdc25-22* were grown at 25 °C until they reached a concentration of 6×10^6 cells ml^{-1}, were arrested before mitosis by shifting to 36 °C for 4.5 h (YEA) or 5 h (EMM), and released by reducing the temperature.

Quantification of GFP signal intensity by WiFDeM. We took several precautions to ensure accuracy of the measurements: we examined functionality of the GFP-fused SAC proteins by analysing growth of the strains, by testing sensitivity to the microtubule-depolymerizing drug benomyl and by performing genetic interaction tests (Supplementary Fig. 1); we ensured that the microscope system responded in a linear fashion to changes in fluorescent protein concentration within the relevant range (Supplementary Fig. 2); we mounted cells in a microfluidics trapping device to ensure parallel orientation of the cells relative to the coverslip, which facilitated capture of the entire cell within the *z*-stack (Supplementary Fig. 2); we performed flat-fielding to eliminate variation caused by unequal illumination; we performed deconvolution to avoid losing out-of-focus light; we subtracted the contribution of autofluorescence by simultaneously measuring cells without GFP (Supplementary Fig. 2); we corrected for errors induced by loss of signal with sample depth[77]; we corrected for variations in lamp intensity between different imaging days by relating all measurements to the *cut9*$^{+}$*–GFP* strain, which was measured on each of the imaging days.

For quantification, asynchronously growing cells were cultured in EMM at 30 °C until they reached a concentration of 6–8 $\times 10^6$ cells ml^{-1}. Cells containing GFP-labelled proteins were mixed with cells containing no GFP, loaded into Y04C plates (CellASIC) and incubated for 2 h at 30 °C on the microscope stage with a constant flow of fresh medium. Imaging was performed on a DeltaVision Core system (Applied Precision) equipped with a climate chamber (EMBL) set to 30 °C. We used a ×60/1.4 Plan Apo oil objective (Olympus) and recorded with a CoolSnap CCD (charge-coupled device) camera (Roper Scientific). *Z*-stacks of 4.8 μm thickness were acquired for both mCherry and GFP fluorescence, with single planes spaced by 0.2 μm. In addition, a differential interference contrast (DIC) reference image of the middle plane was acquired. The imaged area spanned 256 × 256 pixels with 2 × 2 binning. Uneven illumination of the imaged area was corrected by flat-fielding. All images were deconvolved using SoftWorx software. Out of the 24 planes acquired, the 20 central planes were used for further image processing. Only cells of a length above 11 μm were chosen for quantification. The nuclear rim localization of Cut11–mCherry was used as a nuclear marker, and the mitosis-specific localization of Cut11–mCherry to spindle pole bodies was used to differentiate between interphase and early mitotic cells. The nucleus was either tracked in single planes using the SoftWorx 2D polygon tool or by semi-automated segmentation in the *z*-stack using stacked ellipse fitting[78]. The segmentation of the nucleus was projected to the GFP channel and the sum of GFP intensity per sum of area was calculated. Images were corrected for errors introduced by loss of signal with sample depth[77]. To eliminate the contribution of autofluorescence to the signal, we subtracted the sum of intensity per sum of area determined for cells not expressing GFP. To determine the signal from the entire cell, *z*-stacks of 20 planes were sum-projected to a single image and fused to the corresponding DIC image. The outline of individual cells was delineated by hand in the DIC image, projected to the GFP channel and the sum of GFP intensity in this area was calculated. As both the cell width and the cap size are uniform between single cells (data not shown), we used average values for these to calculate the cellular volume from the two-dimensional shape determined by segmentation. The sum of GFP intensities was divided by this volume to determine the GFP concentration. The contribution of autofluorescence was eliminated by performing similar measurements on cells not expressing GFP. The nuclear/cytoplasmic ratio (Supplementary Table 1) was calculated with the measured concentrations in nucleus and whole cell, and with a nucleus to cell volume ratio of 0.08 (ref. 79).

Fluorescence correlation spectroscopy. Cells were cultured in EMM and immobilized on lectin-treated LabTek chambers (Nunc). Fluorescence correlation spectroscopy (FCS) measurements were conducted in the nucleus of G2 cells as judged by cell length (>11 μm) and Cut11–mCherry signal (no spindle pole body localization). Each FCS measurement was acquired for 90 s. The time trace was autocorrelated and fitted with a 1-component anomalous diffusion model, including terms for the photophysics of GFP, using the custom-made Fluctuation Analyser software[80,81]. The parameters resulting from the fit were corrected for background and bleaching. The background correction factor was determined on the basis of the mean fluorescence intensity in the nuclei of wild-type cells (no GFP) that were excited and detected under the same conditions as the experimental measurements. The bleaching correction factor was calculated for each trace as the ratio between the fluorescent intensity within the first 2 s of the measurement and the mean fluorescence intensity. Measurements that showed strong bleaching or strong fluctuations due to cellular movement, resulting in measurement outside the nucleus, were excluded from the analysis based on the time trace. Concentrations were calculated on the basis of the size of the detection volume, which was determined by measurements of the fluorophore Alexa 488 with a known diffusion coefficient of 400 μm^2 s^{-1} (M. Wachsmuth, personal communication).

Size determination of the nucleolus. Cells expressing *cut11*$^{+}$*–mCherry* and either *mad3*$^{+}$*–GFP* or *nuc1*$^{+}$–GFP were cultured in minimal medium (EMM) at 30 °C. Cells were either loaded into Y04C microfluidics plates (CellASIC) or mounted in # 1.5 glass-bottom culture dishes (Ibidi) that had been coated with 35 μg ml^{-1} lectin (Sigma, L-2380). Imaging was performed with conditions identical to those used for relative quantification. The nuclear rim localization of Cut11–mCherry was used as a nuclear marker and the approximate volume of the nucleus was determined by segmenting the nuclear area in each plane (SoftWorx 2D polygon tool) and summing up the areas multiplied by the plane distance of 0.2 μm. The volume of the nucleolus was approximated in a similar way by segmenting the areas occupied by the nucleolar protein Nuc1–GFP, or manually segmenting the areas that exclude Mad3–GFP.

Live-cell imaging to assess SAC functionality. Imaging on a DeltaVision Core system (Applied Precision/GE Healthcare) was performed as previously described[33], with the exception of using 35 μg ml^{-1} lectin (Sigma, L1395 or L-2380) for coating glass-bottom culture dishes (Ibidi).

Quantification of GFP signal in the nucleus and at the kinetochore. Quantification of GFP signal intensity at the kinetochore was performed as previously described[33]. GFP signal intensity in the nucleoplasm was determined by placing two similarly sized regions in the nucleoplasm and in the medium outside the cell. The total intensity measured in the GFP channel per area in the medium was subtracted from the total GFP intensity per area in the nucleoplasm. To analyse differences in kinetochore and nucleoplasmic signals between strains or between population A and B, we used the pooled component test[82]. This is a multivariate test statistic, which accounts for correlation and which can handle missing values. Normality is required for the pooled component test and was verified using the Kolmogorow–Smirnow test taking into account multiple testing by using Bonferroni's correction. As throughout the manuscript, *P* values <0.05 were considered statistically significant.

Single-molecule mRNA fluorescence *in situ* hybridization. Mixtures of DNA probes (Supplementary Table 5) coupled to CAL Fluor Red 610 (Stellaris, synthesized by BioCat) were used for *in situ* hybridization. Except for Slp1, probes were targeted against the GFP moiety of the fusion between gene and GFP coding sequence. Typically, 5×10^7–1×10^8 cells were used for one hybridization reaction. Cells from an asynchronously growing culture were fixed with 4% paraformaldehyde, washed with buffer B (1.2 M sorbitol, 100 mM $KHPO_4$ at pH 7.5, 4 °C) and stored overnight at 4 °C. Cell walls were digested for 45–75 min in spheroplast buffer (1.2 M sorbitol, 100 mM $KHPO_4$ at pH 7.5, 20 mM vanadyl

DOI: 10.1038/ncb2864

ribonuclease complex and 20 μM β-mercaptoethanol) with 1% 100T zymolyase (Medac, 120493-1). The reaction was stopped by washing with buffer B. Cells were incubated for 20 min in 0.01% Triton/1× PBS and washed with 10% formamide/2× SSC. Before hybridization, 25 ng of the probes was mixed with 4μl of a 1:1 mixture between yeast transfer RNA (10 mg ml^{-1}, Life Technologies, AM7119) and salmon-sperm DNA (10 mg ml^{-1}, Life Technologies, 15632-011) and the mixture was dried in a vacuum concentrator. Hybridization buffer F (20% formamide, 10 mM $NaHPO_4$ at pH 7.0; 50 μl per reaction) was added, and the probe/buffer F solution was incubated for 3 min at 95 °C. Buffer H (4× SSC, 4 mg ml^{-1} BSA (acetylated) and 20 mM vanadyl ribonuclease complex; 50 μl per reaction) was added in a 1:1 ratio to the probe/buffer F solution. Cells were resuspended in the mixture and incubated overnight at 37 °C. After three washing steps (10% formamide/2× SSC; 0.1% Triton/2x SSC; 1x PBS), cells were resuspended in 1× PBS and mounted for imaging. Twenty *Z*-planes spaced by 0.3 μm were acquired on a DeltaVision Core system (Applied Precision). We used a ×60/1.4 Plan Apo oil objective (Olympus) and recorded with a CoolSnap CCD camera (Roper Scientific). Images were deconvolved and analysed with FISH-quant software[83] to detect single fluorescent spots in three dimensions. Cells were segmented manually. Dot signals co-localizing with DNA were interpreted as potential transcription sites and excluded from the mRNA counts. Pre-detected spots were narrowed down by thresholds for amplitude, raw intensity and filtered intensity, which were set manually. Typically, the threshold was 1.5× standard deviations below the centre of the distribution of spots that were considered positive. The results were cross-checked by manual counting of a subset of cells. In images of cells not expressing GFP, between 0 and 0.2 spots were detected per cell using similar settings. The value for the number of Slp1 mRNAs in highly expressing cells is underestimated for two reasons: unlike in cells with a low number of mRNAs, fluorescent spots have a range of intensities, indicating that some spots represent more than one mRNA, although we counted these as one; spots close to another spot were sometimes not recognized by the software when the density was high. The frequency distribution of mRNA spots was fitted with a Poisson distribution. The appropriateness of the fits and the corresponding *P* values were determined from the statistics of the root-mean-square error between model and data[84], which were assessed using parametric bootstrapping. For data sets not described by a single Poisson distribution, we fitted a weighted mixture of two Poisson distributions. The appropriateness of the fit was again analysed using the statistics of the root-mean-square error between model and data. For the statistical comparison of the two models, one Poisson distribution and a mixture of two Poisson distributions, we employed the likelihood ratio test.

Immunostaining and fluorescence microscopy of fixed cells. Asynchronously growing cells were fixed with 4% paraformaldehyde (PFA) for 30 min at room temperature, washed three times for 20 min with PEM (100 mM PIPES (pH 6.9), 1 mM EGTA and 1 mM $MgSO_4$) with 0.1% Triton X-100 before resuspending in PEMS (PEM with 1.2 M sorbitol). Beta-mercaptoethanol (0.5%) and zymolyase 100T (1%; Medac, 120493-1) were added and the mixture was incubated for 1 h at 37 °C. Cells were washed once with PEMS, three times with PEM/0.1% Triton X-100 for 20 min each, resuspended in blocking solution PEM-NL (PEM with 5% normal goat serum, 100 mM L-lysine monohydrochloride, 0.1% NaN_3) and incubated for 30 min at room temperature. The primary antibody solution (PEM-NL $^+$ rabbit anti-HA (Cell Signaling 3724S, 1:250) and mouse anti-TAT1 (Gull laboratory, 1:500)) was added and incubated overnight at 4 °C. After washing three times for 20 min with PEM/0.1% Triton X-100, cells were blocked for 5 min with PEM-NL and incubated for 1.5 h with the secondary antibody solution (PEM-NL $^+$ anti-rabbit Alexa-488 (Invitrogen A-11034, 1:250) and anti-mouse Alexa-568 (Invitrogen A-11031, 1:1.000)). Cells were washed three times for 20 min with PEM/0.1% Triton X-100 and resuspended in PEM before imaging. Images were acquired on a Zeiss AxioImager microscope coupled to a CCD camera and were processed with MetaMorph software (Molecular Devices Corporation). Typically, a *z*-stack of about 3 μm thickness, with single planes spaced by 0.3 μm, was acquired and subsequently projected to a single image. To determine the nucleo-cytoplasmic ratio for Slp1–HA, an area was placed over the nucleus of mitotic cells that were identified by the presence of Slp1–HA and a short spindle stained by TAT1. An equally sized area was placed in the cytoplasm. The mean Slp1–HA–Alexa-488 signal measured in the nucleus was divided by the mean Slp1–HA–Alexa-488 signal measured in the cytoplasm. Background measured in interphase cells was subtracted.

Immunoprecipitation. Asynchronously growing cells were collected, washed with extraction buffer (50 mM HEPES at pH 7.5, mM NaCl, 2 mM EDTA and 0.5% NP-40) and frozen as droplets in liquid N_2. Cell extracts were prepared using a mixer mill (RETSCH MM400), followed by resuspension in extraction buffer supplemented with protease inhibitors (Complete EDTA-free, Roche, 1187358001) and phosphatase inhibitors (PhosSTOP, Roche, 4906837001) to a protein concentration of 10 mg ml^{-1}. The extract was spun down for 10 min at 16,600*g* at 4 °C and the supernatant was collected. Protein A-coated magnetic beads (Dynabeads, Invitrogen 10002D) were coupled to rabbit anti-Mad1 antibodies (25 μg per 100 μl beads) and incubated with the supernatant for 15 min at 4 °C. Samples were taken before (input) and after (flow through) incubation with the beads. The beads were washed 5 times with extraction buffer, and elution from the beads was performed by adding 2x SDS sample buffer (125 mM Tris at pH 6.8, 4% SDS, 0.02% bromophenol blue, 20% glycerol and 200 mM dithiothreitol). To quantify input, flow through and immunoprecipitation ratios, the background was subtracted from each band by measuring an equally sized region adjacent to this band. Each Mad1 or Mad2 intensity was normalized to the Cdc2 band intensity in the same lane. As, for each sample, two dilutions were available, ratios were always compared among the more concentrated or among the more diluted samples. The average and standard deviation of these comparisons are shown. As the dilutions of the input were 50 and 25%, whereas the dilutions of the flow through were 100 and 50%, the band intensities for the input were multiplied by two before calculating the ratios. To calculate the immunoprecipitation ratio of Mad2 to Mad1, normalized intensities of Mad2 were divided by normalized intensities of Mad1 individually for each lane. For each strain, the average and standard deviation of the ratios of the two different dilutions (100%, 50%) was then calculated.

Immunoblotting and antibodies. Protein extraction and immunoblotting was performed as previously described[33]. Proteins were detected by mouse anti-GFP (Roche, 11814460001), mouse anti-tubulin (Sigma, T5168), rabbit anti-Mad1 (this study, directed against peptide ADSPRDPFQSRSQL, specificity demonstrated in Supplementary Fig. 5f,i), rabbit anti-Mad2 (ref. 85), rabbit anti-Slp1 (ref. 35) or rabbit anti-Cdc2 (Santa Cruz, SC-53). Secondary antibodies were anti-mouse HRP conjugates (Dianova, 115-035-003) or anti-rabbit HRP conjugates (Dianova, 111-035-003) and were read out using chemiluminescence.

We found that immunoblotting efficiency for recombinant proteins differed when only the recombinant protein was loaded or when the recombinant protein was mixed with a whole-cell extract (data not shown). For quantitative measurement of GFP, we therefore mixed recombinant GFP (Clontech 632373) with a wild-type protein extract not containing GFP. For quantitative measurement of Slp1, we introduced recombinant Slp1 into an extract from G2 cells, which did not contain detectable levels of Slp1. The recombinant GFP that we used for quantification differs from the GFP that was used for tagging of SAC proteins or APC/C subunits by one amino acid (Ser 65 in recombinant GFP, Thr 65 in the fused GFP). The mixture of two monoclonal antibodies that was used for immunoblotting recognizes these two versions similarly well (Supplementary Fig. 3g). We measured the concentration of recombinant GFP both by FCS and by a BCA assay. Both values were in good agreement (0.79 mg ml^{-1} determined by FCS, 0.63 mg ml^{-1} by BCA assay) and were slightly lower than the concentration indicated by the manufacturer (1 mg ml^{-1}). We used the value determined by FCS for all further calculations. The concentration of 6xHis-tagged recombinant Slp1, which was purified under denaturing conditions in 8 M urea, was determined by a Bradford assay. Slp1 and GFP were quantified in *cdc25-22* synchronized mitotic populations. These cells have a larger volume than *cdc25*$^+$ cells, which were used for quantification by microscopy. We determined the nuclear volume increase (Supplementary Fig. 7a), which scales with the cellular volume increase[79], and used this value to derive the presumed protein concentration in a *cdc25*$^+$ cell.

63. Bahler, J. *et al.* Heterologous modules for efficient and versatile PCR-based gene targeting in *Schizosaccharomyces pombe*. *Yeast* **14,** 943–951 (1998).
64. Rosenow, M. A., Huffman, H. A., Phail, M. E. & Wachter, R. M. The crystal structure of the Y66L variant of green fluorescent protein supports a cyclization-oxidation-dehydration mechanism for chromophore maturation. *Biochemistry* **43,** 4464–4472 (2004).
65. Matsuyama, A. *et al.* pDUAL, a multipurpose, multicopy vector capable of chromosomal integration in fission yeast. *Yeast* **21,** 1289–1305 (2004).
66. Russell, P. & Nurse, P. cdc25+ functions as an inducer in the mitotic control of fission yeast. *Cell* **45,** 145–153 (1986).
67. Hagan, I. & Yanagida, M. Novel potential mitotic motor protein encoded by the fission yeast cut7+ gene. *Nature* **347,** 563–566 (1990).

68. Yokobayashi, S. & Watanabe, Y. The kinetochore protein Moa1 enables cohesion-mediated monopolar attachment at meiosis I. *Cell* **123,** 803–817 (2005).
69. Windecker, H., Langegger, M., Heinrich, S. & Hauf, S. Bub1 and Bub3 promote the conversion from monopolar to bipolar chromosome attachment independently of shugoshin. *EMBO Rep.* **10,** 1022–1028 (2009).
70. He, X., Patterson, T. E. & Sazer, S. The *Schizosaccharomyces pombe* spindle checkpoint protein mad2p blocks anaphase and genetically interacts with the anaphase-promoting complex. *Proc. Natl Acad. Sci. USA* **94,** 7965–7970 (1997).
71. Tange, Y. & Niwa, O. Novel mad2 alleles isolated in a *Schizosaccharomyces pombe* gamma-tubulin mutant are defective in metaphase arrest activity, but remain functional for chromosome stability in unperturbed mitosis. *Genetics* **175,** 1571–1584 (2007).
72. Krien, M. J. *et al.* A NIMA homologue promotes chromatin condensation in fission yeast. *J. Cell Sci.* **111,** 967–976 (1998).
73. Grallert, A. & Hagan, I. M. *Schizosaccharomyces pombe* NIMA-related kinase, Fin1, regulates spindle formation and an affinity of Polo for the SPB. *EMBO J.* **21,** 3096–3107 (2002).
74. Funabiki, H., Kumada, K. & Yanagida, M. Fission yeast Cut1 and Cut2 are essential for sister chromatid separation, concentrate along the metaphase spindle and form large complexes. *EMBO J.* **15,** 6617–6628 (1996).
75. Matsumura, T. *et al.* A brute force postgenome approach to identify temperature-sensitive mutations that negatively interact with separase and securin plasmids. *Genes. Cells* **8,** 341–355 (2003).
76. Moreno, S., Klar, A. & Nurse, P. Molecular genetic analysis of fission yeast *Schizosaccharomyces pombe*. *Methods Enzymol.* **194,** 795–823 (1991).
77. Johnston, K. *et al.* Vertebrate kinetochore protein architecture: protein copy number. *J. Cell Biol.* **189,** 937–943 (2010).
78. Widmer, C. *et al.* GRED: graph-regularized 3D shape reconstruction from highly anisotropic and noisy images. Preprint at http://arXiv.org/abs/1309.4426 (2013).
79. Neumann, F. R. & Nurse, P. Nuclear size control in fission yeast. *J. Cell Biol.* **179,** 593–600 (2007).
80. Capoulade, J., Wachsmuth, M., Hufnagel, L. & Knop, M. Quantitative fluorescence imaging of protein diffusion and interaction in living cells. *Nat. Biotechnol.* **29,** 835–839 (2011).
81. Schmidt, U. *et al.* Assembly and mobility of exon-exon junction complexes in living cells. *RNA* **15,** 862–876 (2009).
82. Wu, Y., Genton, M. G. & Stefanski, L. A. A multivariate two-sample mean test for small sample size and missing data. *Biometrics* **62,** 877–885 (2006).
83. Mueller, F. *et al.* FISH-quant: automatic counting of transcripts in 3D FISH images. *Nat. Methods* **10,** 277–278 (2013).
84. Perkins, W., Tygert, M. & Ward, R. Chi-square and classical exact tests often wildly misreport significance; the remedy lies in computers. Preprint at http://arXiv.org/abs/1108.4126 (2011).
85. Yamada, H. Y., Matsumoto, S. & Matsumoto, T. High dosage expression of a zinc finger protein, Grt1, suppresses a mutant of fission yeast slp1(+), a homolog of CDC20/p55CDC/Fizzy. *J. Cell Sci.* **113,** 3989–3999 (2000).

Supplementary Information

nature cell biology

DOI: 10.1038/ncb2864

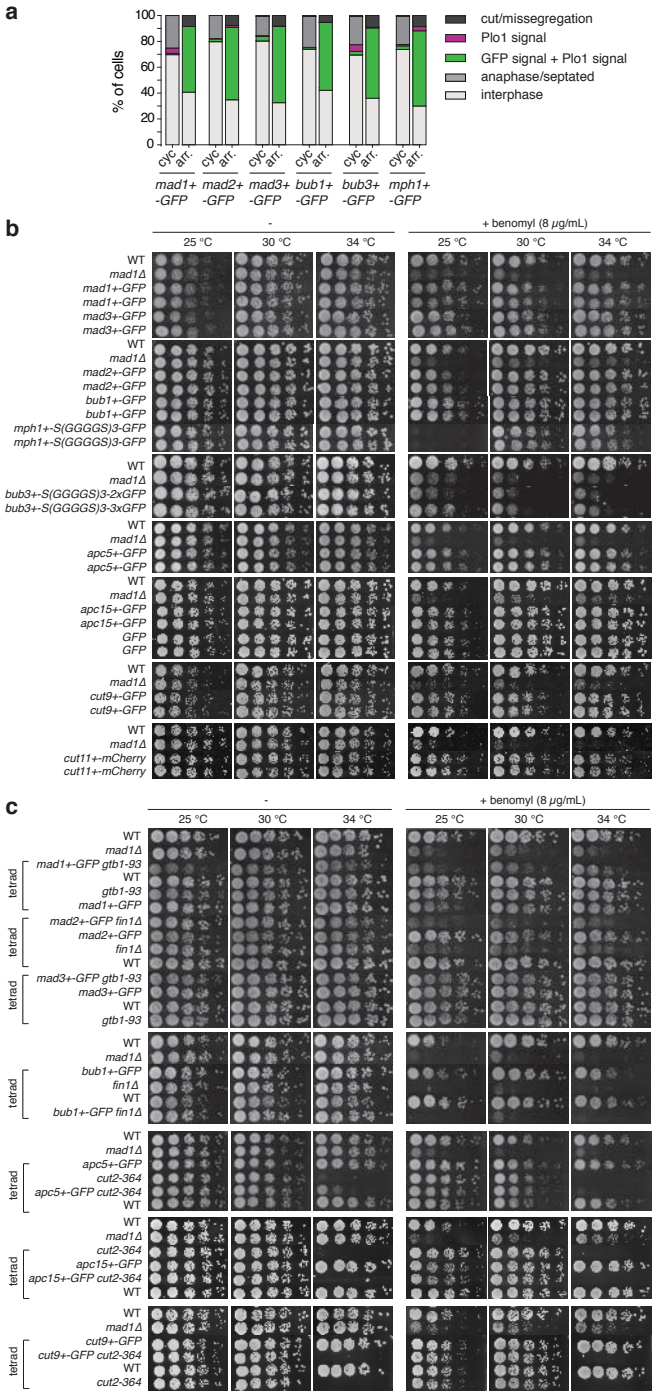

Figure S1 Functionality of GFP fusion proteins. **a** Strains with SAC protein-GFP fusions have a functional SAC. Cells were either grown at permissive temperature for the tubulin mutant *nda3-KM311* (30 °C; cyc; cycling cells) or at restrictive temperature (18 °C; arr.; cells arrested in mitosis) (n > 100 cells for each strain and condition). Plo1 localization to the spindle pole body (Plo1 signal) indicated that cells were in mitosis. Localization of the SAC protein-GFP fusions to kinetochores was additionally scored (GFP signal). Shown is one representative out of two independent experiments. **b** Strains expressing GFP-tagged SAC components grew similar to wild type (WT), with the exception of strains expressing *bub3+-GFP* and *mph1+-GFP*, whose growth was impaired on benomyl-containing medium. A serial dilution of cells was spotted and grown at the indicated temperatures on rich medium or rich medium supplemented with 8 μg/mL of the microtubule drug benomyl. **c** Strains expressing GFP-tagged SAC components were crossed to strains containing mutations that are known to cause a synthetic growth defect when combined with the respective SAC gene deletion. A growth assay of tetrads resulting from these crosses was performed as in (b). Except for the *mad1+-GFP gtb1-93* and *apc5+-GFP cut2-364* double mutant, which had slightly impaired growth, none of the double mutants showed a synthetic growth defect.

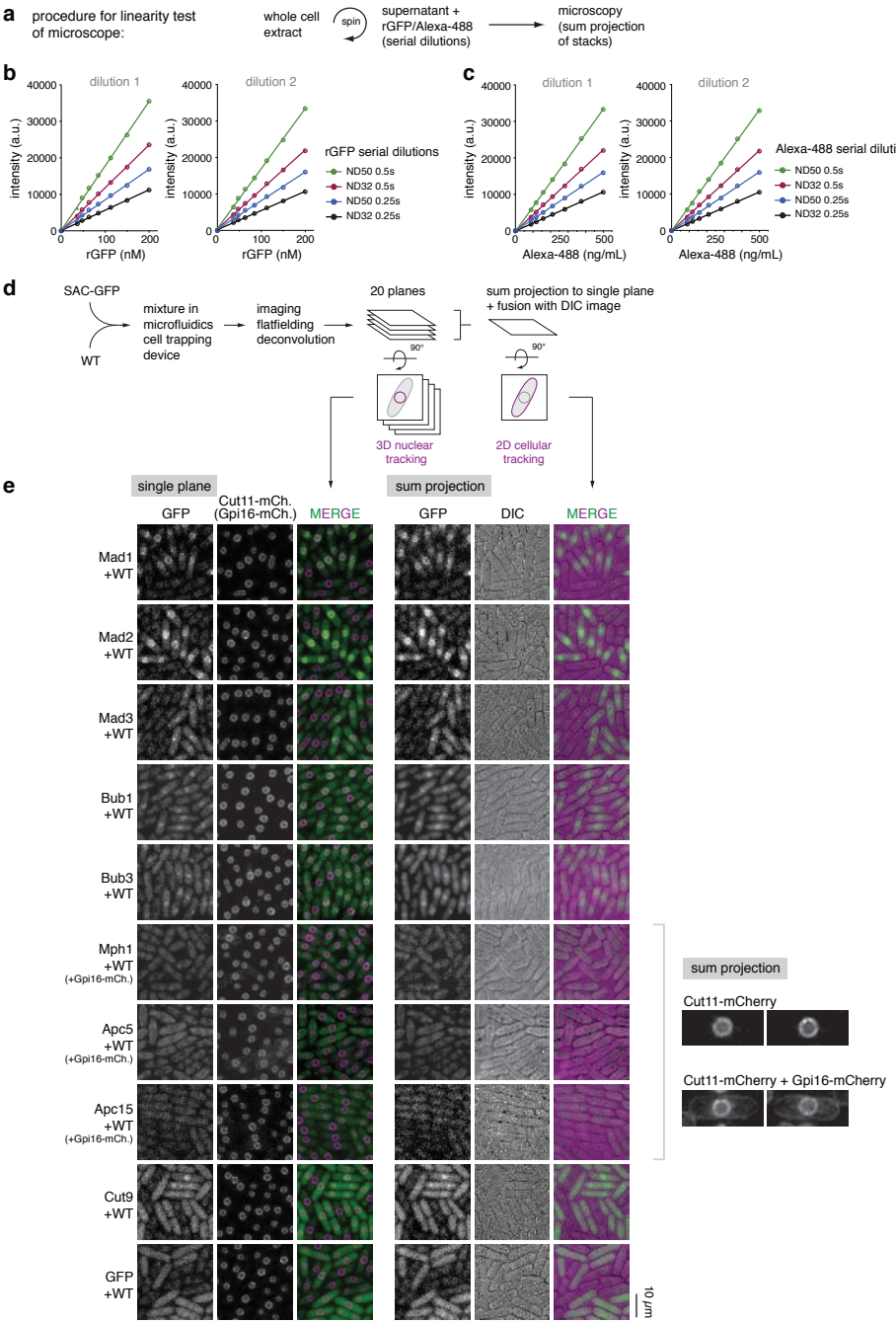

Figure S2 Imaging conditions for quantification by WiFDeM. **a-c** Microscope and camera respond linearly to signals in the relevant range. Protein extracts of wild type cells were mixed with serial dilutions of either recombinant GFP (rGFP; 3:4 dilutions starting from 200 nM) or Alexa-488 coupled antibodies (3:4 dilutions starting from 500 ng/mL). Two independent serial dilutions were imaged (dilution 1 and dilution 2) with different neutral density filters (ND) and different exposure times (0.25 s and 0.5 s). **d** Schematic representation of the quantitative imaging procedure. Cells containing GFP-labelled SAC proteins and cells without GFP (wild type; WT) were mixed and loaded into a microfluidics cell-trapping device. Cells were constantly supplied with fresh medium throughout the imaging process. Image stacks for GFP and mCherry fluorescence were acquired, and a DIC image was taken from the middle of the stack. Uneven illumination of the images was corrected by flatfielding and image stacks were deconvolved. 20 planes of the imaged stack were either used directly for 3D nuclear segmentation or sum-projected to a single plane and fused to the DIC image for 2D cellular segmentation. For 3D nuclear segmentation, the nuclear rim localization of Cut11-mCherry was used as marker. For 2D segmentation, the cellular outline in the DIC image was used and was converted to an estimate of cellular volume. **e** Representative single plane images and sum projections. To differentiate cells with a very weak GFP signal (Apc5-GFP, Apc15-GFP or Mph1-GFP) from cells that do not express GFP (wild type; WT), wild type cells in these cell mixtures expressed the membrane protein Gpi16-mCherry in addition to the nuclear marker Cut11-mCherry, as shown on the right side.

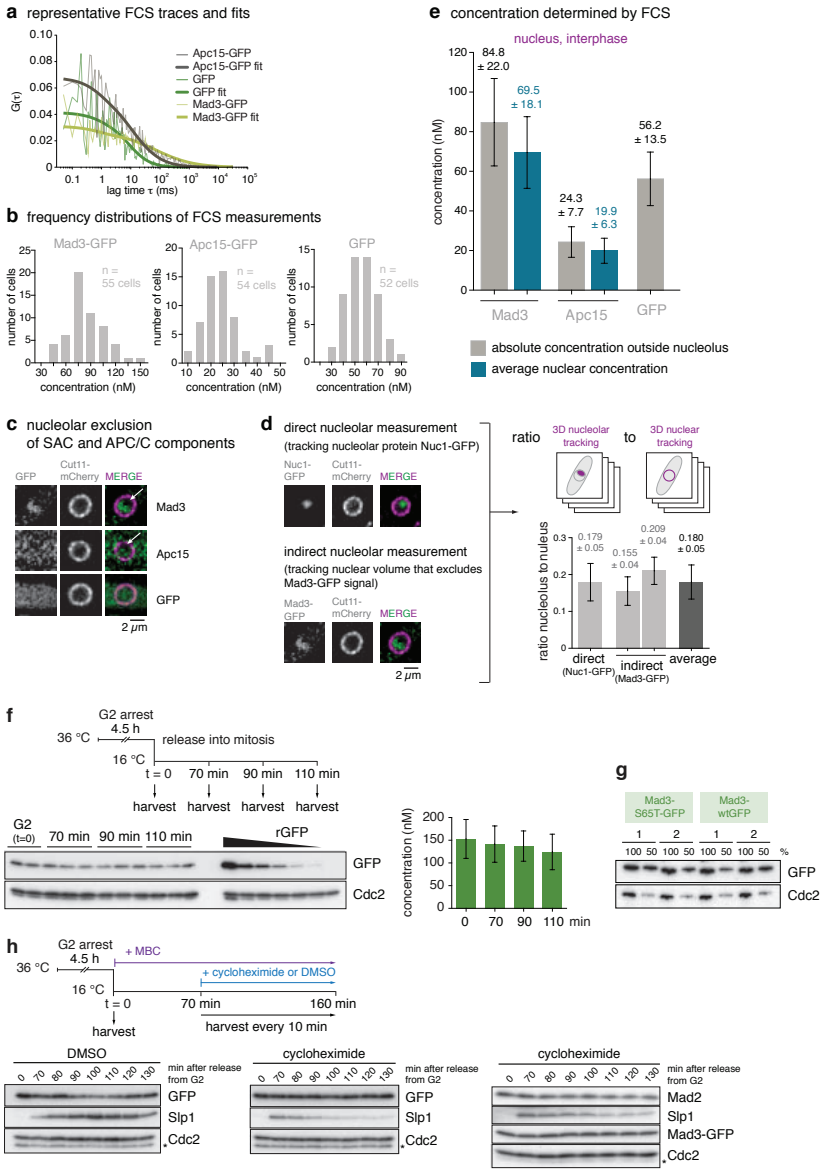

Figure S3 Absolute quantification of SAC proteins and APC/C subunits. **a,b** Quantification of free GFP, Apc15-GFP and Mad3-GFP by fluorescence correlation spectroscopy (FCS). Fluorescence fluctuations were determined in interphase nuclei. Shown in (a) are representative auto-correlation curves and the corresponding fit. The amplitude, G(0), of the autocorrelation curve is inversely proportional to the concentration of the fluorescent protein. The frequency distributions for the nuclear concentration in single cells are shown in (b). **c** Mad3-GFP and Apc15-GFP are excluded from the nucleolus (arrows), but free GFP is not. A single plane of representative nuclei in interphase is shown. GFP signals are differently scaled for different proteins to achieve good visibility. **d** The nucleolus occupies about ~18 % of the nuclear volume. The nucleolar volume was determined by segmentation of either Nuc1-GFP, which localizes to the nucleolus, or by segmentation of the region from which Mad3-GFP is excluded. (n=10 cells (Nuc1-GFP), n=9 and 11 cells (Mad3-GFP); error bars = s.d.). **e** Nuclear concentrations were measured by FCS outside the nucleolus (grey, data from (b)). The average concentration in the nucleus (blue) was calculated using the nucleolar volume determined in (d). (error bars = s.d.) **f** Quantification of free GFP by quantitative immunoblotting. *Cdc25-22* cells expressing *Pmad3-GFP* were arrested before mitosis in rich medium. Three technical replicates were harvested at the indicated time points after release and were analysed by immunoblotting using anti-GFP and anti-Cdc2 (loading control) antibodies. Recombinant GFP (rGFP, Clontech) was mixed with an extract from G2-arrested cells not expressing *Pmad3-GFP* as standard for quantification. The graph on the right shows the average concentration from 4 independent experiments, of which one is shown on the left. (error bars = s.d.; n = 4 experiments). **g** Equal detection of wtGFP and S65T-GFP with anti-GFP antibody. We used recombinant wild type GFP (wtGFP) for quantification of S65T-GFP-tagged checkpoint proteins (f). To confirm that the anti-GFP antibody detected wtGFP and S65T-GFP equally well, Mad3 was tagged with either wtGFP or S65T-GFP. Two independent strains (labelled 1 and 2) were compared by immunoblotting using anti-GFP and anti-Cdc2 (loading control) antibodies. Percentages on top of each lane indicate how much of the original extract was loaded. **h** Incomplete maturation of GFP is unlikely to account for the difference in GFP concentration determined by FCS and immunoblotting. We arrested cells in mitosis by the microtubule drug MBC and additionally treated with cycloheximide to block protein synthesis. GFP, but not Slp1, was stable for 60 min under these conditions. This indicates that protein turnover of GFP is low and that most of the GFP present at any given moment should have had enough time to form the fluorophore. In addition, GFP-tagged Mad3 as well as untagged Mad2 were similarly stable as GFP in cycloheximide-treated cells, indicating low turn-over of these SAC proteins. (*, antibody cross-reaction)

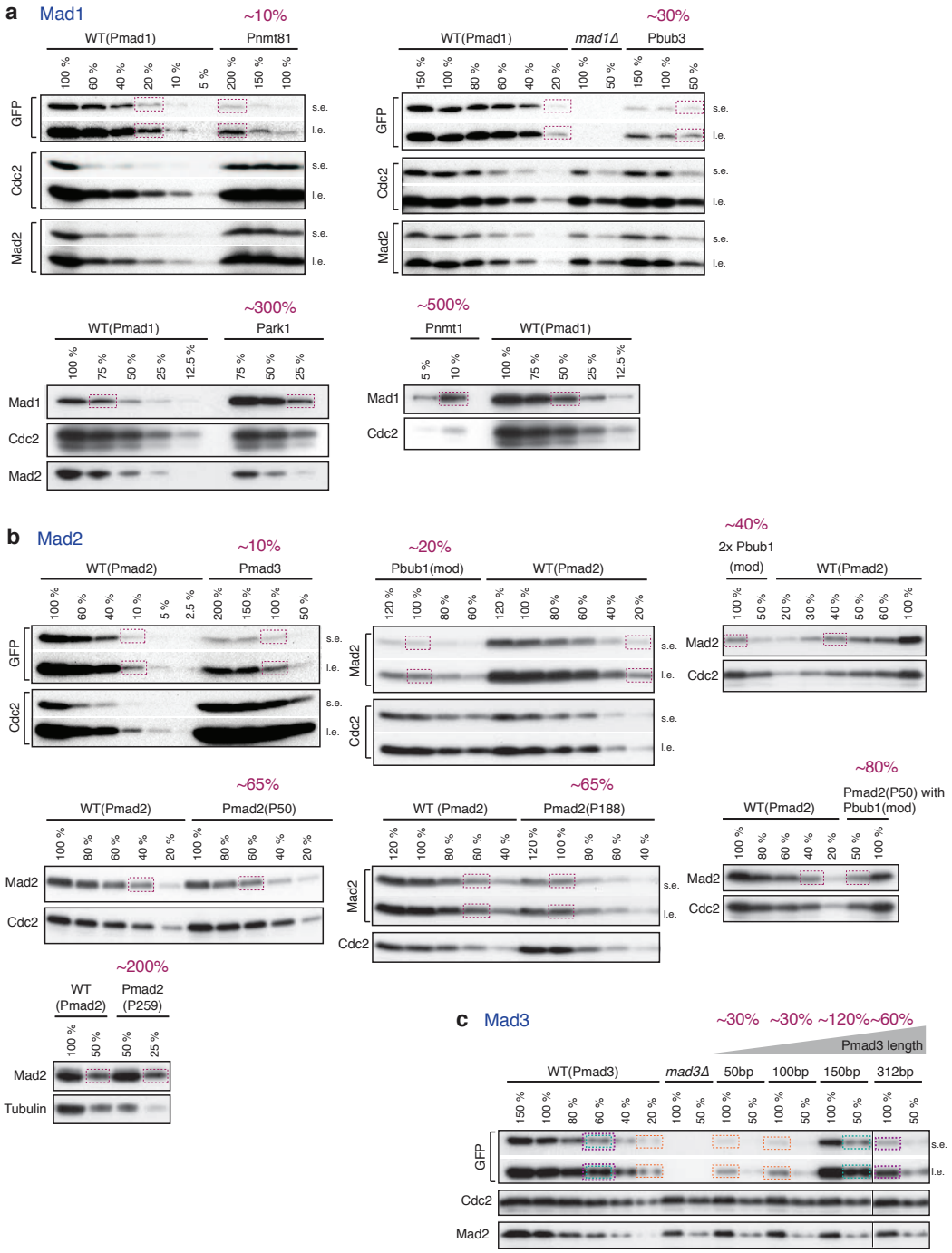

Figure S4 Abundance of Mad1-, Mad2- and Mad3-GFP after promoter modifications. Extracts from asynchronously growing cultures in rich medium were analysed by immunoblotting using anti-GFP, anti-Mad1, anti-Mad2 and either anti-Cdc2 or anti-tubulin antibodies (as loading controls). Mad1-GFP strains are shown in (a), Mad2-GFP strains in (b) and Mad3-GFP strains in (c). Percentages on top of each lane indicate how much of the original extract was loaded. Percentages in purple indicate the estimated protein abundance compared to wild type (WT). Dashed boxes indicate bands with similar signal strength from which protein abundances of the promoter-modified strains were deduced. Estimations of the abundance relative to wild type are typically based on several experiments, of which only one representative experiment is shown. (s.e. = short exposure, l.e. = long exposure, Pmad3 length = length of the remaining *mad3* promoter; see Supplementary Table S3 for the molecular changes in the promoter region).

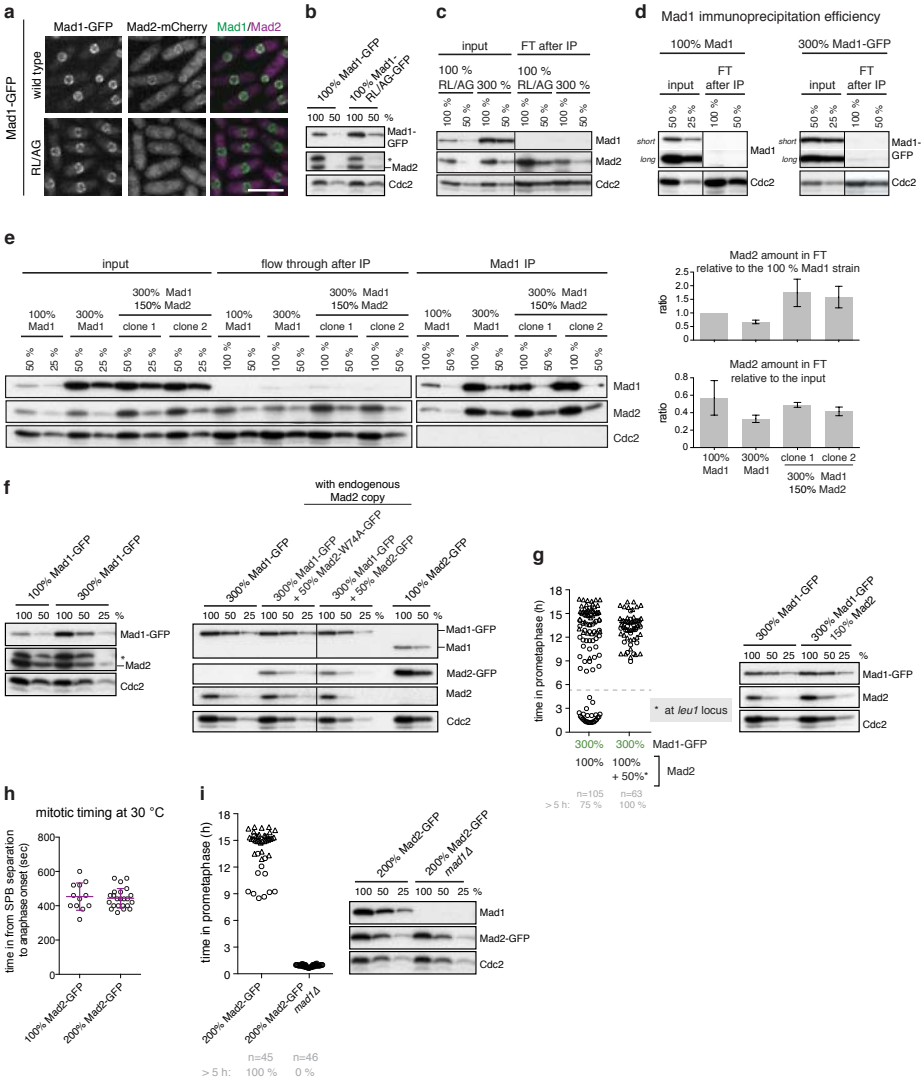

Figure S5 Analysis of the Mad1-RL/AG mutant as well as Mad1 and Mad2 overexpression. **a** Mad2-mCherry does not co-localise with Mad1 that contains two point mutations (CRVLQHRS to CAVGQHRS) in the Mad2-binding site (Mad1-RL/AG). Representative images from asynchronous cultures are shown. Scale bar: 10 µm. **b** Mad1-RL/AG is present at similar levels as wild type Mad1, and Mad2 abundance is unaffected. Extracts from asynchronously growing cultures in rich medium were analysed by immunoblotting using anti-Mad1, anti-Mad2 and anti-Cdc2 (as loading control) antibodies. Percentages on top of each lane indicate how much of the original extract was loaded. The asterisk indicates a cross-reacting band. **c** Input and flow-through of the immunoprecipitation shown in Fig. 4a. Extracts from asynchronously growing cultures in rich medium were used for immunoprecipitation (IP) of Mad1-RL/AG or Mad1-GFP (expressed to 300 %) using anti-Mad1 antibodies. Shown are immunoblots of the extract used for the IP (input) and of the flow through after immunoprecipitation (FT after IP). **d** High immunoprecipitation efficiency for Mad1 or Mad1-GFP. Extracts from asynchronously growing cultures in rich medium were used for immunoprecipitation of Mad1 or Mad1-GFP using anti-Mad1 antibodies and analysed for the amount of Mad1 remaining in the extract after IP (FT (flow through) after IP). **e** 50 % additional Mad2 increases free Mad2 in cells with 300 % Mad1-GFP. Extracts from asynchronously growing cultures in rich medium were used for immunoprecipitation of Mad1 using anti-Mad1 antibodies and analysed for co-immunoprecipitation of Mad2. The input and FT is 6.25 % of the amount used for the IP sample. Mad1 was largely depleted from the flow through after IP. Quantifications of the flow through are shown on the right (see Methods). The depletion of free Mad2 by increasing the Mad1 abundance to 300 % is not as strong as could be expected (Supplementary Note (B1)). Shown is one representative out of two independent experiments. **f** Mad1 and Mad2 abundance in the strains shown in Fig. 4b. Extracts from asynchronously growing cultures in rich medium were analysed by immunoblotting using anti-Mad1 (for Mad1 and Mad1-GFP detection), anti-GFP (for Mad2-GFP detection), anti-Mad2 (for Mad2 detection) and anti-Cdc2 antibodies (as loading control). The asterisk indicates a cross-reacting band. **g** Addition of 50 % untagged Mad2 rescues the checkpoint defect in cells with 300 % Mad1, similar to addition of 50 % Mad2-GFP (Fig. 4b). To determine SAC activity, cells were followed by live cell imaging at 16 °C as in Fig. 2 (left side). Extracts from asynchronously growing cultures from the same strains were analysed by immunoblotting (right side) using anti-Mad1, anti-Mad2 and anti-Cdc2 antibodies (as loading control). Shown is one representative out of two independent experiments. **h** Cells with 200 % Mad2-GFP stay in mitosis for a similar time as cells with 100 % Mad2-GFP. Cells were cultured in rich medium and followed by live cell imaging at 30 °C. The time in mitosis was determined from SPB separation to spindle elongation using Plo1-mCherry as marker for the SPBs. Each circle represents one cell. Shown in purple are mean and s.d. **i** 200 % Mad2-GFP cannot overcome the checkpoint defect of a *mad1* deletion. *nda3-KM311* strains were followed by live cell imaging at 16 °C and the time in mitosis was scored as in Fig. 2 (left side). Extracts from asynchronously growing cultures from the same strains were analysed by immunoblotting (right side) using anti-Mad1, anti-GFP and anti-Cdc2 antibodies (as loading control).

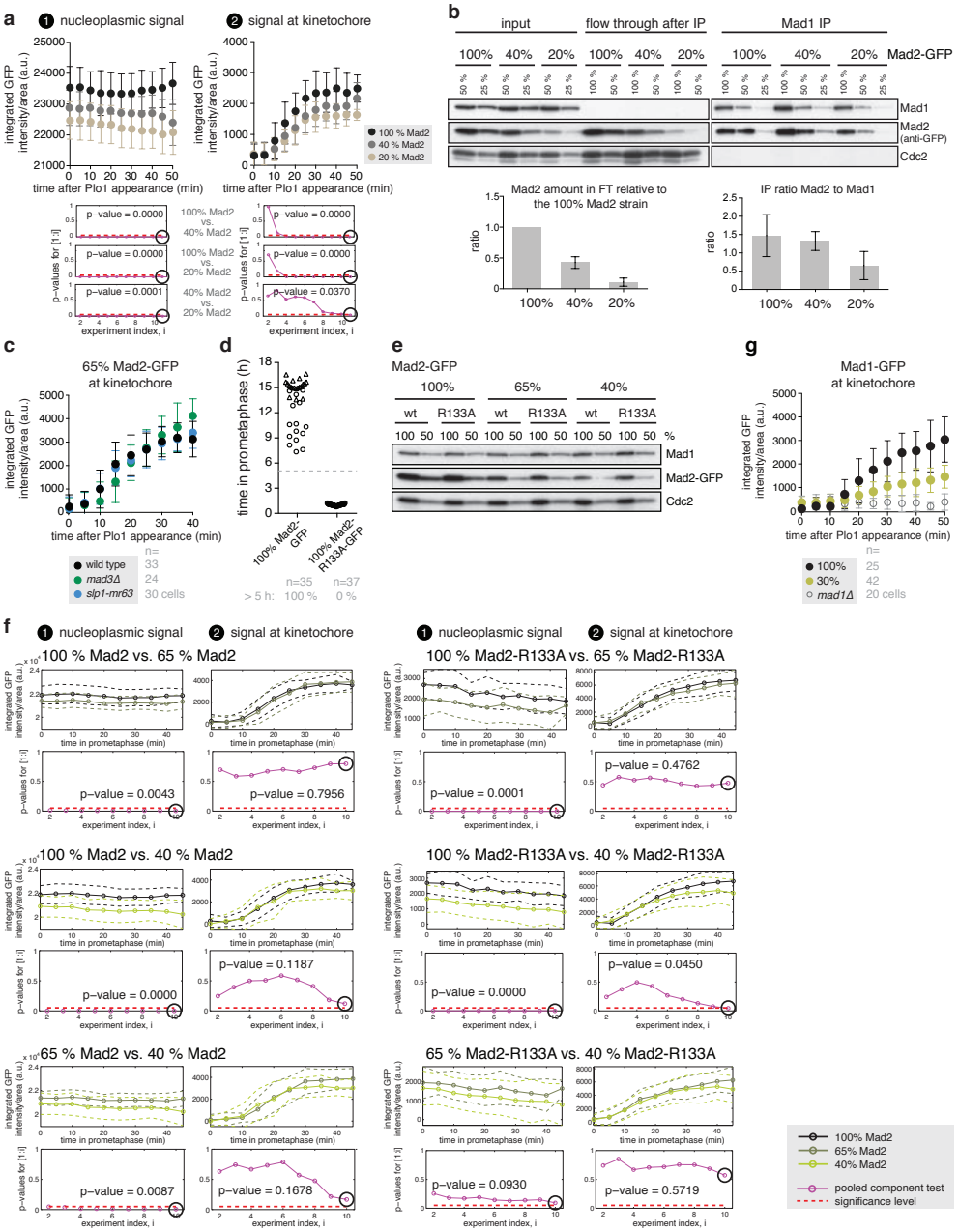

Figure S6 Analysis of Mad2 abundance at kinetochores, in the nucleoplasm and in complex with Mad1. **a** Abundance of 40 % and 20 % Mad2 in the nucleoplasm and at kinetochores. The amount of Mad2-GFP in the indicated strains was followed as cells entered mitosis in the absence of microtubules. (error bars = s.d.; n=41/38/29 cells for 100/40/20 % Mad2). We tested for similarity of the curves by pooled component test. The differences between strains for signals both at the kinetochore and in the nucleoplasm were statistically significant ($p < 0.05$). **b** Reduction of Mad2 to 20 % reduces the Mad1-bound and the free pool of Mad2. Extracts from asynchronously growing cultures in rich medium were used for immunoprecipitation (IP) of Mad1 using anti-Mad1 antibodies and analysed for co-immunoprecipitation of Mad2. Percentages on top of each lane indicate how much of the original extract or the immunoprecipitation was loaded. The input and flow through (FT) loaded is 15 % of the amount used for the IP sample. Quantifications of the flow through and the IP are shown on the right (see Methods). For 100 % and 40 % Mad2, one representative out of three independent experiments is shown. **c** Mad2-GFP recruitment to the kinetochore is not decreased in *mad3D* or *slp1-mr63*. The amount of Mad2-GFP at the kinetochore was recorded as cells entered mitosis in the absence of microtubules. (error bars = s.d.) **d** The Mad2-R133A mutation causes a checkpoint defect. Strains were followed by live cell imaging as in Fig. 2. **e** Mad2-R133A and abundance-reduced versions are present at similar levels as wild type Mad2. Extracts from asynchronously growing cultures in rich medium were analysed by immunoblotting using anti-Mad1, anti-GFP and anti-Cdc2 (as loading control) antibodies. Percentages on top of each lane indicate how much of the original extract was loaded. **f** Statistical analysis of Mad2 abundance in the nucleoplasm and at the kinetochore. Intensity curves for the Mad2-GFP and Mad2-R133A-GFP strains, also shown in Fig. 4d, were compared by a pooled component test. The cumulative p-value is plotted in pink. A p-value of 0.05 is shown as dashed red line. **g** Reduction of Mad1 to 30 % considerably decreases the Mad1 amount at unattached kinetochores. The amount of Mad1-GFP at the kinetochore in the indicated strains was followed as cells entered mitosis in the absence of microtubules (error bars = s.d.).

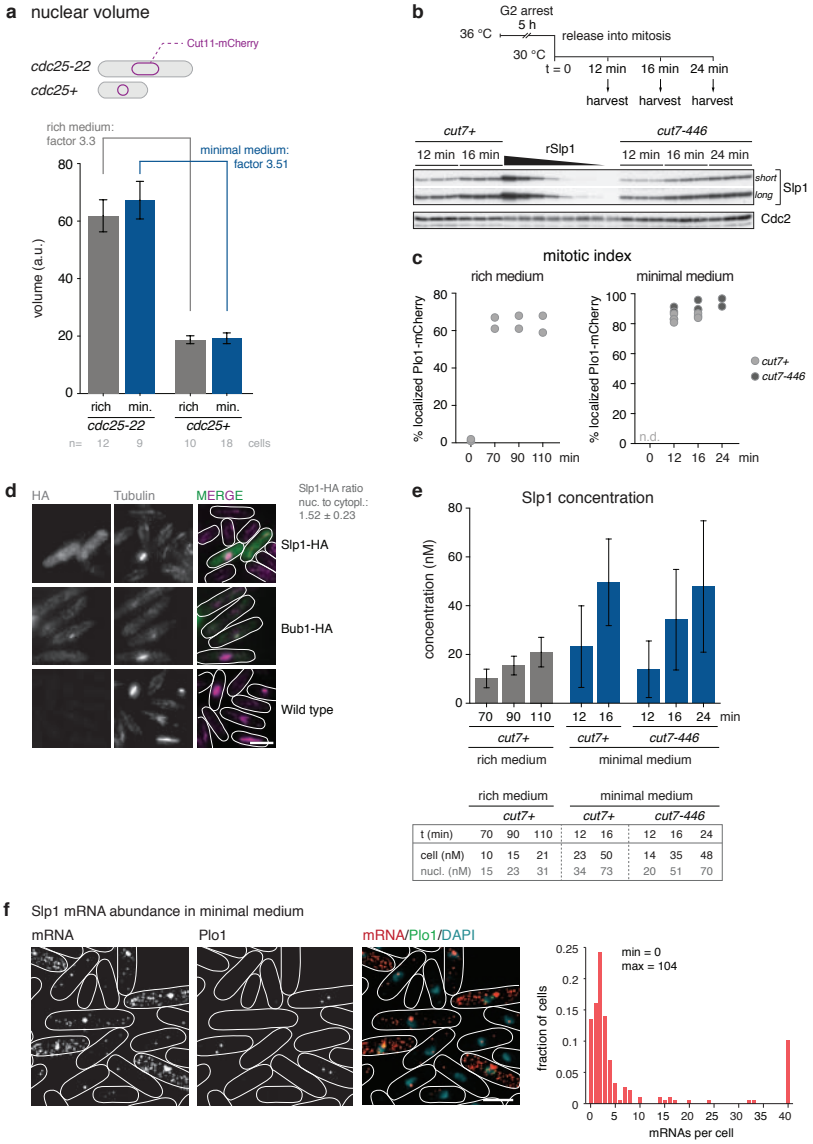

Figure S7 Quantification of Slp1 mRNA and protein abundance. **a** Nuclear volume increase in *cdc25-22* arrest. Cells expressing *cut11+-mCherry* were shifted for 4.5 hours (YEA) or 5 hours (EMM) to 36 °C for synchronization in G2. *Cdc25+* cells were mixed into the G2-arrested *cdc25-22* culture and the mixture was mounted on the microscope stage, which was pre-heated to 36 °C. The nuclear rim localization of Cut11-mCherry was used for nuclear segmentation. (a.u. = arbitrary units, error bars = s.d.) **b** Quantification of Slp1 in minimal medium by quantitative immunoblotting. *Cdc25-22* cells expressing either *cut7+* or the kinesin mutant *cut7-446* were grown in minimal medium (EMM). *Cut7-446* at restrictive temperature causes the formation of a monopolar spindle and activation of the spindle assembly checkpoint (SAC). Three technical replicates were harvested from the start of Slp1 expression until maximal abundance was reached and were analysed by immunoblotting using anti-Slp1 and anti-Cdc2 (loading control) antibodies. Recombinant His_6-Slp1 (rSlp1) was mixed with an extract from G2-arrested cells and was used as standard for quantification. (short = short exposure, long = long exposure) Shown is one representative out of two (*cut7+)* or three (*cut7-446*) independent experiments. **c** Mitotic index of samples used for Slp1 abundance determination by quantitative immunoblotting. Cells were grown in rich medium (for *cut7+* cells; see Fig. 6a) or minimal medium (EMM; for *cut7+* and *cut-446* cells; see (b) and (e) in this figure). After G2 arrest, cells in rich medium were released into mitosis at 16 °C, cells in minimal medium were released into mitosis at 30 °C. The mitotic index was determined from the percentage of cells showing a localized Plo1-mCherry signal at spindle pole bodies (SPBs). **d** Slp1-HA was detectable in mitotic cells and was distributed throughout the cell with a slight enrichment in the nucleus. Cells were immunostained for HA and tubulin. Cells expressing *bub1+-HA* and wild type cells served as specificity controls. The nucleo-cytoplasmic ratio for Slp1-HA was calculated by dividing the mean intensity in the nucleus (nuc.) by the mean intensity in the cytoplasm (cyto.). Background measured in interphase cells was subtracted. (n=30 cells; ± = s.d.) Scale bar: 5 µm. Shown is one representative out of two independent experiments. **e** Slp1 is approximately twice as abundant in minimal medium as in rich medium. Slp1 concentrations determined from the time course experiments shown in Fig. 6a and S6b. The graph shows average concentrations from two (*cut7+,* both rich and minimal medium) or three (*cut7-446*, minimal medium*)* independent experiments. (error bars = s.d.) The table below shows the values for cellular Slp1 concentration (cell) determined by immunoblotting and the estimated nuclear concentration (nucl.) based on the measured nucleo-cytoplasmic ratio (see d). **f** Slp1 mRNA abundance peaks in mitosis. Single molecule FISH was performed on an asynchronous cell culture grown in minimal medium with probes against Slp1 mRNA. A representative image is shown on the left (scale bar: 5 µm). Plo1-GFP indicates cells in prometaphase. The histogram on the right depicts the mRNA frequency distribution in this sample. (n=186 cells).

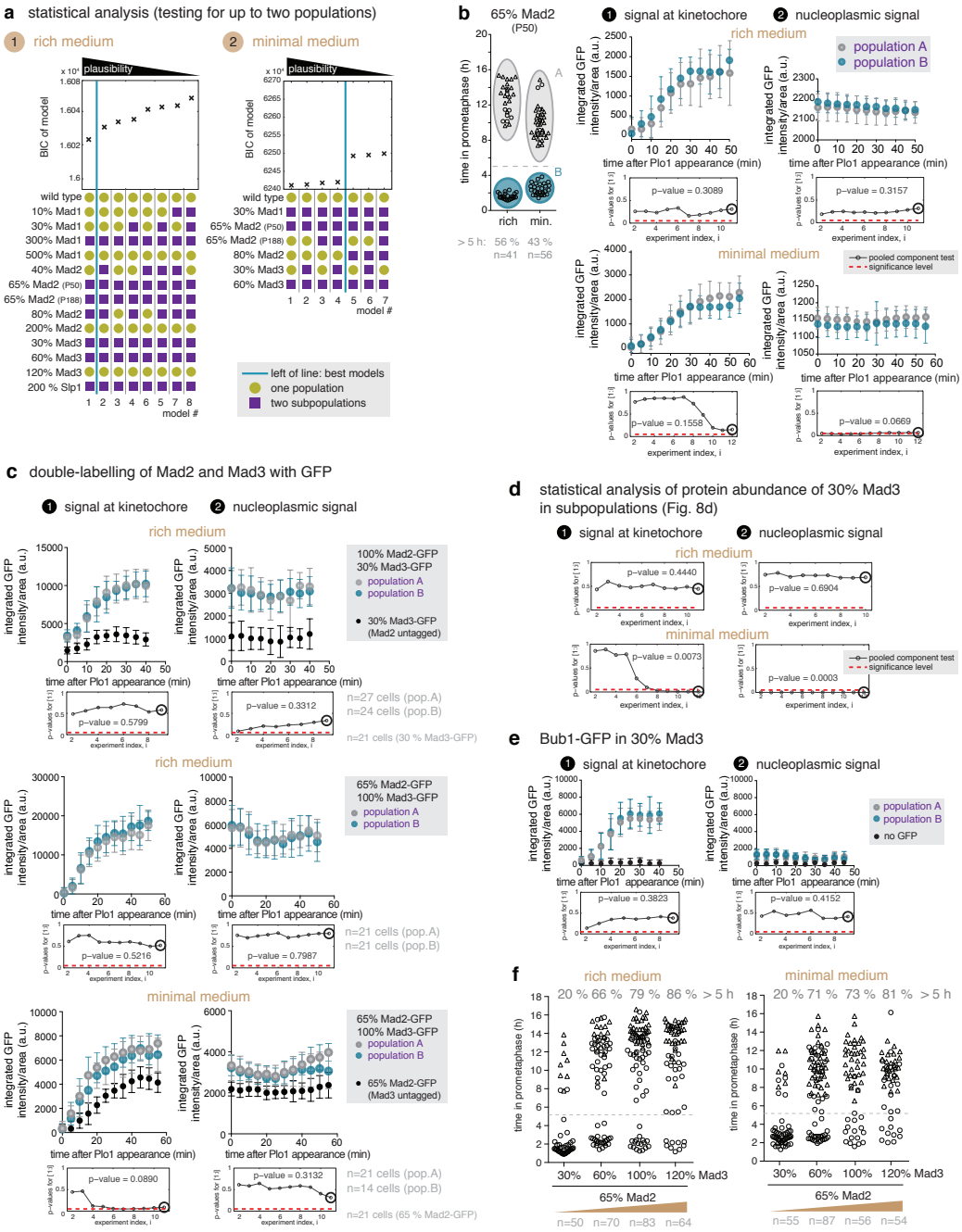

Figure S8 Statistical analysis of distribution of the mitosis times, and protein abundance measurements in the two subpopulations. **a** Distribution of mitosis times assessed by multi-experiment modelling (Supplementary Note). Mitosis times measured in strains with changed SAC protein abundance shown in Fig. 2 were analysed by multi-experiment modelling for the occurrence of up to two subpopulations. More plausible models have a lower Bayesian information criterion (BIC), and ranking of the models according to their BIC is shown. **b** In rich medium, no significant difference in Mad2 abundance was observed between the subpopulations. Strains were followed by live cell imaging as in Fig. 2 in either rich or minimal (min.) medium (left side). Mad2-GFP signals were quantified in each population (A and B) as cells entered mitosis (right side) (a.u. = arbitrary units; error bars = s.d.; n=23/18 cells for population A/B in rich medium; n=24/32 cells for population A/B in minimal medium). Intensity curves for population A and B were compared by a pooled component test. The cumulative p-value is plotted in grey. For rich medium, one representative out of two independent experiments is shown. **c** Combined Mad2 and Mad3 abundance are similar between population A and B. Strains expressing both Mad2- and Mad3-GFP in the indicated abundances were analysed as in (b) (a.u. = arbitrary units; error bars = s.d.). **d** Intensity curves for population A and B from Fig. 8d were compared by a pooled component test. The cumulative p-value is plotted in grey. A p-value < 0.05 is considered significant (dashed red line). Mad3 abundance in minimal medium is different between populations A and B. **e** Bub1-GFP signal intensity in a strain containing non-fluorescent 30 % Mad3-GFP-Y66L was analysed as in (b). ('no GFP' = 30 % Mad3-GFP-Y66L without Bub1-GFP; error bars = s.d.; n=19 cells (no GFP), n=24 cells (population A), n=22 cells (population B)). **f** Titration of Mad3 abundance in a 65 % Mad2-GFP background does not strongly affect the distribution of cells in the two subpopulations. Cells were followed by live cell imaging as in Fig. 2.

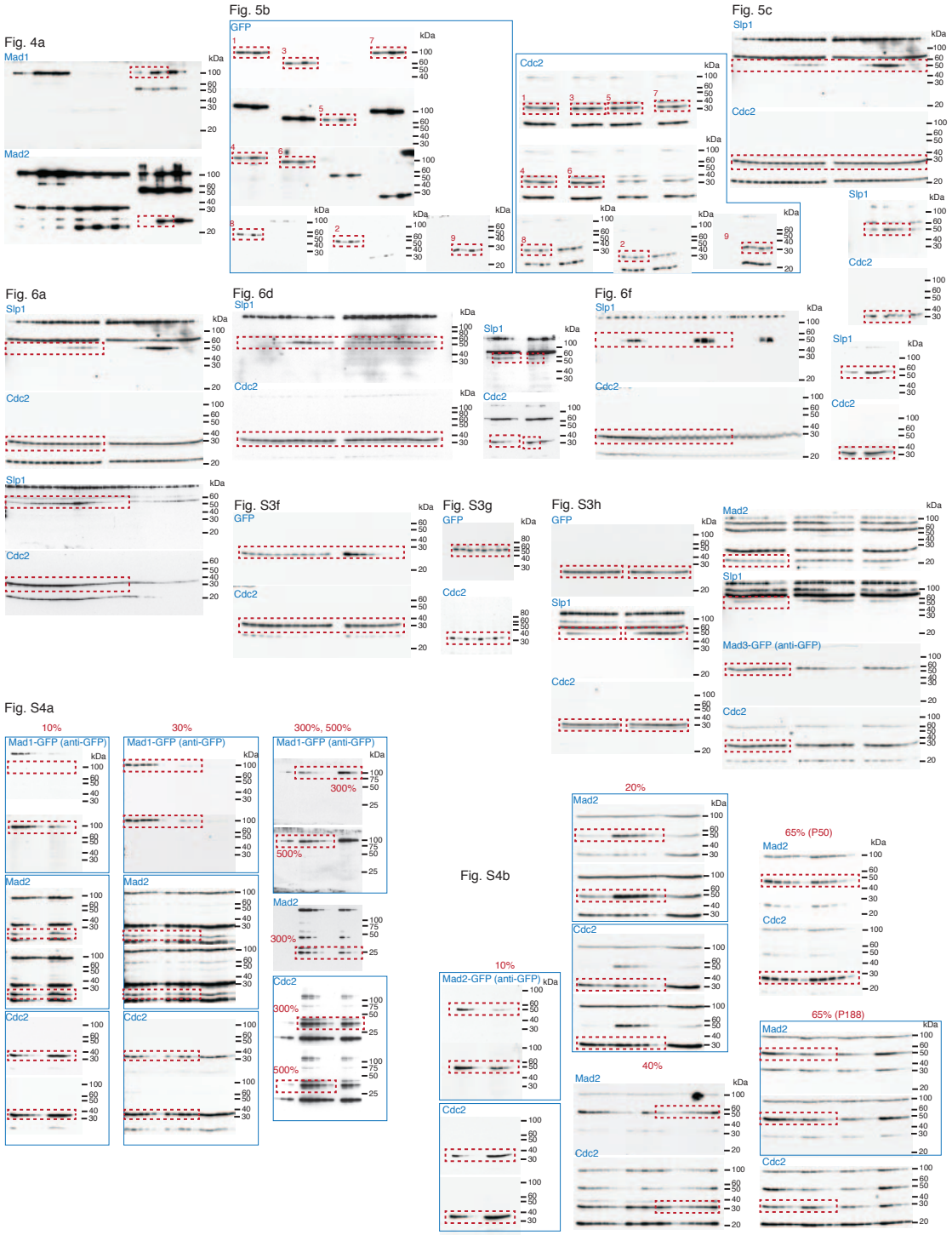

Figure S9 Entire membranes of cropped immunoblots. Blue labels on top indicate the antibody used for detection. Dashed red boxes show which regions of the immunoblot were cropped for the individual figures.

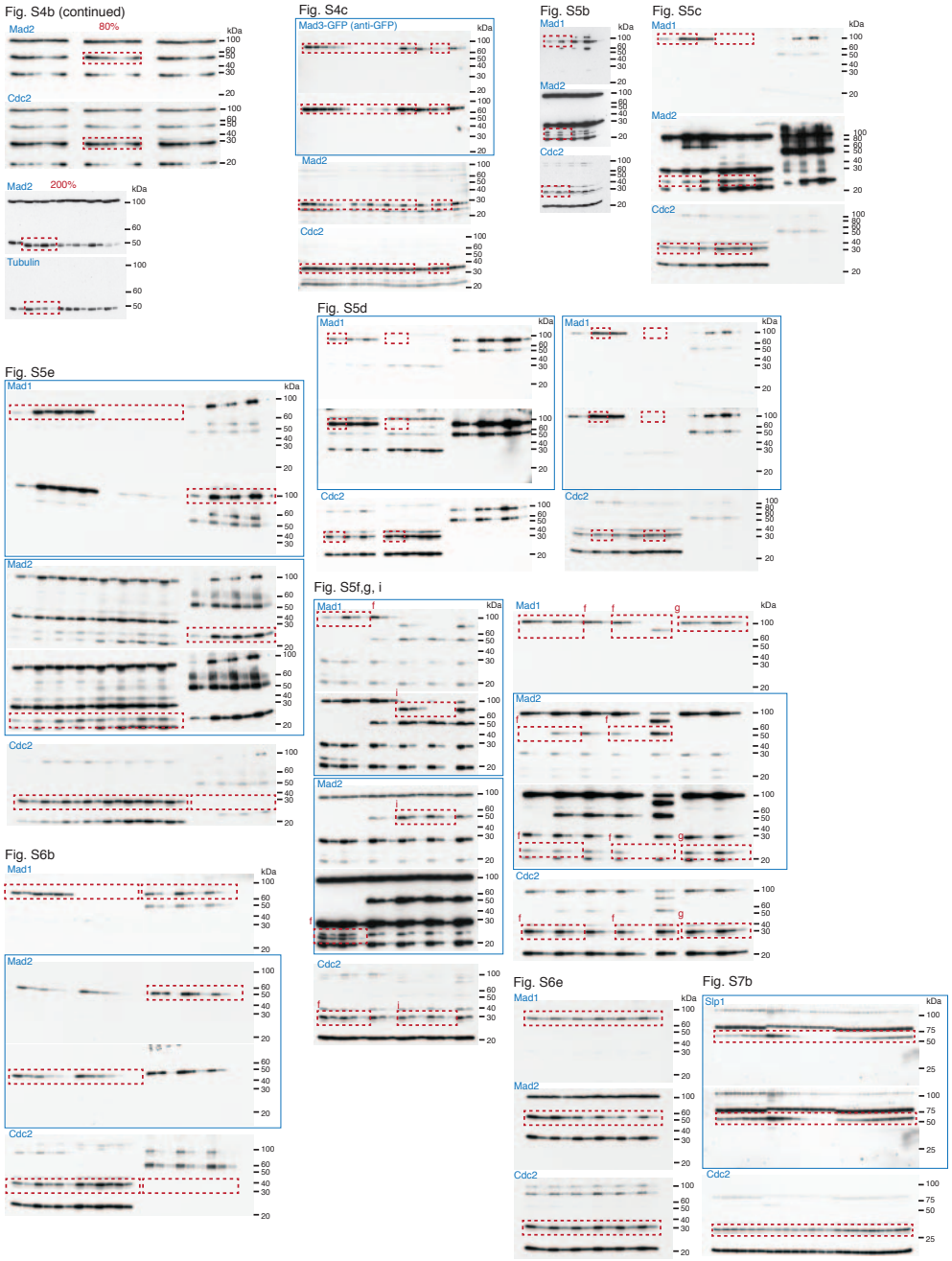

Figure S9 continued

Supplementary Table S1

Relative quantifications

	nucleus						whole cell							
	relative (%; GFP_i=100) **interphase**	CV (%)	# of cells	relative (%; GFP_i=100) **mitosis**	CV (%)	# of cells	relative (%; GFP_i=100) **interphase**	CV (%)	# of cells	relative (%; GFP_i=100) **mitosis**	CV (%)	# of cells	Nuclear/Cytoplasmic ratio interphase	mitosis
Mad1	206 ± 20	9.6	40	204 ± 12	5.95	7	70 ± 24	34.7	28	71 ± 21	30.1	8	3.5	3.4
Mad2	274±22	8.1	57	281 ± 19	6.71	10	109 ± 22	19.8	16	109 ± 25	23.2	11	2.9	3
Mad3	132 ± 13	9.6	36	146 ± 15	10.2	10	78 ± 15	19.2	14	72 ± 12	17	9	1.8	2.2
Bub1	104 ± 11	10.5	31	109 ± 20	18.1	11	23 ± 16	68.6	33	16 ± 11	66.8	9	6.6	13.8
Bub3	98 ± 18	18.5	49	102 ± 15	15	13	21 ± 10	48.7	45	23 ± 12	50.8	16	6.9	6.3
Mph1	23 ± 7	31.4	42	26 ± 6	25.1	14	27 ± 11	40.5	40	31 ± 11	36.4	13	0.8	0.8
Apc5	28 ± 10	36.4	47	52 ± 28	54.2	12	34 ± 13	39	38	33 ± 17	51.5	10	0.8	1.7
Apc15	24 ± 4	16.3	13	53 ± 17	31.7	10	38 ± 8	21.4	14	37 ± 10	28.5	9	0.6	1.5
Cut9	114 ± 15	13	177	183 ± 50	27.3	9	119 ± 15	12.8	113	117 ± 22	18.8	9	1	1.6
GFP	100 ± 17	16.7	60	95 ± 18	18.7	8	100 ± 21	21.3	13	102 ± 24	23.3	8	1	0.9

Table S1 Relative SAC protein-GFP concentrations.

SAC protein abundances measured in the nucleus or whole cell are given as relative (%) values with respect to the concentration of free GFP in interphase (GFP_i) (Fig. 1). (± = s.d.; CV, coefficient of variation =(standard deviation/mean) x 100 (%))

Supplementary Table S2

Absolute quantifications

	FCS			Immunoblotting			Mass spectrometry	
	absolute nuclear conc., determined by FCS (nM)	absolute **nuclear** conc. in interphase based on GFP abundance determined by FCS (nM)	absolute **cellular** conc. in interphase based on GFP abundance determined by FCS (nM)	absolute cellular conc., determined by IB (nM)	absolute **nuclear** conc. in interphase relative to GFP values determined by IB (nM)	absolute **cellular** conc. in interphase relative to GFP values determined by IB (nM)	Marguerat et al. (**cellular** conc., nM)	Carpy et al. (**cellular** conc., nM)
Mad1	n.d.	116± 11	39± 14	n.d.	276± 26	93± 32	11	52
Mad2	n.d.	154± 13	61 ± 12	n.d.	367± 30	146± 29	n.d.	n.d.
Mad3	70± 18	74± 7	44± 8	n.d.	176± 17	104± 20	n.d.	71
Bub1	n.d.	58± 6	13± 9	n.d.	139± 15	30± 21	7	n.d.
Bub3	n.d.	55± 10	12± 6	n.d.	132± 24	28± 14	n.d.	21
Mph1	n.d.	13± 4	15± 6	n.d.	31± 10	36± 15	7	22
Apc5	n.d.	15 ± 6 (29± 16)	19± 7	n.d.	37 ± 14 (69± 38)	45± 17	n.d.	n.d.
Apc15	20 ± 6	13 ± 2 (30± 9)	21 ± 5	n.d.	32 ± 5 (71± 22)	51± 11	n.d.	n.d.
Cut9	n.d.	64± 8 (103± 28)	67± 9	n.d.	152± 20 (246± 67)	160 ± 21	15	39
Slp1	n.d.	n.d.	n.d.	21± 6	30± 9	21 ± 6	n.d.	n.d.
GFP	**56 ± 14**	56± 14	56± 14	**134± 37**	134± 37	134± 37	n.d.	n.d.

Table S2 Estimate of absolute SAC protein-GFP concentrations.

Values for the nuclear concentration in interphase determined by FCS are from Fig. S3e, the value for GFP in mitosis determined by immunoblotting (IB) is from Fig. S3f. GFP is equally distributed between nucleus and cytoplasm, so that nuclear and cellular concentrations are assumed equal. The relative GFP concentrations measured in interphase (Fig. 1a) were used to derive absolute concentrations for SAC proteins and APC/C subunits. Values in parentheses for APC/C subunits denote mitotic values. For Slp1, the measured nucleo-cytoplasmic ratio (Fig. S7) was used to derive the nuclear concentration. Given is the maximum Slp1 concentration reached in rich medium in mitosis. For comparison, mass spectrometry-based quantification of selected checkpoint proteins by Marguerat et al., 2012 (ref. 24), is shown. In addition, absolute cellular abundances of selected proteins were calculated using intensity based absolute quantification (iBAQ) (Schwanhausser et al., 2011 (ref. 56)) applied to a global proteome analysis using SILAC (stable isotope labeling with amino acids in culture)-based quantification (A. Carpy, K. Krug, B. Macek, Proteome Center Tuebingen, personal communication). The iBAQ method correlates the protein mass spectrometric signal intensity to a spiked-in protein standard with known molar amounts and calculates the absolute cellular abundances for each identified protein.

Supplementary Table S3

Promoter modifications to perturb protein abundance

Mad1	estimated abundance relative to wild type	gene modification
Pnmt81	10%	promoter of *nmt81+*, integrated before start of *mad1* open reading frame (ORF), selection via *natNT2* resistance cassette 5' of *Pnmt81*
Pbub3	30%	promoter of *bub3+* (384bp sequence upstream of start of *bub3* ORF) integrated before start of *mad1* ORF, selection via *natNT2* resistance cassette 5' of *Pbub3*
Park1	300%	promoter of *ark1+* (731bp sequence upstream of start of *ark1* ORF) integrated before start of *mad1* ORF, selection via *natNT2* resistance cassette 5' of *Park1*
Pnmt1	500%	promoter of *nmt1+*, integrated before start of *mad1* ORF, selection via *hphNT1* resistance cassette 5' of *Pnmt1;* note: strain was used in rich medium in repressed state, has higher protein noise than other promoter-modified strains

Mad2	estimated abundance relative to wild type	gene modification
Pmad3	10%	promoter of *mad3+* (717bp sequence upstream of start of *mad3* ORF) integrated before start of *mad2* ORF, selection via natNT2 resistance cassette 5' of *Pmad3*
Pbub1(mod)	20%	promoter of *bub1+* (710bp sequence upstream of start of *bub1* ORF, ATG 42bp before natural start was removed) integrated before start of *mad2* ORF, selection via *natNT2* resistance cassette 5' of *Pbub1*
2xPbub1(mod)	40%	into strain containing *Pbub1(mod)*: integrated *Pbub1(mod)-mad2+-GFP<<kanR* at *leu1* locus using pDUAL system
P50	65%	*hphNT1* resistance cassette integrated 50bp upstream of start of *mad2* ORF
P188	65%	*hphNT1* resistance cassette integrated 188bp upstream of start of *mad2* ORF
Pbub1	80%	into strain containing *P50*: integrated *Pbub1(mod)-mad2+-GFP<<kanR* at *leu1* locus using pDUAL system
P259	200%	*hphNT1 resistance cassette integrated 259bp upstream of start of mad2 ORF*

Mad3	estimated abundance relative to wild type	gene modification
P(50bp)	30%	*hphNT1* resistance cassette integrated 50bp 5' of start of *mad3* ORF
P(100bp)	30%	*hphNT1* resistance cassette integrated 100bp 5' of start of *mad3* ORF
P(312bp)	60%	*hphNT1* resistance cassette integrated 312bp 5' of start of *mad3* ORF
P(150bp)	120%	*hphNT1* resistance cassette integrated 150bp 5' of start of *mad3* ORF

Table S3 Promoter modifications to perturb protein abundance.

List of modifications in the *mad1, mad2* and *mad3* genes that were used to change protein abundance. For two strains, 40% Mad2 and 80% Mad2, an extra copy of a modified *mad2* gene was integrated at the *leu1* locus.

Supplementary Table S4

S. pombe strains

Figure 1a

SK570	*h+*	*cut11+-mCherry<<hygR*
SL706	*h-*	*leu1 cut11+-mCherry<< hygR gpi16+-mCherry<<natR*
SK578	*h+*	*leu1 mad1+-GFP<<kanR cut11+-mCherry<<hygR*
SK580	*h+*	*mad2+-GFP<<kanR cut11+-mCherry<<hygR*
SK581	*h+*	*mad3+-GFP<<kanR cut11+-mCherry<<hygR*
SK583	*h+*	*bub1+-GFP<<kanR cut11+-mCherry<<hygR*
SK585	*h+*	*bub3+-S(GGGGS)3-GFP<<kanR cut11+-mCherry<<hygR*
SK829	*h-*	*leu1 mph1+-S(GGGGS)3-GFP<<kanR cut11+-mCherry<<hygR*
SK590	*h-*	*cut9+-GFP<<kanR cut11+-mCherry<<hygR*
SK595	*h+*	*apc5+-GFP<<kanR cut11+-mCherry<<hygR*
SK597	*h-*	*leu1 apc15+-GFP<<kanR cut11+-mCherry<<hygR*
SM558	*h-*	*pDUAL-Pmad3-GFP<<leu1+ cut11+-mCherry<<hygR*

Figure 1c

SK581	*h+*	*mad3+-GFP<<kanR cut11+-mCherry<<hygR*
SK597	*h-*	*leu1 apc15+-GFP<<kanR cut11+-mCherry<<hygR*
SM558	*h-*	*pDUAL-Pmad3-GFP<<leu1+ cut11+-mCherry<<hygR*

Figure 2b

SK893	*h+*	*leu1 ade6-M216 plo1+-mCherry<<natR nda3-KM311 mad1Δ::ura4+*
SL800	*h+*	*leu1 hphNT1<<Pnmt81-mad1+-GFP<<kanR plo1+-mCherry<<natR nda3-KM311*
SK895	*h-*	*leu1 ade6-M216 natNT2<<Pbub3-mad1+-GFP<<kanR plo1+-mCherry<<natR nda3-KM311*
SK896	*h+*	*leu1 (ade6-M216?) natNT2<<Pbub3-mad1+-GFP<<kanR plo1+-mCherry<<natR nda3-KM311*
SK891	*h+*	*leu1 mad1+-GFP<<kanR plo1+-mCherry<<natR nda3-KM311*
SK891'	*h+*	*leu1 mad1+-GFP<<kanR plo1+-mCherry<<natR nda3-KM311*
ST387	*h?*	*leu1 ade6-M216 natNT2<<Park1-mad1+-GFP<<kanR plo1+-mCherry<<natR nda3-KM311*
SL794	*h+*	*leu1 hphNT1<<Pnmt1-mad1+-GFP<<kanR plo1+-mCherry<<natR nda3-KM311*

Figure 2c

SK844	*h+*	*leu1 (ade6-M210? ura4-D18?) plo1+-mCherry<<natR nda3-KM311 mad2Δ::ura4+*
SK835	*h-*	*leu1 natNT2<<Pmad3-mad2+-GFP<<kanR plo1+-mCherry<<natR nda3-KM311*
SM958	*h-*	*leu1 hphNT1<<Pbub1(mod)-mad2+-GFP<<kanR plo1+-mCherry<<natR nda3-KM311*
SM958'	*h-*	*leu1 hphNT1<<Pbub1(mod)-mad2+-GFP<<kanR plo1+-mCherry<<natR nda3-KM311*
SP141	*h-*	*pDUAL-Pbub1(mod)-mad2+-GFP<<leu1+ hphNT1<<Pbub1(mod)-mad2+-GFP<<kanR plo1+-mCherry<<natR nda3-KM311*
SP141'	*h-*	*pDUAL-Pbub1(mod)-mad2+-GFP<<leu1+ hphNT1<<Pbub1(mod)-mad2+-GFP<<kanR plo1+-mCherry<<natR nda3-KM311*
SM985	*h-*	*leu1 hphNT1<<P(50bp)-mad2+-GFP<<kanR plo1+-mCherry<<natR nda3-KM311*
SM987	*h+*	*leu1 hphNT1<<P(50bp)-mad2+-GFP<<kanR plo1+-mCherry<<natR nda3-KM311*
SM880	*h-*	*leu1 hphNT1<<P(188bp)-mad2+-GFP<<kanR plo1+-mCherry<<natR nda3-KM311*
SM880'	*h-*	*leu1 hphNT1<<P(188bp)-mad2+-GFP<<kanR plo1+-mCherry<<natR nda3-KM311*
SP807	*h+*	*pDUAL-Pbub1(mod)-mad2+-GFP<<leu1+ hphNT1<<P(50bp)-mad2+-GFP<<kanR plo1+-mCherry<<natR nda3-KM311*
SK842	*h+*	*leu1 mad2+-GFP<<kanR plo1+-mCherry<<natR nda3-KM311*
SM879	*h-*	*leu1 hphNT1<<P(259bp)-mad2+-GFP<<kanR plo1+-mCherry<<natR nda3-KM311*

Figure 2d

SL756	*h-*	*leu1 ade6-M210 plo1+-mCherry<<natR nda3-KM311 mad3Δ::ura4+*
SM008	*h-*	*leu1 hphNT1<<P(50bp)-mad3+-GFP<<kanR plo1+-mCherry<<natR nda3-KM311*
SM009	*h+*	*leu1 hphNT1<<P(50bp)-mad3+-GFP<<kanR plo1+-mCherry<<natR nda3-KM311*
SM016	*h-*	*leu1 hphNT1<<P(312bp)-mad3+-GFP<<kanR plo1+-mCherry<<natR nda3-KM311*
SM016'	*h-*	*leu1 hphNT1<<P(312bp)-mad3+-GFP<<kanR plo1+-mCherry<<natR nda3-KM311*
SL759	*h-*	*leu1 mad3+-GFP<<kanR plo1+-mCherry<<natR nda3-KM311*
SL760	*h+*	*leu1 mad3+-GFP<<kanR plo1+-mCherry<<natR nda3-KM311*
SM012	*h-*	*leu1 hphNT1<<P(150bp)-mad3+-GFP<<kanR plo1+-mCherry<<natR nda3-KM311*
SM012'	*h-*	*leu1 hphNT1<<P(150bp)-mad3+-GFP<<kanR plo1+-mCherry<<natR nda3-KM311*

Figure 2e

ST387	*h?*	*leu1 ade6-M216 natNT2<<Park1-mad1+-GFP<<kanR plo1+-mCherry<<natR nda3-KM311*
SL794	*h+*	*leu1 hphNT1<<Pnmt1-mad1+-GFP<<kanR plo1+-mCherry<<natR nda3-KM311*
SK891	*h+*	*leu1 mad1+-GFP<<kanR plo1+-mCherry<<natR nda3-KM311*
SK895	*h-*	*leu1 ade6-M216 natNT2<<Pbub3-mad1+-GFP<<kanR plo1+-mCherry<<natR nda3-KM311*
SL800	*h+*	*leu1 hphNT1<<Pnmt81-mad1+-GFP<<kanR plo1+-mCherry<<natR nda3-KM311*
SM879	*h-*	*leu1 hphNT1<<P(259bp)-mad2+-GFP<<kanR plo1+-mCherry<<natR nda3-KM311*
SK842	*h+*	*leu1 mad2+-GFP<<kanR plo1+-mCherry<<natR nda3-KM311*
SP807	*h+*	*pDUAL-Pbub1(mod)-mad2+-GFP<<leu1+ hphNT1<<P(50bp)-mad2+-GFP<<kanR plo1+-mCherry<<natR nda3-KM311*
SM880	*h-*	*leu1 hphNT1<<P(188bp)-mad2+-GFP<<kanR plo1+-mCherry<<natR nda3-KM311*
SM985	*h-*	*leu1 hphNT1<<P(50bp)-mad2+-GFP<<kanR plo1+-mCherry<<natR nda3-KM311*
SP141	*h-*	*pDUAL-Pbub1(mod)-mad2+-GFP<<leu1+ hphNT1<<Pbub1(mod)- mad2+-GFP<<kanR plo1+- mCherry<<natR nda3-KM311*
SM958	*h-*	*leu1 hphNT1<<Pbub1(mod)-mad2+-GFP<<kanR plo1+-mCherry<<natR nda3-KM311*
SK835	*h-*	*leu1 natNT2<<Pmad3-mad2+-GFP<<kanR plo1+-mCherry<<natR nda3-KM311*
SM012	*h-*	*leu1 hphNT1<<P(150bp)-mad3+-GFP<<kanR plo1+-mCherry<<natR nda3-KM311*
SL760	*h+*	*leu1 mad3+-GFP<<kanR plo1+-mCherry<<natR nda3-KM311*
SM016	*h-*	*leu1 hphNT1<<P(312bp)-mad3+-GFP<<kanR plo1+-mCherry<<natR nda3-KM311*
SM008	*h-*	*leu1 hphNT1<<P(50bp)-mad3+-GFP<<kanR plo1+-mCherry<<natR nda3-KM311*

Figure 3b

SI636	*h+*	*leu1 mad1+-GFP<<kanR*
SI607'	*h-*	*leu1 mad2+-GFP<<kanR*
SI640	*h-*	*leu1 mad3+-GFP<<kanR*
PX938	*h-*	*leu1 bub1+-GFP<<kanR*
SK502'	*h-*	*leu1 ade6-M216 bub3+-S(GGGGS)3-GFP<<kanR*
SK820	*h-*	*leu1 mph1+-S(GGGGS)3-GFP<<kanR*
SK820'	*h-*	*leu1 mph1+-S(GGGGS)3-GFP<<kanR*
SI678	*h-*	*leu1 apc5+-GFP<<kanR*
SI641	*h+*	*cut9+-GFP<<kanR*
SI679	*h-*	*leu1 apc15+-GFP<<kanR*
SI680	*h+*	*leu1 apc15+-GFP<<kanR*
SK826	*h-*	*ade6-M216 Pmad3-GFP<<leu1+*

Figure 4a

SK891	*h+*	*leu1 mad1+-GFP<<kanR plo1+-mCherry<<natR nda3-KM311*
ST345	*h-*	*leu1 mad1-R509A/L511G-GFP<<<kanR plo1+-mCherry<<natR nda3-KM311*
ST387	*h?*	*leu1 ade6-M216 natNT2<<Park1-mad1+-GFP<<kanR plo1+-mCherry<<natR nda3-KM311*

Figure 4b

SK891	*h+*	*leu1 mad1+-GFP<<kanR plo1+-mCherry<<natR nda3-KM311*
ST387	*h?*	*leu1 ade6-M216 natNT2<<Park1-mad1+-GFP<<kanR plo1+-mCherry<<natR nda3-KM311*
ST720	*h?*	*ade6-M216 pDUAL-5'(950bp)-mad2+-GFP<<leu1+ natNT2<<Park1-mad1+-GFP<<kanR plo1+-mCherry<<natR nda3-KM311*
ST718	*h?*	*ade6-M216 pDUAL-5'(950bp)-mad2-W74A-GFP<<leu1+ natNT2<<Park1-mad1+-GFP<<kanR plo1+-mCherry<<natR nda3-KM311*
SP247	*h+*	*mad2-W74A-GFP<<kanR plo1+-mCherry<<natR nda3-KM311*

Figure 4d

SK844	*h+*	*leu1 (ade6-M210? ura4-D18?) plo1+-mCherry<<natR nda3-KM311 mad2Δ::ura4+*
SK842	*h+*	*leu1 mad2+-GFP<<kanR plo1+-mCherry<<natR nda3-KM311*
SM987	*h+*	*leu1 hphNT1<<P(50bp)-mad2+-GFP<<kanR plo1+-mCherry<<natR nda3-KM311*
SP141'	*h-*	*pDUAL-Pbub1(mod)-mad2+-GFP<<leu1+ hphNT1<<Pbub1(mod)-mad2+-GFP<<kanR plo1+-mCherry<<natR nda3-KM311*
ST335	*h+*	*leu1 mad2-R133A-GFP<<kanR plo1+-mCherry<<natR nda3-KM311*
ST375	*h-*	*leu1 ade6-M216 hphNT1<<P(50bp)-mad2-R133A-GFP<<kanR plo1+-mCherry<<natR nda3-KM311*
ST392	*h-*	*pDUAL-Pbub1(mod)-mad2-R133A-GFP<<leu1+ hphNT1<<Pbub1(mod)-mad2-R133A-GFP<<kanR plo1+-mCherry<<natR nda3-KM311*

Figure 5a

SK828	*h+*	*leu1 (ade6-M216?) plo1+-mCherry<<natR nda3-KM311*
SK896	*h+*	*leu1 (ade6-M216?) natNT2<<Pbub3-mad1+-GFP<<kanR plo1+-mCherry<<natR nda3-KM311*
SM985	*h-*	*leu1 hphNT1<<P(50bp)-mad2+-GFP<<kanR plo1+-mCherry<<natR nda3-KM311*
SM880	*h-*	*leu1 hphNT1<<P(188bp)-mad2+-GFP<<kanR plo1+-mCherry<<natR nda3-KM311*
SP807	*h+*	*pDUAL-Pbub1(mod)-mad2+-GFP<<leu1+ hphNT1<<P(50bp)-mad2+-GFP<<kanR plo1+-mCherry<<natR nda3-KM311*
SM008	*h-*	*leu1 hphNT1<<P(50bp)-mad3+-GFP<<kanR plo1+-mCherry<<natR nda3-KM311*
SM016	*h-*	*leu1 hphNT1<<P(312bp)-mad3+-GFP<<kanR plo1+-mCherry<<natR nda3-KM311*

Figure 5b

SI636	*h+*	*mad1+-GFP<<kanR*
SI607'	*h-*	*leu1 mad2+-GFP-kanR*
SI639	*h+*	*ade6-M216 mad3+-GFP<<kanR*
PX938	*h-*	*leu1 bub1+-GFP<<kanR*
SK502'	*h-*	*leu1 ade6-M216 bub3+-S(GGGGS)3-GFP<<kanR*
SK820	*h-*	*leu1 mph1+-S(GGGGS)3-GFP<<kanR*
SI641	*h+*	*cut9+-GFP<<kanR*
SI679	*h-*	*leu1 apc15+-GFP<<kanR*
SK826	*h-*	*ade6-M216 pDUAL-Pmad3-GFP<<leu1+*

Figure 5c

SM822	*h+*	*mad1+-GFP<<kanR plo1+-mCherry<<natR cdc25-22*

Figure 6a

SM822	*h+*	*mad1+-GFP<<kanR plo1+-mCherry<<natR cdc25-22*

Figure 6b

SH585	*h-*	*leu1 ade6-M210 plo1+-GFP<<kanR*

Figure 6c

SP458	*h+*	*leu1 ade6-M216? ura4-D18? kanR<<Prad21-slp1+ mad2Δ::ura4+ plo1+-mCherry<<natR nda3-KM311*
SP462	*h-*	*leu1 ade6-M210 kanR<<Prad21-slp1+ mad3Δ::ura4+ plo1+-mCherry<<natR nda3-KM311*
SM958	*h-*	*leu1 hphNT1<<Pbub1(mod)-mad2+-GFP<<kanR plo1+-mCherry<<natR nda3-KM311*
SP430'	*h-*	*kanR<<Prad21-slp1+ hphNT1<<Pbub1(mod)-mad2+-GFP<<kanR plo1+-mCherry<<natR nda3-KM311*
SP141	*h-*	*pDUAL-Pbub1(mod)-mad2+-GFP<<leu1+ hphNT1<<Pbub1(mod)-mad2+-GFP<<kanR plo1+-mCherry<<natR nda3-KM311*
SP421	*h-*	*KM311*
SM987	*h+*	*leu1 hphNT1<<P(50bp)-mad2+-GFP<<kanR plo1+-mCherry<<natR nda3-KM311*
SP427	*h-*	*leu1 kanR<<Prad21-slp1+ hphNT1<<P(50bp)-mad2+-GFP<<kanR plo1+-mCherry<<natR nda3-KM311*
SM008	*h-*	*leu1 hphNT1<<P(50bp)-mad3+-GFP<<kanR plo1+-mCherry<<natR nda3-KM311*
SP423	*h+*	*kanR<<Prad21-slp1+ hphNT1<<P(50bp)-mad3-GFP<<kanR plo1+-mCherry<<natR nda3-KM311*
ST307	*h-*	*GFP<<kanR plo1+-mCherry<<natR nda3-KM311*

Figure 6d

SL240'	*h+*	*leu1 ade6-M210 plo1+-mCherry<<natR cdc25-22*
SP437"'	*h+*	*kanR<<Prad21-slp1 plo1+-mCherry<<natR cdc25-22*

Figure 6e

SK828	*h+*	*leu1 (ade6-M216?) plo1+-mCherry<<natR nda3-KM311*
SP801	*h+*	*(ade6-M216?) pDUAL-5'(1504bp)-slp1+-3'(549bp)<<leu1+ plo1+-mCherry<<natR nda3-KM311*
SK895	*h-*	*leu1 ade6-M216 natNT2<<Pbub3-mad1+-GFP<<kanR plo1+-mCherry<<natR nda3-KM311*
SP802	*h-*	*(ade6-M216?) pDUAL-5'(1504bp)-slp1+-3'(549bp)<<leu1+ natNT2<<Pbub3-mad1+-GFP<<kanR plo1+-mCherry<<natR nda3-KM311*
SM987	*h+*	*leu1 hphNT1<<P(50bp)-mad2+-GFP-kanR plo1+-mCherry<<natR nda3-KM311*
SP804	*h+*	*pDUAL-5'(1504bp)-slp1+-3'(549bp)<<leu1+ hphNT1<<P(50bp)-mad2+-GFP<<kanR plo1+-mCherry<<natR nda3-KM311*
SM008	*h-*	*leu1 hphNT1<<P(50bp)-mad3+-GFP<<kanR plo1+-mCherry<<natR nda3-KM311*
SP805	*h-*	*pDUAL-5'(1504bp)-slp1+-3'(549bp)<<leu1+ hphNT1<<P(50bp)-mad3-GFP<<kanR plo1+-mCherry<<natR nda3-KM311*

Figure 6f

SL240	*h+*	*leu1 ade6-M210 plo1+-mCherry<<natR cdc25-22*
SP500	*h+*	*pDUAL-5'(1504bp)-slp1+-3'(549bp)<<leu1+ ade6-M210 plo1+-mCherry<<natR cdc25-22*

Figure 8a

SM985	*h-*	*leu1 hphNT1<<P(50bp)-mad2+-GFP<<kanR plo1+-mCherry<<natR nda3-KM311*
SM986	*h-*	*leu1 hphNT1<<P(50bp)-mad2+-GFP<<kanR plo1+-mCherry<<natR nda3-KM311*
SM987	*h+*	*leu1 hphNT1<<P(50bp)-mad2+-GFP<<kanR plo1+-mCherry<<natR nda3-KM311*
SM880	*h-*	*leu1 hphNT1<<P(188bp)-mad2+-GFP<<kanR plo1+-mCherry<<natR nda3-KM311*
SM880'	*h-*	*leu1 hphNT1<<P(188bp)-mad2+-GFP<<kanR plo1+-mCherry<<natR nda3-KM311*
SM008	*h-*	*leu1 hphNT1<<P(50bp)-mad3+-GFP<<kanR plo1+-mCherry<<natR nda3-KM311*
SM009	*h+*	*leu1 hphNT1<<P(50bp)-mad3+-GFP<<kanR plo1+-mCherry<<natR nda3-KM311*

Figure 8d

SM008	*h-*	*leu1 hphNT1<<P(50bp)-mad3+-GFP<<kanR plo1+-mCherry<<natR nda3-KM311*

Figure S1a

SK671	*h-*	*mad1+-GFP<<kanR plo1+-mCherry<<natR nda3-KM311 lys1 hygR<<ark1-as3 (L166A, S229A)*
SK673	*h-*	*mad2+-GFP<<kanR plo1+-mCherry<<natR nda3-KM311 lys1 hygR<<ark1-as3 (L166A, S229A)*
SK675	*h-*	*mad3+-GFP<<kanR plo1+-mCherry<<natR nda3-KM311 lys1 hygR<<ark1-as3 (L166A, S229A)*
SK676	*h-*	*bub1+-GFP<<kanR plo1+-mCherry<<natR nda3-KM311 lys1 hygR<<ark1-as3 (L166A, S229A)*
SK678	*h-*	*bub3+-S(GGGGS)3-doublemye-GFP<<kanR plo1+-mCherry<<natR nda3-KM311 lys1 hygR<<ark1-as3 (L166A, S229A)*
SK697	*h+*	*mph1+-GFP<<kanR nda3-KM311 plo1+-mCherry<<natR hygR<<ark1-as3 (L166A, S229A)*

S1b

JY333	*h-*	*ade6-M216 leu1*
AE247	*h-*	*ura4-D18 leu1 mad1D::ura4+*
SI601	*h-*	*ade6-M216 leu1 mad1+-GFP<<kanR*
SI601'	*h-*	*ade6-M216 leu1 mad1+-GFP<<kanR*
SI602	*h-*	*ade6-M216 leu1 mad3+-GFP<<kanR*
SI602'	*h-*	*ade6-M216 leu1 mad3+-GFP<<kanR*
SI607	*h-*	*leu1 ade6-M210 mad2+-GFP<<kanR*
SI607'	*h-*	*leu1 mad2+-GFP<<kanR*
PX937	*h90*	*leu1 bub1+-GFP<<kanR*
PX938	*h-*	*leu1 bub1+-GFP<<kanR*
SI665	*h-*	*ade6-M216 leu1 bub3+-S(GGGGS)3-2xmyeGFP<<kanR*
SI665'	*h-*	*ade6-M216 leu1 bub3+-S(GGGGS)3-3xmyeGFP<<kanR*
SK820	*h-*	*leu1 mph1+-S(GGGGS)3-GFP<<kanR*
SK820'	*h-*	*leu1 mph1+-S(GGGGS)3-GFP<<kanR*
SI677	*h+*	*apc5+-GFP<<kanR*
SI677'	*h+*	*apc5+-GFP<<kanR*
SI664	*h-*	*leu1 ade6-M216 apc15+-GFP<<kanR*
SI664'	*h-*	*leu1 ade6-M216 apc15+-GFP<<kanR*
SI641	*h+*	*cut9+-GFP<<kanR*
SI642	*h-*	*cut9+-GFP<<kanR*
SK826	*h-*	*ade6-M216 leu1 pDUAL-Pmad3-GFP<<leu1+*
SK826'	*h-*	*ade6-M216 leu1 pDUAL-Pmad3-GFP<<leu1+*
SK570	*h+*	*cut11+-mCherry<<hygR*
SK570'	*h+*	*cut11+-mCherry<<hygR*

Figure S1c

JY333	*h-*	*ade6-M216 leu1*
AE247	*h-*	*ura4-D18 leu1 mad1D::ura4+*
SM590	*h?*	*(leu1?) mad1+-GFP<<kanR gtb1-93*
SM591	*h?*	*(leu1?)*
SM592	*h?*	*(leu1?) gtb1-93*

SM593	*h?*	*(leu1?) mad1+-GFP<<kanR*
SM594	*h?*	*leu1 mad2+-GFP<<kanR ura4 fin1Δ::ura4+*
SM595	*h?*	*leu1 mad2+-GFP<<kanR*
SM596	*h?*	*leu1 ura4 fin1Δ::ura4+*
SM597	*h?*	*leu1*
SM598	*h?*	*leu1 mad3+-GFP<<kanR gtb1-93*
SM599	*h?*	*leu1 mad3+-GFP<<kanR*
SM600	*h?*	*leu1*
SM801	*h?*	*leu1 gtb1-93*
SM810	*h?*	*leu1 bub1+-GFP<<kanR*
SM811	*h?*	*leu1 fin1Δ::ura4+*
SM812	*h?*	*leu1*
SM813	*h?*	*leu1 bub1+-GFP<<kanR fin1Δ::ura4+*
ST377	*h-*	*leu1 apc5+-GFP<<kanR*
ST378	*h+*	*apc5+-GFP<<kanR cut2-364*
ST379	*h+*	*cut2-364*
ST380	*h-*	*leu1*
SM806	*h?*	*(leu1?) cut2-364*
SM807	*h?*	*(leu1?) apc15+-GFP<<kanR*
SM808	*h?*	*(leu1?) apc15+-GFP<<kanR cut2-364*
SM809	*h?*	*(leu1?)*
SM802	*h?*	*cut9+-GFP<<kanR*
SM803	*h?*	*cut9+-GFP<<kanR cut2-364*
SM804	*h?*	*wild type*
SM805	*h?*	*cut2-364*

S2e

SK570	*h+*	*cut11+-mCherry<<hygR*
SL706	*h-*	*leu1 cut11+-mCherry<< hygR gpi16+-mCherry<<natR*
SK578	*h+*	*leu1 mad1+-GFP<<kanR cut11+-mCherry<<hygR*
SK580	*h+*	*mad2+-GFP<<kanR cut11+-mCherry<<hygR*
SK581	*h+*	*mad3+-GFP<<kanR cut11+-mCherry<<hygR*
SK583	*h+*	*bub1+-GFP<<kanR cut11+-mCherry<<hygR*
SK585	*h+*	*bub3+-S(GGGGS)3-GFP<<kanR cut11+-mCherry<<hygR*
SK829	*h-*	*leu1 mph1+-S(GGGGS)3-GFP<<kanR cut11+-mCherry<<hygR*
SK595	*h+*	*apc5+-GFP<<kanR cut11+-mCherry<<hygR*
SK597	*h-*	*leu1 apc15+-GFP<<kanR cut11+-mCherry<<hygR*
SK590	*h-*	*cut9+-GFP<<kanR cut11+-mCherry<<hygR*
SM558	*h-*	*pDUAL-Pmad3-GFP<<leu1+ cut11+-mCherry<<hygR*

– c, e

SK581	*h+*	*mad3+-GFP<<kanR cut11+-mCherry<<hygR*
SK597	*h-*	*leu1 apc15+-GFP<<kanR cut11+-mCherry<<hygR*
SM558	*h-*	*pDUAL-Pmad3-GFP<<leu1+ cut11+-mCherry<<hygR*

S3d

SM997	*h90*	*leu1 nuc1+-GFP-HA<<kanR cut11+-mCherry<<hygR*
SK581	*h+*	*mad3+-GFP<<kanR cut11+-mCherry<<hygR*

S3f

SM834'	*h-*	*ade6-M216 Pmad3-GFP<<leu1+ plo1+-mCherry<<natR cdc25-22*
SL240'	*h+*	*ade6-M210 leu1 plo1+-mCherry<<natR cdc25-22*

S3g

SI639	*h+*	*ade6-M216 mad3-GFP<<kanR*
SI640	*h-*	*leu1 mad3-GFP<<kanR*
SP812	*h-*	*leu1 mad3-wtGFP<<kanR*
SP812'	*h-*	*leu1 mad3-wtGFP<<kanR*

S3h

SM834'	*h-*	*ade6-M216 Pmad3-GFP<<leu1+ plo1+-mCherry<<natR cdc25-22*
SP566	*h-*	*leu1 mad3+-GFP<<kanR plo1+-mCherry<<natR cdc25-22*

Figure S4a

SI638	*h-*	*leu1 mad1-GFP<<kanR*
AE247	*h-*	*ura4-D18 leu1 mad1D::ura4+*
SL780	*h-*	*leu1 hphNT1<<Pnmt81-mad1+-GFP<<kanR*
SK876	*h-*	*leu1 natNT2<<Pbub3-mad1+-GFP<<kanR*
SK877'	*h-*	*leu1 natNT2<<Park1-mad1+-GFP<<kanR*
SK891	*h+*	*leu1 mad1+-GFP<<kanR plo1+-mCherry<<natR nda3-KM311*
SL794	*h+*	*leu1 hphNT1<<Pnmt1-mad1+-GFP<<kanR plo1+-mCherry<<natR nda3-KM311*

S4b

SI607‘	*h-*	*leu1 mad2+-GFP-kanR*
JX793	*h90*	*ade6-M216 leu1 ura4-D18 mad2Δ::ura4+*
SK822'	*h-*	*leu1 natNT2<<Pmad3-mad2+-GFP<<kanR*
SM926	*h-*	*leu1 hphNT1<<Pbub1(mod)-mad2+-GFP<<kanR*
SP141'	*h-*	*pDUAL-Pbub1(mod)-mad2+-GFP<<leu1+ hphNT1<<Pbub1(mod)-mad2+-GFP<<kanR plo1+- mCherry<<natR nda3-KM311*
SK842	*h+*	*leu1 mad2+-GFP<<kanR plo1+-mCherry<<natR nda3-KM311*
SM928'	*h-*	*leu1 hphNT1<<P(50bp)-mad2+-GFP<<kanR*
SM858	*h-*	*leu1 hphNT1<<P(188bp)-mad2+-GFP<<kanR*
SP807	*h+*	*pDUAL-Pbub1(mod)-mad2+-GFP<<leu1+ hphNT1<<P(50bp)-mad2+-GFP<<kanR plo1+-mCherry<<natR nda3-KM311*
SK842	*h+*	*leu1 mad2+-GFP<<kanR plo1+-mCherry<<natR nda3-KM311*
SM879	*h-*	*leu1 hphNT1<<P(259bp)-mad2+-GFP<<kanR plo1+-mCherry<<natR nda3-KM311*

Figure S4c

SI640	*h-*	*leu1 mad3+-GFP-kanR*
DM001	*h-*	*ade6-M210 leu1 mad3Δ::ura4+*
SL786	*h-*	*leu1 hphNT1<<P(50bp)-mad3+-GFP<<kanR*
SL787	*h-*	*leu1 hphNT1<<P(100bp)-mad3+-GFP<<kanR*
SL788	*h-*	*leu1 hphNT1<<P(150bp)-mad3+-GFP<<kanR*
SL790	*h-*	*leu1 hphNT1<<P(312bp)-mad3+-GFP<<kanR*

Figure S5a

ST153	*h-*	*mad1+-GFP<kanR mad2+-mCherry<<natR*
ST351	*h+*	*leu1 ade6-M21? mad1-R509A/L511G-GFP<<<kanR mad2+-mCherry<<natR nda3-KM311*

S5b

SK891	*h+*	*leu1 mad1+-GFP<<kanR plo1+-mCherry<<natR nda3-KM311*
ST345	*h-*	*leu1 mad1-R509A/L511G-GFP<<<kanR plo1+-mCherry<<natR nda3-KM311*

Figure S5c

ST345	*h-*	*leu1 mad1-R509A/L511G-GFP<<<kanR plo1+-mCherry<<natR nda3-KM311*
ST387	*h?*	*leu1 ade6-M216 natNT2<<Park1-mad1+-GFP<<kanR plo1+-mCherry<<natR nda3-KM311*

S5d

SK842	*h+*	*leu1 mad2+-GFP<<kanR plo1+-mCherry<<natR nda3-KM311*
ST387	*h?*	*leu1 ade6-M216 natNT2<<Park1-mad1+-GFP<<kanR plo1+-mCherry<<natR nda3-KM311*

S5e

SK891	*h+*	*leu1 mad1+-GFP<<kanR plo1+-mCherry<<natR nda3-KM311*
ST387	*h?*	*leu1 ade6-M216 natNT2<<Park1-mad1+-GFP<<kanR plo1+-mCherry<<natR nda3-KM311*
ST709	*h?*	*ade6-M216 pDUAL-5'(950bp)-mad2+-3'(485bp)<<leu1+ natNT2<<Park1-mad1+-GFP<<kanR plo1+-mCherry<<natR nda3-KM311*

ST709'	*h?*	*ade6-M216 pDUAL-5'(950bp)-mad2+-3'(485bp)<<leu1+ natNT2<<Park1-mad1+-GFP<<kanR plo1+-mCherry<<natR nda3-KM311*
S5f		
SK891	*h+*	*leu1 mad1+-GFP<<kanR plo1+-mCherry<<natR nda3-KM311*
ST387	*h?*	*leu1 ade6-M216 natNT2<<Park1-mad1+-GFP<<kanR plo1+-mCherry<<natR nda3-KM311*
ST718	*h?*	*ade6-M216 pDUAL-5'(950bp)-mad2-W74A-GFP<<leu1+ natNT2<<Park1-mad1+-GFP<<kanR plo1+-mCherry<<natR nda3-KM311*
ST720	*h?*	*ade6-M216 pDUAL-5'(950bp)-mad2+-GFP<<leu1+ natNT2<<Park1-mad1+-GFP<<kanR plo1+-mCherry<<natR nda3-KM311*
SK842	*h+*	*leu1 mad2+-GFP<<kanR plo1+-mCherry<<natR nda3-KM311*
S5g		
ST387	*h?*	*leu1 ade6-M216 natNT2<<Park1-mad1+-GFP<<kanR plo1+-mCherry<<natR nda3-KM311*
ST709	*h?*	*ade6-M216 pDUAL-5'(950bp)-mad2+-3'(485bp)<<leu1+ natNT2<<Park1-mad1+-GFP<<kanR plo1+-mCherry<<natR nda3-KM311*
S5h		
SK842	*h+*	*leu1 mad2+-GFP<<kanR plo1+-mCherry<<natR nda3-KM311*
SM879	*h-*	*leu1 hphNT1<<P(259bp)-mad2+-GFP<<kanR plo1+-mCherry<<natR nda3-KM311*
S5i		
SM879	*h-*	*leu1 hphNT1<<P(259bp)-mad2+-GFP<<kanR plo1+-mCherry<<natR nda3-KM311*
ST386	*h-*	*leu1 hphNT1<<P(259bp)-mad2+-GFP<<kanR plo1+-mCherry<<natR nda3-KM311 mad1Δ::ura4+*
S6a,b		
SK842	*h+*	*leu1 mad2+-GFP<<kanR plo1+-mCherry<<natR nda3-KM311*
SP141'	*h-*	*pDUAL-Pbub1(mod)-mad2+-GFP<<leu1+ hphNT1<<Pbub1(mod)-mad2+-GFP<<kanR plo1+-mCherry<<natR nda3-KM311*
SM958	*h-*	*leu1 hphNT1<<Pbub1(mod)-mad2+-GFP<<kanR plo1+-mCherry<<natR nda3-KM311*
Figure S6c		
SM987	*h+*	*leu1 hphNT1<<P(50bp)-mad2+-GFP<<kanR plo1+-mCherry<<natR nda3-KM311*
SP900	*h+*	*leu1 hphNT1<<P(50bp)-mad2+-GFP<<kanR plo1+-mCherry<<natR nda3-KM311 mad3Δ::ura4+*
SP874	*h+*	*leu1 hphNT1<<P(50bp)- mad2+-GFP<<kanR plo1+-mCherry<<natR nda3-KM311 slp1-mr63*
S6d		
SK842	*h+*	*leu1 mad2+-GFP<<kanR plo1+-mCherry<<natR nda3-KM311*
ST335	*h+*	*leu1 mad2-R133A-GFP<<kanR plo1+-mCherry<<natR nda3-KM311*
S6e		
SK842	*h+*	*leu1 mad2+-GFP<<kanR plo1+-mCherry<<natR nda3-KM311*
ST335	*h+*	*leu1 mad2-R133A-GFP<<kanR plo1+-mCherry<<natR nda3-KM311*
SM987	*h+*	*leu1 hphNT1<<P(50bp)-mad2+-GFP<<kanR plo1+-mCherry<<natR nda3-KM311*
ST375	*h-*	*leu1 ade6-M216 hphNT1<<P(50bp)-mad2-R133A-GFP<<kanR plo1+-mCherry<<natR nda3-KM311*
SP141'	*h-*	*pDUAL-Pbub1(mod)-mad2+-GFP<<leu1+ hphNT1<<Pbub1(mod)-mad2+-GFP<<kanR plo1+-mCherry<<natR nda3-KM311*
ST392	*h-*	*pDUAL-Pbub1(mod)-mad2-R133A-GFP<<leu1+ hphNT1<<Pbub1(mod)-mad2-R133A-GFP<<kanR plo1+-mCherry<<natR nda3-KM311*
S6g		
SK891	*h+*	*leu1 mad1+-GFP<<kanR plo1+-mCherry<<natR nda3-KM311*
SK895	*h-*	*leu1 ade6-M216 natNT2<<Pbub3-mad1+-GFP<<kanR plo1+-mCherry<<natR nda3-KM311*
SK893	*h+*	*leu1 ade6-M216 plo1+-mCherry<<natR nda3-KM311 mad1Δ::ura4+*
Figure S7a		
SM558	*h-*	*pDUAL-Pmad3-GFP<<leu1+ cut11+-mCherry<<hygR*
SM855	*h+*	*pDUAL-Pmad3-GFP<<leu1+ cut11+-mCherry<<hygR cdc25-22*
S7b		
SM347	*h?*	*ade6-M210 mad1+-GFP<<kanR plo1+-mCherry<<natR cdc25-22*
SM823	*h+*	*mad1+-GFP<<kanR plo1+-mCherry<<natR cdc25-22 cut7-446*
S7c,e		
SM822	*h+*	*mad1+-GFP<<kanR plo1+-mCherry<<natR cdc25-22*
SM823	*h+*	*mad1+-GFP<<kanR plo1+-mCherry<<natR cdc25-22 cut7-446*
SM347	*h?*	*ade6-M210 mad1+-GFP<<kanR plo1+-mCherry<<natR cdc25-22*
S7d		
JV356	*h-*	*ade6-M216 leu1 slp1+-3HA<<kanR*
SL337	*h+*	*(ade6-M216?) leu1 bub1+-3HA<<hygR plo1+-mCherry<<natR nda3-KM311*
JY333	*h-*	*ade6-M216 leu1*
S7f		
SH585	*h-*	*leu1 ade6-M210 plo1+-GFP<<kanR*
S8b		
SM985	*h-*	*leu1 hphNT1<<P(50bp)-mad2+-GFP<<kanR plo1+-mCherry<<natR nda3-KM311*
Figure S8c		
SM546	*h+*	*leu1 mad2+-GFP<<kanR hphNT1<<P(50bp)-mad3+-GFP<<kanR plo1+-mCherry<<natR nda3-KM311*
SM008	*h-*	*leu1 hphNT1<<P(50bp)-mad3+-GFP<<kanR plo1+-mCherry<<natR nda3-KM311*
ST301	*h+*	*leu1 hphNT1<<P(50bp)-mad2+-GFP<<kanR mad3+-GFP<<kanR plo1+-mCherry<<natR nda3-KM311*
SM987	*h-*	*leu1 hphNT1<<P(50bp)-mad2+-GFP<<kanR plo1+-mCherry<<natR nda3-KM311*
S8e		
SP849	*h+*	*leu1 hphNT1<<P(50bp)-mad3+-GFP-Y66L<<kanR bub1+-GFP<<kanR plo1+-mCherry<<natR nda3-KM311*
SP851	*h-*	*leu1 hphNT1<<P(50bp)-mad3+-GFP-Y66L<<kanR plo1+-mCherry<<natR nda3-KM311*
S8f		
SM880	*h-*	*leu1 hphNT1<<P(188bp)-mad2+-GFP<<kanR plo1+-mCherry<<natR nda3-KM311*
SM965	*h?*	*leu1 hphNT1<<(188bp)-mad2+-GFP<<kanR hphNT1<<P(100bp)-mad3-GFP<<kanR plo1+-mCherry<<natR nda3-KM311*
SM968	*h?*	*leu1 hphNT1<<P(188bp)-mad2+-GFP<<kanR hphNT1<<P(312bp)-mad3-GFP<<kanR plo1+-mCherry<<natR nda3-KM311*
SM969	*h?*	*leu1 hphNT1<<P(188bp)-mad2+-GFP<<kanR hphNT1<<P(312bp)-mad3-GFP<<kanR plo1+-mCherry<<natR nda3-KM311*
SP101	*h-*	*leu1 hphNT1<<P(188bp)-mad2+-GFP<<kanR hphNT1<<P(150bp)-mad3-GFP<<kanR plo1+-mCherry<<natR nda3-KM311*
SP101'	*h-*	*leu1 hphNT1<<P(188bp)-mad2+-GFP<<kanR hphNT1<<P(150bp)-mad3-GFP<<kanR plo1+-mCherry<<natR nda3-KM311*

Supplementary Table S5

mRNA FISH probes

GFP probes (5' --> 3')	Slp1 probes (5' --> 3')
1: aaaagttcttctcctttact	1: gaattacctgctatctccat
2: caagaattgggacaactcca	2: aagttccttttctttgtggg
3: cccattaacatcaccatcta	3: gttatagggctgttagggaa
4: cctctccactgacagaaaat	4: taaaagtgcctgctgatgca
5: gtaagttttccgtatgttgc	5: tggaagaacgaccgttacgg
6: gtagttttccagtagtgcaa	6: tcgatttttggtgagtttct
7: acaagtgttggccatggaac	7: gatccgcatagtggaataga
8: gcattgaacaccataagtga	8: caggacgacttttgtttcgt
9: tcatgccgtttcatatgatc	9: ataaagcggtcacttcgact
10: gggcatggcactcttgaaaa	10: cattagcagtgtttggacga
11: ttctttcctgtacataacct	11: ggaacgtcactgctgataga
12: gttcccgtcatctttgaaaa	12: aaaaccgcatgcttcagcaa
13: tgacttcagcacgtgtcttg	13: gcgagaacacgcgtgtttaa
14: taacaagggtatcaccttca	14: ctcaggagcatccaatttaa
15: atacctttaactcgattct	15: gcaagtctacaggcttttg
16: gtgtccaagaatgtttccat	16: tgtaaccacaggtctttgag
17: gtgagttatagttgtattcc	17: aactcgttcaggagtagtgt
18: gtctgccatgatgtatacat	18: caatgataccaggagcatct
19: ctttgattccattcttttgt	19: taagtttgaccaatccagca
20: ccatcttcaatgttgtgtct	20: ccaaacatacacattgcgct
21: atggtctgctagttgaacgc	21: taaccgaaccactatcagca
22: cgccaattggagtattttgt	22: aggttgattcatcggtttct
23: gtctggtaaaaggacagggc	23: aaccatcgtgagaccatttt
24: aagggcagattgtgtggaca	24: tatatatcaacgagcccgtt
25: tcttttcgttgggatctttc	25: ctgccattgttcgaagtttt
26:tcaagaaggaccatgtggtc	26: gacaaccaactctagcttga
27: aatcccagcagctgttacaa	27: gacagaacgtgacgattcca
28: tatagttcatccatgccatg	28: gatgaatagcgccagaacgg
	29: ttagcgatacgcacatcatg
	30: ctgaagagtcccaatctgat
	31: ccacagacttcactagagtg
	32: ccaactgaagaccgtctgaa
	33: aacaacgttgtcattaccgc
	34: gaatcgaagatctggcatcc
	35: cgttatggttggttttggta
	36: tagattactttgccaagggc
	37: tggcagcattccaaaagtga
	38: atccacggtgttaactcttg
	39: atcagtgaagtgacctgact
	40: ttctttagaatgagggctcc
	41: tctggaaagccatgagtaga

Table S5 mRNA FISH probes.

List of DNA probes used in fluorescence in situ hybridization (FISH) to detect mRNAs of either gene-GFP fusions (through the GFP moiety) or of *slp1+.*

Supplementary Note for

Determinants of robustness in spindle assembly checkpoint signalling

Stephanie Heinrich, Eva-Maria Geissen, Julia Kamenz, Susanne Trautmann, Christian Widmer, Philipp Drewe, Michael Knop, Nicole Radde, Jan Hasenauer, Silke Hauf

(A) Analysis of noise in checkpoint protein abundance

(A1) Determination of protein noise by WiFDeM

Since we quantified the abundance of SAC proteins or APC/C subunits fused to GFP in single cells, we could determine the variability between cells, both for the nuclear and for the cellular measurements. We took the GFP measurements, from which the contribution of autofluorescence (based on wild type cells present in the same well) had been subtracted, and divided their standard deviation by the mean to obtain the coefficient of variation (CV).

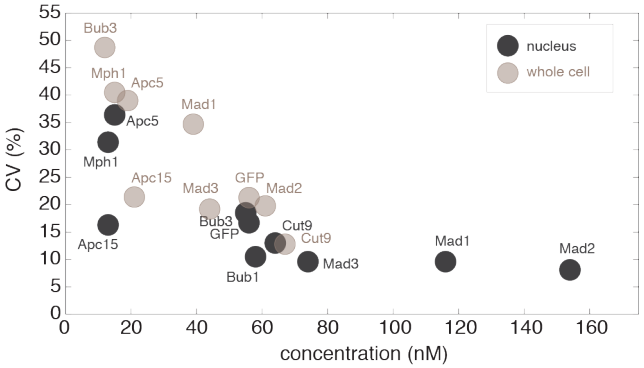

We noticed that noise values tended to be higher when the concentration was lower. This resulted in situations where, for the same cells, cellular noise was higher than nuclear noise (e.g. Mad1). However, in strains where the cellular and nuclear GFP concentration were similar (e.g. Cut9), the CV was also similar. We suspect that in samples with low GFP concentration, the protein noise is obscured by the underlying autofluorescence noise, which leads to an overestimation.

In brief, the fluorescence variability that we observe is a composite of the variability in autofluorescence and the variability in abundance of the GFP fusion protein.

The noise in autofluorescence is

(1) $CV_{AF} = \frac{\sigma_{AF}}{\mu_{AF}}$,

the noise of the GFP fusion protein is

(2) $CV_{GFP} = \frac{\sigma_{GFP}}{\mu_{GFP}}$,

with σ being the standard deviation and μ being the mean. While the noise of the autofluorescence can be measured in control experiments, the noise of the GFP concentration cannot be measured directly. We can merely measure noise of the combined fluorescence.

The combined fluorescence has a standard deviation of

(3) $\sigma_{tot} = \sqrt{{\sigma_{AF}}^2 + {\sigma_{GFP}}^2}$,

and, since we subtract the mean of the autofluorescence to obtain the GFP concentration, has a mean of $\mu_{tot} = \mu_{GFP}$.

We observe $CV_{tot} = \frac{\sigma_{tot}}{\mu_{GFP}}$, and are interested in CV_{GFP}. Equation (2) and (3) can be re-arranged to yield

(4) $$CV_{GFP} = \frac{\sqrt{{\sigma_{tot}}^2 - {\sigma_{AF}}^2}}{\mu_{GFP}} = \sqrt{{CV_{tot}}^2 - \frac{{\sigma_{AF}}^2}{{\mu_{GFP}}^2}}$$

Hence the observed noise (CV_{tot}) overestimates the noise of the SAC-GFP fusion proteins (CV_{GFP}) by a factor that depends on the noise of the autofluorescence and the mean GFP signal intensity. If the GFP signal is high, autofluorescence noise can be neglected and the observed noise will be close to the SAC-GFP fusion protein noise. We therefore grouped our measurements into three categories. Category 1 (darkest grey in Fig. 3a) contains samples, for which the mean GFP concentration is more than 2.5-times the mean autofluorescence concentration: this includes the nuclear measurements for Mad1 and Mad2. In this category, noise is determined quite accurately. Category 2 (intermediate grey intensity in Fig. 3a) contains samples, for which the mean GFP concentration is more than 1.5-times but less than 2.5-times the mean autofluorescence concentration: this includes the nuclear measurements for Mad3, Bub1, Cut9 and free GFP. Category 3 contains all other samples, including all cellular measurements, whose mean GFP concentration is less than 1.5-times the autofluorescence concentration. In those samples, we expect the measured noise to substantially overestimate the protein noise.

The standard deviation of the autofluorescence in the GFP-containing cells, which is needed in equation (4) is unknown, but we can use the standard deviation of the autofluorescence of wild type cells present in the same observation chamber as an estimate. If we perform this correction, the noise estimate of nuclear Mad1 and Mad2 changes only little, whereas the change is more substantial for measurements in category 2 and 3.

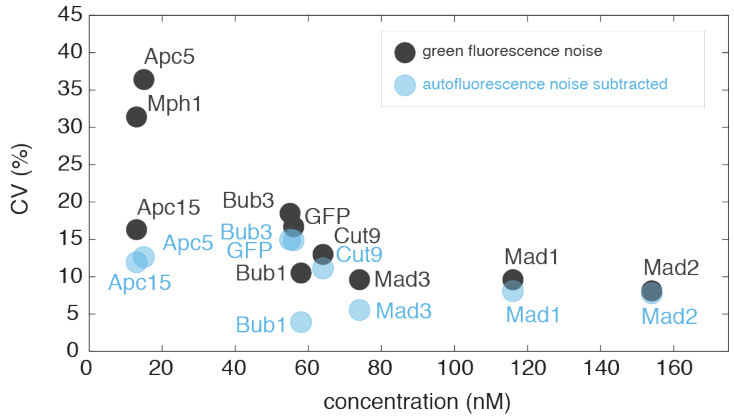

Mph1, whose fluorescence is only 5 % above the autofluorescence, could not be assessed in this way, because the standard deviation of the autofluorescence happened to be higher than the

standard deviation of the fluorescence signal in GFP cells, presumably due to chance variation. We conclude that the observed noise generally overestimates the protein noise and that the noise measurements are more accurate when the GFP concentration is higher, as is the case for Mad1 and Mad2 in the nucleus.

(A2) Comparison of coefficients of variation between our and published data

In budding yeast, low abundant proteins (as the ones we study here) have been reported to have coefficients of variation (CVs) in the order of 20 - 30 %[1,2], whereas our measured CVs for SAC proteins were as low as 8 % (Supplementary Table S1). For a comparison within the species, we plotted our data against a quantification of cytokinesis proteins in fission yeast[3], which used the same microscopy-based method that we used here. Those cytokinesis proteins that had low CVs of around 7 % were about a factor of 10 more abundant than SAC proteins, and those cytokinesis proteins with similar abundance as SAC proteins had higher CVs. This suggests that the cell-to-cell variability of some SAC proteins, including Mad1, Mad2 und Mad3, is remarkably low. Absolute protein abundances for the SAC proteins in the figure below are based on FCS measurements of GFP (Supplementary Table S2).

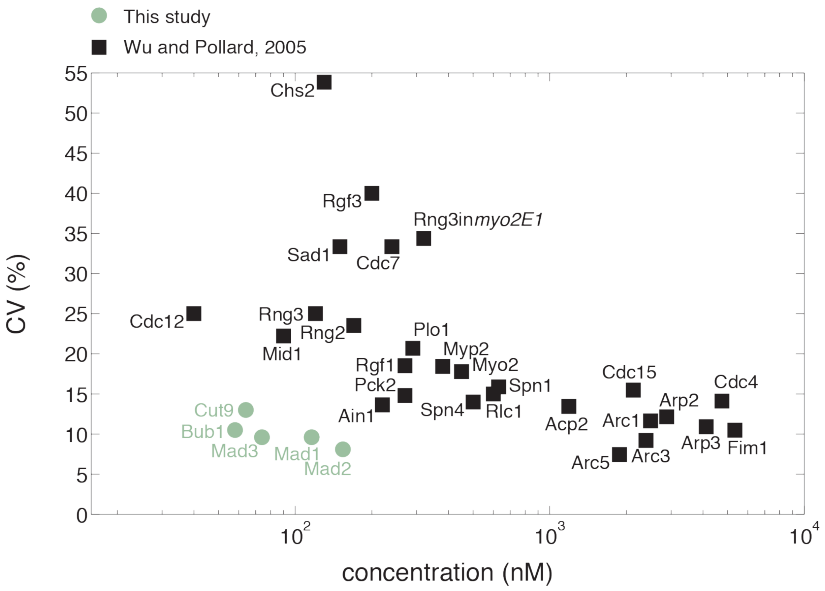

(A3) Stochastic model for the prediction of noise in protein concentration

To predict the minimal mRNA and protein abundance fluctuation of checkpoint proteins, we implemented a stochastic transcription-translation model[4,5], which takes both the stochasticity of biochemical reactions and cell cycle effects into account. The randomness of biochemical

reactions is modelled using the chemical master equation and simulated via Gillespie's simulation algorithm[6]. The reactions in a single cell are:

1. $G \rightarrow G + mRNA,\ w_1 = k_r[G]$ (transcription)
2. $mRNA \rightarrow \emptyset, w_2 = \gamma_r[mRNA]$ (mRNA degradation)
3. $mRNA \rightarrow mRNA + protein, w_3 = k_p[mRNA]$ (translation)
4. $protein \rightarrow \emptyset, w_4 = \gamma_p[protein]$ (protein degradation)

in which G denotes the gene, w_i denotes the reaction propensity of the i-th reaction and brackets denote molecule number of the respective chemical species. We assumed that rates are independent of cell volume. Furthermore, as DNA doubling in *S. pombe* takes place immediately after chromosome segregation[7], the number of gene copies remains constant. Hence, the common Gillespie algorithm can be employed. The transcription rate k_r, the mRNA degradation rate γ_r, the translation rate k_p and the degradation rate γ_p are chosen gene-specific.

The cell cycle introduces additional variability between cells, e.g. by differences in cell cycle length and stochastic partitioning of cell material at cell division. We assumed an inter-division time of 112.5 min (our measurement at 30 °C) and a CV of 10.8 %[8], with a linear increase in cell volume over time[9]. We assumed a log-normal distribution for the inter-division time. A growth rate of 0.632 fL/min (=(average volume increase per cell cycle)/(average cell cycle length) = 71.0 fL/112.5 min) is used, which yields an average cell size of 71.0 fL and 142.0 fL directly after and shortly before cell division, respectively. This is in agreement with our own measurements of the volume of dividing cells. The cell volume is assumed to partition symmetrically at division, yielding in our stochastic simulation cell size CVs of 6.26 % and 6.24 % at the beginning and the end of the cell cycle, respectively. Partitioning of the mRNAs and proteins into the daughter cells is assumed to be a stochastic process, resulting in a binomial distribution.

The simulation has been implemented in MATLAB exploiting fast simulation of the stochastic process using mex-files. Each simulation has been started with a single cell and ran for 40 times the mean inter-division time. This corresponds to roughly 40 generations, a time after which we observed equilibration of the stochastic process for all parameter values.

Simulation routines and parameter estimation routines are provided as supplementary MATLAB code.

(A4) Prediction of noise in protein concentration (Fig. 3c)

To determine protein noise, we required the kinetic parameters of the transcription-translation process. Experimental values for mRNA half-life have been reported[10,11]. We find that SAC proteins are stable for > 60 min (at least at less than 20 °C (Fig. S3)), similar to what others reported[12]. Since longer protein half-life reduces noise (Fig. 3d), we conservatively assumed a protein half-life of 240 min (Fig. 3c) or entirely stable protein (Fig. 3d) whose abundance is only

decreased by dilution in growing cells. The mRNA synthesis rate was estimated from our (Fig. 3b) or published[13] data on mRNA abundance. The protein synthesis rate was estimated from our measurement of protein abundance by FCS and WiFDeM (Fig. 1, Table S2).

As the stochastic process results in a stochastic objective function, we did not use classical gradient-based optimization routines but a simple, robust line search method. This method proved efficient and converged robustly to the global optimum. The optimization was considered converged when the measured values for mean mRNA number and protein concentration were within one standard error of the mean (SEM) interval ([mean-SEM, mean+SEM]) of the stochastic simulation. To ensure sufficient statistics we always averaged over more than 10,000 cells. The parameters were identifiable in all considered scenarios.

mRNA abundances and half-life from this and previous studies that were used in the simulations

	Mad1	Mad2	Mad3	Bub1	Bub3	Mph1	Apc5	Apc15	Cut9
mRNAs per cell[13]	1	0.84	1.4	2.6	0.44	1.9	0.73	2	0.94
mRNAs per cell (this study, Fig. 3b)*	5.2	6.0	4.6	9.2	4.2	8.5	4.2	3.0 13.4**	7.8
mRNA half-life (min)[10]	24.77	34.7	32.6	11.29	36.04	21.41	36.1	15.3	17.41
mRNA degradation rate (min^{-1})[11]	0.024	0.047	0.044	0.027	0.023	0.021	0.021	0.032	0.027

* All values are for the GFP mRNA moiety, i.e. the transcript coding for the quantified proteins.
** Apc15 mRNA counts in an asynchronous population show a bimodal distribution with the given means.

Predicted CV for protein concentration, with different assumptions for mRNA abundance and half-life

Predicted CV of protein conc. (%)	Mad1	Mad2	Mad3	Bub1	Bub3	Mph1	Apc5	Apc15	Cut9
mRNA number from Marguerat *et al.*[13] mRNA half-life from Amorim *et al.*[10]	46.3	56.3	43.0	22.2	76.6	44.6	60.6	n.d.	42.9
mRNA number determined in this study mRNA half-life from Amorim *et al.*[10]	20.4	21.0	23.8	12.2	25.8	15.6	25.6	n.d.	15.0
mRNA number determined in this study mRNA half-life from Sun *et al.*[11]	21.7	15.9	18.5	16.0	24.2	17.6	24.9	n.d.	17.1

All calculations assume a protein half-life of 240 min, and the cellular protein concentrations determined by FCS in this study (Supplementary Table S2). Estimates for Apc15 are not given, because the assumed mRNA half-life cannot reproduce the observed bimodal mRNA abundance distribution in the stochastic simulation.

As exemplified in the graphs for Mad2 below, the mean mRNA counts and the mean protein concentration agree well between measurement and simulation. However, the protein noise is overestimated by the simulation.

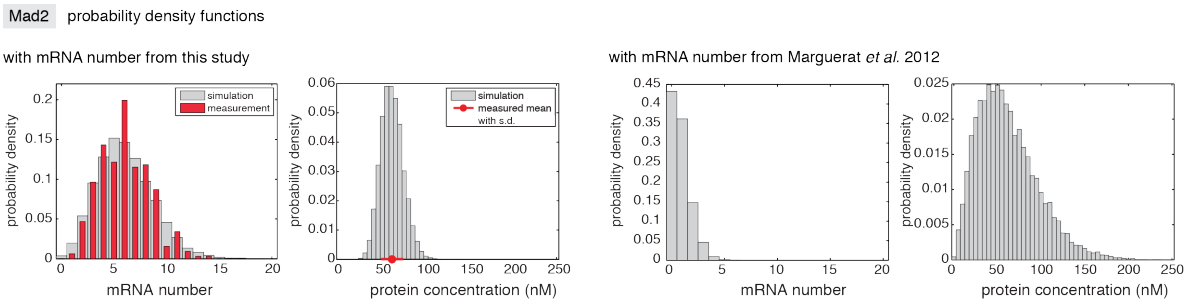

(A5) Comparison of mRNA number obtained in this and previous studies

Large scale studies in both budding and fission yeast have reported that many mRNAs are present in low copy number, often only one mRNA per cell on average[13,14]. Others have already noticed that it is difficult to explain the reliable operation of cell cycle regulatory networks with such low mRNA numbers[15]. For budding yeast, determination of mRNA numbers in single cells yielded slightly higher numbers per cell[16], as we observe it now for fission yeast.

(A6) Prediction of noise depending on protein half-life, protein synthesis rate or mRNA half-life (Fig. 3d)

To predict the changes in the CV of Mad2 protein concentration depending on different protein half-life (Fig. 3d, left), we assumed a mean protein concentration of 61 nM (Supplementary Table S2), a mean mRNA number of 6.03 (Fig. 3b) and an mRNA half-life of 34.7 min[10]. We tested protein half-lifes of 60 min, 240 min, and stable protein, whose abundance is only decreased by dilution in growing cells.

To predict the changes in the CV of Mad2 protein concentration depending on protein concentration (Fig. 3d, middle), we assumed stable protein, the same mean mRNA number and half-life as above, and varied the protein synthesis rate, so that protein concentrations between 15 and 150 nM were reached.

To predict the changes in the CV of Mad2 protein concentration depending on mRNA half-life (Fig. 3d, right), we assumed stable protein with a mean concentration of 61 nM (Supplementary Table S2) and the same mean mRNA number as above. The mRNA half-life was varied between 1 and 60 min.

(B) Computation of Mad1:Mad2 and free Mad2 abundance

The Mad1:Mad2 complex exists throughout interphase[17,18] and we find Mad1 and Mad2 abundance to be constant between interphase and mitosis (Fig. 1). Because Mad1-unbound Mad2 (free Mad2) enters the MCC in checkpoint-activated cells, it is possible that the equilibrium

shifts towards free Mad1 and Mad2 during a checkpoint-mediated mitotic delay. However, since the Mad1:Mad2 complex has repeatedly been shown to be very stable[17,19], we assume that this effect is negligible.

To assess the abundance of the different species in steady state as a function of the stability of the complex, we modelled complex formation

(5) Mad1 + Mad2 <-> Mad1:Mad2

assuming mass action kinetics. As a stability measure for the Mad1:Mad2 complex, we employ the dissociation constant (K_D),

(6) $K_D = \frac{[Mad1][Mad2]}{[Mad1{:}Mad2]}$.

The total protein abundances are assumed to be constant and we use the interphase protein concentrations estimated by FCS (Supplementary Table S2). Hence,

(7) $[Mad1_t] = [Mad1] + [Mad1{:}Mad2] = 39\ nM$

(8) $[Mad2_t] = [Mad2] + [Mad1{:}Mad2] = 61\ nM.$

By re-arranging (7) and (8) and substituting [Mad1] and [Mad2] in equation (6) we obtain

(9) $K_D = \frac{([Mad1_t]-[Mad1{:}Mad2])([Mad2_t]-[Mad1{:}Mad2])}{[Mad1{:}Mad2]}$.

This equation can be solved, which provides the steady-state concentrations of Mad1:Mad2 and Mad2,

(10) $[Mad1{:}Mad2] = \frac{([Mad1_t]+[\mathrm{Mad2}_t]+K_D)-\sqrt{([Mad1_t]+[\mathrm{Mad2}_t]+K_D)^2-4\times[Mad1_t][\mathrm{Mad2}_t]}}{2}$,

(11) $[Mad2] = \frac{([\mathrm{Mad2}_t]-[Mad1_t]-K_D)+\sqrt{([\mathrm{Mad2}_t]-[Mad1_t]-K_D)^2+4[\mathrm{Mad2}_t]K_D}}{2}$.

The abundances of Mad1:Mad2 and Mad2 as a function of dissociation constant are shown in Fig. 4c.

(B1) Plausible range of K_D values

Two pieces of evidence indicate that the K_D for Mad1:Mad2 complex formation is low:

(a) It has been shown that the complex is very stable[17,19,20] and

(b) it has been shown that almost all Mad1 is in complex with Mad2[12,17,21].

To fulfil these conditions, we conclude that the K_D should be 10 nM or lower (see Fig. 4c). Because we observe a reduction of free Mad2 when reducing Mad2 from 40 to 20 % (see Supplementary Fig. S6b), we consider a K_D of 4 nM a plausible, lower bound. We note that, given this low K_D, the expression of 300 % Mad1 should suppress free Mad2 to about one fourth the value in wild type (100 % Mad1) cells. The reduction that we observe is less pronounced (Supplementary Fig. S5e). The reason for the discrepancy is unclear at present, but we consider it possible that a factor like Tpr/Nup211[22] may become limiting in the Mad1 overexpression, so that Mad2 can be less efficiently captured and the soluble pool is less efficiently depleted.

(C) Multi-experiment mixture modelling to assess the distribution of mitosis times

When analysing mitosis time upon SAC activation in wild type or perturbed conditions, we observed strong inter-cell variability and in some situations a split into two subpopulations. For some cells both entry into and exit from mitosis were recorded, whereas for other cells only entry into mitosis was recorded within the observation interval (17 hours). Hence, for the latter cells, only a lower bound of the mitosis time is available. Furthermore cells are only recorded every five minutes. These two types of censoring complicate the statistical analysis. To statistically assess the number of populations and their distribution, we performed multi-experiment mixture modelling suited for censored data (Supplementary Fig. S8a).

To account for the observed inter cell variability we modelled the mitosis times as a stochastic process represented by the probability density function of a parametric distribution. The distribution of uncensored mitosis times was modelled by a log-normal distribution, $\log N(\mu,\sigma^2)$, whereas the distribution of censored times was modelled by a Johnson SU distribution $J(\gamma,\sigma,\lambda,\xi)$. After extensive testing, this combination of distributions was chosen because it resulted in the smallest values for the Bayesian information criterion (BIC). As exit from mitosis and censoring are mutually exclusive events, the realized mitosis and the censoring times depend on the convolution of the mitosis time distribution and censoring time distribution. By integrating these distributions over the inter-observation interval (in our experiments five minutes) we obtained the probability mass functions of the discrete time measurements of mitosis times and censoring times. These were used to derive the likelihood of the data given the model parameters using all perturbation conditions, which were used for fitting the parameters of the log-normal and Johnson SU distributions. Fitting was performed in MATLAB using a multi-start local optimization procedure.

(C1) Analysis for one or two populations

We implemented a mixture model in which every mitosis time distribution was a weighted mixture of up to two components, one for every potential subpopulation. The distribution of censoring times was assumed to be the same for all experimental conditions. To evaluate the different model alternatives and to determine the most parsimonious model still describing the data (evaluated using the BIC), we performed a backward selection. To analyse the distributions of mitosis times in rich medium (YEA), the data shown in Fig. 2b-d (excluding 10 % Mad2 and 20 % Mad2 for computational reasons) were used for the multi-experiment mixture modelling. The data for 200 % Slp1 were taken from Fig. 6e. To analyse the distributions of mitosis times in minimal medium (EMM), the data shown in Fig. 5a were used.

(C2) Comparison of the population A to wild type cells

We also tested the hypothesis that the subpopulation of cells arresting for longer (population A) behaves like the wild type population. In the corresponding mixture model, each dataset could comprise up to two mixture components: an independent, perturbation-caused subpopulation and one with the same parameter values as the wild type population. We considered this model to be favoured over the previous model (both subpopulations were unconstrained) when its BIC value was more than 6 points lower[23]. For rich medium, the hypothesis that population A behaves like the wild type population was favoured (BIC value 66 points lower); for minimal medium, the hypothesis was not supported (BIC value 6 points higher).

(D) Modelling of Slp1 synthesis and MCC formation using ODEs

(D1) Basic assumptions

We formulated a core model of MCC formation (M1; Fig. 7b) based on the following information:

(D1a) Slp1 is synthesized in mitosis[24].

(D1b) Slp1 is an unstable protein with a half-life in the range of 15 min (Supplementary Fig. S3h and Sczaniecka *et al.*[12]).

(D1c) Accumulation of Slp1 is not drastically different in cells with or without an active checkpoint (Supplementary Fig. S7 and data not shown). We therefore assume that the degradation rates of Slp1 and of Slp1 as part of the MCC are similar.

(D1d) Slp1 reaches approx. 20 nM (Fig. 6a and data not shown).

(D1e) Maximal Slp1 concentration is reached in about 120 min after start of mitosis at 16 °C (the temperature at which we assessed checkpoint activity) (Fig. 6a).

(D1f) Mad2 and Mad3 bind Slp1 as stoichiometric inhibitors[25-27].

(D1g) Mad2 and Mad3 are stable proteins (Supplementary Fig. S3h and Sczaniecka *et al.*[12]). Hence, synthesis and degradation can be neglected.

We extended this model by binding of Slp1 and the MCC to the APC/C (M2; Fig. 7d), with the following additional assumptions:

(D1h) APC/C is a stable complex[28]. Hence, synthesis and degradation can be neglected.

(D1i) APC/C is inhibited by binding to the MCC[25,29,30].

(D1j) APC/C is activated by Slp1[31,32].

(D1k) Slp1 is degraded as part of the MCC when bound to the APC/C[33-40].

(D1l) In analogy to M1, we assume APC/C-independent degradation of free Slp1, although the Slp1 ortholog Cdc20 is degraded in an APC/C-dependent manner[41].

(D2) Model M1 for MCC formation (Fig. 7b)

Using mass action kinetics, model M1 shown in Fig.7b is described by the following ordinary differential equations:

(12) $\frac{d[Slp1]}{dt} = k_{syn(Slp1)} - k_{\deg(Slp1)}[Slp1] - k_{on(MCC)}[Slp1][inh] + k_{off(MCC)}[MCC]$

(13) $\frac{d[inh]}{dt} = k_{\deg(Slp1)}[MCC] - k_{on(MCC)}[Slp1][inh] + k_{off(MCC)}[MCC]$

(14) $\frac{d[\mathrm{MCC}]}{dt} = k_{on(MCC)}[Slp1][inh] - k_{off(MCC)}[MCC] - k_{\deg(Slp1)}[MCC]$

in which [Slp1] denotes the concentration of Slp1, [inh] denotes the concentration of inhibitor and [MCC] denotes the concentration of the Slp1:inhibitor complex; $k_{syn(Slp1)}$ is the synthesis rate and $k_{deg(Slp1)}$ the degradation rate of Slp1; $k_{on(MCC)}$ and $k_{off(MCC)}$ are binding and dissociation rate of Slp1 and inhibitor. The degradation rate of Slp1 within the MCC is assumed to be equal to the degradation rate of free Slp1, $k_{deg(Slp1)}$ (see (D1c)). The inhibitor is analogous to Mad2/Mad3 that is competent to bind Slp1 ('active' Mad2/Mad3). The concentration of free Slp1, [Slp1], is considered the model output (Fig. 7b). It is unknown at which rate free Slp1 initiates anaphase. For simplicity, we assume that free Slp1 needs to reach a threshold for anaphase to occur. This is a common simplification[42-44], and is based on the assumption that very small amounts of free Slp1 are insufficient to initiate anaphase, because the system would otherwise not be robust. The threshold should be low, because even low levels of mammalian Cdc20 efficiently promote anaphase[45,46].

(D3) Model M2 for MCC formation with APC/C binding (Fig. 7d)

Using mass action kinetics, the model shown in Fig.7d is described by the following ordinary differential equations:

(15) $\frac{d[APC{:}MCC]}{dt} = \mathrm{v2} - \mathrm{v5}$

(16) $\frac{d[APC{:}Slp1]}{dt} = \mathrm{v1}$

(17) $\frac{d[MCC]}{dt} = -\mathrm{v2} + \mathrm{v3}$

(18) $\frac{d[Slp1]}{dt} = -\mathrm{v1} - \mathrm{v3} + \mathrm{v4} - \mathrm{v6}$

(19) $\frac{d[APC]}{dt} = -\mathrm{v1} - \mathrm{v2} + \mathrm{v5}$

(20) $\frac{d[inh]}{dt} = \mathrm{v5} - \mathrm{v3}$

with

(21) $\mathrm{v1} = k_{\mathrm{on}(APC:Slp1)}[APC][Slp1] - k_{\mathrm{off}(APC:Slp1)}[APC{:}Slp1]$

(22) $v2 = k_{\mathrm{on}(APC:MCC)}[APC][MCC] - k_{\mathrm{off}(APC:MCC)}[APC:MCC]$

(23) $v3 = k_{\mathrm{on}(MCC)}[inh][Slp1] - k_{\mathrm{off}(MCC)}[MCC]$

(24) $v4 = k_{\mathrm{syn(Slp1)}}$

(25) $v5 = k_{\mathrm{deg}(Slp1)}[APC:MCC]$

(26) $v6 = k_{\mathrm{deg}(Slp1)}[Slp1]$

in which [APC:MCC] denotes the concentration of the inhibited APC/C:MCC complex, [APC:Slp1] denotes the concentration of the active APC/C:Slp1 complex, [MCC] denotes the concentration of the Slp1:inhibitor complex MCC, [Slp1] denotes the concentration of free Slp1, [APC] denotes the concentration of APC/C, and [inh] denotes the concentration of the inhibitor. The inhibitor is analogous to Mad2/Mad3 that is competent to bind Slp1 ('active' Mad2/Mad3). The model parameters are the Slp1 synthesis and degradation rates, $k_{syn(Slp1)}$ and $k_{deg(Slp1)}$, and the binding and dissociation rates of different complexes, $k_{on(X)}$ and $k_{off(X)}$. The model fulfils the conservation relations

(27) $[APC_T] = [APC] + [APC:Slp1] + [APC:MCC]$

(28) $[inh_T] = [inh] + [MCC] + [APC:MCC]$

in which $[APC_T]$ denotes the total concentration of APC/C and $[inh_T]$ denotes the total concentration of inhibitor. The concentration of APC/C:Slp1, [APC:Slp1], is considered the model output (Fig. 7d). Anaphase is initiated when APC/C:Slp1 concentration exceeds a certain threshold.

The model includes a double negative feedback loop consisting of inhibition of the APC/C by binding to the MCC and disassembly (and therefore inhibition) of the MCC through the APC/C.

(D4) Parameter estimation for population model from phenotype data

As the models for the signalling pathway should reproduce cell-to-cell variability, the parameter estimation is highly non-trivial. A moment equation based method has been proposed[47], but the required moment closure introduces large errors for the system at hand, which renders it impractical. Furthermore, the measurement data are only phenotypic, namely whether the SAC is functional or dysfunctional, and hence very different from the common concentration measurements.

We employ maximum likelihood estimation to determine the optimal model parameters. We used the number of cells with active and inactive SAC under checkpoint-activating conditions from WT, 30 % Mad1, 65 % Mad2 and 30 % Mad3 strains with both 100 % and 200 % Slp1 and estimated the kinetic parameters (M1: k_{on}, k_{off}, $k_{deg(Slp1)}$; M2: $k_{on(APC:Slp1)}$, $k_{off(APC:Slp1)}$, $k_{on(APC:MCC)}$, $k_{off(APC:MCC)}$, $k_{on(MCC)}$, $k_{off(MCC)}$, $k_{deg(Slp1)}$) and the distribution parameters ($\mu_{k,syn(Slp1)}$, $\sigma_{k,syn(Slp1)}$, $\mu_{inhT,WT}$, $\sigma_{inhT,WT}$, $\mu_{inhT,30\%Mad1}$, $\sigma_{inhT,30\%Mad1}$, $\mu_{inhT,65\%Mad2}$, $\sigma_{inhT,65\%Mad2}$, $\mu_{inhT,30\%Mad3}$, $\sigma_{inhT,30\%Mad3}$).

For each strain:

n_A = number of cells in population A (functional SAC; output below threshold), and

n_B = number of cells in population B (dysfunctional SAC; output above threshold).

The probability of observing n_A and n_B follows a binomial distribution

$$p(n_A, n_A|\theta) = \frac{(n_A + n_B)!}{n_A!\, n_B!} p_A^{n_A}(\theta) p_B^{n_B}(\theta)$$

in which $p_A(\theta)$ is the probability that for a given parameterization θ the concentration of the active species (for M1: Slp1; M2: APC/C:Slp1) is below the threshold, while $p_B(\theta)$ is the probability that for a given parameterization the concentration exceeds the threshold, with $p_A(\theta) + p_B(\theta) = 1$. The binomial distribution provides the likelihood for each individual experiment. The overall likelihood is obtained by multiplying the likelihoods of the individual experiments. An independent optimization of the individual likelihoods is not possible, as the different experiments share the kinetic parameters, the threshold and the distribution parameters of the Slp1 synthesis rate.

The probabilities $p_A(\theta)$ and $p_B(\theta)$ for each strain can in principle be computed by simulating the model for different values of Slp1 synthesis rates and inhibitor concentrations, drawn from the corresponding distribution defined by $\mu_{k,syn(Slp1)}$, $\sigma_{k,syn(Slp1)}$, μ_{inhT} and σ_{inhT}. By evaluating for each simulated cell whether the threshold is reached or not, one obtains a Monte Carlo estimate of the probabilities $p_A(\theta)$ and $p_B(\theta)$. However, the number of simulations required to achieve a high precision is large and the resulting objective function would exhibit stochastic fluctuations. This renders application of efficient gradient-based methods impractical and the optimization of the process computationally intractable.

To estimate the parameters of the population model we developed a sigma-point based estimation method. Our method is based on the decomposition of the overall parameter distribution into smaller parts using mixtures of log-normal distributions. For the individual log-normal parameter distribution we approximate the mean and the variance of the systems states, e.g., the Slp1 concentration, using the sigma-point method[48]. Based on the means and variances provided by the sigma-point method, we construct an approximating normal distribution for each mixture component. By computing the weighted sum of the mixture components we obtain an approximation of the probability density of the state for the full parameter distribution. This approximation of the state density can directly be used to approximate the probabilities $p_A(\theta)$ and $p_B(\theta)$. While a high-quality estimate of $p_A(\theta)$ and $p_B(\theta)$ still requires the decomposition into many small distributions, which all have to be propagated forward by simulating the system, this method is still orders of magnitude faster than classical Monte Carlo integration. Furthermore, as the sigma-points are deterministic, we can derive the gradient of the objective function, resulting in a further acceleration of the optimization and in better convergence properties.

In addition to the computational speed-up provided by our sigma-point based method, we wanted

to ensure robustness of the model predictions with respect to the chosen threshold. To achieve this, we evaluated the objective function not only for the current threshold, but also for thresholds smaller and larger by a factor of 3.162. The likelihood functions obtained for these three thresholds are multiplied and the third root is computed. The resulting values can be interpreted as average likelihood function of the interval [1/3.162, 3.162] x threshold. This interval spans one order of magnitude. By using this average in the optimization, we search for parameter combinations for which $p_A(\theta)$ and $p_B(\theta)$ are not sensitive with respect to the threshold.

Using the likelihood function approximation based on sigma-points, for which we ensured a good approximation quality, we optimized M1 and M2. We employed multi-start local optimization using the MATLAB optimization routine fmincon.

Further details regarding the sigma point method and the implementation of the parameter estimation can be found in the supplementary MATLAB code and its documentations. Beyond the implementation of the estimation and the analysis of model 1 and model 2, we also provide illustrations of the sigma point approximation.

(D5) Parameter estimation for M1

The synthesis rate of Slp1 ($k_{syn(Slp1)}$) as well as [inh_T] in the different strains are assumed to be log-normally distributed with parameters μ and σ. This yields in total 14 parameters that we constrained to the following ranges:

- CV of $k_{syn(Slp1)}$ between 0.05 and 0.5
- lower bound of mean of $k_{syn(Slp1)}$: 0.17 mol/min; calculated from 20 nM Slp1 after 120 min (see (D1d) and (D1e)), assuming no degradation
- upper bound of mean of $k_{syn(Slp1)}$: 1.98 mol/min calculated from 20 nM Slp1 after 120 min, assuming the upper bound for the degradation rate
- degradation rates should result in a Slp1 half-life between 7 and 40 min (see (D1b))
- 1e-5 $nM^{-1}min^{-1} < k_{on} <$ 1e5 $nM^{-1}min^{-1}$
- 1e-5 nM < $K_d = k_{off}/k_{on}$ < 1e5 nM
- 1 nM < [inh_T] < 50 nM (Supplementary Table S2) with corresponding CV between 0.05 and 0.5
- Slp1 threshold for anaphase onset between 0.1 and 20 nM

The dissociation constant K_d and the CV and mean of the total inhibitor concentration [inh_T] are lumped parameters of several biological parameters that are not included in this simple model. Hence, these model parameters do not have an exact biological equivalent.

Parameter boundaries for estimation:

	$\sigma_{k,syn(Slp1)}$	$\mu_{k,syn(Slp1)}$	σ_{inhT}	μ_{inhT}	$k_{deg(Slp1)}$
min	0.04997	-1.793	0.04997	-0.1116	0.01733 min^{-1}
max	0.47238	0.5717	0.47238	3.9108	0.09902 min^{-1}

The optimization using the sigma-point method (D4) yields the following maximum likelihood estimates:

$\sigma_{k,syn(Slp1)}$	$\mu_{k,syn(Slp1)}$	$k_{deg(Slp1)}$	K_d	threshold
0.3096	-0.4077	0.0353 min^{-1}	6.6156 10^{-5} nM	0.1034 nM

$[inh_T]$	wild type	30 % Mad1	65 % Mad2	30 % Mad3
μ	3.8734	3.5366	2.9306	3.0791
σ	0.0507	0.0572	0.4719	0.2167

Based on these parameters the mean of the total inhibitor concentrations and of the synthesis rate $k_{syn(Slp1)}$ can be calculated together with the respective CVs.

	wild type $[inh_T]$	30 % Mad1 $[inh_T]$	65 % Mad2 $[inh_T]$	30 % Mad3 $[inh_T]$	$k_{syn(Slp1)}$
Mean	48.1675 nM	34.4063 nM	20.9464 nM	22.2551 nM	0.6978 nM min^{-1}
CV	0.0507	0.0573	0.4995	0.2192	0.3172

To assess how well the model describes the data parameterized with the maximum likelihood estimate found using our sigma-point method, we computed the probability density to measure the fraction of cells in population A and B for a particular strain. These probability densities can be computed from the binomial distribution (underlying the likelihood function) using the probabilities $p_A(\theta)$ and $p_B(\theta)$ computed by the model and the total number of measured cells. Using the probability densities, we evaluate the 98 % confidence interval of the measurement assuming that our model is correct. These 98 % confidence intervals are depicted below (light resp. dark grey area) for a range of threshold values around the best fit for each experimental condition. Bold lines indicate the resulting fraction of cells in population B when assuming the corresponding threshold.

We find that for the nominal threshold (x-axis value = 1) the experimentally observed fractions are inside the 98 % confidence intervals for all strains. By varying the threshold, we find that the model fit is not sensitive to the choice of the threshold. We conclude that M1 can describe the main characteristics of the process while satisfying our requirement to be robust with respect to the threshold for anaphase activation.

model analysis M1

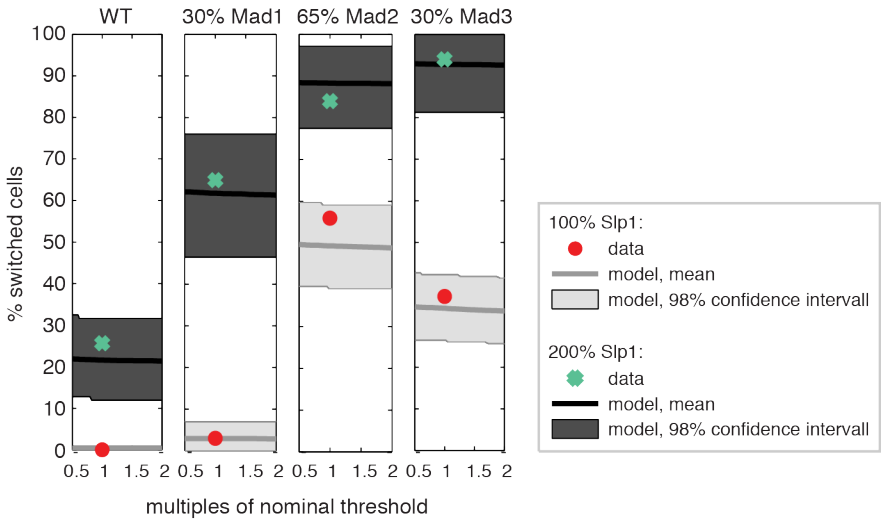

A representative sample of single-cell trajectories for model M1 is shown below and in Fig. 7c. We simulated 100 cells by sampling inhibitor concentration and Slp1 synthesis rate for each cell from the estimated distribution for each strain. In the large plot the time-dependent concentration of Slp1 in individual cells is shown. The frequency distribution is plotted on the right. The small plot shows the trajectories using a nonlinear y-axis, which is roughly linear for [Slp1] < 0.01 and becomes progressively logarithmic (Y = log([Slp1]+0.01)). The scale is related to the logicle scale used for the visualization of flow cytometry data[49].

The trajectory plots reveal that the Slp1 response is highly heterogeneous within the simulated populations. Depending on the strain, many cells keep very small values of [Slp1] (indicating a functional SAC, population A), while others reach high [Slp1] levels above the threshold (indicating a non-functional SAC, population B).

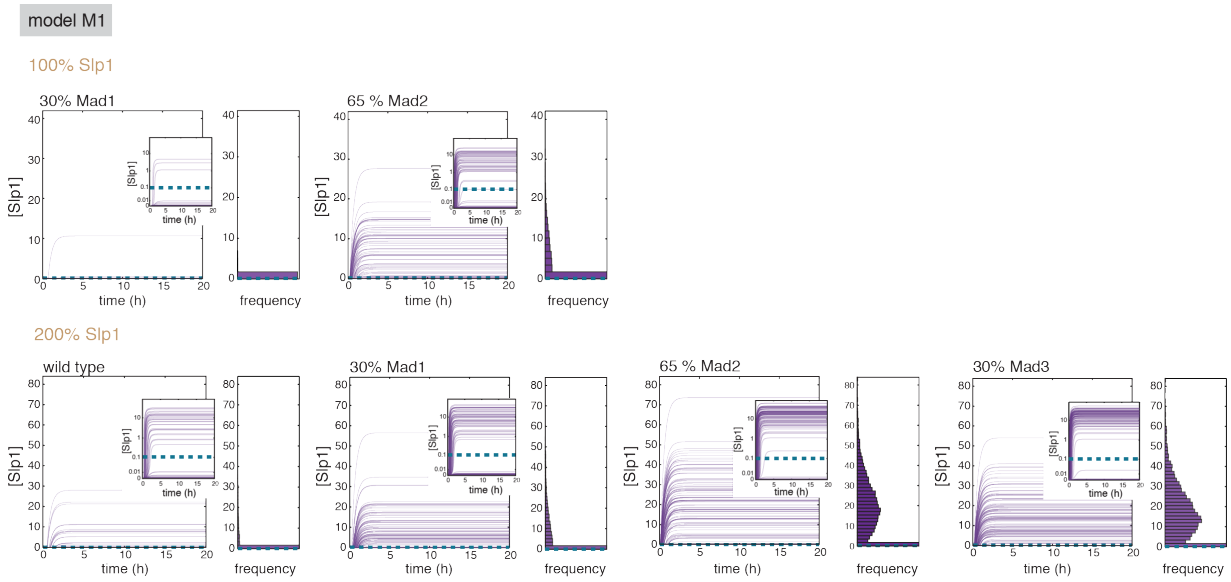

(D6) Bayesian uncertainty analysis for M1 using steady state assumption

Even with our sigma-point based method the parameter estimation for the time-dependent system is computationally intensive and a rigorous uncertainty analysis is currently impracticable. However, the estimation results in (D5) suggest that the system almost reached its steady state after 20 hours. We therefore decided to consider for the uncertainty analysis the steady state of M1, for which an analytical solution can be derived (see below). Using the analytical solution for the steady state of a single cell and the distribution of inhibitor and Slp1 synthesis rates, we can efficiently compute the probabilities $p_A(\theta)$ and $p_B(\theta)$. The efficient computation of $p_A(\theta)$ and $p_B(\theta)$ enables the fast evaluation of the likelihood function and thus a rigorous uncertainty analysis.

To study the uncertainty of the kinetic and distribution parameters of M1, we employed a Bayesian approach with a flat prior constraint to the parameter set specified above. To explore the parameter set we employed adaptive Markov chain Monte Carlo (adaptive MCMC) sampling. Using the MATLAB Toolbox DRAM (http://helios.fmi.fi/~lainema/mcmc/) we generated a converged MCMC sample and evaluated its statistics.

The MCMC sampling of the steady state version of M1 found the maximum a posteriori parameter estimate (the optimal parameters):

$\sigma_{k,syn(Slp1)}$	$\mu_{k,syn(Slp1)}$	$k_{deg(Slp1)}$	$K_D = k_{off} / k_{on}$	threshold
0.2908	0.3175	0.0716 min^{-1}	0.1066 nM	1.1788 nM

$[inh_T]$	wild type	30 % Mad1	65 % Mad2	30 % Mad3
μ	3.8945	3.5694	2.9338	3.1228
σ	0.0733	0.1058	0.4710	0.2882

This estimate is for many parameters surprisingly close to the estimate for the dynamic version of M1 and the fits of the observed data are almost indistinguishable. This substantiated our simplification and we analysed the parameter uncertainties based upon the MCMC sample.

The key finding of this analysis is that the variability in the inhibitor concentration in WT cells has to be small to explain the observed fraction of population A and B. Furthermore, the variability in the Slp1 synthesis rate is high compared to the variability of inhibitor concentrations in WT cells. The marginal for these two properties is illustrated in Fig. 8b.

(D7) Analysis of steady state ultrasensitivity of M1

Our analysis in (D5) revealed that the concentration of free Slp1 predicted by M1 is insensitive with respect to the threshold but yields two populations. To understand the underlying mechanism we analysed the steady state properties of M1 using methods developed by Buchler and Louis[50]. In particular, we analysed the steady state, the steady state fluxes and the point where the system changes its buffering behaviour (the equivalence point).

The *in vivo* dissociation constant[50] is

(29) $K_{\mathrm{D}} = \frac{k_{\mathrm{off}} + k_{\deg(Slp1)}}{k_{\mathrm{on}}}$.

In steady state, the fluxes are balanced,

(30) $k_{syn(Slp1)} = k_{\deg(Slp1)}[Slp1] + k_{\deg(Slp1)}[MCC]$.

As Mad2 and Mad3 are stable (see (D1g)), the overall inhibitor abundance is constant

(31) $[inh_T] = const. = [inh] + [MCC]$.

Employing these properties, we can determine an analytical expression for the steady state,

(32) $$k_{\deg\,(Slp1)}[Slp1] = \frac{k_{syn(Slp1)} - [inh_T]k_{\deg(Slp1)} - k_{\deg\,(Slp1)}K_D}{2} + \sqrt{\left(\frac{k_{syn(Slp1)} - [inh_T]k_{\deg(Slp1)} - k_{\deg\,(Slp1)}K_D}{2}\right)^2 + k_{syn(Slp1)}k_{\deg\,(Slp1)}K_D}$$

(33) $$k_{\deg\,(Slp1)}[inh] = \frac{-k_{syn(Slp1)} + [inh_T]k_{\deg(Slp1)} - k_{\deg(Slp1)}K_D}{2} + \sqrt{\left(\frac{-k_{syn(Slp1)} + [inh_T]k_{\deg(Slp1)} - k_{\deg(Slp1)}K_D}{2}\right)^2 + [inh_T]k_{\deg(Slp1)}k_{\deg(Slp1)}K_D}$$

(34) $$k_{\deg\,(Slp1)}[MCC] = \frac{k_{syn(Slp1)} + [inh_T]k_{\deg(Slp1)} + k_{\deg\,(Slp1)}K_D}{2} - \sqrt{\left(\frac{k_{syn(Slp1)} + [inh_T]k_{\deg(Slp1)} + k_{\deg\,(Slp1)}K_D}{2}\right)^2 - k_{syn(Slp1)}[inh_T]k_{\deg(Slp1)}}.$$

The comparison of these equations to equation (S4) from Buchler and Louis[50] yields the following relations:

(S4)	A	B	AB
our model	$k_{deg(Slp1)}$[Slp1]	$k_{deg(Slp1)}$[inh]	$k_{deg(Slp1)}$[MCC]

(S4)	A_T	B_T	K_D
our model	$k_{syn(Slp1)}$	$k_{deg(Slp1)}[inh_T]$	$k_{deg(Slp1)}K_D$

Thus, in analogy to Buchler and Louis[50], the system reaches its equivalence point when

(35) $k_{\mathrm{syn}\,(Slp1)} = k_{\mathrm{deg}\,(Slp1)}[inh_T]$

Slp1 synthesis rate $k_{syn(Slp1)}$, MCC degradation rate $k_{deg(Slp1)}$, and the amount of Slp1-inhibition competent Mad2/Mad3 ($[inh_T]$) define the regimes in which the checkpoint operates. Within the transition zone (regime II), the steady state of free Slp1 has high sensitivity with respect to changes in inhibitor concentration, i.e. it shows ultrasensitivity towards differences in the total amount of inhibitor. This sensitivity reaches its maximum at the so called equivalence point, which is the smallest total amount of inhibitor sufficient to roughly balance Slp1 synthesis given a certain rate for the degradation of Slp1 from the MCC. In Regime I, which is characterised by an excess of the inhibitor, changes are buffered and do not strongly influence the steady state. In Regime III, which is characterised by saturation of the inhibitor and an excess of free Slp1, changes in Slp1 synthesis rate or $[inh_T]$ result in equal fold changes of the steady state of Slp1.

Regime I **(buffering)**	**Regime II** **(transition zone)**	**Regime III** **(saturation)**
$k_{syn(Slp1)} \ll k_{deg(Slp1)}\,[inh_T]$	$k_{syn(Slp1)} \approx k_{deg(Slp1)}\,[inh_T]$	$k_{syn(Slp1)} \gg k_{deg(Slp1)}\,[inh_T]$

(D8) Parameter estimation for M2

To distinguish between qualitatively different outcomes (functional SAC vs. dysfunctional SAC) for different cells we assume that APC/C:Slp1 needs to reach a threshold for anaphase to occur.
The synthesis rate of Slp1($k_{syn(Slp1)}$) as well as $[inh_T]$ in the different strains are assumed to be log-normally distributed with parameters μ and σ. This yields in total 19 parameters that we constrained to the following ranges:

- CV of $k_{syn(Slp1)}$ between 0.05 and 0.5
- lower bound of mean of $k_{syn(Slp1)}$: 0.17 mol/min; calculated from 20 nM Slp1 after 120 min (see (D1d) and (D1e)), assuming no degradation
- upper bound of mean of $k_{syn(Slp1)}$: 1.98 mol/min calculated via 20 nM Slp1 after 120 min assuming maximum degradation rate
- degradation rates should result in a Slp1 half-life between 7 and 40 min (see (D1b))

- 1e-5 $nM^{-1}min^{-1} < k_{on} <$ 1e5 $nM^{-1}min^{-1}$
- 1e-5 nM $< K_d = k_{off}/k_{on} <$ 1e5 nM
- 1 nM $< [inh_T] <$ 50 nM (Supplementary Table S2) with corresponding CV between 0.05 and 0.5
- APC/C:Slp1 threshold for anaphase onset between 0.1 and 20 nM

Parameter boundaries for estimation:

	$\sigma_{k\_syn(Slp1)}$	$\mu_{k\_syn(Slp1)}$	σ_{inhT}	μ_{inhT}	$k_{deg(Slp1)}$
min	0.04997	-1.793	0.04997	-0.1116	0.01733 min^{-1}
max	0.47238	0.5717	0.47238	3.9108	0.09902 min^{-1}

Optimization using the sigma-point method (D4) yields the following maximum likelihood estimate for the model parameters:

$\sigma_{k,syn(Slp1)}$	$\mu_{k,syn(Slp1)}$	$k_{deg(Slp1)}$	$[APC_T]$	threshold
0.3446	-1.0654	0.0616 min^{-1}	19.2690 nM	1.0147 nM

$k_{on(Slp1:inh)}$	$K_{d(Slp1:inh)}$	$k_{on(APC:MCC)}$	$K_{d(APC:MCC)}$	$k_{on(APC:Slp1)}$	$K_{d(APC:Slp1)}$
1.4225e03 nM^{-1} min^{-1}	22.7780e-04 nM	1.9263 nM^{-1} min^{-1}	2.5582 nM	4.0955 nM^{-1} min^{-1}	0.2560 nM

$[inh_T]$	wild type	30 % Mad1	65 % Mad2	30 % Mad3
μ	3.2600	2.6577	1.9059	2.1000
σ	0.0922	0.0845	0.3854	0.2087

Based on these parameters the mean of the total inhibitor concentrations and of the synthesis rate $k_{syn(Slp1)}$ can be calculated as well as the respective CVs.

	wild type $[inh_T]$	30 % Mad1 $[inh_T]$	65 % Mad2 $[inh_T]$	30 % Mad3 $[inh_T]$	$k_{syn(Slp1)}$
Mean	26.1606 nM	14.3145 nM	7.2440 nM	8.3459 nM	0.3684 nM min^{-1}
CV	0.0924	0.0847	0.4002	0.2110	0.3551

For the maximum likelihood estimate we assess, as before, the fit of M2. The corresponding illustration is depicted below. As for M1, we find that M2 can describe the main characteristics of the process while satisfying our requirement to be robust with respect to the threshold for anaphase activation.

model analysis M2

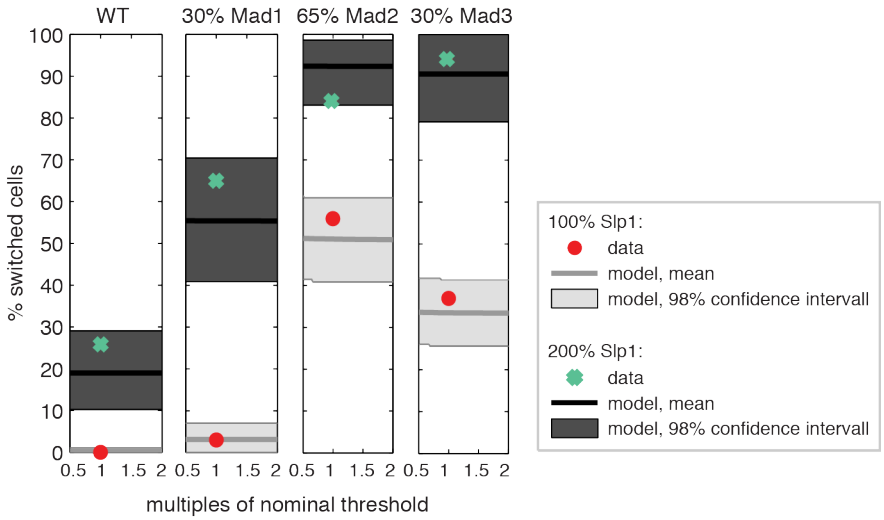

While the fits of the experimentally observed fractions of population A and B are similar for M1 and M2, the dynamics of the underlying pathways are quite different. This becomes apparent from exemplary trajectories of model M2 simulated with the maximum likelihood estimate. While M1 showed a long tail towards high concentrations of the active species ([Slp1]), which is a result of ultrasensitivity, M2 shows a bimodal distribution of the concentration of the active species ([APC:Slp1]). Individual cells either have [APC:Slp1] close to zero or have high [APC:Slp1] as depicted in the plot below and in Fig. 8e.

model M2

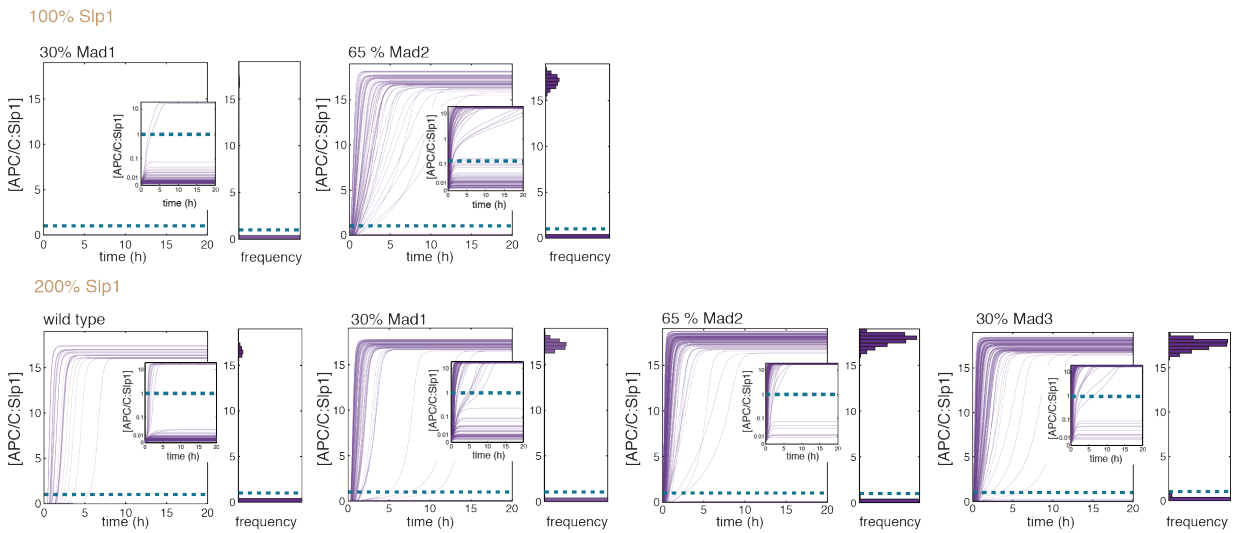

To analyse whether inhibitor concentration or Slp1 synthesis rate in populations A and B could be distinguished experimentally, we evaluated the parameter distributions corresponding to the individual populations. For [APC:Slp1] trajectories that exceeded or that remained below the threshold, we collected the inhibitor concentrations and the Slp1 synthesis rates and computed the corresponding frequency distributions. Shown in Fig. 8c are the histograms for a strain with 30 % Mad3 and 100 % Slp1. We find that the distributions of inhibitor concentrations differ only slightly between population A and B for most strains. The Slp1 synthesis rate allows for a better discrimination but this rate cannot be measured experimentally.

(D9) Bifurcation analysis for model M2

To understand the cause of the bimodality and the resulting robustness to threshold alterations we performed a bifurcation analysis using the maximum likelihood parameters and the estimated mean inhibitor concentration in WT cells. The resulting bifurcation diagram is shown below and revealed that: (1) For low $k_{syn(Slp1)}$, model M2 possesses a globally asymptotic stable steady state with low [APC:Slp1], corresponding to a functional SAC. (2) For high $k_{syn(Slp1)}$, there exists a globally asymptotic stable steady state with high [APC:Slp1] above the threshold, corresponding to a dysfunctional checkpoint. (3) For intermediate values of $k_{syn(Slp1)}$, M2 possesses three steady states of which two are stable and correspond to a functional and a dysfunctional SAC, respectively. This multi-stability allows for a threshold behaviour with respect to $k_{syn(Slp1)}$, meaning that below a certain Slp1 synthesis the SAC is functional, while above the threshold the SAC is deficient. For the maximum likelihood estimates of the parameters and the mean wild type inhibitor concentration, the critical Slp1 synthesis rate is 0.943 nM/min. Furthermore, the multi-stability and the switch-like change allow for robustness with respect to the threshold as lower and upper steady state are separated.

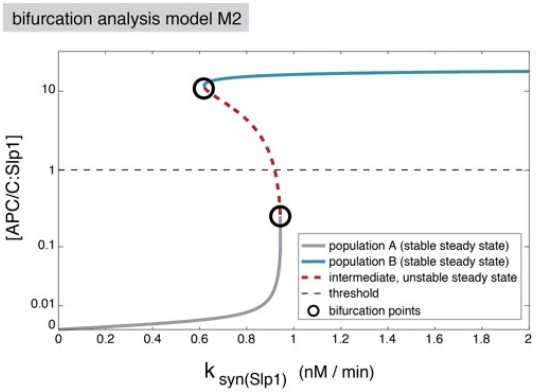

(E) References

1. Newman, J.R. *et al.* Single-cell proteomic analysis of S. cerevisiae reveals the architecture of biological noise. *Nature* **441**, 840-846 (2006).
2. Bar-Even, A. *et al.* Noise in protein expression scales with natural protein abundance. *Nature genetics* **38**, 636-643 (2006).
3. Wu, J.Q. & Pollard, T.D. Counting cytokinesis proteins globally and locally in fission yeast. *Science* **310**, 310-314 (2005).
4. Swain, P.S., Elowitz, M.B. & Siggia, E.D. Intrinsic and extrinsic contributions to stochasticity in gene expression. *Proc Natl Acad Sci U S A* **99**, 12795-12800 (2002).
5. Huh, D. & Paulsson, J. Non-genetic heterogeneity from stochastic partitioning at cell division. *Nature genetics* **43**, 95-100 (2011).
6. Gillespie, D.T. Exact Stochastic Simulation of Coupled Chemical-Reactions. *J Phys Chem-Us* **81**, 2340-2361 (1977).
7. Forsburg, S.L. & Nurse, P. Cell cycle regulation in the yeasts Saccharomyces cerevisiae and Schizosaccharomyces pombe. *Annual review of cell biology* **7**, 227-256 (1991).
8. Sveiczer, A., Novak, B. & Mitchison, J.M. The size control of fission yeast revisited. *J Cell Sci* **109 (Pt 12)**, 2947-2957 (1996).
9. Neumann, F.R. & Nurse, P. Nuclear size control in fission yeast. *J Cell Biol* **179**, 593-600 (2007).
10. Amorim, M.J., Cotobal, C., Duncan, C. & Mata, J. Global coordination of transcriptional control and mRNA decay during cellular differentiation. *Molecular systems biology* **6**, 380 (2010).
11. Sun, M. *et al.* Comparative dynamic transcriptome analysis (cDTA) reveals mutual feedback between mRNA synthesis and degradation. *Genome research* **22**, 1350-1359 (2012).
12. Sczaniecka, M. *et al.* The spindle checkpoint functions of Mad3 and Mad2 depend on a Mad3 KEN box-mediated interaction with Cdc20-anaphase-promoting complex (APC/C). *The Journal of biological chemistry* **283**, 23039-23047 (2008).
13. Marguerat, S. *et al.* Quantitative analysis of fission yeast transcriptomes and proteomes in proliferating and quiescent cells. *Cell* **151**, 671-683 (2012).
14. Holstege, F.C. *et al.* Dissecting the regulatory circuitry of a eukaryotic genome. *Cell* **95**, 717-728 (1998).
15. Kar, S., Baumann, W.T., Paul, M.R. & Tyson, J.J. Exploring the roles of noise in the eukaryotic cell cycle. *Proc Natl Acad Sci U S A* **106**, 6471-6476 (2009).
16. Zenklusen, D., Larson, D.R. & Singer, R.H. Single-RNA counting reveals alternative modes of gene expression in yeast. *Nature structural & molecular biology* **15**, 1263-1271 (2008).
17. Chen, R.H., Brady, D.M., Smith, D., Murray, A.W. & Hardwick, K.G. The spindle checkpoint of budding yeast depends on a tight complex between the Mad1 and Mad2 proteins. *Mol Biol Cell* **10**, 2607-2618 (1999).
18. Ikui, A.E., Furuya, K., Yanagida, M. & Matsumoto, T. Control of localization of a spindle checkpoint protein, Mad2, in fission yeast. *J Cell Sci* **115**, 1603-1610 (2002).
19. Sironi, L. *et al.* Mad2 binding to Mad1 and Cdc20, rather than oligomerization, is required for the spindle checkpoint. *Embo J* **20**, 6371-6382 (2001).
20. Vink, M. *et al.* In vitro FRAP identifies the minimal requirements for Mad2 kinetochore dynamics. *Curr Biol* **16**, 755-766 (2006).
21. Shah, J.V. *et al.* Dynamics of centromere and kinetochore proteins; implications for checkpoint signaling and silencing. *Curr Biol* **14**, 942-952 (2004).
22. Lee, S.H., Sterling, H., Burlingame, A. & McCormick, F. Tpr directly binds to Mad1 and Mad2 and is important for the Mad1-Mad2-mediated mitotic spindle checkpoint. *Genes Dev* **22**, 2926-2931 (2008).

23. Kass, R.E. & Raftery, A.E. Bayes Factors. *J Am Stat Assoc* **90**, 773-795 (1995).
24. Yamada, H.Y., Matsumoto, S. & Matsumoto, T. High dosage expression of a zinc finger protein, Grt1, suppresses a mutant of fission yeast slp1(+), a homolog of CDC20/p55CDC/Fizzy. *J Cell Sci* **113 (Pt 22)**, 3989-3999 (2000).
25. Fang, G. Checkpoint protein BubR1 acts synergistically with Mad2 to inhibit anaphase-promoting complex. *Mol Biol Cell* **13**, 755-766 (2002).
26. Burton, J.L. & Solomon, M.J. Mad3p, a pseudosubstrate inhibitor of APCCdc20 in the spindle assembly checkpoint. *Gene Dev* **21**, 655-667 (2007).
27. Chao, W.C., Kulkarni, K., Zhang, Z., Kong, E.H. & Barford, D. Structure of the mitotic checkpoint complex. *Nature* **484**, 208-213 (2012).
28. Schwanhausser, B. *et al.* Global quantification of mammalian gene expression control. *Nature* **473**, 337-342 (2011).
29. Herzog, F. *et al.* Structure of the anaphase-promoting complex/cyclosome interacting with a mitotic checkpoint complex. *Science* **323**, 1477-1481 (2009).
30. Sudakin, V., Chan, G.K. & Yen, T.J. Checkpoint inhibition of the APC/C in HeLa cells is mediated by a complex of BUBR1, BUB3, CDC20, and MAD2. *J Cell Biol* **154**, 925-936 (2001).
31. Fang, G., Yu, H. & Kirschner, M.W. Direct binding of CDC20 protein family members activates the anaphase-promoting complex in mitosis and G1. *Molecular cell* **2**, 163-171 (1998).
32. Kramer, E.R., Gieffers, C., Holzl, G., Hengstschlager, M. & Peters, J.M. Activation of the human anaphase-promoting complex by proteins of the CDC20/Fizzy family. *Curr Biol* **8**, 1207-1210 (1998).
33. Pan, J. & Chen, R.H. Spindle checkpoint regulates Cdc20p stability in Saccharomyces cerevisiae. *Genes Dev* **18**, 1439-1451 (2004).
34. Reddy, S.K., Rape, M., Margansky, W.A. & Kirschner, M.W. Ubiquitination by the anaphase-promoting complex drives spindle checkpoint inactivation. *Nature* **446**, 921-925 (2007).
35. Nilsson, J., Yekezare, M., Minshull, J. & Pines, J. The APC/C maintains the spindle assembly checkpoint by targeting Cdc20 for destruction. *Nat Cell Biol* **10**, 1411-1420 (2008).
36. Mansfeld, J., Collin, P., Collins, M.O., Choudhary, J.S. & Pines, J. APC15 drives the turnover of MCC-CDC20 to make the spindle assembly checkpoint responsive to kinetochore attachment. *Nat Cell Biol* **13**, 1234-1243 (2011).
37. Ma, H.T. & Poon, R.Y. Orderly inactivation of the key checkpoint protein mitotic arrest deficient 2 (MAD2) during mitotic progression. *J Biol Chem* **286**, 13052-13059 (2011).
38. Ge, S., Skaar, J.R. & Pagano, M. APC/C- and Mad2-mediated degradation of Cdc20 during spindle checkpoint activation. *Cell Cycle* **8**, 167-171 (2009).
39. Foster, S.A. & Morgan, D.O. The APC/C subunit Mnd2/Apc15 promotes Cdc20 autoubiquitination and spindle assembly checkpoint inactivation. *Molecular cell* **47**, 921-932 (2012).
40. Uzunova, K. *et al.* APC15 mediates CDC20 autoubiquitylation by APC/C(MCC) and disassembly of the mitotic checkpoint complex. *Nature structural & molecular biology* **19**, 1116-1123 (2012).
41. Foe, I.T. *et al.* Ubiquitination of Cdc20 by the APC occurs through an intramolecular mechanism. *Curr Biol* **21**, 1870-1877 (2011).
42. Doncic, A., Ben-Jacob, E. & Barkai, N. Evaluating putative mechanisms of the mitotic spindle checkpoint. *Proc Natl Acad Sci U S A* **102**, 6332-6337 (2005).
43. Doncic, A., Ben-Jacob, E. & Barkai, N. Noise resistance in the spindle assembly checkpoint. *Molecular systems biology* **2**, 2006 0027 (2006).
44. Mistry, H.B., MacCallum, D.E., Jackson, R.C., Chaplain, M.A. & Davidson, F.A. Modeling the temporal evolution of the spindle assembly checkpoint and role of Aurora B kinase. *Proc Natl Acad Sci U S A* **105**, 20215-20220 (2008).

45. Wolthuis, R. *et al.* Cdc20 and Cks direct the spindle checkpoint-independent destruction of cyclin A. *Molecular cell* **30**, 290-302 (2008).
46. Malureanu, L. *et al.* Cdc20 hypomorphic mice fail to counteract de novo synthesis of cyclin B1 in mitosis. *J Cell Biol* **191**, 313-329 (2010).
47. Zechner, C. *et al.* Moment-based inference predicts bimodality in transient gene expression. *Proc Natl Acad Sci U S A* **109**, 8340-8345 (2012).
48. Julier, S. & Uhlmann, J.K. New extension of the Kalman filter to nonlinear systems. *Proc. SPIE 3068, Signal Processing, Sensor Fusion, and Target Recognition VI* **182** (1997).
49. Parks, D.R., Roederer, M. & Moore, W.A. A new "Logicle" display method avoids deceptive effects of logarithmic scaling for low signals and compensated data. *Cytometry. Part A : the journal of the International Society for Analytical Cytology* **69**, 541-551 (2006).
50. Buchler, N.E. & Louis, M. Molecular titration and ultrasensitivity in regulatory networks. *J Mol Biol* **384**, 1106-1119 (2008).

3 Discussion

3.1 Hierarchical kinetochore recruitment of checkpoint components with Mph1 as upstream and crucial part of the signaling network (results part 2.1)

3.1.1 Kinetochore recruitment of SAC components shows almost no feedback

Our live cell imaging experiments revealed a clear hierarchy in the kinetochore localization of *S. pombe* checkpoint proteins with Ark1 on top recruiting Mph1, which then recruits Bub1 and Bub3, which in turn recruit Mad1, Mad2 and Mad3 (part 2.1, Fig. 4A). Bub1 and Bub3 depend on each other for their kinetochore localization, which can be explained by their direct interaction; a Bub1-ΔGLEBS mutant unable to bind to Bub3 cannot localize to kinetochores but also fails to co-recruit Bub3. The mutual dependency that we observed supports the finding that the interaction of both proteins is necessary for binding to the kinetochore protein KNL1 (Yamagishi et al, 2012). One level below Bub1 and Bub3, kinetochore localization of Mad1 and Mad2 partially requires Mad3, but not vice versa. This defines Mad2 as the most downstream checkpoint component recruited to kinetochores. Data from other organisms is fragmentary or sometimes contradictory (part 2.1, Figure S11), but the overall hierarchical dependencies seem to be conserved between organisms, with Mad3 and BubR1 being the most variable (Chen, 2002; Heinrich et al, 2012; Lampson et al, 2004; Meraldi et al, 2004). Although we describe the *S. pombe* kinetochore recruitment dependencies to be hierarchical without strong feedback signaling from downstream to upstream SAC components, Ark1 recruitment to centromeres is partially affected in *mph1Δ*, *bub1Δ* and *bub3Δ* cells. The strongest effect was observed in cells lacking Bub1. Bub1 has been shown to phosphorylate histone H2A (Kawashima et al, 2010), which is required for recruiting the protein Sgo2 to centromeres, which then recruits Aurora B (Kawashima et al, 2007; Kawashima et al, 2010; Tsukahara et al, 2010). Bub1 recruitment has been shown to indirectly reinforce Mph1 recruitment to kinetochores via regulation of the Sgo2-Ark1 pathway (Kawashima et al, 2007; Kawashima et al, 2010; Tsukahara et al, 2010). This positive feedback further enforces

Mph1 recruitment to kinetochores and might aid in robust SAC signaling (van der Waal et al, 2012). The weaker effect of *mph1* or *bub3* deletion on Ark1 localization probably is a result of Bub1 still being present, but mislocalizing. We observed additional spots of Ark1 in *mph1Δ* and *bub3Δ,* but not in *bub1Δ.* The data is reminiscent to Sgo2 localization in *bub3Δ,* which also showed an increase in the number of Sgo2 dots in mitosis compared to wild type (Windecker et al, 2009). It might reflect an additional pathway with Bub3 and Mph1 shielding telomeres from Bub1 phosphorylation, thereby blocking Sgo2 recruitment and subsequent Ark1 localization. It is unclear if this is relevant for mitotic progression or conserved in evolution.

3.1.2 Essentiality of SAC protein kinetochore recruitment

Kinetochore recruitment of some checkpoint proteins does not seem to be essential for SAC signaling. Both *C. elegans* BubR1 and *S. cerevisiae* Mad3 are not enriched at kinetochores during mitosis, which suggests that Mad3 kinetochore recruitment in these organisms is not essential (Essex et al, 2009; Gillett et al, 2004). If kinetochore localization of Mad3/BubR1 is essential for checkpoint function in other organisms or if checkpoint function can be maintained with solely a cytosolic version of Mad3/BubR1 has not been investigated. *S. pombe* cells lacking *bub3* do not enrich Bub1, Mad1, Mad2 and Mad3 at kinetochores, but still displayed a functional checkpoint (Windecker et al, 2009; Vanoosthuyse et al, 2009). In our study, we now found that kinetochores in *bub3Δ* cells are not completely ‘empty’ of checkpoint components as both Ark1 and Mph1 were still recruited to unattached kinetochores. How the checkpoint signal is transferred from Mph1 at the kinetochore to the downstream components in the nucleoplasm is unclear. One possibility could be that, although we were unable to detect an enrichment of these downstream factors at kinetochores, they still pass by and transiently bind kinetochores, which is sufficient for these proteins to become activated. Another possibility that has been put forward is based on the idea that Bub3 could act as an inhibitor of Bub1 (Yamagishi et al, 2012). This hypothesis originated from experiments showing that mutations in the kinetochore protein Spc7, which eliminate kinetochore localization of Bub1 and Bub3, only cause a checkpoint defect when Bub3 is present, but not in the absence of Bub3 (Yamagishi et al, 2012). Hence, kinetochore localization of Bub1 and Bub3 may be required to release Bub1 from an inhibitory effect of Bub3. In cells lacking Bub3, Bub1 could be precociously activated,

thereby artificially boosting SAC signaling strength and/or dynamics. As a consequence neither Bub1 enrichment at kinetochores nor enrichment of the Mad1-Mad2 complex may be needed for checkpoint activity. Alternatively or additionally, active Mph1 could cycle between the kinetochore and the nucleoplasm, which might allow for binding and activation of the checkpoint components away from the kinetochore. Indeed, Mps1 turnover at kinetochores has been shown to be highly dynamic (Howell et al, 2004; Jelluma et al, 2010). We furthermore find that kinetochore localization of Mph1 cells is important, because an N-terminal truncation of Mph1 (Δ1-302) that impairs kinetochore localization causes a checkpoint failure in *bub3Δ* cells.

Tethering of Mph1-Δ1-302 to kinetochores also bypassed the requirement of Ark1 function for checkpoint signaling, which showed that in *S. pombe* the only checkpoint function of Ark1 is to recruit Mph1 to kinetochores. Therefore, if Ark1 is solely required to localize Mph1 to kinetochores, then Mph1 is the only crucial SAC component that needs to be enriched at kinetochores to facilitate SAC signaling. This strongly emphasizes the central role of Mph1 in checkpoint signaling. Similar observations have been made for human cells showing that Aurora B inhibition in cells containing kinetochore-tethered Mps1 does not affect checkpoint signaling (Saurin et al, 2011).

Having shown that only some checkpoint proteins need to be at kinetochores for proper checkpoint function raises the question if kinetochores themselves are essential for SAC signaling or if enrichment at other spots within the nucleus would be sufficient to facilitate checkpoint function. Recruitment of Mad1 or Bub1 to chromosome arms has been shown to be insufficient for SAC signaling (Maldonado & Kapoor, 2011; Rischitor et al, 2007). However, tethering of these proteins away from kinetochores potentially only co-recruited a subset of checkpoint components, which limits the interpretation. Only recruitment of all SAC proteins to spots away from kinetochores could elucidate whether kinetochores are essential for checkpoint signaling. In addition, it will be interesting to address why checkpoint components enrich at kinetochores, and why this feature has been evolutionary conserved, although at least for some checkpoint proteins kinetochore enrichment is non-essential for SAC signaling (Essex et al, 2009; Gillett et al, 2004; Vanoosthuyse et al, 2009; Windecker et al, 2009). Possibly, this is a consequence of additional, non-checkpoint functions of these proteins at kinetochores (Lampson & Kapoor, 2005; Logarinho et al, 2008; Meraldi & Sorger, 2005; Rahmani et al, 2009; van der Waal et al, 2012; Warren et al, 2002; Windecker et al, 2009).

3.2 The Mad1 C-terminus has an active role in checkpoint signaling and links the Bub1:Bub3 complex with downstream checkpoint signaling (results part 2.2)

3.2.1 Dissecting the connection between Bub1 and Mad1

In recent years, a detailed view emerged on the molecular events of Mps1-dependent Bub1:Bub3 recruitment to the kinetochore on the one hand and Mad1:Mad2 interaction, Cdc20 sequestration and MCC-dependent APC/C inhibition on the other hand. However, how these two sets of events are connected is only fragmentarily understood. Experiments in budding yeast described a mitosis-specific Mad1:Bub1:Bub3 complex, whose formation was abolished by mutating the C-terminal RLK motif in Mad1 to triple alanines (AAA) (Brady & Hardwick, 2000). Interaction of budding yeast Bub1 with Mad1 required the central region of Bub1 (Warren et al, 2002). This region contains the conserved motif 1 (cm1), which in human cells has been found to be necessary for Mad1 kinetochore recruitment and checkpoint function (Klebig et al, 2009). It remained unclear if the connection between Mad1 and Bub1 is direct, how Mad1 is incorporated into the constitutive Bub1:Bub3 complex during mitosis and if the Mad1-Bub1 relationship is an evolutionary conserved feature of SAC signaling.

In our study, we addressed the question if the link between Mad1 and Bub1 is evolutionary conserved. Indeed, in *S. pombe* we found that a Bub1-cm1 mutant abolished SAC function and strongly impaired Mad1 (Nadine Schmidt, personal communication) and Mad2 localization, but was still able to localize to kinetochores similar to wild type, mirroring results from Klebig et al. (2009) in human cells. Conversely, a Mad1-RLK/AAA or Mad1-RLK/ALA mutant was unable to localize to kinetochores and failed to establish a checkpoint-dependent mitotic arrest, while Bub1 localization was preserved. Despite this similar phenotype between *bub1-cm1* and *mad1-rlk* mutants, we could not detect any interaction between Bub1 and Mad1 by co-immunoprecipitation (Nicole Hustedt, personal communication). This could be explained if only a minor fraction of the two proteins (e.g. the kinetochore-bound pool) interacts. Immunoprecipitations with higher sensitivity, or testing of the interaction *in vitro* or by yeast-two-hybrid will be required to address this. Since artificial recruitment of Bub1 to the kinetochore is not sufficient for Mad1 recruitment (Ito et al, 2012), it will also be important to determine the additional factors that influence the kinetochore localization of Mad1.

3.2.2 The Mad1 RLK motif facilitates an additional function in the checkpoint

Interestingly, if Mad1-RLK/AAA, which by itself does not localize to kinetochores, was tethered to kinetochores via Mis12, checkpoint function was not restored. Similarly, the checkpoint remained non-functional when Mad1 was tethered to kinetochores in *bub1Δ* cells (Katharina Sewart, personal communication). This indicates that Bub1 and Mad1-RLK have a function in checkpoint signaling beyond Mad1 kinetochore recruitment. Interestingly, kinetochore-tethered Mad1-RLK/AAA interacted with Mad2 to a similar extent as wild type Mad1, and additionally Mad2:Mad2 dimerization at the kinetochore seemed unaffected. This indicated that signaling events downstream of Mad2:Mad2 dimerization are perturbed in this mutant. One particular process that could be affected in the Mad1-RLK/AAA mutant (and possibly be affected by Bub1) could be the binding and sequestration of Cdc20 at the kinetochore by Mad2 as this is the step in checkpoint signaling that directly follows Mad2:Mad2 dimerization. (Yamagishi et al, 2012). Further analysis is required to understand the role of the RLK motif in checkpoint function.

3.2.3 Additional, Mad2 dimerization-independent checkpoint function of the Mad1 C-terminal tail (CTD)

Since the Mad1 C-terminus was required for both Mad1 kinetochore localization and this additional, unknown checkpoint function, we screened the region for separation-of-function mutants that showed wild type like kinetochore localization but were impaired in checkpoint signaling (part 2.2, Fig. S4A and Fig. 3). We identified two Mad1-CTD mutants that maintained kinetochore localization but abolished checkpoint signaling: a deletion of the last alpha-helix in the CTD (Δhelix) as well as a triple point mutant (EDD/QNN) in the same region. Similar to the kinetochore-tethered Mad1-RLK/AAA mutant, both Mad1:Mad2 complex formation as well as Mad2 dimerization were unaffected, again indicating a defect in downstream signaling events. Comparable results have been obtained in human cells (Kruse et al., manuscript submitted), arguing that the requirement for the Mad1 C-terminus in SAC signaling is conserved in eukaryotes.

An interesting concept on how the Mad1 C-terminus influences Mad1 function mechanistically has been proposed by Sironi et al (2002). Based on their crystal structure of the tetrameric Mad1:Mad2 complex, the authors suggested that the two

alpha-helices after the Mad2 binding site could potentially fold back onto each other (part 2.2, Fig. 4), thereby flipping the Mad1 CTD back towards the Mad2 binding site. As the crystal structure of both the CTD and the Mad1:Mad2 complex only included one of the two alpha helices, it remains to be seen if the Mad1 C-terminus folds back onto itself *in vivo*, whether this conformation could be dynamic, and which part of the SAC process is regulated through the C-terminus of Mad1.

Taken together, further experiments are needed to decipher the additional function of Mad1 in SAC signaling, for example by searching for potential Mad1-CTD interaction partners in mitosis using unbiased approaches such as Mad1 immunoprecipitations followed by mass spectrometry, or protein-protein interaction screens such as yeast two-hybrid assays. Chemical cross-linking followed by mass spectrometry (CX-MS) could be used to address the potential intramolecular interactions to analyze the native structure of Mad1 and would provide a higher sensitivity in the search for intermolecular interactions. CX-MS has the advantage that it can provide information of the interaction topology in heterologous protein samples from a cellular context, compared to structure determination techniques such as X-ray crystallography or NMR that need homologous samples of proteins and complexes. Clearly, there is still a gap in our understanding how the checkpoint signal is propagated, and Bub1 and the Mad1 C-terminus seem to have an important role in this.

3.3 The spindle assembly checkpoint displays fragility towards abundance changes of checkpoint components, which is potentially detrimental for its functionality (results part 2.3)

3.3.1 Abundance changes in checkpoint proteins differentially affect SAC signaling capacity, reflecting their functions within the checkpoint

We have shown that varying the abundance different checkpoint components had different effects on SAC signaling. The checkpoint displays its greatest tolerance towards reduction of Mad1 and Bub1 (unpublished results) abundance, an intermediate flexibility towards reducing Mad3 levels and a low tolerance to reduction of Mad2. For Mad2, a mere 20% decrease in protein levels already impairs checkpoint function. The high tolerance of the SAC to reduction of Mad1 suggests that Mad1 is either in large excess over checkpoint targets or that Mad1 has a catalytic role. The low tolerance towards reduction of Mad2 and Mad3 is consistent with their role as stoichiometric inhibitors of Cdc20 (Nilsson et al, 2008; Sudakin et al, 2001).

Mad2 is only slightly more abundant than Mad1 as determined by relative nuclear and cellular abundance measurements. If all Mad1 is bound to Mad2, as shown for human cells (Shah et al, 2004), the free Mad2 pool available for Cdc20 binding should be small, which may pose a risk for robust checkpoint signaling. We currently do not know if in fission yeast all Mad1 is bound to Mad2, but we suspect that only a fraction of Mad1 may be used for Mad1:Mad2 complex formation as we can still detect Mad1-free Mad2 in a strain expressing only 40 % Mad2, while the amount of Mad1:Mad2 complex was very similar compared to a strain expressing 100% Mad2. This indicates that Mad1 is incapable to titrate out Mad2. This is further supported by the fact that overexpression of Mad1 to 300% does not fully sequester the available pool of Mad2 and only partially impairs checkpoint function, although it does bind more Mad2 than the wild type Mad1. Interestingly, slight reduction of Mad2 mainly affected the Mad1-free pool of Mad2, but did not visibly change the formation of the Mad1:Mad2 complex. Similarly, slight overexpression of Mad2 in 300% did not strongly alter the abundance of the Mad1:Mad2 complex compared to 300% Mad1 with wild type amount of Mad2. This suggests that the process of Mad1:Mad2 formation is regulated and is not strongly affected by slight variations in the abundance of either Mad1 or Mad2. The nuclear

pore complex component Tpr (Nup211 in *S. pombe*) has been suggested to aid in Mad1:Mad2 complex formation and checkpoint function (Lee et al, 2008). Human Tpr binds to both Mad1 and Mad2 *in vitro* and *in vivo*, and is important for Mad1:Mad2 activation (Lee et al, 2008). Tpr/Nup211 could therefore be the limiting factor for Mad1:Mad2 complex formation. To test this idea, it would be useful to overexpress Tpr/Nup211, which should exacerbate the partial checkpoint defect observed in strains expressing 300% Mad1. However, Nup abundance changes have been shown to artificially 'cluster' NPCs at local spots in the nuclear membrane (DuBois et al, 2012). This could in principle affect checkpoint signaling as it concentrates and/or sequesters Mad1:Mad2 away from kinetochores, making an interpretation of a Tpr/Nup211 overexpression experiment difficult.

The situation for Mad2 and Mad3 is different. Both proteins bind Cdc20 to form the MCC and inhibit Cdc20. This interaction seems to be stoichiometric, as already slight reduction of Mad2 to 80% and reduction of Mad3 to 60% of the wild type level cause defects in checkpoint signaling. Mad3 binding to Cdc20 seems to strictly depend on Mad2 binding, but not vice versa, implying a sequential action of Mad2 and Mad3 (Kulukian et al, 2009; Nilsson et al, 2008; Sczaniecka et al, 2008). This would in principle suggest that Mad2 is the limiting factor. However, we observe that reduction of Mad3 in a 65% Mad2 background further reduces checkpoint activity, whereas an increase of Mad3 attenuated the defect. This suggests cooperativity in MCC formation and might be facilitated through multiple contacts between all three proteins, as shown in the crystal structure (Chao et al, 2012). It is reasonable to assume that MCC formation is strongly impaired when both Mad2 and Mad3 are expressed at reduced levels. Conversely, improved checkpoint signaling in 65% Mad2 with increased Mad3 is potentially facilitated by Mad3 either stabilizing the Mad2:Cdc20 complex or by accelerated extraction of Cdc20 from Mad2:Cdc20 by Mad3 to form the final APC/C inhibitor.

3.3.2 Physiologic and pathologic changes in checkpoint protein abundance

Changes in checkpoint protein abundance have been shown to occur both under physiologic and pathologic conditions (Baker et al, 2004; Kops et al, 2005; Uhlen et al, 2010). Our study shows that nutrient conditions can influence the robustness of the checkpoint as cells with altered SAC protein abundance display a different SAC

response profile in rich medium and minimal medium, with the most apparent difference in mitotic arrest time in cells with 30 % Mad1. Wild type cells grown in minimal medium display a robust checkpoint, but accumulated Slp1 to approximately twice the abundance compared to wild type cells grown in rich medium. The abundance of other checkpoint components was not affected. Strikingly, if Slp1 abundance was artificially doubled in cells grown in rich medium, checkpoint function was clearly impaired, indicating that the checkpoint can adapt to Slp1 changes in minimal medium and that additional, Slp1-independent processes have been altered in minimal medium to confer robustness in a mitotic arrest.

Other physiological changes in checkpoint protein abundance have been described for various human tissues (The Human Protein Atlas; Uhlen et al, 2010). In addition, BubR1 abundance has been shown to decrease in testis and ovary tissue of ageing mice (Baker et al, 2004). Creating similarly low levels in haploinsufficient BubR1 mutant mice caused mitotic defects, early-onset senescence and infertility, mirroring the phenotypes observed in naturally ageing mice (Baker et al, 2004).

Alterations in checkpoint protein abundance have also been linked with pathological changes in mitotic progression, such as aneuploidy and cancer development (Kops et al, 2010; Pinto et al, 2008; Ricke et al, 2011; Ryan et al, 2012; Schuyler et al, 2012). Initially, it was thought that checkpoint signaling was abrogated in cancer cells, but recent evidence indicates that an attenuated rather than abrogated checkpoint might facilitate tumorigenesis, possibly in conjunction with mutated tumor suppressors (Kops et al, 2005; Thoma et al, 2009). Similar to our observations of a highly variable checkpoint response in some fission yeast strains with altered checkpoint protein abundance, cancer cells also display a non-genetic variability in response to microtubule drugs that activate the checkpoint (Gascoigne & Taylor, 2008). A weakened checkpoint in a fraction of the cells forming a tumor might ultimately favor their survival.

3.3.3 Cells keep noise in protein abundance unusually low to avoid critical zones of SAC signaling

Our study is the first single cell analysis of SAC protein abundance using live cell imaging approaches that provide information on cell-to cell variability of checkpoint components. Other studies have reported protein numbers on a subset of checkpoint

proteins, but lacked single cell data as most of the protein quantification was done on bulk cell extracts (Ghaemmaghami et al, 2003; Howell et al, 2000; Marguerat et al, 2012; Nilsson et al, 2008; Poddar et al, 2005). These studies agree with our finding that checkpoint protein concentrations are in a nanomolar range, presumably in the lower third of protein abundances. Low abundant proteins have been shown to be 'noisy', i.e. they tend to show a high cell-to-cell variability (Bar-Even et al, 2006; Newman et al, 2006). We now show that this is not the case for many of the checkpoint components, with the greatest noise constraints on nuclear Mad1, Mad2 and Mad3, where cell-to-cell variability was measured to be below 10%. The noise in checkpoint protein levels might be unusually low for proteins of this abundance, as cell-to-cell variability of similarly low-abundant proteins involved in cytokinesis was higher (Wu & Pollard, 2005). The low noise in checkpoint protein levels also explains why wild type cells can signal robustly even though a mere 20 % reduction of Mad2 causes problems in checkpoint signaling: the variability in wild type cells is too low to reach the critical borders for checkpoint functionality. How cells regulate protein abundance within this tight window is not understood. We suspect that checkpoint proteins may influence their own protein abundance through negative feedback on their translation. Proteins involved in temperature shock response, cell growth or development have been shown to auto-regulate the translation of their own mRNA (Skabkina et al, 2005; Yanowitz et al, 1999; Zhao et al, 2012), but if this reflects the mechanism of how checkpoint protein noise is regulated remains to be investigated.

Regarding the general robustness of the SAC signaling pathway, it is also unclear why the Mad2 abundance is so dangerously close to the critical zone of SAC signaling. Because we quantified GFP-tagged versions of checkpoint proteins, rather than the endogenous protein, we can at present not exclude that the levels of Mad2 are higher than is suggested by the level of Mad2-GFP. In vertebrate cells and budding yeast, Mad2 seems to be in larger excess over Mad1 (Ghaemmaghami et al, 2003; Shah et al, 2004) compared to our result in fission yeast, which will probably make checkpoint signaling less susceptible to reduction of Mad2. However, it is also possible that there is an advantage in having Mad2 abundance so close to the critical zone. Checkpoint function requires fast activation but also fast inactivation. We hypothesize that Mad2 levels may need to be relatively low to allow fast inactivation. This remains to be tested; but very high levels of Mad2 artificially activate the checkpoint and impair cellular viability (He et al, 1997) suggesting that Mad2 levels could be critical for checkpoint inactivation.

3.3.4 Slp1 variability as the basis of the bimodal split in SAC signaling

We have shown that varying the abundance of some checkpoint proteins can cause a bimodal split in the checkpoint response. The occurrence of two distinct populations of cells with different checkpoint signaling capacity is of non-genetic nature and presumably created by cell-to-cell variability (noise) in protein abundance. The two populations can be most prominently observed in Mad2 and Mad3 perturbations as well as in a 200 % over-expression of Slp1, which suggests that stoichiometric MCC formation as downstream signaling event is involved in the population split. Stoichiometric binding reactions have been shown to allow ultrasensitivity (Buchler & Louis, 2008). A computational model, which included MCC formation, Slp1-synthesis/-degradation and Mad2/Mad3 re-cycling, predicted that Slp1 synthesis differs between the two populations and is higher in the population that cannot arrest in mitosis, thereby potentially overriding the SAC. In contrast, Mad2 and Mad3 abundance was predicted to be similar in the two populations. We can substantiate this model prediction with biological experiments. On the Mad2/Mad3 side, when analyzing the kinetochore-bound and nucleoplasmic pool of both proteins we could not observe abundance differences between the two populations in rich medium and at best slight differences in minimal medium. On the Slp1 side, we could not determine protein abundance in single living cells, because tagging impairs functionality and the turn-over of the protein is too high for most fluorescent proteins to mature. However, Slp1 mRNA abundance in single cells fluctuates in a cell cycle-dependent manner, strongly increases in mitosis and is highly variable (ranging from 40 to over 100 mRNA molecules), which could reflect a high variability in Slp1 synthesis. To substantiate this proposition, we will continue our efforts to engineer a fully functional fluorescent version of Slp1, which will be essential to test if there are differences in Slp1 synthesis or abundance between the two populations.

In addition, a drawback of our measurements is that we only look at the total pool of protein, and cannot differentiate this from individual, active checkpoint complexes. We therefore need to develop new live-cell imaging based approaches such as Fluorescence (Förster) resonance energy transfer (FRET) or optogenetic tools to be able to detect dynamic checkpoint complex formation in single cells, which will help to understand the bimodal behavior of the SAC.

Data from human cells also suggests non-genetic cell-to-cell variability in checkpoint signaling, for example when checkpoint function was assayed after titrating small

molecule inhibitors or performing partial RNAi experiments. However, unlike in yeast, where we can regulate protein levels relatively homogeneously within a population, the degree of knock-down can vary considerably from cell to cell in RNAi experiments, making the interpretation of these experiments difficult. A functional checkpoint in RNAi-treated cells is therefore typically interpreted as failed knock-down. For example, Morrow et al. (2005) show a population split in Bub1 and BubR1 RNAi cells treated with the Aurora B inhibitor ZM447439, but interpret this as a consequence of incomplete knock-down in the fraction of cells that remains arrested (Morrow et al, 2005). Some other publications show a bimodal checkpoint response upon checkpoint perturbations (Saurin et al, 2011; Thoma et al, 2009), but do not comment on this phenomenon. Whether these observed population differences are due to noise in protein abundance can only be answered by simultaneously measuring both protein amount and the checkpoint response. This requires cell lines with endogenously tagged checkpoint proteins, and such data will hopefully become available soon.

4 References

Andreassen PR, Margolis RL (1994) Microtubule dependency of p34cdc2 inactivation and mitotic exit in mammalian cells. *The Journal of cell biology* **127:** 789-802

Bailer SM, Siniossoglou S, Podtelejnikov A, Hellwig A, Mann M, Hurt E (1998) Nup116p and nup100p are interchangeable through a conserved motif which constitutes a docking site for the mRNA transport factor gle2p. *The EMBO journal* **17:** 1107-1119

Baker DJ, Jeganathan KB, Cameron JD, Thompson M, Juneja S, Kopecka A, Kumar R, Jenkins RB, de Groen PC, Roche P, van Deursen JM (2004) BubR1 insufficiency causes early onset of aging-associated phenotypes and infertility in mice. *Nature genetics* **36:** 744-749

Bar-Even A, Paulsson J, Maheshri N, Carmi M, O'Shea E, Pilpel Y, Barkai N (2006) Noise in protein expression scales with natural protein abundance. *Nature genetics* **38:** 636-643

Barnhart EL, Dorer RK, Murray AW, Schuyler SC (2011) Reduced Mad2 expression keeps relaxed kinetochores from arresting budding yeast in mitosis. *Molecular biology of the cell* **22:** 2448-2457

Biggins S, Murray AW (2001) The budding yeast protein kinase Ipl1/Aurora allows the absence of tension to activate the spindle checkpoint. *Genes & development* **15:** 3118-3129

Bolanos-Garcia VM, Kiyomitsu T, D'Arcy S, Chirgadze DY, Grossmann JG, Matak-Vinkovic D, Venkitaraman AR, Yanagida M, Robinson CV, Blundell TL (2009) The crystal structure of the N-terminal region of BUB1 provides insight into the mechanism of BUB1 recruitment to kinetochores. *Structure* **17:** 105-116

Brady DM, Hardwick KG (2000) Complex formation between Mad1p, Bub1p and Bub3p is crucial for spindle checkpoint function. *Current biology : CB* **10:** 675-678

Brito DA, Rieder CL (2006) Mitotic checkpoint slippage in humans occurs via cyclin B destruction in the presence of an active checkpoint. *Current biology : CB* **16:** 1194-1200

Buchler NE, Louis M (2008) Molecular titration and ultrasensitivity in regulatory networks. *Journal of molecular biology* **384:** 1106-1119

Buffin E, Lefebvre C, Huang J, Gagou ME, Karess RE (2005) Recruitment of Mad2 to the kinetochore requires the Rod/Zw10 complex. *Current biology : CB* **15:** 856-861

Burgess DR, Chang F (2005) Site selection for the cleavage furrow at cytokinesis. *Trends in cell biology* **15:** 156-162

Burton JL, Solomon MJ (2007) Mad3p, a pseudosubstrate inhibitor of APCCdc20 in the spindle assembly checkpoint. *Genes & development* **21:** 655-667

Campbell L, Hardwick KG (2003) Analysis of Bub3 spindle checkpoint function in Xenopus egg extracts. *Journal of cell science* **116:** 617-628

Carmena M, Wheelock M, Funabiki H, Earnshaw WC (2012) The chromosomal passenger complex (CPC): from easy rider to the godfather of mitosis. *Nature reviews Molecular cell biology* **13:** 789-803

Chao WC, Kulkarni K, Zhang Z, Kong EH, Barford D (2012) Structure of the mitotic checkpoint complex. *Nature* **484:** 208-213

Cheeseman IM, Anderson S, Jwa M, Green EM, Kang J, Yates JR, 3rd, Chan CS, Drubin DG, Barnes G (2002) Phospho-regulation of kinetochore-microtubule attachments by the Aurora kinase Ipl1p. *Cell* **111:** 163-172

Cheeseman IM, Chappie JS, Wilson-Kubalek EM, Desai A (2006) The conserved KMN network constitutes the core microtubule-binding site of the kinetochore. *Cell* **127:** 983-997

Chen RH (2002) BubR1 is essential for kinetochore localization of other spindle checkpoint proteins and its phosphorylation requires Mad1. *The Journal of cell biology* **158:** 487-496

Chen RH, Brady DM, Smith D, Murray AW, Hardwick KG (1999) The spindle checkpoint of budding yeast depends on a tight complex between the Mad1 and Mad2 proteins. *Molecular biology of the cell* **10:** 2607-2618

Chen RH, Shevchenko A, Mann M, Murray AW (1998) Spindle checkpoint protein Xmad1 recruits Xmad2 to unattached kinetochores. *The Journal of cell biology* **143:** 283-295

Chung E, Chen RH (2002) Spindle checkpoint requires Mad1-bound and Mad1-free Mad2. *Molecular biology of the cell* **13:** 1501-1511

Ciferri C, Pasqualato S, Screpanti E, Varetti G, Santaguida S, Dos Reis G, Maiolica A, Polka J, De Luca JG, De Wulf P, Salek M, Rappsilber J, Moores CA, Salmon ED, Musacchio A (2008) Implications for kinetochore-microtubule attachment from the structure of an engineered Ndc80 complex. *Cell* **133:** 427-439

Collin P, Nashchekina O, Walker R, Pines J (2013) The spindle assembly checkpoint works like a rheostat rather than a toggle switch. *Nature cell biology*

Coudreuse D, Nurse P (2010) Driving the cell cycle with a minimal CDK control network. *Nature* **468:** 1074-1079

Courtheoux T, Gay G, Reyes C, Goldstone S, Gachet Y, Tournier S (2007) Dynein participates in chromosome segregation in fission yeast. *Biol Cell* **99:** 627-637

D'Arcy S, Davies OR, Blundell TL, Bolanos-Garcia VM (2010) Defining the molecular basis of BubR1 kinetochore interactions and APC/C-CDC20 inhibition. *The Journal of biological chemistry* **285:** 14764-14776

Dai W, Wang Q, Liu T, Swamy M, Fang Y, Xie S, Mahmood R, Yang YM, Xu M, Rao CV (2004) Slippage of mitotic arrest and enhanced tumor development in mice with BubR1 haploinsufficiency. *Cancer research* **64:** 440-445

De Antoni A, Pearson CG, Cimini D, Canman JC, Sala V, Nezi L, Mapelli M, Sironi L, Faretta M, Salmon ED, Musacchio A (2005) The Mad1/Mad2 complex as a template for Mad2 activation in the spindle assembly checkpoint. *Current biology : CB* **15:** 214-225

De Rop V, Padeganeh A, Maddox PS (2012) CENP-A: the key player behind centromere identity, propagation, and kinetochore assembly. *Chromosoma* **121:** 527-538

DeAntoni A, Sala V, Musacchio A (2005) Explaining the oligomerization properties of the spindle assembly checkpoint protein Mad2. *Philosophical transactions of the Royal Society of London Series B, Biological sciences* **360:** 637-647, discussion 447-638

DeLuca JG, Gall WE, Ciferri C, Cimini D, Musacchio A, Salmon ED (2006) Kinetochore microtubule dynamics and attachment stability are regulated by Hec1. *Cell* **127:** 969-982

DeLuca JG, Musacchio A (2012) Structural organization of the kinetochore-microtubule interface. *Curr Opin Cell Biol* **24:** 48-56

Dick AE, Gerlich DW (2013) Kinetic framework of spindle assembly checkpoint signalling. *Nature cell biology*

Ding R, West RR, Morphew DM, Oakley BR, McIntosh JR (1997) The spindle pole body of Schizosaccharomyces pombe enters and leaves the nuclear envelope as the cell cycle proceeds. *Molecular biology of the cell* **8:** 1461-1479

Ditchfield C, Johnson VL, Tighe A, Ellston R, Haworth C, Johnson T, Mortlock A, Keen N, Taylor SS (2003) Aurora B couples chromosome alignment with anaphase by targeting BubR1, Mad2, and Cenp-E to kinetochores. *The Journal of cell biology* **161:** 267-280

DuBois KN, Alsford S, Holden JM, Buisson J, Swiderski M, Bart JM, Ratushny AV, Wan Y, Bastin P, Barry JD, Navarro M, Horn D, Aitchison JD, Rout MP, Field MC (2012) NUP-1 Is a large coiled-coil nucleoskeletal protein in trypanosomes with lamin-like functions. *PLoS biology* **10:** e1001287

Essex A, Dammermann A, Lewellyn L, Oegema K, Desai A (2009) Systematic analysis in Caenorhabditis elegans reveals that the spindle checkpoint is composed of two largely independent branches. *Molecular biology of the cell* **20:** 1252-1267

Fang G (2002) Checkpoint protein BubR1 acts synergistically with Mad2 to inhibit anaphase-promoting complex. *Molecular biology of the cell* **13:** 755-766

Fang G, Yu H, Kirschner MW (1998) The checkpoint protein MAD2 and the mitotic regulator CDC20 form a ternary complex with the anaphase-promoting complex to control anaphase initiation. *Genes & development* **12:** 1871-1883

Fava LL, Kaulich M, Nigg EA, Santamaria A (2011) Probing the in vivo function of Mad1:C-Mad2 in the spindle assembly checkpoint. *The EMBO journal* **30:** 3322-3336

Foley EA, Kapoor TM (2013) Microtubule attachment and spindle assembly checkpoint signalling at the kinetochore. *Nature reviews Molecular cell biology* **14:** 25-37

Foster SA, Morgan DO (2012) The APC/C subunit Mnd2/Apc15 promotes Cdc20 autoubiquitination and spindle assembly checkpoint inactivation. *Molecular cell* **47:** 921-932

Fraschini R, Beretta A, Sironi L, Musacchio A, Lucchini G, Piatti S (2001) Bub3 interaction with Mad2, Mad3 and Cdc20 is mediated by WD40 repeats and does not require intact kinetochores. *The EMBO journal* **20:** 6648-6659

Gascoigne KE, Taylor SS (2008) Cancer cells display profound intra- and interline variation following prolonged exposure to antimitotic drugs. *Cancer cell* **14:** 111-122

Gascoigne KE, Taylor SS (2009) How do anti-mitotic drugs kill cancer cells? *Journal of cell science* **122:** 2579-2585

Gassmann R, Holland AJ, Varma D, Wan X, Civril F, Cleveland DW, Oegema K, Salmon ED, Desai A (2010) Removal of Spindly from microtubule-attached kinetochores controls spindle checkpoint silencing in human cells. *Genes & development* **24:** 957-971

Ghaemmaghami S, Huh WK, Bower K, Howson RW, Belle A, Dephoure N, O'Shea EK, Weissman JS (2003) Global analysis of protein expression in yeast. *Nature* **425:** 737-741

Gillett ES, Espelin CW, Sorger PK (2004) Spindle checkpoint proteins and chromosome-microtubule attachment in budding yeast. *The Journal of cell biology* **164:** 535-546

Han JS, Holland AJ, Fachinetti D, Kulukian A, Cetin B, Cleveland DW (2013) Catalytic assembly of the mitotic checkpoint inhibitor BubR1-Cdc20 by a Mad2-induced functional switch in Cdc20. *Molecular cell* **51:** 92-104

Hardwick KG, Johnston RC, Smith DL, Murray AW (2000) MAD3 encodes a novel component of the spindle checkpoint which interacts with Bub3p, Cdc20p, and Mad2p. *The Journal of cell biology* **148:** 871-882

Hauf S, Cole RW, LaTerra S, Zimmer C, Schnapp G, Walter R, Heckel A, van Meel J, Rieder CL, Peters JM (2003) The small molecule Hesperadin reveals a role for Aurora B in correcting kinetochore-microtubule attachment and in maintaining the spindle assembly checkpoint. *The Journal of cell biology* **161:** 281-294

He X, Patterson TE, Sazer S (1997) The Schizosaccharomyces pombe spindle checkpoint protein mad2p blocks anaphase and genetically interacts with the anaphase-promoting complex. *Proceedings of the National Academy of Sciences of the United States of America* **94:** 7965-7970

He X, Rines DR, Espelin CW, Sorger PK (2001) Molecular analysis of kinetochore-microtubule attachment in budding yeast. *Cell* **106:** 195-206

Heinrich S, Windecker H, Hustedt N, Hauf S (2012) Mph1 kinetochore localization is crucial and upstream in the hierarchy of spindle assembly checkpoint protein recruitment to kinetochores. *Journal of cell science* **125:** 4720-4727

Herzog F, Primorac I, Dube P, Lenart P, Sander B, Mechtler K, Stark H, Peters JM (2009) Structure of the anaphase-promoting complex/cyclosome interacting with a mitotic checkpoint complex. *Science* **323:** 1477-1481

Hewitt L, Tighe A, Santaguida S, White AM, Jones CD, Musacchio A, Green S, Taylor SS (2010) Sustained Mps1 activity is required in mitosis to recruit O-Mad2 to the Mad1-C-Mad2 core complex. *The Journal of cell biology* **190:** 25-34

Hori T, Fukagawa T (2012) Establishment of the vertebrate kinetochores. *Chromosome Res* **20:** 547-561

Howell BJ, Hoffman DB, Fang G, Murray AW, Salmon ED (2000) Visualization of Mad2 dynamics at kinetochores, along spindle fibers, and at spindle poles in living cells. *The Journal of cell biology* **150:** 1233-1250

Howell BJ, McEwen BF, Canman JC, Hoffman DB, Farrar EM, Rieder CL, Salmon ED (2001) Cytoplasmic dynein/dynactin drives kinetochore protein transport to the spindle poles and has a role in mitotic spindle checkpoint inactivation. *The Journal of cell biology* **155:** 1159-1172

Howell BJ, Moree B, Farrar EM, Stewart S, Fang G, Salmon ED (2004) Spindle checkpoint protein dynamics at kinetochores in living cells. *Current biology : CB* **14:** 953-964

Hoyt MA, Totis L, Roberts BT (1991) S. cerevisiae genes required for cell cycle arrest in response to loss of microtubule function. *Cell* **66:** 507-517

Hwang LH, Lau LF, Smith DL, Mistrot CA, Hardwick KG, Hwang ES, Amon A, Murray AW (1998) Budding yeast Cdc20: a target of the spindle checkpoint. *Science* **279:** 1041-1044

Ito D, Saito Y, Matsumoto T (2012) Centromere-tethered Mps1 pombe homolog (Mph1) kinase is a sufficient marker for recruitment of the spindle checkpoint protein Bub1, but not Mad1. *Proceedings of the National Academy of Sciences of the United States of America* **109:** 209-214

Jaspersen SL, Winey M (2004) The budding yeast spindle pole body: structure, duplication, and function. *Annual review of cell and developmental biology* **20:** 1-28

Jelluma N, Brenkman AB, van den Broek NJ, Cruijsen CW, van Osch MH, Lens SM, Medema RH, Kops GJ (2008) Mps1 phosphorylates Borealin to control Aurora B activity and chromosome alignment. *Cell* **132:** 233-246

Jelluma N, Dansen TB, Sliedrecht T, Kwiatkowski NP, Kops GJ (2010) Release of Mps1 from kinetochores is crucial for timely anaphase onset. *The Journal of cell biology* **191:** 281-290

Jia L, Kim S, Yu H (2013) Tracking spindle checkpoint signals from kinetochores to APC/C. *Trends Biochem Sci* **38:** 302-311

Jia L, Li B, Warrington RT, Hao X, Wang S, Yu H (2011) Defining pathways of spindle checkpoint silencing: functional redundancy between Cdc20 ubiquitination and p31(comet). *Molecular biology of the cell* **22:** 4227-4235

Kadura S, He X, Vanoosthuyse V, Hardwick KG, Sazer S (2005) The A78V mutation in the Mad3-like domain of Schizosaccharomyces pombe Bub1p perturbs nuclear accumulation and kinetochore targeting of Bub1p, Bub3p, and Mad3p and spindle assembly checkpoint function. *Molecular biology of the cell* **16:** 385-395

Kalitsis P, Earle E, Fowler KJ, Choo KH (2000) Bub3 gene disruption in mice reveals essential mitotic spindle checkpoint function during early embryogenesis. *Genes & development* **14:** 2277-2282

Karess R (2005) Rod-Zw10-Zwilch: a key player in the spindle checkpoint. *Trends in cell biology* **15:** 386-392

Kastenmayer JP, Lee MS, Hong AL, Spencer FA, Basrai MA (2005) The C-terminal half of Saccharomyces cerevisiae Mad1p mediates spindle checkpoint function, chromosome transmission fidelity and CEN association. *Genetics* **170:** 509-517

Kawashima SA, Tsukahara T, Langegger M, Hauf S, Kitajima TS, Watanabe Y (2007) Shugoshin enables tension-generating attachment of kinetochores by loading Aurora to centromeres. *Genes & development* **21:** 420-435

Kawashima SA, Yamagishi Y, Honda T, Ishiguro K, Watanabe Y (2010) Phosphorylation of H2A by Bub1 prevents chromosomal instability through localizing shugoshin. *Science* **327:** 172-177

Kerscher O, Crotti LB, Basrai MA (2003) Recognizing chromosomes in trouble: association of the spindle checkpoint protein Bub3p with altered kinetochores and a unique defective centromere. *Molecular and cellular biology* **23:** 6406-6418

Kim S, Sun H, Tomchick DR, Yu H, Luo X (2012) Structure of human Mad1 C-terminal domain reveals its involvement in kinetochore targeting. *Proceedings of the National Academy of Sciences of the United States of America* **109:** 6549-6554

Kim SH, Lin DP, Matsumoto S, Kitazono A, Matsumoto T (1998) Fission yeast Slp1: an effector of the Mad2-dependent spindle checkpoint. *Science* **279:** 1045-1047

King EM, van der Sar SJ, Hardwick KG (2007) Mad3 KEN boxes mediate both Cdc20 and Mad3 turnover, and are critical for the spindle checkpoint. *PloS one* **2:** e342

Kiyomitsu T, Murakami H, Yanagida M (2011) Protein interaction domain mapping of human kinetochore protein Blinkin reveals a consensus motif for binding of spindle assembly checkpoint proteins Bub1 and BubR1. *Molecular and cellular biology* **31:** 998-1011

Klebig C, Korinth D, Meraldi P (2009) Bub1 regulates chromosome segregation in a kinetochore-independent manner. *The Journal of cell biology* **185:** 841-858

Kops GJ, Saurin AT, Meraldi P (2010) Finding the middle ground: how kinetochores power chromosome congression. *Cell Mol Life Sci* **67:** 2145-2161

Kops GJ, Weaver BA, Cleveland DW (2005) On the road to cancer: aneuploidy and the mitotic checkpoint. *Nature reviews Cancer* **5:** 773-785

Krenn V, Wehenkel A, Li X, Santaguida S, Musacchio A (2012) Structural analysis reveals features of the spindle checkpoint kinase Bub1-kinetochore subunit Knl1 interaction. *The Journal of cell biology* **196:** 451-467

Kulukian A, Han JS, Cleveland DW (2009) Unattached kinetochores catalyze production of an anaphase inhibitor that requires a Mad2 template to prime Cdc20 for BubR1 binding. *Developmental cell* **16:** 105-117

Lampson MA, Kapoor TM (2005) The human mitotic checkpoint protein BubR1 regulates chromosome-spindle attachments. *Nature cell biology* **7:** 93-98

Lampson MA, Renduchitala K, Khodjakov A, Kapoor TM (2004) Correcting improper chromosome-spindle attachments during cell division. *Nature cell biology* **6:** 232-237

Lara-Gonzalez P, Scott MI, Diez M, Sen O, Taylor SS (2011) BubR1 blocks substrate recruitment to the APC/C in a KEN-box-dependent manner. *Journal of cell science* **124:** 4332-4345

Lara-Gonzalez P, Westhorpe FG, Taylor SS (2012) The spindle assembly checkpoint. *Current biology : CB* **22:** R966-980

Larsen NA, Al-Bassam J, Wei RR, Harrison SC (2007) Structural analysis of Bub3 interactions in the mitotic spindle checkpoint. *Proceedings of the National Academy of Sciences of the United States of America* **104:** 1201-1206

Lau DT, Murray AW (2012) Mad2 and Mad3 cooperate to arrest budding yeast in mitosis. *Current biology : CB* **22:** 180-190

Lee KK, Gruenbaum Y, Spann P, Liu J, Wilson KL (2000) C. elegans nuclear envelope proteins emerin, MAN1, lamin, and nucleoporins reveal unique timing of nuclear envelope breakdown during mitosis. *Molecular biology of the cell* **11:** 3089-3099

Lee SH, Sterling H, Burlingame A, McCormick F (2008) Tpr directly binds to Mad1 and Mad2 and is important for the Mad1-Mad2-mediated mitotic spindle checkpoint. *Genes & development* **22:** 2926-2931

Li D, Morley G, Whitaker M, Huang JY (2010) Recruitment of Cdc20 to the kinetochore requires BubR1 but not Mad2 in Drosophila melanogaster. *Molecular and cellular biology* **30:** 3384-3395

Li R, Murray AW (1991) Feedback control of mitosis in budding yeast. *Cell* **66:** 519-531

Li X, Nicklas RB (1995) Mitotic forces control a cell-cycle checkpoint. *Nature* **373:** 630-632

Logarinho E, Resende T, Torres C, Bousbaa H (2008) The human spindle assembly checkpoint protein Bub3 is required for the establishment of efficient kinetochore-microtubule attachments. *Molecular biology of the cell* **19:** 1798-1813

London N, Ceto S, Ranish JA, Biggins S (2012) Phosphoregulation of Spc105 by Mps1 and PP1 regulates Bub1 localization to kinetochores. *Current biology : CB* **22:** 900-906

Lopes CS, Sampaio P, Williams B, Goldberg M, Sunkel CE (2005) The Drosophila Bub3 protein is required for the mitotic checkpoint and for normal accumulation of cyclins during G2 and early stages of mitosis. *Journal of cell science* **118:** 187-198

Luo X, Tang Z, Rizo J, Yu H (2002) The Mad2 spindle checkpoint protein undergoes similar major conformational changes upon binding to either Mad1 or Cdc20. *Molecular cell* **9:** 59-71

Luo X, Tang Z, Xia G, Wassmann K, Matsumoto T, Rizo J, Yu H (2004) The Mad2 spindle checkpoint protein has two distinct natively folded states. *Nature structural & molecular biology* **11:** 338-345

Ma HT, Poon RY (2011) Orderly inactivation of the key checkpoint protein mitotic arrest deficient 2 (MAD2) during mitotic progression. *The Journal of biological chemistry* **286:** 13052-13059

Maciejowski J, George KA, Terret ME, Zhang C, Shokat KM, Jallepalli PV (2010) Mps1 directs the assembly of Cdc20 inhibitory complexes during interphase and mitosis to control M phase timing and spindle checkpoint signaling. *The Journal of cell biology* **190:** 89-100

Maldonado M, Kapoor TM (2011) Constitutive Mad1 targeting to kinetochores uncouples checkpoint signalling from chromosome biorientation. *Nature cell biology* **13:** 475-482

Mansfeld J, Collin P, Collins MO, Choudhary JS, Pines J (2011) APC15 drives the turnover of MCC-CDC20 to make the spindle assembly checkpoint responsive to kinetochore attachment. *Nature cell biology* **13:** 1234-1243

Mapelli M, Filipp FV, Rancati G, Massimiliano L, Nezi L, Stier G, Hagan RS, Confalonieri S, Piatti S, Sattler M, Musacchio A (2006) Determinants of conformational dimerization of Mad2 and its inhibition by p31comet. *The EMBO journal* **25:** 1273-1284

Mapelli M, Massimiliano L, Santaguida S, Musacchio A (2007) The Mad2 conformational dimer: structure and implications for the spindle assembly checkpoint. *Cell* **131:** 730-743

Marguerat S, Schmidt A, Codlin S, Chen W, Aebersold R, Bahler J (2012) Quantitative analysis of fission yeast transcriptomes and proteomes in proliferating and quiescent cells. *Cell* **151:** 671-683

Mariani L, Chiroli E, Nezi L, Muller H, Piatti S, Musacchio A, Ciliberto A (2012) Role of the Mad2 dimerization interface in the spindle assembly checkpoint independent of kinetochores. *Current biology : CB* **22:** 1900-1908

Martin-Lluesma S, Stucke VM, Nigg EA (2002) Role of Hec1 in spindle checkpoint signaling and kinetochore recruitment of Mad1/Mad2. *Science* **297:** 2267-2270

Maure JF, Kitamura E, Tanaka TU (2007) Mps1 kinase promotes sister-kinetochore bi-orientation by a tension-dependent mechanism. *Current biology : CB* **17:** 2175-2182

McIntosh JR, Grishchuk EL, Morphew MK, Efremov AK, Zhudenkov K, Volkov VA, Cheeseman IM, Desai A, Mastronarde DN, Ataullakhanov FI (2008) Fibrils connect

microtubule tips with kinetochores: a mechanism to couple tubulin dynamics to chromosome motion. *Cell* **135:** 322-333

Meadows JC, Shepperd LA, Vanoosthuyse V, Lancaster TC, Sochaj AM, Buttrick GJ, Hardwick KG, Millar JB (2011) Spindle checkpoint silencing requires association of PP1 to both Spc7 and kinesin-8 motors. *Developmental cell* **20:** 739-750

Meraldi P, Draviam VM, Sorger PK (2004) Timing and checkpoints in the regulation of mitotic progression. *Developmental cell* **7:** 45-60

Meraldi P, Sorger PK (2005) A dual role for Bub1 in the spindle checkpoint and chromosome congression. *The EMBO journal* **24:** 1621-1633

Michel LS, Liberal V, Chatterjee A, Kirchwegger R, Pasche B, Gerald W, Dobles M, Sorger PK, Murty VV, Benezra R (2001) MAD2 haplo-insufficiency causes premature anaphase and chromosome instability in mammalian cells. *Nature* **409:** 355-359

Millband DN, Hardwick KG (2002) Fission yeast Mad3p is required for Mad2p to inhibit the anaphase-promoting complex and localizes to kinetochores in a Bub1p-, Bub3p-, and Mph1p-dependent manner. *Molecular and cellular biology* **22:** 2728-2742

Miniowitz-Shemtov S, Teichner A, Sitry-Shevah D, Hershko A (2010) ATP is required for the release of the anaphase-promoting complex/cyclosome from inhibition by the mitotic checkpoint. *Proceedings of the National Academy of Sciences of the United States of America* **107:** 5351-5356

Morgan DO (1995) Principles of CDK regulation. *Nature* **374:** 131-134

Morgan DO (1997) Cyclin-dependent kinases: engines, clocks, and microprocessors. *Annual review of cell and developmental biology* **13:** 261-291

Morgan DO (2007) *The cell cycle : principles of control*, London
Sunderland, MA: Published by New Science Press in association with Oxford University Press ;
Distributed inside North America by Sinauer Associates, Publishers.

Morrow CJ, Tighe A, Johnson VL, Scott MI, Ditchfield C, Taylor SS (2005) Bub1 and aurora B cooperate to maintain BubR1-mediated inhibition of APC/CCdc20. *Journal of cell science* **118:** 3639-3652

Musacchio A, Salmon ED (2007) The spindle-assembly checkpoint in space and time. *Nature reviews Molecular cell biology* **8:** 379-393

Newman JR, Ghaemmaghami S, Ihmels J, Breslow DK, Noble M, DeRisi JL, Weissman JS (2006) Single-cell proteomic analysis of S. cerevisiae reveals the architecture of biological noise. *Nature* **441:** 840-846

Nezi L, Rancati G, De Antoni A, Pasqualato S, Piatti S, Musacchio A (2006) Accumulation of Mad2-Cdc20 complex during spindle checkpoint activation requires binding of open and closed conformers of Mad2 in Saccharomyces cerevisiae. *The Journal of cell biology* **174:** 39-51

Nilsson J, Yekezare M, Minshull J, Pines J (2008) The APC/C maintains the spindle assembly checkpoint by targeting Cdc20 for destruction. *Nature cell biology* **10:** 1411-1420

Oliveira RA, Nasmyth K (2010) Getting through anaphase: splitting the sisters and beyond. *Biochem Soc Trans* **38:** 1639-1644

Orth JD, Tang Y, Shi J, Loy CT, Amendt C, Wilm C, Zenke FT, Mitchison TJ (2008) Quantitative live imaging of cancer and normal cells treated with Kinesin-5 inhibitors indicates significant differences in phenotypic responses and cell fate. *Molecular cancer therapeutics* **7:** 3480-3489

Pereira G, Schiebel E (1997) Centrosome-microtubule nucleation. *Journal of cell science* **110 (Pt 3):** 295-300

Peters JM (2006) The anaphase promoting complex/cyclosome: a machine designed to destroy. *Nature reviews Molecular cell biology* **7:** 644-656

Petrovic A, Pasqualato S, Dube P, Krenn V, Santaguida S, Cittaro D, Monzani S, Massimiliano L, Keller J, Tarricone A, Maiolica A, Stark H, Musacchio A (2010) The MIS12 complex is a protein interaction hub for outer kinetochore assembly. *The Journal of cell biology* **190:** 835-852

Pines J (2011) Cubism and the cell cycle: the many faces of the APC/C. *Nature reviews Molecular cell biology* **12:** 427-438

Pines J, Rieder CL (2001) Re-staging mitosis: a contemporary view of mitotic progression. *Nature cell biology* **3:** E3-6

Pinsky BA, Nelson CR, Biggins S (2009) Protein phosphatase 1 regulates exit from the spindle checkpoint in budding yeast. *Current biology : CB* **19:** 1182-1187

Pinto M, Vieira J, Ribeiro FR, Soares MJ, Henrique R, Oliveira J, Jeronimo C, Teixeira MR (2008) Overexpression of the mitotic checkpoint genes BUB1 and BUBR1 is associated with genomic complexity in clear cell kidney carcinomas. *Cellular oncology : the official journal of the International Society for Cellular Oncology* **30:** 389-395

Poddar A, Stukenberg PT, Burke DJ (2005) Two complexes of spindle checkpoint proteins containing Cdc20 and Mad2 assemble during mitosis independently of the kinetochore in Saccharomyces cerevisiae. *Eukaryotic cell* **4:** 867-878

Powers AF, Franck AD, Gestaut DR, Cooper J, Gracyzk B, Wei RR, Wordeman L, Davis TN, Asbury CL (2009) The Ndc80 kinetochore complex forms load-bearing attachments to dynamic microtubule tips via biased diffusion. *Cell* **136:** 865-875

Primorac I, Musacchio A (2013) Panta rhei: the APC/C at steady state. *The Journal of cell biology* **201:** 177-189

Primorac I, Weir JR, Chiroli E, Gross F, Hoffmann I, van Gerwen S, Ciliberto A, Musacchio A (2013) Bub3 reads phosphorylated MELT repeats to promote spindle assembly checkpoint signaling. *Elife* **2:** e01030

Przewloka MR, Venkei Z, Bolanos-Garcia VM, Debski J, Dadlez M, Glover DM (2011) CENP-C is a structural platform for kinetochore assembly. *Current biology : CB* **21:** 399-405

Rahmani Z, Gagou ME, Lefebvre C, Emre D, Karess RE (2009) Separating the spindle, checkpoint, and timer functions of BubR1. *The Journal of cell biology* **187:** 597-605

Reddy SK, Rape M, Margansky WA, Kirschner MW (2007) Ubiquitination by the anaphase-promoting complex drives spindle checkpoint inactivation. *Nature* **446:** 921-925

Ricke RM, Jeganathan KB, van Deursen JM (2011) Bub1 overexpression induces aneuploidy and tumor formation through Aurora B kinase hyperactivation. *The Journal of cell biology* **193:** 1049-1064

Rieder CL, Cole RW, Khodjakov A, Sluder G (1995) The checkpoint delaying anaphase in response to chromosome monoorientation is mediated by an inhibitory signal produced by unattached kinetochores. *The Journal of cell biology* **130:** 941-948

Rieder CL, Maiato H (2004) Stuck in division or passing through: what happens when cells cannot satisfy the spindle assembly checkpoint. *Developmental cell* **7:** 637-651

Rieder CL, Schultz A, Cole R, Sluder G (1994) Anaphase onset in vertebrate somatic cells is controlled by a checkpoint that monitors sister kinetochore attachment to the spindle. *The Journal of cell biology* **127:** 1301-1310

Rischitor PE, May KM, Hardwick KG (2007) Bub1 is a fission yeast kinetochore scaffold protein, and is sufficient to recruit other spindle checkpoint proteins to ectopic sites on chromosomes. *PloS one* **2:** e1342

Rosenberg JS, Cross FR, Funabiki H (2011) KNL1/Spc105 recruits PP1 to silence the spindle assembly checkpoint. *Current biology : CB* **21:** 942-947

Rossio V, Galati E, Ferrari M, Pellicioli A, Sutani T, Shirahige K, Lucchini G, Piatti S (2010) The RSC chromatin-remodeling complex influences mitotic exit and adaptation to the spindle assembly checkpoint by controlling the Cdc14 phosphatase. *The Journal of cell biology* **191:** 981-997

Ryan SD, Britigan EM, Zasadil LM, Witte K, Audhya A, Roopra A, Weaver BA (2012) Up-regulation of the mitotic checkpoint component Mad1 causes chromosomal instability and resistance to microtubule poisons. *Proceedings of the National Academy of Sciences of the United States of America* **109:** E2205-2214

Santaguida S, Tighe A, D'Alise AM, Taylor SS, Musacchio A (2010) Dissecting the role of MPS1 in chromosome biorientation and the spindle checkpoint through the small molecule inhibitor reversine. *The Journal of cell biology* **190:** 73-87

Saurin AT, van der Waal MS, Medema RH, Lens SM, Kops GJ (2011) Aurora B potentiates Mps1 activation to ensure rapid checkpoint establishment at the onset of mitosis. *Nat Commun* **2:** 316

Schuyler SC, Wu YF, Kuan VJ (2012) The Mad1-Mad2 balancing act - a damaged spindle checkpoint in chromosome instability and cancer. *Journal of cell science* **125:** 4197-4206

Scott RJ, Lusk CP, Dilworth DJ, Aitchison JD, Wozniak RW (2005) Interactions between Mad1p and the nuclear transport machinery in the yeast Saccharomyces cerevisiae. *Molecular biology of the cell* **16:** 4362-4374

Screpanti E, De Antoni A, Alushin GM, Petrovic A, Melis T, Nogales E, Musacchio A (2011) Direct binding of Cenp-C to the Mis12 complex joins the inner and outer kinetochore. *Current biology : CB* **21:** 391-398

Sczaniecka M, Feoktistova A, May KM, Chen JS, Blyth J, Gould KL, Hardwick KG (2008) The spindle checkpoint functions of Mad3 and Mad2 depend on a Mad3 KEN box-mediated interaction with Cdc20-anaphase-promoting complex (APC/C). *The Journal of biological chemistry* **283:** 23039-23047

Shah JV, Botvinick E, Bonday Z, Furnari F, Berns M, Cleveland DW (2004) Dynamics of centromere and kinetochore proteins; implications for checkpoint signaling and silencing. *Current biology : CB* **14:** 942-952

Sharp-Baker H, Chen RH (2001) Spindle checkpoint protein Bub1 is required for kinetochore localization of Mad1, Mad2, Bub3, and CENP-E, independently of its kinase activity. *The Journal of cell biology* **153:** 1239-1250

Shepperd LA, Meadows JC, Sochaj AM, Lancaster TC, Zou J, Buttrick GJ, Rappsilber J, Hardwick KG, Millar JB (2012) Phosphodependent recruitment of Bub1 and Bub3 to Spc7/KNL1 by Mph1 kinase maintains the spindle checkpoint. *Current biology : CB* **22:** 891-899

Simonetta M, Manzoni R, Mosca R, Mapelli M, Massimiliano L, Vink M, Novak B, Musacchio A, Ciliberto A (2009) The influence of catalysis on mad2 activation dynamics. *PLoS biology* **7:** e10

Sironi L, Mapelli M, Knapp S, De Antoni A, Jeang KT, Musacchio A (2002) Crystal structure of the tetrameric Mad1-Mad2 core complex: implications of a 'safety belt' binding mechanism for the spindle checkpoint. *The EMBO journal* **21:** 2496-2506

Sironi L, Melixetian M, Faretta M, Prosperini E, Helin K, Musacchio A (2001) Mad2 binding to Mad1 and Cdc20, rather than oligomerization, is required for the spindle checkpoint. *The EMBO journal* **20:** 6371-6382

Sivaram MV, Wadzinski TL, Redick SD, Manna T, Doxsey SJ (2009) Dynein light intermediate chain 1 is required for progress through the spindle assembly checkpoint. *The EMBO journal* **28:** 902-914

Skabkina OV, Lyabin DN, Skabkin MA, Ovchinnikov LP (2005) YB-1 autoregulates translation of its own mRNA at or prior to the step of 40S ribosomal subunit joining. *Molecular and cellular biology* **25:** 3317-3323

Sotillo R, Hernando E, Diaz-Rodriguez E, Teruya-Feldstein J, Cordon-Cardo C, Lowe SW, Benezra R (2007) Mad2 overexpression promotes aneuploidy and tumorigenesis in mice. *Cancer cell* **11:** 9-23

Sudakin V, Chan GK, Yen TJ (2001) Checkpoint inhibition of the APC/C in HeLa cells is mediated by a complex of BUBR1, BUB3, CDC20, and MAD2. *The Journal of cell biology* **154:** 925-936

Suijkerbuijk SJ, van Dam TJ, Karagoz GE, von Castelmur E, Hubner NC, Duarte AM, Vleugel M, Perrakis A, Rudiger SG, Snel B, Kops GJ (2012a) The vertebrate mitotic checkpoint protein BUBR1 is an unusual pseudokinase. *Developmental cell* **22:** 1321-1329

Suijkerbuijk SJ, Vleugel M, Teixeira A, Kops GJ (2012b) Integration of kinase and phosphatase activities by BUBR1 ensures formation of stable kinetochore-microtubule attachments. *Developmental cell* **23:** 745-755

Sullivan M, Morgan DO (2007) Finishing mitosis, one step at a time. *Nature reviews Molecular cell biology* **8:** 894-903

Tange Y, Niwa O (2008) Schizosaccharomyces pombe Bub3 is dispensable for mitotic arrest following perturbed spindle formation. *Genetics* **179:** 785-792

Taylor SS, Ha E, McKeon F (1998) The human homologue of Bub3 is required for kinetochore localization of Bub1 and a Mad3/Bub1-related protein kinase. *The Journal of cell biology* **142:** 1-11

Teichner A, Eytan E, Sitry-Shevah D, Miniowitz-Shemtov S, Dumin E, Gromis J, Hershko A (2011) p31comet Promotes disassembly of the mitotic checkpoint complex in an ATP-dependent process. *Proceedings of the National Academy of Sciences of the United States of America* **108:** 3187-3192

Thoma CR, Toso A, Gutbrodt KL, Reggi SP, Frew IJ, Schraml P, Hergovich A, Moch H, Meraldi P, Krek W (2009) VHL loss causes spindle misorientation and chromosome instability. *Nature cell biology* **11:** 994-1001

Tipton AR, Wang K, Link L, Bellizzi JJ, Huang H, Yen T, Liu ST (2011) BUBR1 and closed MAD2 (C-MAD2) interact directly to assemble a functional mitotic checkpoint complex. *The Journal of biological chemistry* **286:** 21173-21179

Tsukahara T, Tanno Y, Watanabe Y (2010) Phosphorylation of the CPC by Cdk1 promotes chromosome bi-orientation. *Nature* **467:** 719-723

Uhlen M, Oksvold P, Fagerberg L, Lundberg E, Jonasson K, Forsberg M, Zwahlen M, Kampf C, Wester K, Hober S, Wernerus H, Bjorling L, Ponten F (2010) Towards a knowledge-based Human Protein Atlas. *Nature biotechnology* **28:** 1248-1250

Uzunova K, Dye BT, Schutz H, Ladurner R, Petzold G, Toyoda Y, Jarvis MA, Brown NG, Poser I, Novatchkova M, Mechtler K, Hyman AA, Stark H, Schulman BA, Peters JM (2012) APC15 mediates CDC20 autoubiquitylation by APC/C(MCC) and disassembly of the mitotic checkpoint complex. *Nature structural & molecular biology* **19:** 1116-1123

van der Waal MS, Saurin AT, Vromans MJ, Vleugel M, Wurzenberger C, Gerlich DW, Medema RH, Kops GJ, Lens SM (2012) Mps1 promotes rapid centromere accumulation of Aurora B. *EMBO reports* **13:** 847-854

Vanoosthuyse V, Hardwick KG (2009) A novel protein phosphatase 1-dependent spindle checkpoint silencing mechanism. *Current biology : CB* **19:** 1176-1181

Vanoosthuyse V, Meadows JC, van der Sar SJ, Millar JB, Hardwick KG (2009) Bub3p facilitates spindle checkpoint silencing in fission yeast. *Molecular biology of the cell* **20:** 5096-5105

Vanoosthuyse V, Valsdottir R, Javerzat JP, Hardwick KG (2004) Kinetochore targeting of fission yeast Mad and Bub proteins is essential for spindle checkpoint function but not for all chromosome segregation roles of Bub1p. *Molecular and cellular biology* **24:** 9786-9801

Varma D, Wan X, Cheerambathur D, Gassmann R, Suzuki A, Lawrimore J, Desai A, Salmon ED (2013) Spindle assembly checkpoint proteins are positioned close to core microtubule attachment sites at kinetochores. *The Journal of cell biology* **202:** 735-746

Vernieri C, Chiroli E, Francia V, Gross F, Ciliberto A (2013) Adaptation to the spindle checkpoint is regulated by the interplay between Cdc28/Clbs and PP2ACdc55. *The Journal of cell biology* **202:** 765-778

Vigneron S, Prieto S, Bernis C, Labbe JC, Castro A, Lorca T (2004) Kinetochore localization of spindle checkpoint proteins: who controls whom? *Molecular biology of the cell* **15:** 4584-4596

Vink M, Simonetta M, Transidico P, Ferrari K, Mapelli M, De Antoni A, Massimiliano L, Ciliberto A, Faretta M, Salmon ED, Musacchio A (2006) In vitro FRAP identifies the minimal requirements for Mad2 kinetochore dynamics. *Current biology : CB* **16:** 755-766

Wan X, O'Quinn RP, Pierce HL, Joglekar AP, Gall WE, DeLuca JG, Carroll CW, Liu ST, Yen TJ, McEwen BF, Stukenberg PT, Desai A, Salmon ED (2009) Protein architecture of the human kinetochore microtubule attachment site. *Cell* **137:** 672-684

Warren CD, Brady DM, Johnston RC, Hanna JS, Hardwick KG, Spencer FA (2002) Distinct chromosome segregation roles for spindle checkpoint proteins. *Molecular biology of the cell* **13:** 3029-3041

Weiss E, Winey M (1996) The Saccharomyces cerevisiae spindle pole body duplication gene MPS1 is part of a mitotic checkpoint. *The Journal of cell biology* **132:** 111-123

Westhorpe FG, Straight AF (2013) Functions of the centromere and kinetochore in chromosome segregation. *Curr Opin Cell Biol* **25:** 334-340

Westhorpe FG, Tighe A, Lara-Gonzalez P, Taylor SS (2011) p31comet-mediated extraction of Mad2 from the MCC promotes efficient mitotic exit. *Journal of cell science* **124:** 3905-3916

Windecker H, Langegger M, Heinrich S, Hauf S (2009) Bub1 and Bub3 promote the conversion from monopolar to bipolar chromosome attachment independently of shugoshin. *EMBO reports* **10:** 1022-1028

Wu JQ, Pollard TD (2005) Counting cytokinesis proteins globally and locally in fission yeast. *Science* **310:** 310-314

Xia G, Luo X, Habu T, Rizo J, Matsumoto T, Yu H (2004) Conformation-specific binding of p31(comet) antagonizes the function of Mad2 in the spindle checkpoint. *The EMBO journal* **23:** 3133-3143

Yamagishi Y, Yang CH, Tanno Y, Watanabe Y (2012) MPS1/Mph1 phosphorylates the kinetochore protein KNL1/Spc7 to recruit SAC components. *Nature cell biology* **14:** 746-752

Yamaguchi S, Decottignies A, Nurse P (2003) Function of Cdc2p-dependent Bub1p phosphorylation and Bub1p kinase activity in the mitotic and meiotic spindle checkpoint. *The EMBO journal* **22:** 1075-1087

Yang M, Li B, Liu CJ, Tomchick DR, Machius M, Rizo J, Yu H, Luo X (2008) Insights into mad2 regulation in the spindle checkpoint revealed by the crystal structure of the symmetric mad2 dimer. *PLoS biology* **6:** e50

Yang M, Li B, Tomchick DR, Machius M, Rizo J, Yu H, Luo X (2007) p31comet blocks Mad2 activation through structural mimicry. *Cell* **131:** 744-755

Yang Z, Kenny AE, Brito DA, Rieder CL (2009) Cells satisfy the mitotic checkpoint in Taxol, and do so faster in concentrations that stabilize syntelic attachments. *The Journal of cell biology* **186:** 675-684

Yanowitz JL, Deshpande G, Calhoun G, Schedl PD (1999) An N-terminal truncation uncouples the sex-transforming and dosage compensation functions of sex-lethal. *Molecular and cellular biology* **19:** 3018-3028

Zhao X, Wu N, Ding L, Liu M, Liu H, Lin X (2012) Zebrafish p53 protein enhances the translation of its own mRNA in response to UV irradiation and CPT treatment. *FEBS letters* **586:** 1220-1225

LIST OF PUBLICATIONS

Accepted manuscripts:

1. **Heinrich S**, Geissen EM, Kamenz J, Trautmann S, Widmer C, Drewe P, Knop M, Radde N, Hasenauer J, Hauf S (2013)
   Determinants of robustness in spindle assembly checkpoint signalling
   Nature Cell Biology, 2013 Nov;15(11):1328-39

2. Widmer C, Drewe P, Lou X, Umrania S, **Heinrich S**, Raetsch G (2013)
   GRED: Graph-regularized 3D shape reconstitution from highly anisotropic and noisy images.
   arxiv.org 1309.4426

3. **Heinrich S**, Windecker H, Hustedt N, Hauf S (2012)
   Mph1 kinetochore localization is crucial and upstream in the hierarchy of spindle assembly checkpoint protein recruitment to kinetochores.
   Journal of Cell Science, 2012 Oct 15; 125(Pt 20):4720-7

4. Windecker H, Langegger M, **Heinrich S**, Hauf S (2009)
   Bub1 and Bub3 promote the conversion from monopolar to bipolar chromosome attachment independently of shugoshin.
   EMBO Reports, 2009 Sep;10(9):1022-8

Submitted manuscripts:

1. **Heinrich S**, Sewart K, Windecker H, Langegger M, Schmidt N, Hauf S
   Mad1 promotes checkpoint function independently of recruiting Mad1:Mad2 to kinetochores.
   EMBO Reports, under review